ABSTRACTS*

Oral and Poster

1. Use of Magnetization Transfer Imaging to Identify Atherosclerotic Plaque Components: Evaluation on Carotid Endarterectomy Specimens

William Kerwin,[1] Marina Ferguson,[2] Chun Yuan.[3] [1]*University of Washington, Department of Radiology, Seattle, WA USA;* [2]*Marina Ferguson, Inc., 1914 N 34th St, Seattle, WA USA;* [3]*University of Washington, Box 357115, Seattle, Washington United States*

Introduction: Research indicates that high resolution MRI can be used to identify atherosclerotic plaque components in vivo and assess vulnerabiltiy to rupture. Such efforts may be facilitated by magnetization transfer contrast (MTC), which highlights the macromolecular environment of each tissue type. MTC was previously shown to vary with tissue type in microdissected plaque samples [1]. The purpose of this study is to verify MTC tissue dependencies in intact plaque.

Methods: Five intact atherosclerotic plaque samples were obtained via carotid endarterectomy surgery. Within four hours of removal, the plaques were scanned at body temperature on a 1.5T GE Signa scanner using a 3D time-of-flight sequence (TR/TE/flip = 23 msec/3.6 msec/25 deg) that was previously found to provide good tissue contrast within plaque [2]. The sequence was then repeated with MTC generated using 14 msec CW pulses centered 1200 Hz off resonance. Finally, the magnetization transfer ratio (MTR) was computed for each 3 × 3 pixel region using the formula

$$MTR = (1 - I_{MTC}/I_0) \times 100\%$$

where I_{MTC} is the average MTC image intensity within a 3 × 3 pixel region and I_0 is the average intensity without MTC.

After the scan, histology was obtained for each sample after sequential sectioning and H & E staining as in [3]. Each section was then radially divided into eight regions that were examined under high power magnification. For each of these regions, the presence or absence was established of the following tissue types: necrotic lipid core (LC), intraplaque hemorrhage (H), fibrous tissue (F), neovascular ingrowth (NV), and calcium (Ca).

Finally, histology sections corresponding to available image planes were manually identified and oriented using the carotid bifurcation as a landmark. Image/histology pairs were restricted to the 2 image planes above and below the bifurcation to ensure proper correspondence. The same radial division into eight regions was performed on the images and within each region, the maximal MTR was recorded. These maximal MTR values were then investigated for correlation with the presence or absence of each identified tissue type.

Results: A typical image showing MTR results for a plaque specimen is depicted in Figure 1. The image has been gray scale encoded to depict MTR ranging from 0% (black) to 50% (white). The large black circle is the saline-filled vessel and the plaque is the object slightly offset to the upper left. Arrows indicate a region (1) with large MTR corresponding to LC in histology and two regions (2) with low MTR corresponding to neovasculature.

The relationship between LC and high MTR was observed in all plaques studied. Table 1 shows the average value of the maximum MTR in regions with (LC+) and without (LC−) LC for each of the plaques studied. In parentheses are the number of regions of each type. This shows a correlation of high MTR and the presence of LC. No other tissue type showed a consistent correlation with high MTR.

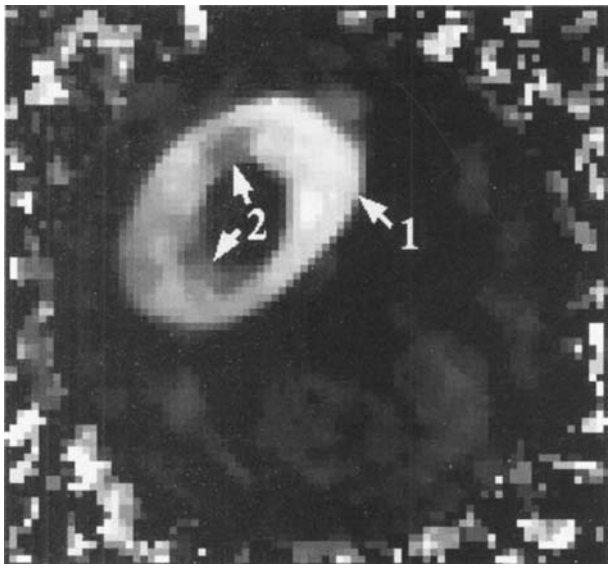

Figure 1.

Table 1

MTR Dependence on LC

	Sample 1	Sample 2	Sample 3	Sample 4	Sample 5
LC+	44.5(15)	52.0(3)	34.8(7)	39.8(27)	34.6(12)
LC−	37.0(8)	45.6(19)	30.2(24)	35.7(14)	32.8(22)

Discussion: Figure 1 shows that MTR varies with tissue type in intact plaque fresh from surgery. This suggests that MTC may be a valuable tool for identifying plaque components in vivo. In particular, large MTR indicates the presence of LC. The mechanism for the MT sensitivity of LC remains uncertain and the macromolecule responsible for the observation must be identified. MTC also shows promise for identifying NV as regions with little sensitivity to MTC. Presumably, the low MTR of these regions is due to the lack of magnetization transfer within the fluid filled neovessels.

2. True-FISP Navigator-Gated Free-Breathing Projection MRA with a 2D Selective Aortic Labeling Pulse

Elmar Spuentrup,[1] Peter Boernert,[2] Kraig V Kissinger,[3] Warren Manning,[4] Matthias Stuber.[5] [1]*Beth Israel Deaconess Medical Center, 330 Brookline Avenue, Boston, Massachusetts United States;* [2]*Beth Israel Deaconess Medical Center, Cardiovascular Division, Boston, MA USA;* [3]*Beth Israel Deaconess Medical Center, 330 Brookline Avenue, Boston, MA USA;* [4]*Beth Israel Deaconess Medical Center, Cardiovascular Divison, Boston, MA USA;* [5]*Beth Israel Deaconess Medical Center, 330 Brookline Ave, Boston, Massachusetts United States*

*For some of the abstracts, original art was not available.

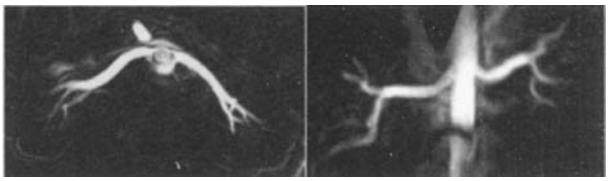

Figure 1. Double-oblique transverse (left) and coronal (right) projection MRA of the renal arteries (MIP) with 2D selective aortic labeling pulse and cardiac triggered, 3D True-FISP imaging sequence acquired during free-breathing with navigator technology.

Purpose: To develop a navigator-gated, free-breathing projection MRA imaging technique, which selectively visualizes the arteries originating from the aorta and completely suppresses the surrounding tissue and veins without exogenous contrast agent.

Introduction: Contrast-enhanced 3D gradient-echo MR angiography (MRA) in a breath hold during the first pass is the most common technique for visualization of the aorta and the thoracic and abdominal arteries. But their are several limitations associated with this technique: many patients cannot hold on their breath for prolonged periods, and most accurate timing of the imaging sequence is crucial for maximized contrast. Furthermore, only one slice orientation can be acquired during the first pass.

Projection MRA uses arterial spin labeling as contrast for selective MR angiograms (1–3). During a time delay between labeling and imaging, the labeled blood flows into the imaged volume. Subsequently, two acquisitions with and without preceding labeling are subtracted. This results in an selective MR arteriogram without exogenous contrast agent. We sought to combine a 2D selective pencil beam for selective labeling of the aortic blood with a free-breathing 3D True-FISP imaging sequence and real-time navigator technology for respiratory motion artifact suppression.

Materials and Methods: A right hemi-diaphragm navigator gated free-breathing projection MRA technique with a 2D selective pencil beam for aortic spin labeling was implemented on a 1.5T clinical MR scanner (ACS-NT, Philips, Best, The Netherlands) and applied for renal MRA in 6 healthy adult subjects. For imaging, a free-breathing, cardiac triggered segmented k-space 3D balanced gradient-echo sequence (3D True-FISP, TE 1.2 ms, FA 85°, 20 start-up cycles to obtain steady-state, 13–15 2mm thick slices, 1.1 × 1.1 mm in-plane resolution) was applied with and without preceding aortic spin-labeling. Subsequently, both data sets were complex subtracted (3). The time delay between the labeling pulse and imaging part of the sequence was 150–200 ms, which allowed for inflow of the labeled blood into the renal arteries. Data were collected in late diastole to use high diastolic flow in the renal arteries but to avoid motion artifacts during the aortic pulse wave. For suppression of respiratory motion artifacts during free-breathing, a right hemi-diaphragmatic 2D selective navigator was used (5 mm end-expiratory gating window). Coronal and a double-oblique transverse orientated projection MRA images were acquired using a 3-Point Plan-scan Tool and a 5-element synergy coil.

Results: In 6/6 subjects, renal arteries including more distal branches were selectively visualized on the projection MRA images with a high CNR (>120). Signal from static tissue and renal veins was successfully suppressed (Figure 1).

Conclusion: A projection MRA techniques with a 2D selective aortic labeling pulse was successfully combined with a free-breathing navigator-gated 3D True-FISP imaging sequence and allows for selective visualization of the renal arteries without exogenous contrast media. This selective aortic labeling technique shows potential for combination with other imaging sequences and for visualization of variable arteries originating from the aorta.

3. Free-Breathing Coronary Vessel Wall Imaging Using a Navigator and Spiral Data Acquisition

René Botnar,[1] Peter Börnert,[2] Won Kim,[3] Matthias Stuber,[4] Kraig Kissinger,[3] Warren Manning,[1] *[1]Beth Israel Deaconess Medical Center, 330 Brookline Ave, Boston, MA USA; [2]Philips Research Laboratory, Röntgenstrasse 24-26, Hamburg, Schleswig-Holstein Germany; [3]Beth Israel Deaconess Medical Center, 330 Brookline Ave, Boston, MA USA; [4]Beth Israel Deaconess Medical Center, 330 Brookline Ave, Boston, Massachusetts United States*

Introduction: Recently, MR coronary vessel wall imaging was demonstrated by several groups [1-3]. Coronary vessel wall imaging is primarily hampered by the small size of the coronary vessel wall, by respiratory and intrinsic cardiac motion, the low contrast between the wall and epicardial fat and the relatively long imaging time. Due to the thin coronary vessel wall thickness, images with sub-millimeter spatial resolution are required. The spiral readout trajectory is a very efficient way of sampling k-space with respect to time and signal-to-noise. SNR per unit time is high, which translates into shorter scanning times compared to Cartesian sampling schemes. Due to the short acquisition window (<27ms@500 microns) it is also relatively insensitive to intrinsic cardiac motion. Meyer and co-workers proposed a breathhold spiral approach [1], which can be difficult to apply in patients. We therefore thought to develop a free-breathing black blood spiral imaging sequence for coronary vessel wall and plaque imaging.

Purpose: The purpose of this study was to develop a free-breathing navigator gated black blood spiral imaging sequence for faster coronary vessel wall imaging.

Methods: Seven healthy adult subjects without clinical history of vascular disease and two patients with multi-vessel coronary artery disease were examined in supine position with a Philips Gyroscan ACS-NT MR scanner (Philips Medical Systems, Best, NL) using a commercial 5-element cardiac synergy coil and an interactive cardiac software package (INCA2). Cross-sectional images of the right coronary artery (RCA) and the left anterior descending (LAD) coronary artery were acquired. K-space was covered with 42 spiral interleaves (1 interleave per RR-interval) resulting in an in-plane resolution of 390–660 microns and a slice thickness of 5 mm. Negative contrast between coronary blood and vessel wall was achieved using a double inversion (Dual-IR) pre-pulse, which was immediately followed by an inversion slab [4] positioned on the dome of the right hemi-diaphragm (RHD) to facilitate navigator detection on the diaphragm. The 2D spiral imaging sequence was preceded by a 2D selective RHD navigator. Fat suppression was either performed using a chemical shift (CHESS) pre-pulse or using a water selective spectral spatial excitation pulse (1331). The parameters of the imaging sequence were TE = 1.6 (CHESS), TE = 5.3 ms (1331), TR = 2 heartbeats, AQ-window = 21–35 ms, NSA = 1, resulting in a scanning-time of 1:24 min per slice. Imaging was done during late diastole to minimize intrinsic cardiac motion.

Results: In all subjects the coronary vessel wall could be successfully visualized. The spectral spatial excitation pulse (1331) resulted in a more consistent suppression of epicardial fat than the frequency selective CHESS pre-pulse (Figure 1). In Figure 1 (right) a small branch vessel is visible that is not visible with the CHESS pre-pulse. All images were free from major respiratory and cardiac motion artifacts. Scanning time was three fold shorter than with a previously published TSE sequence (1:24 min vs. 4:16 min) without a penalty in signal-to-noise.

Conclusions: We successfully implemented a free-breathing black blood spiral imaging sequence for coronary vessel wall imaging. The ability to visualize such small structures without breathholding demonstrates the effectiveness of respiratory motion compensation with a MR navigator. The short acquisition window helped to reliably suppress artifacts from intrinsic cardiac motion. The ability to visualize small branch vessels demonstrates the effectiveness of the spectral spatial RF pulse for epicardial fat suppression. Due to the shortened imaging time

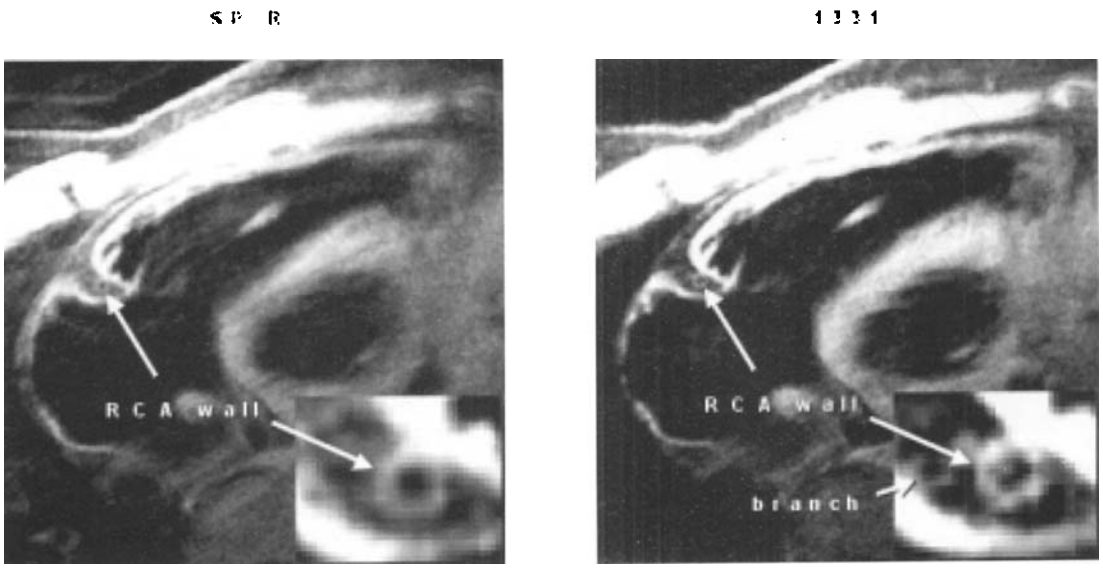

Figure 1. Image of the cross-sectional RCA using a navigator gated Dual-IR spiral imaging sequence using a CHESS pre-pulse (left) and a spectral spatial excitation RF pulse (right).

it helps to improve patient comfort and makes the sequence less motion sensitive.

4. Myocardial Perfusion Reserve and Endo-/Epicardial Perfusion Ratio After Cardiac Transplantation Assessed with Magnetic Resonance First-Pass Perfusion Imaging

Olaf Muehling,[1] Prasad Panse,[2] Andrey Zenovich,[2] M. Jerosch-Herold,[3] Betsy Wilson,[4] Robert Wilson,[5] Leslie Miller,[6] Norbert Wilke.[7] [1]*University of Minnesota, 420 Delaware St, Minneapolis, Minnesota United States;* [2]*University of Minnesota, 420 Delaware St. SE, Minneapolis, Minnesota USA;* [3]*University of Minnesota, 420 Delaware St. SE, Minneapolis, Minnesota United States;* [4]*University of Minnesota Division of Cardiology, 401 E River Rd, Minneapolis, Minnesota USA;* [5]*University of Minnesota, University of Minnesota, Minneapolis, Minnesota United States;* [6]*University of Minesota Division of Cardiology, 401 E River Rd, Minneapolis, Minnesota USA;* [7]*University of Minnesota, CMRR, Minneapolis, Minnesota United States*

Introduction: Magnetic Resonance First-Pass Perfusion (MRFP) imaging allows non-invasive assessment of myocardial perfusion reserve (MPR) (1) and endocardial/epicardial perfusion ratio (Endo/Epi) (2). Abnormalities in myocardial perfusion in transplanted hearts have been related to prior rejection (3) and hypertrophy (4). In the present study we assessed MPR and Endo/Epi ratio using MRFP imaging to elucidate the effects of prior rejection or hypertrophy on transmural myocardial perfusion in cardiac transplant recipients.

Methods: We examined 13 healthy volunteers (N) and 2 groups, A (n = 6) and B (n = 6), of clinically healthy cardiac recipients (7 ± 3 yrs. after transplantation). Both groups of patients had normal ejection fraction, angiographically normal coronary arteries, no acute rejection at biopsy and a coronary flow reserve (CFR) ≥2.5. CFR was calculated by the ratio of peak/resting coronary blood flow velocity measured at catheterization using an intra-coronary Doppler-flow wire and intra-coronary adenosine. Group B patients had increased wall thickness assessed on 2-D echo or MRI, a prior episode of rejection and a higher prevalence of hypertension and/or hypercholesterolemia compared to group A. Patients and volunteers underwent MRFP imaging in a 1.5 T MR Scanner (Vision, Siemens/Germany). Perfusion was assessed using a multi-slice saturation recovery turboFLASH sequence using a TR, TE and a flip angle of 2.4, 1.2 and 18°, a spatial resolution of 2–3 mm, a temporal resolution of 120–200 ms/image at 1 image/slice/heart beat. During image acquisition at rest and adenosine-induced hyperemia (140 µg/kg/min) a bolus of 0.02 mmol/l Gd-DTPA was injected. Spatial signal intensity (SI) time curves were generated using the ARGUS software (Siemens, Medical Systems, Iselin, NJ). Myocardial perfusion was determined from the SI-curves using a previously validated Fermi-model of constrained deconvolution (5). MPR was calculated from the ratio of hyperemic/resting perfusion and was corrected for the pressure-rate product (PRP) using the formula MPR × (mean group PRP at stress × individual PRP at rest/mean group PRP at rest × individual patient PRP at stress).

Results: Demographic data of patients and volunteers are shown in table 1. Group A and B did not differ in age, years after transplant and cold ischemia time. Group B had a higher incidence of risk factors associated with microvascular dysfunction (hypercholesterolemia and hypertension) than group A. For CFR, MPR, Endo/Epi and PRP see

Table 1

	Group A (n = 6)	Group B (n = 6)	Volunteers (n = 13)
Age (Yrs.)	53 ± 10	53 ± 10	34 ± 9
Gender	2♀	2♀	2♀
Tx-Age (Yrs.)	8 ± 4	7 ± 3	—
Cold-Ischemia Time (min.)	186 ± 33	140 ± 51	—
S/P Rejection (n)	0	5	—
LV Hypertrophy (n)	0	6	—
Hypertension (n)	2	5	—
Hypercholesteremia (n)	2	6	—

Table 2

Group	CFR	PR	Endo/Epi	PRP Rest/Hyperemia
A (n = 6)	3.7 ± 0.4	3.9 ± 0.8	1.7 ± 0.2	9.3 ± 1.7/9.0 ± 2.3
B (n = 6)	3.0 ± 0.4*	2.2 ± 0.3†	1.3 ± 0.3†	9.8 ± 2.7/9.8 ± 1.0#
Volunteers (n = 13)	—	4.1 ± 1.2	1.7 ± 0.4	6.3 ± 1.0‡/8.5 ± 2.5**

* $p < 0.05$ vs. A, † $p < 0.05$ vs. A and N, ‡ $p < 0.01$ vs. A and B, # $p < 0.01$ vs. N, ** $p <$ 0.01 vs. rest; PRP = pressure rate product in mmHg/min/1000 during rest and hyperemia

table 2. MPR and Endo/Epi ratio were not different between group A and volunteers. MPR and Endo/Epi ratio of group B were markedly reduced compared to group A and volunteers. PRP did not differ between group A and B. PRP at rest in volunteers was significantly lower compared to both groups of patients and increased significantly during adenosine infusion, while the transplant recipients showed no increase in PRP under adenosine.

Conclusion: In accordance with earlier published results (6) MRFP-imaging shows the functional integrity of the coronary microvasculature several years after cardiac transplantation. In regard to a group of healthy volunteers, Endo/Epi ratios are normal when MPR is normal. Prior episodes of rejection or hypertrophy, however, are related to a reduced MPR and Endo/Epi ratio. Other than in the group of healthy volunteers, the hyperemic response in the group of transplant recipients was not accompanied by changes in hemodynamic parameters (PRP). This indicates, that the transplanted heart seems to more rely on regional regulation of its hyperemic response than on systemic changes. MRFP imaging provides a new powerful tool to non-invasively assess the coronary microcirculation after cardiac transplantation.

5. Breathhold Myocardial Tagging of the Entire Cardiac Cycle

Frederick Epstein,[1] Daniel B. Ennis,[2] Peter Kellman,[3] Andrew Arai,[4] Elliot McVeigh.[5] [1]*University of Virginia, Radiology Department, Charlottesville, VA USA;* [2]*Johns Hopkins University School of Medicine, Department of Biomedical Engineering, Baltimore, MD USA;* [3]*National Institutes of Health, 10 Center Drive (Bldg 10, Room B1D416), Bethesda, Maryland United States;* [4]*National Institutes of Health, Laboratory of Cardiac Energetics, Bethesda, MD USA;* [5]*National Institutes of Health, Laboratory of Cardiac Energetics, Bethesda, Maryland United States*

Introduction: Myocardial tagging is used to image regional cardiac function. Conventional tags fade across the cardiac cycle and tag analysis is generally limited to systole. However, diastolic dysfunction occurs in diseases such as heart failure and ischemic heart disease. A breathhold CSPAMM pulse sequence using an echo-planar readout has recently been shown which increases tag persistence through systole

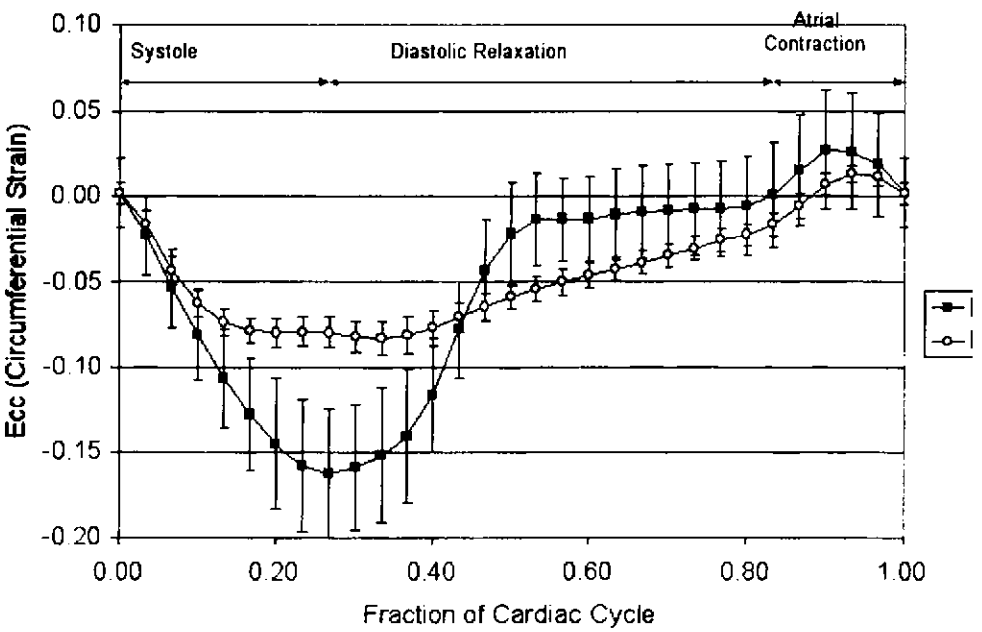

Figure 1. Normal volunteer and HCM midwall circumferential strain versus time.

and diastole (1). However, like many prospectively gated techniques, a trigger window is used prior to an upcoming heartbeat, and the last 10–20% of the cardiac cycle, including much of diastole, is not imaged. A method for imaging the entire cardiac cycle with a breathhold sequence, using Cardiac Phase To Order Reconstruction (CAPTOR), has also been reported (2). We investigated combining breathhold CSPAMM with CAPTOR to perform myocardial tagging over the entire cardiac cycle.

Methods: All imaging was performed on a 1.5T GE cardiac MRI scanner. CSPAMM tagging was implemented in a Fast Gradient Echo sequence with an Echo-Train readout (FGRE-ET). The slice following technique was not used because our tag analysis methods perform tissue tracking using short-axis and long-axis images. The FGRE-ET sequence supported CAPTOR acquisition and reconstruction. Three normal volunteers (NV) and three patients with hypertrophic cardiomyopathy (HCM) were scanned. Scan parameters included: FOV = 32–36 cm, matrix = 160 × 128, TR = 30 ms, echo train length = 8, bandwidth = ±62.5 kHz, slice thickness = 8 cm, views per segment = 8, phase FOV factor = 0.75, nex = 0.75, flip angle = ramped (8–21 degrees), and 1 dummy heartbeat, resulting in a scan time of 19 heartbeats. In NVs, 10 short-axis and 8 long-axis images were acquired. In HCM patients, 4 short-axis images were acquired. Image reconstruction, including homodyne processing and CSPAMM subtraction, was performed off-line using MATLAB. Three-dimensional strain analysis for the NV data and 2-dimensional strain analysis for the patient data was performed using continuous multi-dimensional b-spline based motion analysis (3).

Results: Tag persistence and image SNR was rated as good for all subjects. Tags were analyzable for all subjects across the entire cardiac cycle. Figure 1 shows regional left ventricular (LV) midwall circumferential strain (E_{cc}) from all regions spanning base to apex sampled from the continuous model for one NV (210 regions) and one HCM patient (48 regions). The normal volunteer exhibits typical systolic shortening, rapid early diastolic lengthening, diastasis, and lengthening during atrial contraction. The patient with HCM shows normal shortening during early systole, but an abnormal plateau during late systole. Diastole is markedly abnormal with no period of rapid lengthening and a prolonged period of slow lengthening. In the HCM patient a larger fraction of total lengthening is due to atrial contraction.

Conclusions: By combining the breathhold CSPAMM pulse sequence with the CAPTOR acquisition and reconstruction technique, myocardial tagging and strain analysis can be performed over the entire cardiac cycle.

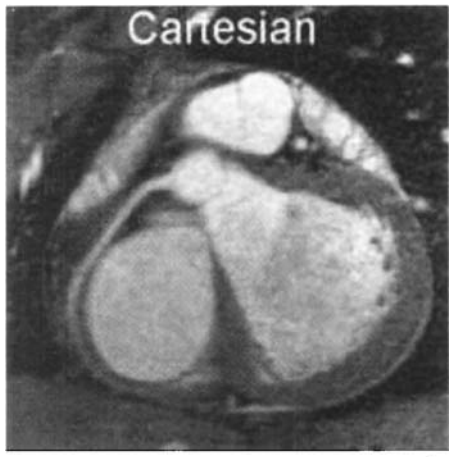

Figure 1a.

Figure 1b.

Figure 1c.

6. Superiority of Spiral Imaging for 3D Coronary MR Angiography

Peter Börnert,[1] Matthias Stuber,[2] Kraig Kissinger,[3] René Botnar,[4] Peter Koken,[5] Elmar Spuentrup,[6] Warren Manning.[7] [1]*Philips Research Laboratories, Technical Systems, Hamburg, Hamburg, Germany Germany;* [2]*Beth Israel Deaconess Medical Center, 330 Brookline Ave, Boston, Massachusetts United States;* [3]*Beth Israel Deaconess Medical Center, 330 Brookline Ave., Boston, MA MA;* [4]*Beth Israel Deaconess Medical Center, Cardiovascular Div., Cardiac MR, Boston, MA USA;* [5]*Philips Research Hamburg, Roentgenstrasse 24-26, Hamburg, Hamburg Germany;* [6]*Beth Israel Deaconess Medical Center, 330 Brookline Avenue, Boston, Massachusetts United States;* [7]*Beth Israel Deaconess Medical Center, Division of Cardiology, Boston, MA USA*

Introduction: Imaging of the human coronary arteries remains a challenge. 3D spiral imaging, which is a more efficient way to sample k-space data, has recently been considered [1,2]. However, to the present date, no comparative study between spiral acquisition and more conven-

Table 1

	Cartesian	Single Interl. Spiral	Double Interl. Spiral
SNR	15 ± 4	49 ± 12	33 ± 7
CNR	13 ± 5	36 ± 11	22 ± 7
Scan time (hb)	380	400	210
Quality (1-3 score)	2.5 ± 0.7	1.3 ± 0.4	2.2 ± 0.5

tional gradient echo techniques about the performance has been made. Therefore, in the present work, free-breathing, sub-millimeter 3D spiral coronary MRA was investigated in detail and objectively compared to more a conventional gradient-echo sequence.

Material and Methods: Nine healthy adults and one patient were studied using a commercial 1.5 T whole body scanner (Gyroscan, ACS-NT15, Philips Medical Systems) and a five-element cardiac synergy coil. Coronary MRA was performed using magnetization prepared (T2-preparation, regional signal pre-saturation, fat suppression) 3D imaging [3]. MR Signal was acquired using a Cartesian gradient-echo technique (c.f. ref. [3]) a stack of spirals in which one single interleave per R-R interval (with a 90° excitation angle, c.f. ref. [1]) was acquired and a stack of spirals in which two spiral interleaves (with 45°–90° excitation angle, c.f. ref. [2])) were measured within one R-R interval. Real-time navigator gating and prospective motion correction was applied. In all experiments the in-plane spatial resolution was 0.7×0.7 mm^2 with a slice thickness of 1.5 mm (after zero padding). The final matrix size was set to $512 \times 512 \times 20$. Evaluation of the SNR, CNR and visual scoring (test by three observers) was subsequently performed for the acquired data sets.

Results and Discussion: In all the measured individuals and for all of the different imaging techniques the major parts of the proximal coronaries (RCA, LAD, LCX) could consistently be visualized with a high contrast between the arterial blood pool and the surrounding tissue. In Fig. 1, selected reformatted images for the three techniques are shown. The results of the entire study are summarized in Table 1. The conventional spiral scan (b) (single interleave per R-R) with identical scanning duration as for the Cartesian scan (a) showed a three-fold improvement in SNR and was scored on average as the best scan with the best image quality. When compared to the Cartesian scan, the accelerated spiral protocol scan (c) (two interleaves per R-R) reduced the scanning time by a factor of two, showed an SNR improvement of a factor of two, and was scored to be of slightly improved image quality when compared to the Cartesian acquisition.

Conclusion: Accelerated 3D spiral coronary MRA allows for high-resolution visualization of the proximal coronary arteries with a 50% reduced scanning duration and without penalty in SNR or image quality when compared to standard Cartesian image acquisition. This may contribute to an increased image quality as well as improved patient comfort and throughput. The three-fold signal gain in the single interleave spiral suggested that this technique may have a potential for spatial resolution coronary MRA towards x-ray angiography standards.

References

1. Thedens DR, Irarrazaval P, Sachs TS, et al. MRM 1999; 41: 1170–1179.
2. Börnert P, Aldefeld A, Groen J, et al. 6th Meeting of ISMRM, (1999) p. 1271
3. Stuber M, Botnar RM, Danias PG, et al. J Am Coll Cardiol 1999; 34:524–531.

7. Contrast Enhanced 3D MRI Improves Measurement of Atherosclerotic Plaque Volume and Identification of Tissue Types

Jianming Cai,[1] William Kerwin,[2] Ying Luo,[3] Marina Ferguson,[4] Thomas Hatsukami,[5] Chun Yuan.[6] *[1]University of Washington, Department of Raidology, Seattle, WA USA; [2]University of Washington, Department of Radiology, Seattle, WA USA; [3]University of Washington, Department of Electrical Engineering, Seattle, WA USA; [4]Marina Ferguson, Inc., 1914 N 34th St, Seattle, WA USA; [5]University of Washington, Veterans Affairs Puget Sound Health Care System, Seattle Division, Seattle, Washington United States; [6]University of Washington, Box 357115, Seattle, Washington United States*

Introduction: Atherosclerotic lesion size and tissue characteristics may be directly linked to lesion stability. Viewing lesion structures in vivo may therefore permit the assessment of lesion stability and the diagnosis of vulnerable lesions. MRI has shown great potential to view lesion structures in vivo, particularly for atherosclerosis of the carotid arteries [1]. However, certain plaque features, such as neovasculature, are difficult to identify with existing techniques. Additionally, the outer boundary of the vessel wall can be obscured in places by adjacent tissue with similar contrast, thus hindering wall area measurement. This study's aim was to determine if the use of contrast enhanced MRI can improve the accuracy of wall area measurement and assist in tissue characterization in atherosclerotic lesions.

Methods: Ten subjects scheduled for carotid endarterectomy (CEA) underwent an MRI scan using a custom made phased-array coil [2] on a SIGNA scanner (GE Medical Systems). Pre- and post-contrast images were acquired with a gadolinium agent (0.2 mmol/kg) using an axial 3D fast gradient echo (3DFGRE) protocol (TR/TE/flip = 9 msec/2.4 msec/20deg).

CEA was then performed within 1 week of the MRI with the plaque removed intact. An identical 3DFGRE scan was conducted on the excised plaque at 37°C as a reference before obtaining plaque histology. Histological processing described in [3] has been completed on six of the plaques with the remaining four expected in the near future. Histology slices corre-

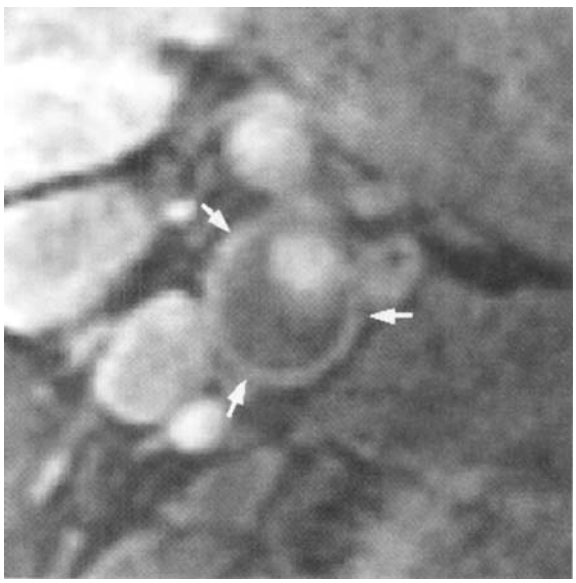

Figure 1.

sponding to in vivo image planes were identified by matching features such as lumen shape and proximity to the bifurcation. Enhancing plaque regions were then associated with tissue type from histology.

Additionally, for six of the plaques, tracing of carotid artery boundaries was conducted on pre, post and ex vivo 3DFGRE images by 2 raters. Wall areas (WA) were measured based on the outlines. After matching locations, the accuracy and precision of WA measurements in vivo were investigated using ex vivo results as a gold standard.

Results: Varying degrees of contrast enhancement were observed within the artery wall. As previously reported [4], the outer wall of the vessel enhanced relative to the necrotic core as depicted by arrows in Figure 1 (on previous page). In general, the plaque interior showed no enhancement. However, in three of the six plaque specimens for which histology is available regional enhancement did occur within the plaque itself. The enhanced regions were found to contain neovasculature or loose fibrous matrix.

For the wall area comparison, a total of 103 matched image locations were evaluated. The average difference in WA between pre-contrast and ex vivo images was 10.72 mm^2 with a standard deviation of 7.04 mm^2. The average difference between post-contrast and ex vivo was 6.23 mm^2 with a standard deviation of 5.88 mm^2. The smaller ex vivo WA observed in both cases is expected, since a portion of the artery wall remains in vivo after CEA. The fact that the difference is smaller for post-contrast images is attributable to an apparent increase in lumen size after contrast injection. This effect, which is also utilized in contrast enhanced MRA, occurs because regions of slow flow are less saturated after enhancement. Because it eliminates these slow flow regions from the wall area measurement, the post-contrast result is likely to be more accurate. The somewhat smaller standard deviation in the area measurements for post-contrast images (5.88 mm^2 versus 7.04 mm^2 without contrast) also suggests that the post-contrast measurements are more precise. Most likely, this is the result of better boundary identification because of the enhanced outer walls.

Conclusions: These results show that post-contrast 3DFGRE may be useful for vessel volume measurement and tissue characterization. The most significant benefits appear to be improved outer wall visibility and enhancement of neovasculature and loose fibrous matrix. These two types of tissue, in particular, may be important clinical indicators of destabilizing processes such as inflammation. The improved outer wall visibility, on the other hand, will be valuable in future studies examining the relationship between plaque volume changes and clinical outcome.

8. Segmental Myocardial Function Visualization During Tagged MRI Dobutamine Stress Testing

Rosa Maria Piva,[1] Carlos Rochitte,[2] Luiz Francisco Ávila,[3] Cláudio Campi de Castro,[4] Giovanni Guido Cerri,[2] José Rodrigues Parga Filho.[2] [1]*Heart Institute–InCor–University of Sao Paulo Medical School, Av. Dr. Eneas Carvalho Aguiar, São Paulo, São Paulo Brazil;* [2]*Heart Institute (InCor), University of São Paulo Medical School, Av. Dr. Eneas Carvalho Aguiar, 44–AB, São Paulo, São Paulo Brazil;* [3]*Heart Institute (InCor)–University of São Paulo Medical School, Av. Dr. Eneas Carvalho Aguiar, 44–AB, São Paulo, São Paulo Brazil;* [4]*Heart Institute (InCor)–University of São Paulo Medical School, Av. Dr. Eneas Carvalho Aguiar, 44–AB, São Paulo, São Paulo Brazil*

Introduction: Early detection of myocardial ischemia is important for the diagnosis and therapy of coronary artery disease. High spatial/temporal resolution of magnetic resonance imaging (MRI) associated with myocardial tagging can provide, non-invasively, detailed information on regional transmural function. These features are very attractive for evaluation of inotropic stimulation of myocardium during pharmacologically induced-stress testing. Multi-plane imaging at continuous drug infusion is desirable for full left ventricular (LV) coverage. In this work,

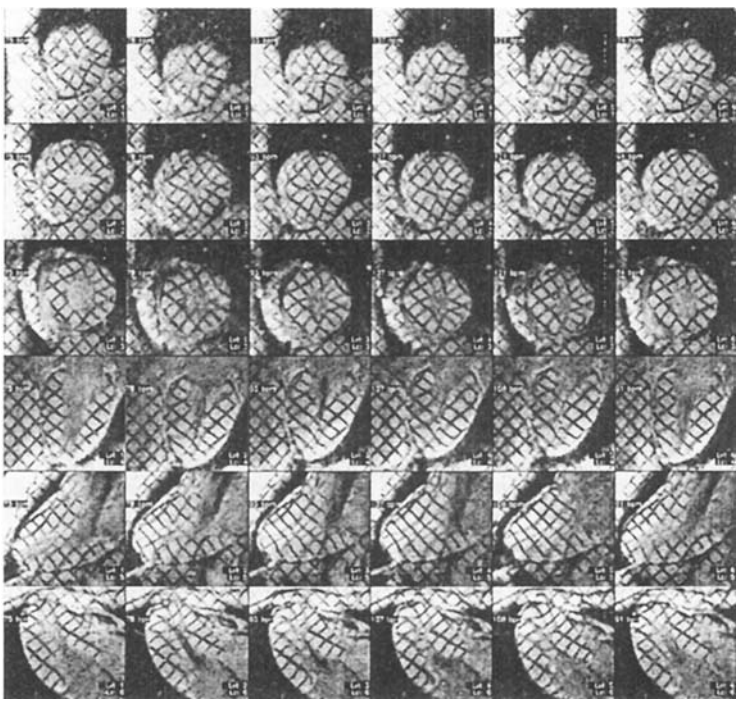

Figure 1.

Table 1

Results of Tagged MRI Dobutamine Stress Testing with Real Time Slice Prescription, Fast Cine Imaging and Multi-Stress Level Cine Display

Ex.	Sex	Age	ECG-Pré	ECG-Pós	Results	Adverse Reactions	Coronary Angyography
1	M	64	N	N	Conclusive. Ischemia: No	None	No
2	M	60	N	N	Conclusive. Ischemia: No	None	No
3	M	43	Ab	Ab	Conclusive. Ischemia: Yes	None	Yes. Agreed
4	M	79	N	N	Cancelled. Hypertension	—	No
5	F	74	Ab	Ab	Conclusive. Ischemia: No. Viability: Yes	None	No
6	M	75	Ab	Ab	Cancelled. Unreported metal implant	—	No
7	F	36	Ab	Ab	Conclusive. Ischemia: No. Viability: Yes	None	Yes. Agreed
8	M	53	MI	MI	Inconclusive	None	No
9	F	65	N	N	Conclusive. Ischemia: Yes	HA	Yes. Agreed
10	M	73	MI	MI	Conclusive. Ischemia: No. Viability: No	None	No
11	F	57	N	N	Cancelled. Clautrophobia	—	Yes
12	M	58	Ab	Ab	Inconclusive	None	Yes
13	M	33	LBBB	LBBB	Inconclusive	None	Yes
14	M	63	Ab	Ab	Inconclusive. Viability: No	HI	No
15	M	46	N	N	Inconclusive	HA, HI	Yes
16	M	73	LBBB	LBBB	Inconclusive. Ischemia: Yes by chest pain	FT, CP	No
17	F	73	MI	MI	Conclusive: Ischemia: Yes	FT	Yes. Agreed
18	M	74	Ab	Ab	Inconclusive. Viability: Yes	HI	Yes
19	F	58	MI	MI	Conclusive: Ischemia: yes. Viability: Yes	HP	Yes. Agreed
20	M	56	N	N	Conclusive. Ischemia: No	HI	Yes. Agreed
21	F	51	N	N	Inconclusive. Viability: Yes	HI, HA	No
22	F	61	N	N	Conclusive. Ischemia: No	ES	No
23	F	45	N	N	Inconclusive	HA	No
24	M	52	N	N	Conclusive. Ischemia: Yes	CP	No

we have assessed regional myocardial function in patients referred for MRI stress testing, using real time image acquisition, EPI-based fast cine tagged MRI and simultaneous image display at different levels of stress.

Methods: Twenty-four patients underwent tagged MRI dobutamine stress testing. A new specially designed software package developed by GE was used for image acquisition and display. Slice prescription was performed using real time image acquisition, with a rate of 7 to 8 frames per second and acceptable image quality. Six LV slices were prescribed, including 3 short-axis (basal, medium and apical) and 3 long axis slices (two and four chambers and LV outflow tract). Tagged images (grid pattern) were obtained at rest, different levels of stress and at recovery. At all levels of dobutamine dosage, the imaging acquisition section started after 2 minutes of infusion and lasted for the next three minutes, which was the period required for acquisition of 6 cine slices, with a breath held EPI fast cine pulse sequence (TR/TE = 14/1.4 ms). Stepwise dobutamine infusions of 5, 10, 20, 30 and 40 mg/kg/min were used. If the heart rate did not increase, atropine was infused simultaneously at 30 mg/kg/min dobutamine level. The software allowed the reacquisition of selected single slice cine sequence at any time, when image quality was degraded due to motion and respiratory artifacts.

Results: In order to illustrate the feasibility of MRI dobutamine stress testing using the given resources, Table 1 shows the results of all studies, including presence of adverse reactions such as hypertension (HI), hypotension (HP), chest pain (CP), headache (HA), facial tickling (FT), extra-systole (ES), and the agreement with coronary angiography. Studies where the patient reached the sub maximal heart rate predicted for her/his age were considered conclusive, otherwise, were classified as inconclusive for ischemia evaluation. Out of 24 studies, 3 were cancelled for the reasons shown in Table 1. From the remaining 21 studies, 12 were conclusive and 9 were not. Figure 1 (on previous page) shows the simultaneous display of the tagged MRI at end systole of all dose levels of the stress test of a patient study. Direct visualization of regional myocardial deformation through MR tag curvature and inter-tag distance shortening in a screen displaying images of all stress levels simultaneously was essential for determining any new regional wall motion abnormality that could appear during dobutamine and/or atropine infusion. Myocardial viability was detected in 3/12 conclusive, and 2/9 inconclusive studies. Conclusive dobutamine-MRI were in agreement in all 6 patients who underwent coronary angiography (Table 1. N = Normal. Ab = Abnormal. MI = Myocardial Infarction. LBBB = Left Bundle Branch Block).

Discussion and Conclusions: The use of real time slice prescription, EPI-based fast cine imaging techniques with tagged MRI, slice reacquisition and multi-stress level image display can provide direct means for visual inspection of segmental myocardial motion and deformation during pharmacologically induced-stress. Tagging MRI contributes with valuable data for accurate regional localization of a new wall motion abnormality and, consequently, for interrupting the test and improving examination safety. Fast imaging and real time monitoring while dobutamine is infused can also increase the safety of MRI stress testing. Single slice image reacquisition is crucial to diagnosis enhancement by assuring data quality and appropriate timing for exam realization. Our initial results are promising in detecting significant coronary

artery stenosis. Future works include the quantitative analysis of tagged MRI in all levels of stress using in-house developed software.

9. Real-Time Black-Blood Imaging and Active Tracking for Catheter-Based MRI

Krishna Nayak,[1] Pedro Rivas,[2] *Michael McConnell*,[3] Juan Santos,[1] Greig Scott,[4] Dwight Nishimura,[5] John Pauly,[6] Bob Hu.[7] [1]*Stanford University, Department of Electrical Engineering, Stanford, CA USA;* [2]*Stanford University, Division of Cardiovascular Medicine, Stanford, CA USA;* [3]*Stanford University, Cardiovascular Medicine, Stanford, CA United States;* [4]*Stanford University, Department of Electrical Engineering, Stanford, CA USA;* [5]*Stanford University, Department of Electrical Engineering, Stanford, California United States;* [6]*Stanford University, 206 Packard Electrical Engineering, Stanford, California United States;* [7]*Stanford University, Mail Code: 5233, Stanford, California United States*

Introduction: MRI is an emerging technology for catheter-based imaging and interventions. Advantages include detailed cross-sectional imaging, high tissue contrast, and no ionizing radiation. Real-time MRI offers the ideal platform to overcome catheter and physiologic motion and to provide image feedback to guide interventions. We have previously demonstrated the feasibility of small-FOV real-time imaging from catheter coils (1). Here we present an enhanced real-time system that allows blood-signal suppression for improved vessel wall imaging and active catheter tracking.

Methods: Imaging was performed on a 1.5 T Signa MRI scanner (General Electric Medical Systems, Milwaukee, WI) with a cardiac gradient set (40 mT/m, 150 mT/m/msec). This system is augmented with a Sun workstation for real-time data acquisition, image reconstruction, and interactive control and display. A catheter RF coil (opposed-solenoid or twin-lead) was used for signal reception. Phantom studies were performed using a continuous flow system through an 8-mm plastic tube surrounded by a 6-mm-thick layer of water-based silicone gel. Animal studies were performed on anesthetized 3–4 kg New Zealand White rabbits under a protocol approved by the Stanford University Administrative Panel on Laboratory Animal Care. The catheter coil was placed in the esophagus for transesophageal imaging or inserted through a 6F right iliac artery sheath into the aorta for intravascular imaging. The real-time imaging sequence uses a spectral-spatial excitation followed by interleaved spiral acquisitions. Typical imaging parameters were: FOV 1–2 cm, in-plane resolution 120–440 microns, slice thickness 5 mm, TR 40 ms. Temporal resolution could be adjusted from 240–800 ms per full image, using 6–20 interleaves per image. A sliding reconstruction algorithm provided images at up to 16 frames/sec. Real-time black-blood imaging was enabled by integrating two out-of-slice saturation pulses, one on each side of the imaging plane (4-cm thick, with a 1.5-cm deadband between saturation slab and imaging slice). Real-time tracking was performed by integrating a pulse sequence to identify the x, y, z location of the maximal catheter signal. The real-time interactive system uses this location to adjust the scan plane in all three directions, centering the image on the catheter coil.

Results: The real-time black-blood sequence was tested in a vessel phantom (Figure 1A, 1B). With flow on, the bright flow signal and resultant artifacts obscured the phantom wall. With the black-blood saturation pulses turned on, the lumen signal was almost completely suppressed, showing the wall. Intravascular imaging in the rabbit aorta revealed similar results (Figure 1C, 1D). Without the saturation pulses turned on, the large blood signal and artifacts dominated the image. With the black-blood saturation pulses on, the vessel wall could be seen. Initial results with the real-time tracking in a phantom and the rabbit esophagus demonstrated that the imaging plane automatically centered on the catheter coil and was adjusted in real-time when the catheter was moved.

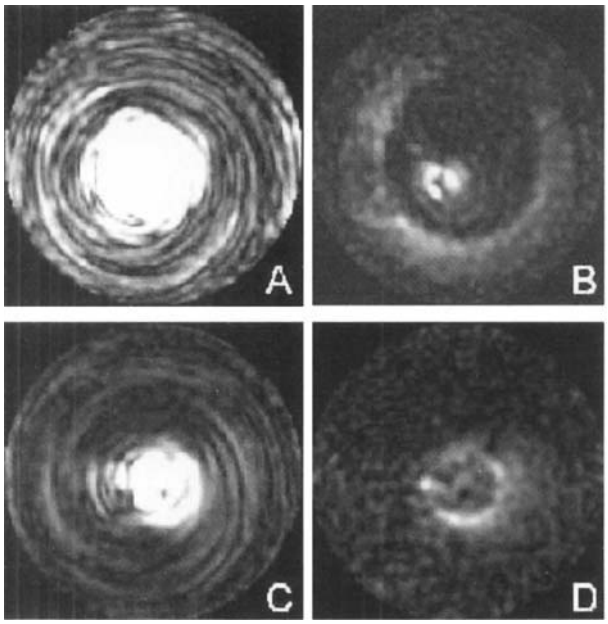

Figure 1. Real-time intravascular MRI of flow phantom (A,B) and rabbit aorta in vivo (C,D). Flow artifacts obscuring the wall (A,C) are suppressed with black-blood saturation pulses (B,D).

Conclusions: Real-time black blood imaging and active tracking provide significant enhancements to catheter-based MRI, establishing a promising platform for intravascular diagnosis and interventions.

10. Direct Clot Detection with MRI Using a Novel Fibrin-Targeted Gadolinium Agent

Philip Graham,[1] Randall Lauffer,[1] Katariina Lahti,[2] Shrikumar Nair,[1] Peter Caravan,[1] Andrew Kolodziej,[1] Robert Weisskoff.[1] [1]*EPIX Medical, Inc., 71 Rogers Street, Cambridge, MA USA;* [2]*EPIX Medical, Inc., 71 Rogers Street, Cambrige, MA USA*

Purpose: To evaluate a prototype small-molecule clot-enhancing MRI agent, in fibrin-binding/relaxivity assays and in vivo animal imaging studies. The agent is composed of a fibrin-binding peptide derivative, obtained from phage display screening, coupled to a signal-enhancing group with several gadolinium chelates.

Method and Materials: In vitro studies included whole blood clot uptake as well as clot relaxation time (1/T1) analysis at 0.5 T. In the animal studies, the jugular vein of a rabbit was clamped, blood removed by catheter, and human fibrin clots (with added rabbit red blood cells to approximate the composition of whole blood clots) injected and aged 1 hour prior to clamp release and MR (1.5T, gradient echo, TR = 36, TE = 5, flip = 30 deg.) images acquired.

Results: The agent, EP-862, binds strongly to fibrin clots and whole blood clots, with concommittant increases in the 1/T1 relaxation rate. No significant binding was detected to albumin or fibrinogen. The strong binding and high relaxivity of EP-862 led to strong, persistent enhancement of jugular vein clots on T1-weighted images, with approximately 300% enhancement. Magnevist showed no enhancement when infused as a solution with equivalent relaxivity. Infusion of a diamag-

netic analog of EP-862 greatly diminished the clot signal intensity, presumably due to specific displacement at the fibrin binding site.

Conclusions: This prototype agent has the specificity and signal-enhancing ability to enhance clots in vivo using MRI. This "bright spot" approach may allow the detection of small clots in a wide range of conditions including pulmonary embolism, deep vein thrombosis, arterial thrombosis, ventricular and atrial clots, and potentially, unstable atherosclerotic plaque.

11. Comparison of Gadolinium-Based Extracellular and Bloodpool Contrast Agents Versus Manganese-Based Contrast Agents in the Differentiation of Viable and Non-viable Tissues Using a Rat Myocardial Infarction Model

Sebastian Flacke,[1] John Stacy Allen,[2] Jonathan Chia,[1] James H. Wible,[3] MP Periasamy,[4] I. Kofi Adzamli,[5] Christine Lorenz.[6]
[1]*Washington University, Cardiovascular Division, St. Louis, MO USA;* [2]*Washington University, Cardiovascular Division, St. Louis, Missouri USA;* [3]*Mallinckrodt Inc., 675 McDonnell Blvd, St. Louis, MO USA;* [4]*Mallinckrodt, Inc., Radiology and Cardiology R, St. Louis, MO USA;* [5]*Mallinckrodt Inc., Radiology and Cardiology R, St. Louis, MO USA;* [6]*Washington University, 660 S. Euclid Avenue, St. Louis, MO USA*

Introduction: There is growing interest in the use of extracellular MR contrast agents for differentiating viable and non-viable myocardium after infarction using the delayed MRI enhancement method [1,2]. This method takes advantage of the fact that Gd-DTPA, an extracellular agent, accumulates in irreversibly damaged tissue while it washes out of normal myocardium, providing a time window for T1-weighted imaging of infarction. Other classes of MR agents may also be useful for this application. For example, manganese-based agents are of interest since manganese is potent for T1 shortening and is only taken up in cells capable of active calcium transport [3,4], providing an analog to thallium imaging. Another approach is to use gadolinium-based agents that bind to albumin in the bloodpool hence have longer blood residence times and release an unbound component that accumulates in infarcted myocardium similar to extracellular agents. Therefore, the purpose of this study was to compare the advantages and disadvantages of these three classes of agents (extracellular, manganese, and albumin-binding) in a rat model of myocardial infarction.

Methods: One extracellular gadolinium-based agent (OptiMARK Mallinckrodt Inc., 0.1 millimole/kg) and one albumin-binding gadolinium-based agent (MP-2269, Mallinckrodt Inc., 0.03 millimole/kg), with >80% binding and long residence time in the bloodpool [5], were used. MnCl2 and MP-680 (Mallinckrodt Inc.), a weakly-chelated analog of Mn-DPDP (Teslascan, Nycomed Amersham) represented the Mn-based agents. Further, because manganese competes with calcium uptake, concerns about the potential for negative inotropic effects also led to the evaluation of a formulation of MnCl2 dissolved in calcium gluconate for injection [6]. 35 rats underwent ligation of the LAD or LCX [7]. 5 animals died. One week following surgery, rats were imaged on a 1.5T Philips Gyroscan NT (PT6000) using a custom surface coil as described previously [8]. Each animal was randomized to one of 5 contrast agents (n = 6 in each group). The following three manganese-based agents were used: MnCl2 (15 micromoles/kg administered over 60 seconds); MP-680, 45 micromole/kg administered over 60 seconds; and MnCl2/Ca, with Mn/Ca ratio of 1/8 (15 micromole/kg, administered over 60 seconds.) [5] Short axis cine imaging was performed from base to apex to localize the infarct region. Imaging was performed at baseline and post contrast (t = 1, 5, 10, 15, 30, 45 & 60 min) with a segmented inversion recovery gradient echo sequence (inv. time 430 ms, pixel size 0.7 mm by 0.7 mm, TR/TE/flip angle 5.2ms/2.5ms/15). Images were ECG triggered and each was acquired over 100 heartbeats (5 TFE shots, NEX 20). Heart rate was 300-350 beats per minute. After sacrifice, triphenyl tetrazolium chloride (TTC) staining was performed for measurement of infarct size. Images were analyzed by measuring signal intensity in the bloodpool, normal myocardium and in the infarct region. To account for variations in absolute signal intensity between animals, each animal's signal intensity data was normalized to the maximum signal intensity for each tissue. Relative contrast between blood and myocardium, and between normal and infarcted myocardium was calculated, as was the contrast to noise ratio.

Results: The time course for the contrast to noise ratio (CNR) between normal and infarcted myocardium for the three manganese based agents is shown in Fig 1. For all three agents, the contrast clears from the bloodpool rapidly, and uptake of the contrast agents in the normal myocardium was apparent by 5 minutes for MnCl2, and by 15 minutes for MnCl2/Ca and MP680. All agents showed persistent signal increase in the normal myocardium throughout the imaging period of 60 minutes. For the Gd-based agents, the time course for CNR between infarct and normal myocardium is shown in Fig 2. OptiMARK, the extracellular agent, washes out of the blood rapidly, while MP-2669 persists in the bloodpool for the duration of the imaging (60 min). Accumulation of either contrast agent in the infarct area was apparent as early as 1 min after administration of the agent, but diminished significantly after approximately 15 min for OptiMARK. However, the high contrast between normal and infarcted myocardium persisted throughout the imaging period with MP-2269. Sample images for each agent are shown in Fig 3. The gadolinium agents on the left show the infarct region as

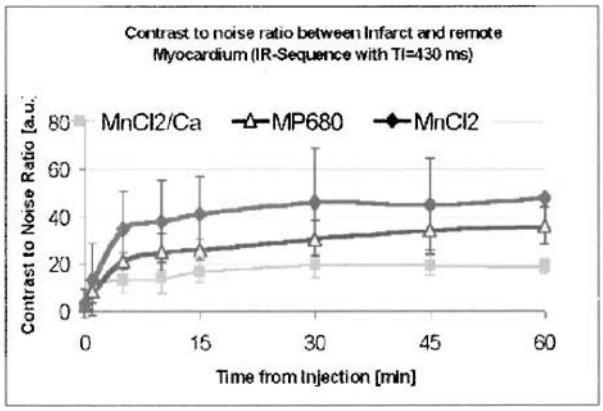

Figure 1.

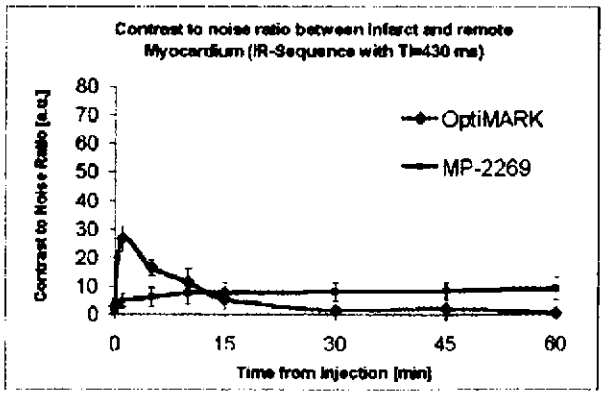

Figure 2.

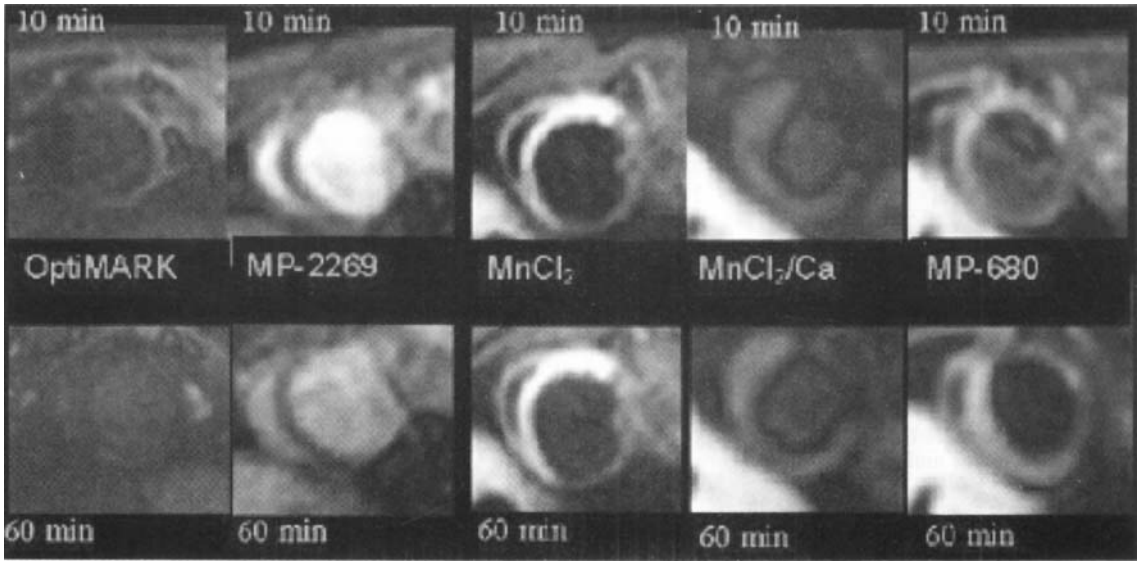

Figure 3.

bright, while the manganese based agents on the right show the infarct as dark. The infarct size and location matched that identified by TTC staining with all agents.

Discussion: The contrast behavior of the extracellular agent OptiMARK was similar to that reported for other extracellular MR agents, with an imaging window of approximately 15–20 minutes. MP-2269 showed persistent contrast between normal and infarcted myocardium for the entire imaging period (60 minutes). However, the bloodpool also remained enhanced over this time period, so visualization of thin subendocardial infarcts may be problematic with MP-2269 and analogous albumin binding blood pool agents. The manganese-based agents cleared rapidly from the bloodpool, facilitating visualization of the myocardium throughout the imaging period. Discrimination between the normal and infarcted myocardium was possible approximately 15 minutes after injection and persisted throughout the 60 minute imaging period. In summary, amongst the three classes of agents tested, the albumin-binding Gd-based agent and the manganese agents may be potentially useful for viability imaging due to the long imaging window possible. The manganese based agents may offer additional benefit over the albumin binding agent since they also provide good bloodpool-myocardial contrast and higher contrast to noise than the Gd-based agents. However, the safety profile of these agents has to be evaluated further before clinical trials could be undertaken.

12. Stress and Strain Relationship: Novel MRI Assessment of Ventricular Function in Severe Aortic Insufficiency

Giridhar Vedala,[1] Pavlos Moustakidis,[2] Brian Cupps,[2] Randall Scheri,[2] Nancy Nickerson,[2] Nicholas Kouchoukos,[3] Robert Gropler,[4] Michael Pasque,[5] Victor Davila.[6] [1]*Washington University, Cardiovascular Division, Box 8086, St. Louis, MO U.S.A.;* [2]*Washington University, St. Louis, MO U.S.A.;* [3]*Missouri Baptist Medical Center, St. Louis, MO U.S.A.;* [4]*Washington University, 510 S Kingshighway Boulevard, Saint Louis, Missouri United States;* [5]*Washington University, Washington University, St Louis, Missouri United States;* [6]*Washington University, Medical School, Campus Box 8086, Saint Louis, Missouri United States*

The timing of aortic valve surgery in patients with significant aortic insufficiency (AI) can be difficult. Many indices of myocardial contractile performance are load-dependent and/or require assumptions in left ventricular (LV) geometry. We propose to measure load-independent indices of LV contractility which do not require geometric assumptions. LV end-systolic stress (LVESS) and LV strain relationships were measured using magnetic resonance imaging (MRI).

Methods: 7 patients with significant AI (6 male, 48 ± 17 yrs.) and normal LV function, scheduled to undergo aortic valve surgery, and 15 normal volunteers (N) (7 male, 45 ± 22 yrs.) underwent MRI at rest and during inotropic stimulation (dobutamine, 10μg/kg/min). AI patients had no significant coronary atherosclerosis by cardiac catheterization. All healthy volunteers had normal rest/stress echocardiograms. Midventricular, short-axis MR images were used for all analyses. 2-dimensional (2D) LVESS was measured using finite element analysis. Pressures were obtained from calibrated noninvasive Millar carotid artery tracings. 2D LV strains were obtained by measuring deformation of splines superimposed on MRI tag lines.

Results: Fractional area change and LVESS were similar between the AI group and the N group (43 ± 6% vs. 48 ± 7%, 15.0 × 10^4 ±

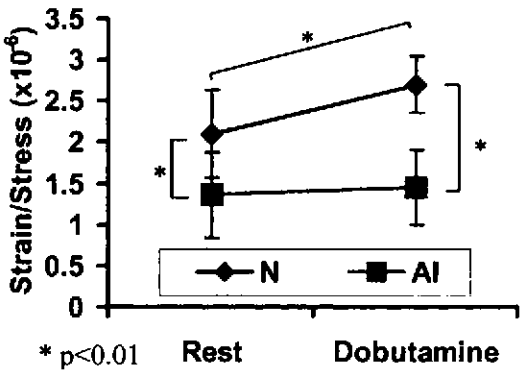

Figure.

3.0×10^4 vs. $12.6 \times 10^4 \pm 2.6 \times 10^4$ dynes/cm,^{2} respectively, p = NS for both). LV strain at rest was significantly lower in the AI group ($2.0 \times 10^{-1} \pm 4.0 \times 10^{-2}$ vs. $2.5 \times 10^{-1} \pm 3.2 \times 10^{-2}$, $p < 0.01$). At rest, the strain / stress ratio was significantly reduced in the AI group compared with the N group ($1.36 \times 10^{-6} \pm 3.4 \times 10^{-7}$ vs. $2.1 \times 10^{-6} \pm 5.3 \times 10^{-7}$ cm^2/dyne, $p < 0.01$, see figure). This ratio did not increase with inotropic stimulation in the AI group ($1.45 \times 10^{-6} \pm 4.6 \times 10^{-7}$, p = NS vs. rest), compared to the N group ($2.7 \times 10^{-6} \pm 5.2 \times 10^{-7}$, $p < 0.01$ vs. rest, see figure).

Conclusions: Patients with significant AI have diminished contractile reserve, assessed by MRI-derived strain/stress relationship. This is a noninvasive, load-independent index that does not require geometric assumptions. This method may uncover subclinical myocardial dysfunction, and may be useful in determining the optimal time for surgery.

13. Na^+-Overload During Ischemia and Reperfusion in Rat Hearts: Comparison of the Na^+/H^+-Exchange Blockers EIPA, HOE642 and EMD96785

Michiel ten Hove,[1] Jan G. Van Emous,[2] Cees Van Echteld.[3]
[1]*Interuniversity Cardiology Institute of the Netherlands, P.O. Box 85500, Utrecht, Utrecht Netherlands;* [2]*Interuniversity Cardiology Institute of the Netherlands, HPn G02-523, Utrecht, Utrecht the Netherlands;* [3]*University Medical Center, Cardiology, Room G02.523, Utrecht, Utrecht Netherlands*

Introduction: Intracellular myocardial Na^+ overload during ischemia is an important cause of reperfusion damage via reversed Na^+/Ca^{2+}-exchange.

The relative importance of the different influx routes of Na^+ is still a matter of debate. Previously it has been shown that the Na^+-channel plays an important role and its blockade can result in a 60% reduction in Na^+-overload[1]. Another important influx route is via the sarcolemmal Na^+/H^+-exchanger (NHE). In this study we tested the effect of ischemic inhibition of the NHE on intracellular Na^+ ($[Na^+]_i$), intracellular pH (pH_i), high energetic phosphates (HEP's) and post-ischemic contractile recovery in isolated rat hearts, using three different NHE-blockers: EIPA, HOE642 and EMD96785.

Materials and Methods: Isolated rat hearts were perfused according to Langendorff at a constant pressure of 73.5 mmHg at 37°C with a modified Krebs-Henseleit buffer (pH 7.4) with glucose as substrate and were paced at 5 Hz. Contractile performance was measured with an intraventricular balloon. $[Na^+]_i$, pH_i and HEP's were measured simulta-

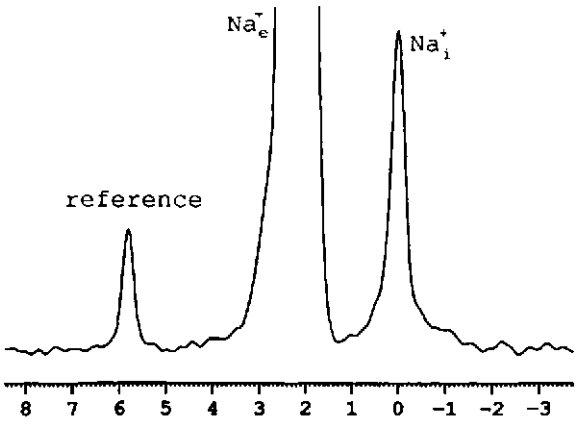

Figure 1. 1 min ^{23}Na spectrum.

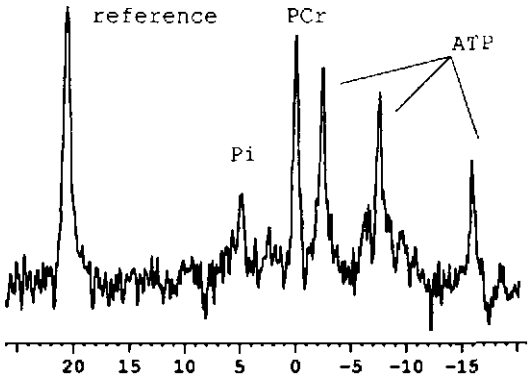

Figure 2. 1 min ^{31}P spectrum.

Table 1

$[Na^+]_i$ as % of Baseline (:p < 0.001)*

	30′ Ischemia	30′ Reperfusion
Untreated	305 ± 23%	162 ± 14%
EIPA	212 ± 6%*	127 ± 7%
HOE642 1	7 ± 5%*	123 ± 15%
EMD96785	146 ± 6%*	132 ± 5%

Table 2

pH_i After 5′ Reperfusion

	5′ R
Untreated	6.90 ± 0.05
EIPA	6.78 ± 0.07
HOE642	6.79 ± 0.04
EMD96785	6.68 ± 0.04

Table 3

RPP (:p < 0.05)*

	Start Protocol	30′ Reperfusion
Untreated	16.4 ± 1.2	11.5 ± 2.7
EIPA	15.8 ± 1.9	12.1 ± 2.1
HOE642	16.9 ± 1.3	19.6 ± 2.0*
EMD96785	15.6 ± 1.4	20.4 ± 2.3*

neously using ^{23}Na and ^{31}P NMR spectroscopy, respectively, on a Bruker Avance DRX400 spectrometer equipped with a dual tuned probe and two digital receivers. ^{31}P and ^{23}Na spectra were both collected with a time resolution of 1 minute. To quantify PCr and ATP five ^{31}P spectra were added. To discriminate between intra- and extracellular Na^+, the shift reagent $TmDOTP^{5-}$ (3.5 mM) was added to the perfusate, necessitating a lower free Ca^{2+} concentration (0.85 mM). NHE-blockers were administered in a concentration of 3 μM during 5 minutes immediately prior to 30 minutes of global ischemia and 30 minutes of drug-free reperfusion. Data are presented as mean ± SEM.

Results: Na^+ overload after 30 min of ischemia was reduced with 30, 58 and 60% using EIPA, HOE642 and EMD96785, respectively (table 1). Administration of NHE-blockers did not result in any significant difference in pH_i during ischemia. During reperfusion recovery of pH_i was delayed (table 2). During ischemia PCr content decreased to <5% within 15 min in all groups. After 30 min of reperfusion PCr had recovered to 81 ± 6, 95 ± 8, 94 ± 10 and 105 ± 7% in untreated (n = 7) and EIPA (n = 6), HOE642 (n = 6) and EMD96785 (n = 6) treated hearts, respectively (NS). ATP content had decreased to <10% after 30 min of ischemia in all groups. After 30 min of reperfusion ATP had recovered to 29 ± 1, 44 ± 8, 35 ± 3 and 42 ± 4% in untreated and EIPA, HOE642 and EMD96785 treated hearts, respectively (NS). Administration of HOE642 and of EMD96785 resulted in a better recovery of the rate pressure product (RPP; heart rate * LVDP) after 30 min of reperfusion (table 3). At the end of reperfusion EDP was 38.0 ± 3.8, 38.3 ± 2.2, 31.9 ± 4.6 and 23.5 ± 4.3 $*10^3$ mmHg in untreated and EIPA, HOE642 and EMD96785 treated hearts, respectively.

Discussion: Our results show that the NHE mediates an important Na^+ influx during ischemia, reflected in a reduced Na^+ overload when the NHE is inhibited. EIPA was less effective than the two more specific NHE-blockers, HOE642 and EMD96785, in the concentrations used. Although drugs were not administered during reperfusion, treated hearts showed a slower recovery of pH_i, indicating that the NHE is still (partly) inhibited at that time, probably due to the fact that a complete washout of the drug takes a few minutes. The NHE-inhibition upon reperfusion will reduce reversed Na^+/Ca^{2+}-exchange via decreased NHE-mediated Na^+ influx and, reportedly, via direct inhibition of the Na^+/Ca^{2+}-exchanger protein by the prolonged acidosis. The more pronounced delay in recovery of pH_i in the EMD96785 treated hearts correlates to the better recovery of the EDP in that group, indicating that a higher concentration of the two other blockers is required to achieve a similar recovery of the EDP.

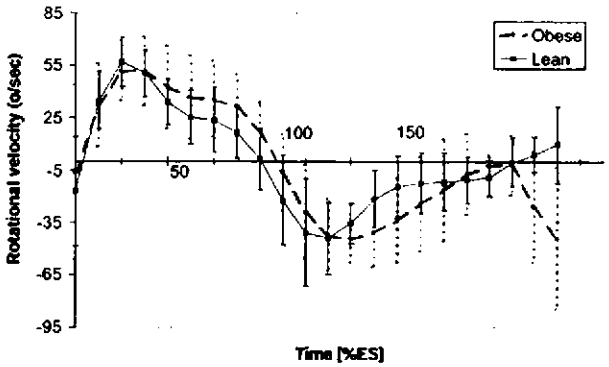

Figure 1. Apical LV rotational velocity over the RR cycle, expressed as % of end-systole [%ES] in the obese and lean. Error bars are equal to SD.

14. Altered Apical Left Ventricular Rotation in Obesity—A Cardiac Magnetic Resonance Tagging Study

Peter Danias,[1] Nicholas A. Tritos,[2] Matthias Stuber,[3] Carol Salton,[3] Kraig V. Kissinger,[1] Warren J. Manning.[4] [1]*Beth Israel Deaconess Medical Center, 330 Brookline Avenue, Boston, Massachusetts United States;* [2]*Joslin Diabetes Center, One Joslin Place, Boston, Massachusetts United States;* [3]*Beth Israel Deaconess Medical Center, 330 Brookline Ave, Boston, Massachusetts United States;* [4]*Beth Israel Deaconess Medical Center, 330 Brookline Avenue, Boston, Massachusetts United States*

Background: Obesity affects 1/3 of the adult US population and carries increased morbidity and mortality. Several echocardiographic studies have demonstrated an increase in left ventricular (LV) mass and abnormal diastolic function in the obese. Although cardiac MRI has confirmed the LV mass increase in obese individuals (1), MR evaluation of LV rotation has not been previously reported. Thus we used Complementary SPAtial Modulation of Magnetization (CSPAMM) to assess the apical LV rotation, a correlate of diastolic function, in otherwise healthy adult male obese subjects and lean controls.

Methods: We evaluated 47 men (20–40 yr) including 23 obese (body mass index BMI>30 kg/m^2) (30 ± 8 yr; BMI 35 ± 3 kg/m^2) and 24 lean (BMI 19–25 kg/m^2) (29 ± 5 yr; BMI 23 ± 2 kg/m^2). Imaging was performed using a 1.5T whole body scanner (Gyroscan NT/ACS, Philips Medical Systems, Best, The Netherlands) with advanced cardiac software (CPR6) and enhanced gradient hardware (PT 6000, 21 mT/m, slew rate 105 mT/m/msec). Single breath-hold (duration 15–20 sec) ECG-gated slice following CSPAMM images (2) were acquired at the apical LV (approximately 1 cm from the apex). Depending on the subjects' heart rate, 15–24 cardiac phases per RR interval, extending throughout ventricular diastole were acquired. The following parameters were used: FOV 300 mm; matrix 128 (in-plane resolution 2.3 × 2.3 mm^2); tagged slice thickness 8 mm, with imaged volume thickness 20 mm; 9 EPI readouts for each RF excitation; TE of 5.4 msec. Temporal resolution was 35 msec. A standard breath-hold

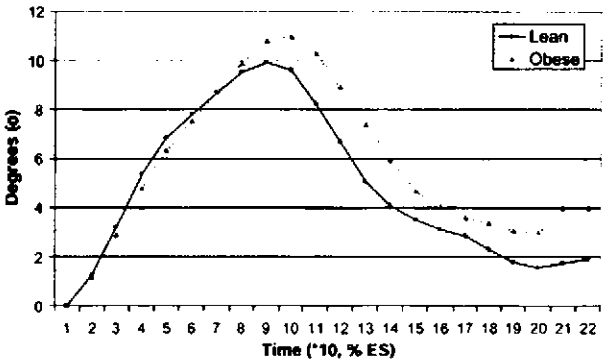

Figure 2. LV apical torsion in the obese and lean subjects over the RR cycle, expressed as % of end-systole [%ES].

FFE-EPI sequence was used to obtain short-axis cine images to cover the whole LV. Manual segmentation of endocardial and epicardial borders was performed offline on an analysis workstation (Easyvision, Philips Medical System, NL) for determination of LV mass. Tagged image analysis was done offline on a Linux workstation using a custom-LV tagging analysis package (2) written on PV-Wave 6.0® platform (Visual Numerics, Houston, TX). The apical LV rotational velocity (°/sec) and rotation (°) were measured in a blinded fashion and expressed as percent of end-systole (%ES). LV mass and LV wall thickness-to-cavity radius ratio were also measured.

Results: The twisting and untwisting pattern of the apical LV (Figure 1) was significantly different between obese and lean individuals ($p = 0.01$, repeated measures ANOVA). The peak untwisting diastolic velocity of the obese (62 ± 26°/sec) was similar to that of the lean (57 ± 20°/sec, $p = 0.5$). The LV rotation (Figure 2) was similar in the obese and lean throughout the whole cardiac cycle ($p = 0.1$). However, in early diastole (110–140% ES) there was significantly higher apical torsion in the obese ($p = 0.03$). The peak LV systolic rotation in the obese (11.3 ± 3.6°) was slightly higher than in the lean (10.2 ± 2.5°, $p = 0.2$) and tended to occur later in relation to end-systole (ES), (88 ± 9% ES vs. 81 ± 13% ES, obese vs. lean, respectively, $p = 0.07$). The absolute LV mass and the height-adjusted LV mass in the obese (202 ± 37 g and 113 ± 18g/m, respectively) were significantly higher ($p < 0.001$) than in the lean (164 ± 22 g and 93 ± 12 g/m, respectively). However, the LV wall thickness-to-cavity radius ratio was similar in the obese (0.59 ± 0.08) and lean individuals (0.61 ± 0.1, $p = 0.4$).

Conclusion: Obesity is associated with an altered apical LV rotation pattern, characterized by delayed twisting with increased twisting and untwisting velocities, and sustained torsion throughout early diastole. CSPAMM tagging MRI is a unique tool to assess subclinical changes of LV rotation and may be helpful in evaluation of obese individuals.

15. MR Myocardial Perfusion Reserve Index Early After PTCA for the Prediction of Restenosis

Nidal Al-Saadi,[1] Holger Langrek,[2] Eike Nagel,[3] Eckart Fleck.[4]
[1]German Heart Institute, Berlin Germany, Augustenburger Pl. 1, Berlin, Berlin Germany; [2]German Heart Institute, Augustenburger Pl 1, Berlin, Berlin Germany; [3]German Heart Institue, Augustenburger Pl 1, Berlin, Berlin Germany; [4]German Heart Institute, Augustenburger Pl 1, Berlin, Berlin Germany

Reduced myocardial perfusion reserve early after PTCA has been reported in a variable fraction of patients and has been mainly attributed to incomplete dilatation of the coronary artery. Impaired myocardial perfusion after coronary intervention could be detected by MR perfusion analysis. We have investigated the predictive value of an impaired magnetic resonance (MR) myocardial perfusion reserve index for restenosis.

Patients and Methods: Twenty seven patients with single and multi vessel coronary artery disease were examined 24 hours after PTCA with a 1.5 T MR tomograph (Philips ACS NT) using fast gradient systems (23 mT/m amplitude, 105 T/m/sec slew rate) and a dedicated 5-element cardiac coil. A short axis image at the base of the papillary muscle was acquired every heart beat using an ECG-triggered T1-weighted inversion recovery single shot turbo-gradient echo sequence (inversion pulse, pre-pulse delay 360 ms, acquisition duration 360 ms, flip angle 15°, echo time 1.7 ms, repetition time 9 ms). Slice thickness was 8 mm with a spatial resolution of 1.7 × 1.9 mm. During an expiratory breath hold, a bolus of Gd 0.025 mmol/kg body weight was injected. The signal intensity time curves of the first pass of a gadolinium-DTPA bolus injected via a central vein catheter (0.025 mmol/kg) were evaluated before and after dipyridamole infusion using the MASS perfusion software (Medis, Leiden, The Netherlands) the endo- and epicardial contours were traced in all images. The myocardium was divided into 6 equiangular segments. Signal intensity was determined for all dynamics and segments. The upslope of the resulting signal intensity time curve was determined by the use of a linear fit. The results were corrected for the input function by dividing the upslope of each myocardial segment by the upslope of the left ventricular signal intensity curve (relative upslope) and perfusion reserve index was calculated. Follow up coronary angiography was performed 6 months after PTCA. A restenosis was defined as an area reduction of ≥75% assessed by quantitative angiography.

Results: Nine patients developed restenosis (30%). Myocardial perfusion reserve index 24 hrs after PTCA was 1.7 ± 0.43 in segments which developed restenosis and 2.05 ± 0.31 in segments without restenosis ($p = 0.05$). A cut off value of 1.8 myocardial perfusion reserve index showed the best positive and negative predictive values (table).

Cut off Values

	1.7	1.8	1.9	2.0
Positive prediction	66%	66%	61%	53%
Negative prediction	75%	88%	89%	92%

Conclusion: Measurements of myocardial perfusion index with cardiac MR is very sensitive. After coronary intervention MR perfusion measurements may allow for the prediction of restenosis and can be used for the follow up of patients after coronary intervention.

16. Real Time TrueFISP Imaging for the Assessment of Regional Wall Motion Abnormalities

James Moon,[1] Gillian Smith,[2] Jane Francis,[3] Nicholas Bunce,[4] Christine Lorenz,[5] Dudley Pennell.[6] *[1]Royal Brompton Hospital, CMR Unit, London, England UK; [2]Royal Brompton Hospital, CMR unit, London, England UK; [3]Royal Brompton Hospital, CMR unit, London, England UK; [4]Royal Brompton Hospital, CMR unit, London, England UK; [5]Royal Brompton Hospital and Siemens Engineering, CMR unit and Siemens engineering, London, England UK; [6]Royal Brompton Hospital, CMR Unit, London, England UK*

Background: Left ventricular regional wall motion abnormality assessment by CMR is established with conventional gradient echo cine imaging. Recently, faster imaging techniques have been introduced and early studies suggest real-time imaging can be used for global left ventricular volume and mass assessment [1,2]. These are quicker and are less dependent on the breath-holding capacity of the patient and do not require ECG triggering, advantageous in breathless patients or in those with arrhythmias. However, the current spatial and temporal resolution is below that of conventional imaging. Therefore, we sought to determine whether real time imaging using real-time TrueFISP (rt-TrueFISP) could accurately assess regional wall motion abnormalities in patients with heart failure by comparison with conventional breath hold TrueFISP (bh-TrueFISP) imaging.

Methods: 15 patients (12 males, 3 females aged 19–84, mean 62) with either ischaemic cardiomyopathy (13), dilated cardiomyopathy (1) or left ventricular dysfunction as a result of valvular disease (1), were assessed. Ejection fraction was 43% (25–69%), RR interval 900 ms (600–1100 ms). 4 patients were in atrial fibrillation. Imaging was performed on a 1.5T Sonata scanner (Siemens Medical, Erlangen, Germany).

Imaging consisted of scout views to determine the cardiac axes. Short axis slice positioning was identical for both acquisitions. For the bh-TrueFISP, up to 13 × 7 mm slices with a 3 mm gap, 1 slice per breath hold were acquired. Imaging parameters were, TE/TR 1.6/3.2 ms, in plane pixel size 2.27 × 1.37 mm, temporal resolution 48 ms, flip

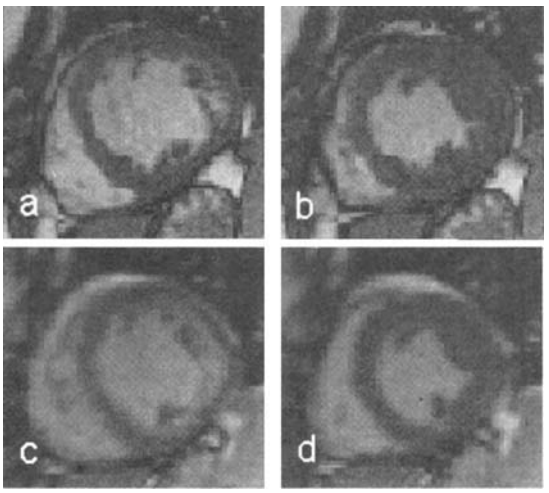

Figure 1. Representative sample images: bh-TrueFISP diastole (a), systole (b). rt-TrueFISP diastole (c), systole (d).

angle 60° acquired in approximately 12 seconds. For the rt-TrueFISP imaging, slices were acquired in two interleaved breath-holds covering the entire ventricle, each breath-hold acquiring seven, 7 mm slices, with a 13 mm gap; the second breath-hold offset by 10 mm. Imaging parameters were TE/TR 1.1/2.2 ms, 77 ms temporal resolution, flip angle 47–55°, in plane pixel size approximately 2.8 × 3.8 mm [3] and a breath-hold of approximately 15 seconds.

Images were viewed using in-house developed software (CMRtools). A 12 segment model was used including basal, mid ventricular and apical short axis slices, each with 4 segments. Segmental assessment was by the consensus of two observers, and wall motion was categorised on a 4 point scale (normal = 2, hypokinetic = 1, akinetic = 0, dyskinetic = −1). A total wall motion score for each patient was computed as the sum the 12 segments. The mean difference between total wall motion score was computed between the techniques. Sensitivity and specificity for detection of wall motion abnormalities was computed with bh-TrueFISP as the reference method.

Results: Representative images are shown in Figure 1. Of 180 segments assessed, 77 (43%) were abnormal (hypokinetic, akinetic or dyskinetic). No normal segments were classified as abnormal by rt-TrueFISP, and 4 hypokinetic segments were classified as normal by rt-TrueFISP. Therefore, rt-TrueFISP had a specificity of 100% (95% ci 96.7%–100%) and a sensitivity of 94.7 (95% ci 90.2%–100%) for the detection of abnormal segments. 10 additional segments were scored as abnormal but mis-classified by rt-TrueFISP. Of these 10 segments, the severity of the wall motion abnormality was under-reported by one grade in 9 segments and over-reported by one grade in 1 segment by rt-TrueFISP. The mean difference in total wall motion score between rt-TrueFISP and bh-TrueFISP was −0.87 ± 1.25 or −0.07 ± 0.1 per segment.

Conclusion: Real-time imaging with TrueFISP is sensitive and specific for detection of regional wall motion abnormalities in patients with resting left ventricular dysfunction. However, due to reduced temporal and spatial resolution, there is a trend to underestimate severity of wall motion abnormalities with real-time TrueFISP. Due to the limited temporal resolution, however, this technique cannot yet be recommended for application with elevated heart rates such as during dobutamine stress testing. This technique is a viable alternative to conventional cine imaging in patients who cannot tolerate multiple breath-holds, who have significant arrhythmias, or who are uncooperative.

17. Non-Uniform Flow Dynamics of the Normal Aorta in Children: A Velocity Mapping Study

Mark Fogel,[1] Paul Weinberg,[2] Anne Hubbard,[1] James Meyer,[3] John Haselgrove.[3] [1]*The Children's Hospital of Philadelphia, CHOP–Division of Cardiology, Philadelphia, Pennsylvania United States;* [2]*The Children's Hospital of Philadelphia, 34th & Civic Center Blvd, Philadelphia, Pennsylvania United States;* [3]*The Children's Hospital of Philadelphia, 34th St and Civic Center Blvd, Philadelphia, PA USA*

Objectives & Methods: Understanding flow dynamics in normal aortas (Ao) in children is important to designing improved Ao reconstructions by crafting the surgery to mimic normal Ao flow. We performed magnetic resonance velocity mapping on 13 subjects with normal Aos (ages 7.2 ± 6.2 years) to determine flow dynamics in 4 equal quadrants (Q) in the ascending (AAo) and descending aorta (DAo) aligned along the Ao long axis. Significance = $P < .05$.

Results: In the AAo, the left posterior Q displayed significantly less blood flow (16 ± 5%) than the other Qs (26–29%) over the cardiac cycle (see graph) while in the DAo, both anterior Qs carried significantly less blood flow (20 & 21%) than the posterior Qs (27 & 32%).

At maximum flow (15 ± 5% into the cardiac cycle for the AAo, 27 ± 15% for the DAo), there was significantly more flow in the right posterior Q (28 ± 2%) than other Qs (22–23%) in the AAo while in the DAo, both posterior Qs had significantly higher flow rates (27 & 30%) than the anterior Qs (21 & 22%). Maximum velocity in both AAo & DAo occurred in the left posterior Q in 10/13 at 16–24% into the cardiac cycle. At end-systole, a short flow reversal was noted in the posterior Qs in the AAo in 11/13 (see graph) while in the DAo, this occurred in the anterior Qs in 10/13.

Conclusion: Flow dynamics in the normal Ao in children are not homogeneous with an asymmetric distribution of flow in the AAo & DAo throughout systole including flow reversal related to the dicrotic notch. These results may help improve Ao surgery.

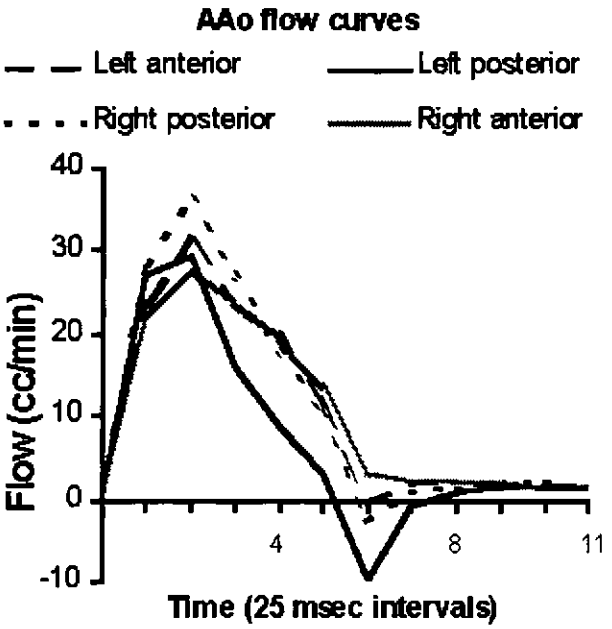

Figure 1. Flow Curves in Various Ao Qs Over Time.

18. The Impact of Right Aortic Arch Geometry on Aortic Flow Dynamics Using Through Plane Velocity Mapping

Mark Fogel,[1] James Meyer,[2] Anne Hubbard,[3] Paul Weinberg,[4] John Haselgrove.[5] [1]*The Children's Hospital of Philadelphia, CHOP–Division of Cardiology, Philadelphia, Pennsylvania United States;* [2]*The Children's Hospital of Philadelphia, The Children's Hospital of Philadelphia, Phildelphia, PA USA;* [3]*Children's Hospital of Philadelphia, 34th & Civic Center Boulevard, Philadelphia, Pennsylvania United States;* [4]*The Children's Hospital of Philadelphia, 34th & Civic Center Blvd, Philadelphia, Pennsylvania United States;* [5]*The Children's Hospital of Philadelphia, 34th St and Civic Center Blvd, Philadelphia, PA USA*

Background: Flow dynamics in the aortic arch (AO) is affected by a number of parameters including geometry. We sought to determine the impact of flow dynamics of right AO geometry as compared to left AO.

Methods: 24 patients (15 with left AO and 9 with right AO) underwent magnetic resonance through-plane phase-encoded velocity mapping in the ascending (AAO) and descending aorta (DAO). The cross-sectional area was divided into 4 equal quadrants (Q) aligned along the AO long-axis for analysis. Significance = $P < 0.05$.

Results: In the AAO, there was a significantly higher % of total flow throughout the cardiac cycle in the left posterior Q of right AO than left ($P = .007$) which was compensated for by significantly lower flow in right anterior Q of right AO than left ($P = .02$). This is illustrated in the diagram which displays values in all Qs.

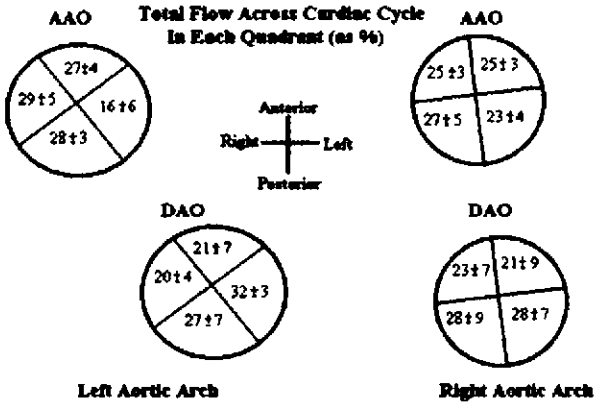

Figure 1. Distribution of Flow in Various Qs of Left and Right AO Archs.

In right AO, maximum velocity (100 ± 14 cm/s) occurred in 7/9 patients in the right half of the AO while in left AO, maximum velocity (107 ± 20 cm/s) occurred in 13/15 in the left half of the AO. In the DAO, whether left or right AO, the posterior half had greater flow than the anterior half (56 ± 11 vs. 44 ± 11% respectively, $P = .02$ for right AO and 59 ± 10 vs. 41 ± 10% respectively, $P = .02$ for left AO). In both AAO and DAO, no differences were noted in distribution of flow among Qs at maximum flow, the maximum flows in each Q, and the maximum range of flows across all Qs in the cardiac cycle.

Conclusion: Right AO geometry significantly impacts flow dynamics in the AAO whereas it is not altered in the DAO, where flow is predominantly in the posterior half of the AO. Alternatively, this also may suggest that hemodynamics could have played a role in the development of right AO in certain individuals.

19. Magnetic Resonance Angiography of Coronary Arteries in Children after Arterial Switch Operation

Sander Starreveld,[1] Martha Sobotka-Plojhar,[2] Aernout Beek,[3] J. Hruda,[4] Mark Hofman,[5] Albert van Rossum.[3] [1]*University Hospital Vrije Universiteit, Department of Pediatrics, Amsterdam, Netherlands;* [2]*University Hospital Vrije Universiteit, Department of Pediactrics, Amsterdam, Netherlands;* [3]*University Hospital Vrije Universiteit, Department of Cardiology, Amsterdam, Netherlands;* [4]*University Hospital Vrije Universiteit, Department of Pediatrics, Amsterdam, Netherlands;* [5]*University Hospital Vrije Universiteit, Department of Clinical Physics & Informatics, Amsterdam, Netherlands*

Introduction: In children with transposition of the great arteries (TGA), as a consequence of transferring the coronary arteries to the neoaorta during arterial switch operations (ASO), coronary flow abnormalities are a recognized long-term problem. Since coronary involvement may remain asymptomatic, many centers advise to perform coronary angiography routinely, being the only reliable method to assess coronary arteries in children. In adults MRI and MRA have proven to be useful in the assessment of coronary artery origin and course.

The purpose of the study was to investigate the value of MRI/MRA in the assessment of coronary arteries in children.

Methods: Thirteen children, age 9.0–13.6 year (median 11.9y) were studied; 4 healthy volunteers, 9 after ASO (all patients older than 8 years in follow-up at our department; operated 1–41 days after birth; median 5d). MR imaging was performed on a whole body imaging system (Vision, Siemens, Erlangen, Germany, 1.5T) using a body phased array coil. No sedation was used. Coronary arteries were visualized using gradient echo imaging obtained during breathholding in mild expiration using both a 2D MRA and 3D MRA technique triggered at the ECG to mid-diastole with a 100–120 ms acquisition window. Frequency selective fat saturation was applied. Partial Fourier encoding was applied to limit the duration of the breath-hold for the 3D technique.

Results: Image quality was good to excellent. In 11 children offspring and proximal course of both coronary arteries could be identified. Three ASO patients revealed abnormal findings. One of them had a fragile LCA but no complaints or ECG abnormalities. The second had an unexpected origin and course of the RCA. The third, whose proximal LCA could not be identified, had chest pain and ECG changes during exercise. LCA kinking was confirmed by coronary angiography and surgery.

Figure 1 shows the LCA and RCA in a healthy volunteer (age 9 year). Figure 2 shows the LCA and RCA in a patient after ASO. (age 13 year).

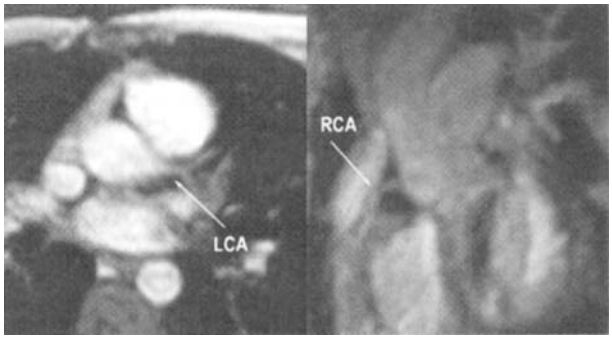

Figure 1. LCA and RCA in a healthy volunteer (age 9 year).

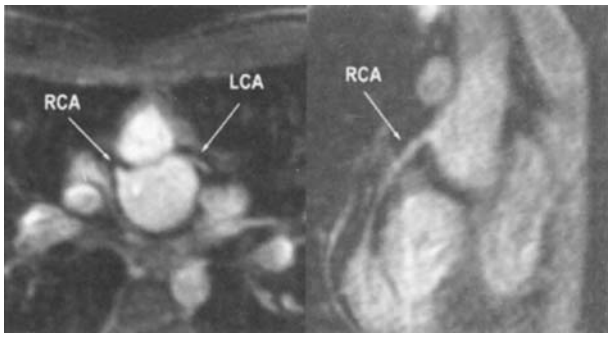

Figure 2. LCA and RCA in a patient after ASO (age 13 year).

Conclusion: MRI/MRA is a useful non-invasive tool for the assessment of coronary artery patency in children after ASO and might in these patients replace coronary angiography in the future.

20. Are Pulmonary Flow Dynamics Uniform in Young Children? A Magnetic Resonance Velocity Mapping Study

Mark Fogel,[1] Paul Weinberg,[2] Anne Hubbard,[3] James Meyer,[4] John Haselgrove.[4] *[1]The Children's Hospital of Philadelphia, CHOP–Division of Cardiology, Philadelphia, Pennsylvania United States; [2]The Children's Hospital of Philadelphia, 34th & Civic Center Blvd, Philadelphia, Pennsylvania United States; [3]Children's Hospital of Philadelphia, 34th & Civic Center Boulevard, Philadelphia, Pennsylvania United States; [4]The Children's Hospital of Philadelphia, 34th St and Civic Center Blvd, Philadelphia, PA USA*

Background: It has been thought that the flow profile in the normal main pulmonary artery (MPA) is parabolic. When that flow is distributed at the branch point to right (RPA) and left pulmonary arteries(LPA), the profile in theory should skew towards the flow divider (ie medially). We sought to test this hypothesis in vivo.

Methods: 9 young children (1.1 ± 8.3 years old) with normal pulmonary anatomy underwent magnetic resonance through-plane phase-encoded velocity mapping in the MPA just proximal to the bifurcation and in the RPA and LPA just distal to the bifurcation. The cross-sectional area was divided into 4 equal quadrants (Q) aligned anatomically for analysis. Significance = $P < 0.05$.

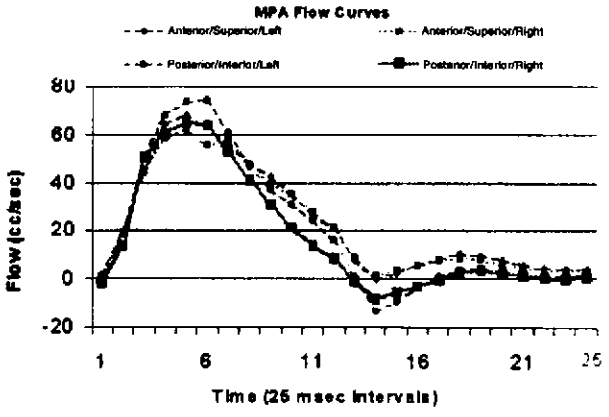

Figure 1. Flow Curves in Various Qs of the Main Pulmonary Artery in Young Children.

Results: In the MPA, there was a significantly lower % of total flow throughout the cardiac cycle in the posterior, inferior and right Q than all other Qs (20 ± 4 vs. 25–27% respectively, P = .01).

In the RPA and LPA, flow dynamics were remarkably similar with no differences noted in total flow, distribution of flow among Qs at maximum flow, and maximum flow in each Q. Maximum velocity and the range of velocities, however, were greater in the LPA than the RPA (127 ± 22 vs 107 ± 22 cm/s respectively for maximum velocity and 48 ± 33 vs. 21 ± 6 cm/s respectively for range of velocities.

Conclusion: In very young children, flow in the MPA is not parabolic as more flow occurs in the posterior, inferior and right Q. In addition, flow in RPA and LPA are remarkably similar without the skewing towards the flow divider with the exception that there appears to be a more heterogeneous profile to velocities in the LPA than the RPA. This information may be useful in designing better pulmonary artery reconstructions, such as in the Fontan operation.

21. Prognostic Value of Aortic Elasticity on Aortic Complications in Patients with Marfan Syndrome

Gijs Nollen,[1] Maarten Groenink,[2] Barbara Mulder,[2] Albert De Roos,[3] Digna Kool,[2] Ernst van der Wall.[4] *[1]Academisch Medisch Centrum Amsterdam, Meibergdreef 9, Amsterdam, Noord Holland Netherlands; [2]Academic Medical Center, Meibergdreef 9, Amsterdam, Noord Holland The Netherlands; [3]University Hospital Leiden, Dept. of Diagnostic Radiology, Leiden, Zuid Holland Netherlands; [4]Leiden University Medical Center, Albinusdreef 2, Leiden, Zuid Holland The Netherlands*

Background: In Marfan patients survival is mainly determined by aortic complications at a relatively young age. The occurrence of aortic dissection and rupture in Marfan patients is difficult to predict by mere aortic dimensions. Assessment of aortic elasticity may be of additional value for risk stratification.

Methods: To assess the prognostic value of aortic elasticity on aortic complications (defined as: 1. aortic root diameter increase >2 mm/year, 2. aortic dissection or 3. death), 73 Marfan patients (aged 31 ± 8 years, 41 men and 32 women) underwent magnetic resonance imaging of the entire aorta in 1997 and were followed up for 3 years. Aortic diameter and ascending aortic distensibility were assessed. MR velocity mapping was used to assess flow wave velocity along the descending aorta as an additional index of elasticity.

Results: 10 patients (12.8%) of the 73 patients examined in 1997 reached one of the endpoints (7 patients with an increase in aortic root diameter >2 mm/year, 3 acute dissections) after 3 years (3.1 ± 0.2 years). The remaining 63 patients did not reach an endpoint. The patients were divided in a complicated and a non-complicated group. There was no significant difference in baseline characteristics and in aortic root diameter (46.9 ± 4.4 vs. 42.7 ± 7.3 mm, respectively) between the two groups. However the 10 complicated patients had a significantly decreased ascending aortic distensibility (2 ± 1 vs. 3 ± 1 10-3 mmHg 10-, respectively) and significantly higher descending aorta flow wave velocity (6.6 ± 1.6 vs. 5.8 ± 1.3 ms −1, respectively) compared to the non-complicated Marfan patients.

Conclusion: Descending aorta flow wave velocity and ascending aorta distensibility are related to the occurrence of aortic complications in Marfan patients, and could be of additional prognostic value for risk stratification.

22. Magnetic Resonance Measurement of Factors Predisposing to Fatal Arrhythmias Late After Repair of Fallot's Tetralogy

Philip Kilner,[1] Periklis Davlouros,[2] Timothy Hornung,[3] Jane Francis,[4] Michael Gatzoulis.[2] [1]*Royal Brompton Hospital, CMR Unit, London, London UK;* [2]*Royal Brompton Hospital, Sydney Street, London, London UK;* [3]*Royal Brompton Hospital, Sydney Street, London, London UK;* [4]*The Royal Brompton Hospital, CMR Unit, London, London England, UK*

Introduction: After repair of Fallot's tetralogy, free pulmonary regurgitation is common, and the right ventricle may dilate. Prolongation of the QRS complex on the ECG has been shown to be associated with increased cardiothoracic ratio on chest x-ray, and to predispose to the devastating late complications of sustained ventricular tachycardia and sudden death (1,2). Causal relationships between pulmonary regurgitation, right ventricular dilatation and ECG changes have been suspected, but not established.

Methods: We studied 26 adults with repaired tetralogy of Fallot (mean age 31 ± 10 years, mean time since repair 23 ± 5 years) using a Picker Edge 1.5T system to acquire 12–14 contiguous breathold FLASH cine acquisitions through both ventricles for measurement of biventricular volume, mass and function (3). Measurements were indexed to body surface area where appropriate. Phase velocity mapping, TE = 5.2 ms, was used to measure systolic and diastolic pulmonary artery flow curves for calculation of regurgitant fraction (4). QRS duration was measured manually from standard ECG traces. The above measurements plus gender, age and time from surgery were analysed by Spearman correlation and linear regression.

Results: Mean pulmonary regurgitant fraction was 22.8 ± 17% (range 0%–51%). Multivariate linear regression analysis showed that pulmonary regurgitant fraction was the only independent variable influencing right ventricular end diastolic volume index (RVEDVi) ($R2 = 0.49$, $R = 0.7$, $P < 0.0001$), and that RVEDVi was the only significant predictor of QRS duration ($R2 = 0.7$, $R = 0.8$, $P < 0.0001$). There was no correlation between QRS duration and left ventricular volume or mass, suggesting that it related to changes of the right ventricle alone.

Conclusions: These results help to clarify causes leading to arrhythmogenesis late after repair of Fallot's tetralogy. Pulmonary regurgitation appears to be the principal cause of right ventricular dilatation, which in turn leads to QRS prolongation. The latter has previously been shown to predispose to malignant arrhythmias and sudden death (1,2). As more data are gathered and patients continue to be followed up, we anticipate that magnetic resonance measurements will play an increasingly important role in deciding if and when to re-operate to place a valve in the pulmonary position.

23. Towards X-Ray Angiographic Resolution–3D Black-Blood Coronary MRA

Matthias Stuber,[1] Elmar Spuentrup,[1] Rene M. Botnar,[1] Kraig V. Kissinger,[1] Warren J. Manning.[1] [1]*Beth Israel Deaconess Medical Center, Cardiovasc. Div., Boston, MA USA*

Introduction: Due to signal-to-noise ratio (SNR) constraints, current 'bright-blood' 3D coronary MRA approaches still suffer from limited spatial resolution when compared to conventional x-ray coronary angiography (~300μm). Recent 2D black-blood techniques (1) have shown to maximize the SNR for coronary MRA at no loss in image spatial resolution. This suggests that the extension of black-blood coronary MRA with a 3D imaging technique would allow for a further increase in SNR, which may be traded for an enhanced image spatial resolution towards X-ray angiographic standards. We therefore extended black-blood coronary MRA with a 3D fast spin-echo imaging technique and prospective real-time navigator technology for the suppression of respiratory motion artifacts.

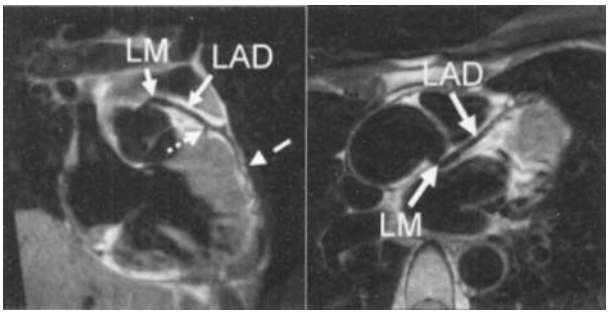

Figure 1. 3D black-blood coronary MRA.

Methods: Free-breathing 3D black-blood coronary MRA was implemented on a Philips Gyroscan ACS-NT system including a 5-element cardiac synergy coil, a Vector ECG for cardiac triggering, and a 3-Point Planscan Tool for volume targeting of the coronary arteries. Five healthy adult subjects were examined. For enhanced black-blood characteristics, a dual-inversion pre-pulse was used with a heart-rate dependent inversion time (~600 ms) (2). Subsequent to the dual-inversion pre-pulse, a 2D selective NAV-RESTORE pre-pulse was applied, which enables lung-liver interface detection of the navigator in the presence of the dual-inversion pre-pulse. For respiratory motion suppression, a real-time navigator for gating (5 mm gating window) and prospective motion correction (factor 0.6) in foot-head direction of the imaged volume position was utilized. The imaging part of the sequence included a 3D fast spin-echo technique with a linear k-space acquisition scheme, 7.6 ms inter-echo spacing, 28 ms TE, echo-train length of 17 and TR of 2 cardiac cycles. The field of view was 200 to 360 mm with a 512 scan matrix (spatial resolution 390. .700μm). Two signal averages were acquired using oversampling in ky-direction. A 16 mm thin 3D slab was imaged consisting of 8 adjacent slices with 2 mm slice thickness each.

Results: In all investigated individuals, free-breathing 3D black-blood coronary MRA could be successfully acquired and the targeted vessels including smaller-diameter coronary branch vessels could be consistently visualized with high contrast. Figure 1 (left) shows a 3D black-blood coronary MRA of a left coronary system acquired with an in-plane resolution of 500μm and a slice thickness of 2 mm. In this image, an 11cm contiguous segment of the left main (LM) and the left anterior descending (LAD) is shown. In parallel to the LAD, proximal portions of a diagonal (dotted arrow) and a septal branch (dashed arrow) are visualized. The image on Figure 1 (right) shows a left coronary system acquired with an in-plane resolution of 390 × 390μm and a slice thickness of 2 mm. In this image, the LM and LAD are visualized together with more distal branching vessels of the LAD.

Conclusions: The extension of black-blood coronary MRA with a 3D fast spin echo imaging sequence and real-time navigator technology allows for thin-slice black-blood coronary MRA image data acquisition with an in-plane image resolution approaching that of X-ray angiography. Hereby, coronary MRA data can be acquired during free-breathing without restrictions related to breath-hold duration/cooperation. The present results warrant a further assessment in patients with x-ray angiographically defined disease.

24. Three-Dimensional TrueFISP Coronary Magnetic Resonance Angiography

Matthias Stuber,[1] Peter Boernert,[2] Rene M. Botnar,[1] Kraig V. Kissinger,[1] Elmar Spuentrup,[1] Warren Manning.[1] [1]*Beth Israel Deaconess Medical Center, Cardiovasc. Div., Boston, MA USA;* [2]*Beth Israel Deaconess Medical Center and Philips Research Laboratory Hamburg, Cardiovasc. Div., Boston, MA USA*

Background: Recent developments of magnetic resonance imaging (MRI) hardware and software allow for the acquisition of high-quality functional images of the heart using TrueFISP imaging sequences (1). With this technique, a substantial 'T2 like' contrast between the ventricular blood-pool and the myocardium may be obtained without the application of exogenous contrast agents or special pre-pulses. For three-dimensional coronary MRA, the inflow effect is reduced, thereby minimizing the contrast between the coronary blood-pool and the surrounding tissue. Hereby, the application of TrueFISP may offer a valuable source of contrast enhancement between the coronary blood-pool and the surrounding tissue. But the commonly used ECG triggered, diastolic coronary MRA data acquisition in a short acquisition window may pose major challenges to successful TrueFISP signal steady-state imaging. We propose the combination of real-time navigator technology with a TrueFisp imaging sequence including signal steady-state preparatory pulses for high-contrast 3D coronary MRA data acquisition during free-breathing.

Methods: Three-dimensional double-oblique TrueFISP coronary MRA was implemented on a commercial 1.5T Philips Gyroscan ACS-NT system equipped with a 5-element cardiac synergy coil and a 3-Point Planscan Tool for volume targeting of the coronary arteries. Coronary MRA were acquired using a vector ECG triggered (2) 3D TrueFISP imaging sequence with a centric ordered k-space acquisition scheme, a TR of 4 ms and a TE of 2 ms. Thirty-four RF excitations with a constant excitation angle of 75° were applied per RR interval. Signal sampling was performed during the last 14 RF excitations resulting in an acquisition window of 56ms. The field of view was 320 mm with a 256 scan matrix. This resulted in an in-plane resolution of 1.25 mm. The slice thickness was 3 mm and 12 slices were acquired. During reconstruction, 24 slices with a slice thickness of 1.5mm each were reconstructed using zero-filling in kz-direction. For the suppression of respiratory motion artifacts, a 2D selective navigator utilized for gating and prospective adaptive 3D motion correction was localized at the dome of the right hemidiaphragm (5 mm gating window, correction factor 0.6 in superior-inferior direction) and applied prior to the excitations.

Results: MR studies were completed in all subjects without complications. Average scanning duration for each 3D acquisition during free breathing was 6 minutes. On all acquired coronary MRA images, long contiguous segments of the targeted coronary vessels could be successfully visualized with high contrast and a good visual vessel definition. Figure 1 displays representative multiplanar reformatted 3D TrueFISP coronary MRA image data acquired during free breathing in a healthy adult subject. A left and a right coronary system acquired with an in-plane resolution of 1.25 × 1.25 mm are displayed. A 10.0 cm contiguous segment of the RCA including a 6cm portion of the left coronary circumflex (LCX) are displayed with a high SNR and visual contrast between the coronary blood-pool and the myocardium (Figure 1, left). Similar observations apply for the left main (LM), the anterior descending (LAD), and the left circumflex (LCX) (Figure 1, right). Signal from the great cardiac vein (GCV) appears to be mildly attenuated when compared to the signal observed in the ventricular cavities or in the coronary arteries.

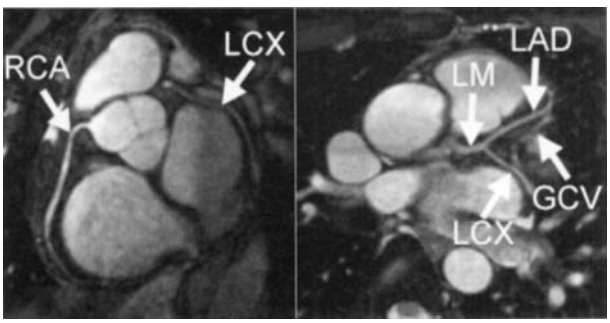

Figure 1. 3D TrueFISP Coronary MRA.

Discussion: TrueFISP has been successfully implemented for contrast enhancement between the coronary blood-pool and the surrounding tissue in 3D coronary MRA. The combination with prospective real-time navigator technology enables free-breathing data acquisition and the application of signal enhancement techniques such as signal averaging or 3D data acquisition. No specific pre-pulses, exogenous contrast agents or fat saturation pre-pulses were necessary. TrueFisp offers a valuable alternative for contrast enhancement in 3D coronary MRA. Its clinical role remains to be defined by future studies.

25. Comparison of Black-Blood and Bright-Blood Coronary MRA in Patients with Coronary Disease–Preliminary Results

Matthias Stuber,[1] Elmar Spuentrup,[1] Rene M. Botnar,[1] Kraig V. Kissinger,[1] Warren J. Manning.[1] [1]*Beth Israel Deaconess Medical Center, Cardiovasc. Div., Boston, MA USA*

Background: Over the last decade, 'bright-blood' coronary MRA techniques with or without the application of exogenous contrast enhancement have been successfully applied to visualize the proximal to mid portions of the coronary anatomy in healthy and diseased states. As an alternative to a bright-blood visualization of the coronary anatomy, free-breathing navigator gated and corrected dual-inversion 'black-blood' coronary MRA has recently been introduced (1). Using this technique, the coronary lumen appears dark and the surrounding tissue (epicardial fat and myocardium) displays high signal intensity. In the present study, black-blood vs. bright-blood coronary MRA was compared in patients with x-ray angiographically confirmed coronary disease and in healthy adult subjects.

Methods: Free-breathing ECG triggered black-blood and bright-blood coronary MRA were acquired in 20 patients (61 ± 14 yrs, 17 male) with x-ray angiographically confirmed coronary disease and in 6 healthy young adults (23 ± 5, 2 male). Volume targeted coronary MRA data were acquired on a commercial 1.5T Philips Gyroscan ACS-NT system equipped with a 5-element cardiac synergy coil (2). A real-time 2D selective navigator was used for gating and prospective adaptive motion correction of the imaged volume position (gating window = 5mm; correction factor = 0.6 in superior-inferior direction). For black-blood coronary MRA, a previously described dual-inversion 2D fast spin-echo imaging sequence (inversion time ~600 ms, NAV-RESTORE, 5.2 ms inter-echo spacing; 25 ms TE; echo-train length of 23; TR = 2 cardiac cycles; acquisition window = 120 ms; field of view = 360 mm; 512 × 384 scan matrix, 3 mm slice thickness, 6–12 slices) was applied (1). For bright-blood coronary MRA, a fat-suppressed 3D segmented k-space gradient echo technique (TR = 8.4 ms; TE = 2.4 ms; acquisition window = 120 ms; field-of-view = 360 mm; scan matrix = 512 × 360, 30 mm volume thickness, 10 slices with 3 mm thick-

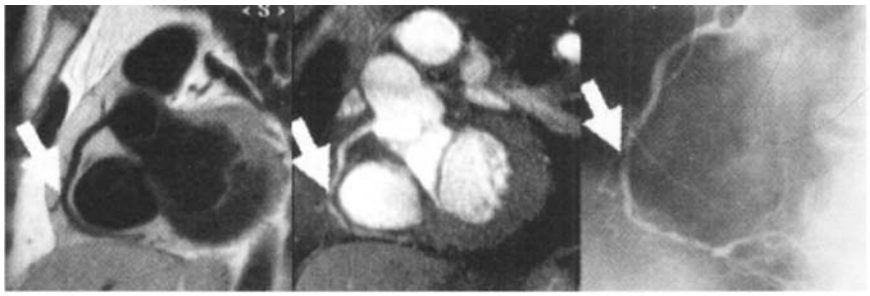

Figure 1.

ness) was combined with a T2 pre-pulse (TE = 50 ms) for contrast enhancement between the coronary blood-pool and the surrounding tissue (3). Vessel diameter, vessel sharpness and the contrast-to-noise ratio (CNR) between the coronary blood-pool and myocardial muscle were subsequently quantified on both, the black-blood and the bright-blood coronary MRA. Vessel sharpness and vessel diameter were determined based on a local first-order derivation (3).

Results: In the patient subgroup, black-blood coronary MRA resulted in a 33% improvement in vessel sharpness when compared to bright-blood coronary MRA (0.6 ± 0.2 black-blood vs. 0.4 ± 0.1 bright-blood; $p < 0.01$). In healthy adults, a trend for an increased vessel sharpness was observed (0.7 ± 0.2 black-blood vs. 0.6 ± 0.2 bright-blood; $p = 0.2$). In the patients with x-ray confirmed coronary disease, we found an increased normal coronary vessel diameter for black-blood coronary MRA (3.2 ± 0.6 mm black-blood vs 2.7 ± 0.5 mm bright-blood; $p < 0.01$). However, in the healthy adults no significant difference in vessel diameter could be found (2.6 ± 0.3 mm black-blood vs. 2.4 ± 0.3 mm bright-blood; p = NS). A significantly increased improvement in CNR was found for black-blood coronary MRA when compared to bright-blood coronary MRA. These findings were consistent among patients (18 ± 8 black-blood vs. 5 ± 2 bright-blood; $p < 0.01$) and healthy adults (22 ± 9 black-blood vs. 5 ± 3 bright-blood; $p < 0.01$). In Figure 1, a black-blood coronary MRA (left), a bright-blood coronary MRA (center) and an x-ray angiogram (right) of the RCA of the same patient are displayed. The white arrow refers to an x-ray confirmed 50% focal stenosis visible on the bright-blood coronary MRA but not on the black-blood image. At this location, local calcifications could be observed on the x-ray angiogram.

Discussion: This preliminary study suggests that CNR is substantially improved for 2D black-blood coronary MRA when compared to the present 3D bright-blood coronary MRA approach. On the black-blood coronary MRA, an increased objectively determined vessel diameter was found in patients with x-ray angiographically defined coronary disease (when compared to the bright-blood method), but not in healthy adults. This small but significant difference may be attributed to calcifications or plaque in the coronary arteries of the patients. Calcifications and various plaque components appear signal attenuated on both, the black-blood and the bright-blood coronary MRA (Figure 1). While this signal attenuation contributes to a visual narrowing of the vessel on bright-blood coronary MRA, it contributes to a visual enlargement of the same vessel on the black-blood coronary MRA. Consistent with the findings for the vessel diameter, a significantly improved vessel sharpness was only found in the patients using the black-blood technique. This may also be related to alterations in the composition of the coronary vessel wall. However, these findings remain to be further investigated.

26. Interrogation of Both Cardiac Function and Delayed Enhancement in Mice Using a Single Pulse Sequence

Zequan Yang,[1] Antwone J. Ross,[2] Wesley Gilson,[3] Stuart Berr,[4] John N. Oshinski,[5] Brent French Ph.D.[6] *[1]University of Virginia, Dept. of Biomedical Engineering, Charlottesville, VA USA; [2]University of Virginia, Dept. of Biomedical Engineering, Charlottesvillle, VA USA; [3]University of Virginia, 111B Maywood Lane, Charlottesville, Virginia United States; [4]University of Virginia, MR4 Building, Room 1192, Charlottesville, Virginia United States; [5]Emory University School of Medicine, Frederik Philips MR Research Lab, Atlanta, GA USA; [6]University of Virginia, 300 Park Place, MR4 Room 5021, Charlottesville, VA USA*

Introduction: Transgenic and "knock-out" mice have provided fundamental insights into the genetic mechanisms underlying atherosclerosis, hypertension, and diabetes. However, similar advances in the field of myocardial infarction (MI) have been slow due to the challenges of performing coronary ligation and assessing cardiac function in such small animals with high heart rates (>500 bpm). Upon implementing a murine model of reperfused coronary occlusion, we sought to develop methods for simultaneously assessing left ventricular (LV) function and myocardial infarct size in intact mice using cardiac MRI.

Methods: Six agouti mice were anesthetized with pentobarbital and subjected to a 60 min occlusion of the major left anterior descending coronary artery followed by 24 hrs of reperfusion. For imaging, Gd-DTPA (0.3 mmol/kg) was administered as an IV bolus through the femoral vein 10 min before the start of the imaging session. Imaging was performed on a Varian Inova 4.7T MRI scanner equipped with Magnex gradients (80 G/cm max). An ECG-triggered, 2D-cine FLASH sequence was used to acquire a set of contiguous short-axis images

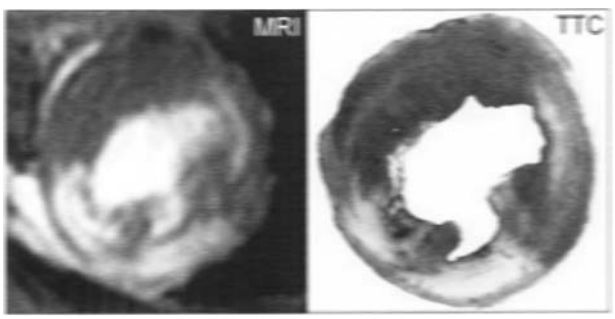

Figure 1. Infarct size by Gd-DTPA and TTC.

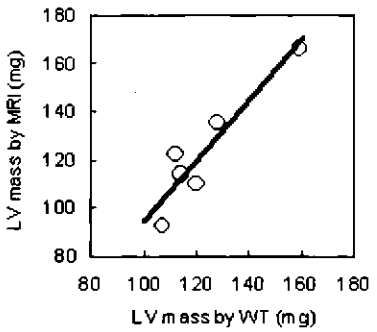

Figure 2. LV mass by MRI and wet weight.

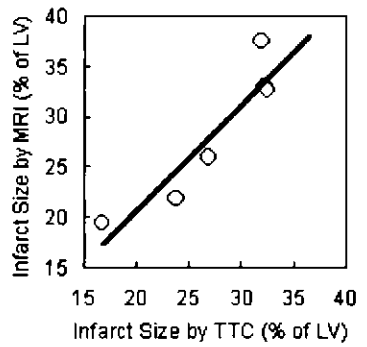

Figure 3. Infarct size by Gd-DTPA and TTC.

spanning the entire LV. A flip angle of 60° was used to increase T1 weighting. Twelve evenly-spaced images were acquired over the heart cycle with an echo time of 3.9 ms. A 2.5 cm Helmholtz transceiver coil and a 2.56 cm × 2.56-cm field of view yielded a final resolution of 0.1 × 0.1 × 1.0 mm^3. Image analysis was performed using the ARGUS package (Siemens Medical Systems) to determine LV end diastolic volume (LVEDV), end systolic volume (LVESV), ejection fraction (LVEF) and LV mass. Hyperenhanced regions at end-diastole were planimetered from cine images acquired 10–30 min after Gd-DTPA injection using similar methods. After imaging, the isolated hearts were stained with TTC for comparison with the hyperenhanced images.

Results: Excellent correspondence was noted between the size and shape of Gd-enhanced regions in the LV and infarcted myocardium as revealed by TTC staining (Fig. 1). As shown in Fig. 2, there was good correlation (R = 0.935) between the LV mass (mean ± SEM) in the 6 mice as determined by MRI (122 ± 10 mg) and as determined by wet weight (125 ± 7 mg). As shown in Fig. 3, there was also good correlation (R = 0.925) between infarct size (expressed as% of LV mass, mean ± SEM) as determined by delayed Gd-enhancement (27.4 ± 2.5%) and by TTC staining (28.4 ± 2.9%). LVESV and LVEF (mean ± SEM) in the 6 mice 24 hrs post-MI were 12.6 ± 2.5 uls and 56.0 ± 4.7%, respectively. There was little correlation between infarct size and either LVESV or LVEF (R = 0.55 & R = −0.54, respectively) as measured with cardiac MRI 24 hrs post-MI.

Conclusions: A single 2D-cine FLASH sequence provides all the information necessary to simultaneously interrogate both infarct size (by delayed Gd-enhancement) and global cardiac function (by LVEF). Infarct size does not correlate well with either LVESV or LVEF when assessed 24 hrs after reperfusion, indicating the existence of post-infarct stunning in this murine model of reperfused MI. These dynamic cardiac MR microimaging techniques, applied in combination with genetically-manipulated mice and murine models of MI, should prove valuable in elucidating the role of individual genes in the pathophysiology of myocardial infarction.

27. Absolute Levels of High-Energy Phosphates in Human Heart Disease by 31P-SLOOP MRS

Meinrad Beer,[1] Joern Sandstede,[2] Wilfried Landschuetz,[3] Herbert Koestler,[2] Thomas Pabst,[2] Werner Kenn,[2] Kerstin Harre,[4] Markus von Kienlin,[3] Dietbert Hahn,[2] Stefan Neubauer.[5] *[1]Uniklinik Wuerzburg, Josef-Schneider-Str. 2, D-97080 Wuerzburg, Wuerzburg, Bavaria Germany; [2]Institut fuer Roentgendiagnostik, Josef-Schneider-Str. 2, Wuerzburg, Bavaria Germany; [3]Institut fuer Biophysik, Am Hubland, Wuerzburg, Bavaria Germany; [4]Medizinische Klinik, Josef-Schneider-Str. 2, Wuerzburg, Bavaria Germany; [5]Oxford University, John Radcliffe Hospital, Headley Way, Oxford, England UK*

Whether alterations of myocardial high-energy phosphate (HEP) levels occur in hypertrophied and failing human heart remains a controversy; biopsy measurements are problematic (degradation) and non-invasive 31P-MR spectroscopy (MRS) allows detection of relative levels of HEP (PCr/ATP ratio) only. Here, we report on the first highly accurate non-invasive measurements of absolute HEP levels in human hypertrophy/heart failure.

We examined 4 age-matched groups (n = 10 each): Volunteers (VOL), patients with severe hypertension (HYP), aortic stenosis requiring valve replacement (AST, valve area <.7 cm2) and dilated cardiomyopathy (DCM, normal coronaries) (see table below). Ejection fraction (EF), LV end-systolic volume (LVESV), LV mass (LVM) were measured with cine-MR imaging, relative (PCr/ATP) and absolute (PCr, ATP) levels of HEP by 31P-SLOOP-MRS. SLOOP takes into account anatomic compartments, local flip angles and a 31P-standard.

Conclusions: 1) In heart failure, but not in LV hypertrophy, ATP is reduced significantly by 36% 2) PCr/ATP ratios underestimate changes of HEP in heart failure 3) In spite of similar increases in LVM, PCr is reduced in AST but not in HYP.

Functional and Metabolic Data Determined Using MRI and 31P-MRS

	VOL	HYP	AST	DCM
EF (%)	69 ± 2	67 ± 2	58 ± 4	20 ± 3*
ESV (ml)	31 ± 3	39 ± 3	57 ± 12	263 ± 26*
M (g)	140 ± 7	217 ± 21*	230 ± 12*	223 ± 18*
PCr/ATP	1.69 ± 0.17	1.50 ± 0.09	1.34 ± 0.10*	1.26 ± 0.11*
PCr (mmol/kg)	8.5 ± 0.5	8.2 ± 0.5	6.5 ± 0.6*	4.4 ± 0.4*
ATP (mmol/kg)	5.7 ± 0.5	5.5 ± 0.3	4.9 ± 0.3	3.7 ± 0.2*

28. 3D Magnetization-Prepared True-FISP: A New Technique for the MR Imaging of Coronary Arteries

Vibhas Deshpande,[1] Steven Shea,[2] Gerhard Laub,[3] Orlando Simonetti,[4] John Finn,[5] Debiao Li.[6] [1]*Northwestern University, Department of Radiology, Chicago, Illinois United States;* [2]*Northwestern University, Department of Radiology, Chicago, IL USA;* [3]*Siemens Medical Systems, 448 E. Ontario St., Chicago, IL USA;* [4]*Siemens Medical Systems, Ontario Center East Tower, Chicago, IL USA;* [5]*Northwestern University, Morton Building 5-681310 E. Superior Street, Chicago, Illinois United States;* [6]*Northwestern University, Department of Radiology, Chicago, IL USA*

Discussion: Volume targeted breath-hold imaging (VCATS) using a FLASH (fast low-angle shot) sequence has recently been described for MR angiography of the coronary arteries (1). Destruction of the transverse magnetization in each TR, high bandwidths, and signal saturation at high flip angles result in relatively low signal-to-noise ratio (SNR). The steady-state coherent gradient-echo sequence, or True-FISP has been shown to substantially improve the blood SNR and blood/myocardium contrast-to-noise ratio (CNR) in cine images (2) because the transverse magnetization is re-used and the signal is T2/T1-weighted. The aim of this work was to evaluate the utility of True-FISP for coronary artery imaging. Specifically, a magnetization preparation scheme was developed to allow fat saturation in a true-FISP sequence for coronary artery imaging.

Methods: The sequence structure was a 3D segmented data acquisition with 'n' centrically reordered phase-encoding lines per cardiac cycle. All gradients were balanced in every rf cycle to ensure that the transverse magnetization was maintained in coherence. Alternating rf pulses were used (180° phase alternation) to maintain a relatively uniform signal in presence of field inhomogeneities. A spectral fat saturation pulse (flip angle 110°) was applied, followed by an $\alpha 2$ (α = flip angle for data acquisition) preparation pulse to force a quick approach to steady-state (3). A number of dummy cycles after the $\alpha/2$ preparation allowed a reduction in the signal oscillations of off-resonant spins.

Simulations and Phantom Studies: Simulations were performed to determine the optimal number of dummy cycles that would allow fat saturation and reduced blood signal oscillations during the approach to steady state (TR/TE = 3.9/1.9 ms, α = 50°). Results show that the fat signal was minimum at approximately 20 dummy cycles. Phantom imaging was used to validate the simulation results.

Volunteer Imaging: Healthy volunteers were studied (n = 24) to evaluate improvements in SNR and CNR using true-FISP as compared to FLASH with the same imaging parameters. The imaging parameters include: TR/TE = 3.8/1.9 ms, (25–39) lines per cardiac cycle, matrix size = (75–117) × 256, slab thickness = 32 mm, number of partitions = 8, imaging time = 24 cardiac cycles. The readout bandwidth for the FLASH sequence was 480 Hz/pixel and for the true-FISP sequence, 781 Hz/pixel.

Results: The simulations and phantom studies demonstrate an effective fat suppression using the proposed preparation scheme. Volunteer studies show a 55% increase in the SNR ($p < 0.001$) and 178% increase in the CNR ($p < 0.001$) over FLASH. Clear improvements in coronary artery delineation, especially the distal portions were observed in True-FISP images.

Conclusion: A new method for imaging the coronary arteries was proposed using a True-FISP sequence. The designed magnetization preparation scheme allows fat saturation and suppression of image artifacts caused by the approach to steady-state. A significantly higher SNR and CNR were observed as compared to FLASH. Thus, it can potentially challenge contrast-enhanced FLASH imaging for coronary MRA.

29. Cardiac MRI for Assessing the Effects of Antioxidant Therapy on Cardiac Structure and Function in a Mouse Model of Post-Infarction Heart Failure

Zequan Yang,[1] Stuart Berr,[2] John Oshinski,[3] Antwone J. Ross,[4] Brent French.[5] [1]*University of Virginia, UVA Health System Box 800759, Charlottesville, Virginia United States;* [2]*University of Virginia, MR4 Building, Room 1192, Charlottesville, Virginia United States;* [3]*Emory University School of Medicine, Frederik Philips MR Research Lab, Atlanta, Georgia United States;* [4]*University of Virginia, Dept. of Biomedical Engineering, Charlottesville, VA USA;* [5]*University of Virginia, 300 Park Place, MR4 Room 5021, Charlottesville, Virginia United States*

Background: Recent advances allow cardiac MRI to be applied in small animals, thus facilitating the study of both cardiovascular pharmacology and pathophysiology in mice. In this study, cardiac MRI was used to serially assess cardiac structure and function in a mouse model of heart failure secondary to reperfused myocardial infarction (MI), and to evaluate the efficacy of a potent antioxidant (alpha-lipoic acid, ALA) in this model.

Methods: MI was induced in 23 C57BL/6N mice by temporarily occluding the LAD coronary artery for 2 hrs. One day after MI, the mice were divided into two groups. Mice in the control group (n = 14) were fed vehicle (water, 2 ul/g body weight) daily by gavage for 56 days. Mice in the treatment group (n = 9) were fed ALA (75 mg/kg) daily by gavage for 56 days. Cardiac MR was used to serially assess changes in cardiac structure and function over time following MI. Imaging was performed with a Helmholtz RF coil on a Varian Inova 4.7T MR scanner with Magnex gradients (80 G/cm max). An ECG-triggered, 2D-cine FLASH sequence was employed with a slice thickness of 1 mm and an in-plane resolution of 0.1 × 0.1 mm^2. The flip angle was 20° and the TR was 10–20 ms. During each imaging session, the entire LV was assessed using 7 to 9 contiguous short-axis slices. Cardiac MRI

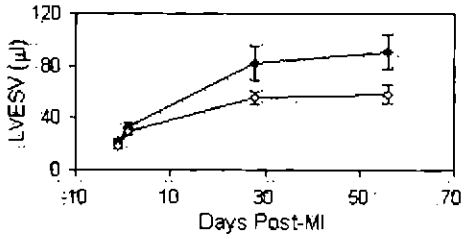

Figure 1. LVESV in control (solid) and ALA-treated mice (open).

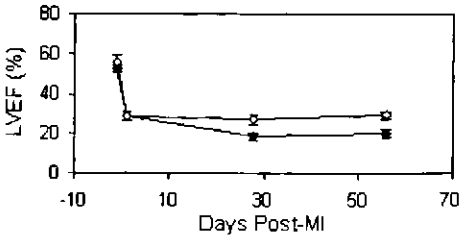

Figure 2. LVEF in control (solid) and ALA-treated mice (open).

was performed 1 day before MI and on days 1, 28 and 56 post-MI. LV end-systolic volume (LVESV) and ejection fraction (LVEF) were calculated using the ARGUS software package from Siemens Medical Systems.

Results: No differences were found in either LVESV or LVEF between the control and ALA-treated groups at baseline or at 1 day post-MI. When measured by cardiac MR on the day after LAD occlusion, MI produced a 60% increase in LVESV (from 21 ± 2 ul to 33 ± 3 ul) and a precipitous 50% reduction in LVEF (from 54 ± 2% down to 27 ± 2%). LVESV in control mice gradually increased at later time points to a value of 82 ± 14 ul at day 28 and 91 ± 13 ul at day 56 (Fig. 1). In contrast, LVESV in mice treated with ALA was only 56 ± 5 ul at day 28 and 58 ± 7 ul at day 56 (both time points $p < 0.05$ vs control). After the initial decline resulting from MI, LVEF in control mice further deteriorated to a steady-state level of 19 ± 2% at day 28 and 20 ± 2 at day 56 (Fig. 2). In contrast, LVEF in mice treated with ALA was maintained at near post-MI values, remaining at 27 ± 3% on day 28 at 29 ± 2% on day 56 (both time points $p < 0.05$ vs control). Thus ALA attenuated LV remodeling and helped preserve LVEF. Furthermore, the salutary effects of ALA on cardiac structure and function were also evidenced by an enhanced survival rate (100% vs 57% on day 28 and 89% vs 43% on day 56, $p < 0.05$).

Conclusions: MRI provides for accurate, non-invasive, serial evaluation of cardiac structure and function in a mouse model of post-infarction heart failure. Cardiac MRI proved particularly valuable in verifying that both control and treatment groups had similar chamber volumes and suffered similar declines in cardiac function on day 1 post-MI. Furthermore, cardiac MR provided the sensitivity necessary to detect the beneficial effects of antioxidants in the mouse model using a reasonable number of animals. In this study, cardiac MR proved invaluable in demonstrating that antioxidant therapy exerts beneficial effects on LV remodeling and helps preserve cardiac function after large MI, resulting in an enhanced rate of survival.

30. TrueFISP and Conventional Turbo Gradient Echo MRI Result in Significantly Different Estimations of Left Ventricular Dimensions and Function

Sven Plein,[1] Timothy Bloomer,[1] John Ridgway,[2] Mohan Sivananthan.[1] [1]*Leeds General Infirmary, Cardiac MRI Unit, Leeds, West Yorkshire United Kingdom;* [2]*University of Leeds, Department of Medical Physics, Leeds, West Yorkshire United Kingdom*

Introduction: Steady state gradient echo imaging with balanced gradients (TrueFISP or BFFE = Balanced Fast Field Echo) is increasingly used in cardiac MRI. The main applications of TrueFISP include the assessment of global and regional ventricular dimensions and function. TrueFISP sequences provide substantially better contrast between blood and myocardium than conventional Turbo Gradient Echo sequences and this contrast depends mainly on T1/T2 properties of tissue. As a consequence, estimations of cardiac volumes might differ between TrueFISP and conventional Gradient Echo acquisition. The purpose of this study is to compare a TrueFISP and a standard Turbo Gradient Echo acquisition sequence in the evaluation of global and regional left ventricular dimensions and function.

Methods: Twenty-five consecutive patients were studied (6 left ventricular hypertrophy, 9 dilated cardiomyopathy, 10 normal cardiac dimensions). Studies were performed on a 1.5T Philips ACS NT system with Master gradients (Philips Medical Systems, Best, The Netherlands). ECG gated, breath-hold, multi-slice multi-phase data sets covering the left ventricle in 10–12 short axis slices were acquired using a Turbo Gradient Echo sequence (Turbo Field Echo = TFE: TR 8.1, TE 4.9, Flip angle 35°) and a TrueFISP equivalent sequence (BFFE: TR 3.34, TE 1.67, Flip angle 55°). Slice thickness was 6mm with 4mm gap for both scans. Analysis was performed offline on a Sun workstation with MASS software (Medis, Leiden, The Netherlands). Endocardial and epicardial contours were drawn manually by two experienced observers. End-diastolic volume (EDV), end-systolic volume (ESV), Ejection fraction (EF), Stroke volume (SV) and left ventricular mass (LVM) were determined using conventional methods. End-diastolic (EDWT) and end-systolic wall thickness (ESWT) was measured and diastolic to systolic wall-thickening (WT) and wall motion (WM) calculated using the centreline method. Data is expressed as mean ± SD and was compared using Bland-Altman analysis and a paired t-test. Intra- and interobserver variabilities were assessed.

Results: Figure 1 shows corresponding images acquired with BFFE (left) and TFE (right). Analysis revealed significantly higher EDV and ESV on TrueFISP data sets while EDWT, ESWT and LVM were significantly lower (Table 1). Differences for EF and WM were lower but also significant. SV and WT did not differ significantly. The observed differences were similar for all patient groups (no table). Intra- and interobserver variabilities were less than 5%.

Discussion: This study demonstrates significant differences in measurements of ventricular dimensions and function between TrueFISP and Turbo Gradient Echo Imaging. These differences are largely due to lower wall thickness measurements in both diastole and systole. They are consistent and reproducible in subjects with normal, dilated and hypertrophied ventricles.

One reason for the observed results is likely to be the improved contrast between blood and myocardium with the TrueFISP acquisition. This improves the visualisation of trabeculation in TrueFISP and may lead to positioning of the endocardial contours more towards the myocardium. In Turbo Gradient Echo, slow blood flow can be mistaken for myocardium and wall thickness overestimated. This would explain lower EDWT, ESWT, LVM and higher EDV and ESV. The calculated parameters SV and EF and the functional parameters (WT and WM) showed substantially lower differences, in keeping with a systematic reduction in measurements of wall thickness throughout the cardiac cycle.

Other inherent differences in the two sequences and imaging artefacts specific to each sequence could also have contributed to the observed differences.

In conclusion, steady state gradient echo MRI with balanced gradients results in lower measurements of LV dimensions and some functional parameters than Turbo Gradient Echo MRI. This has to be considered in the interpretation of results, definition of normal values and in particular in the long-term follow up if different acquisition sequences are used.

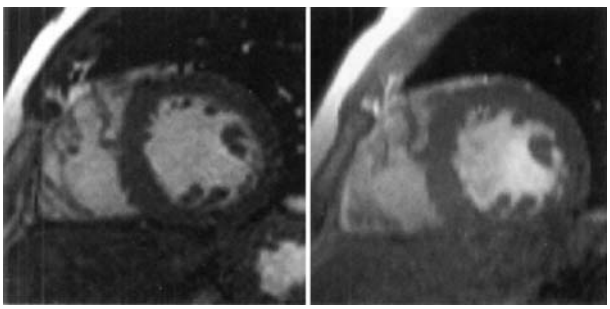

Figure 1.

Table 1

Differences Between TFE and TrueFISP Measurements

	EDV (ml)	ESV (ml)	SV (ml)	EF (%)	LVM (g)	EDWT (mm)	ESWT (mm)	WT (%)	WM (mm)
TFE	161.4 (87.1)	74.9 (84.9)	93.1 (23.4)	63.4 (18.3)	163.8 (51.1)	8.2 (1.8)	13.0 (3.5)	63.0 (29.7)	7.5 (2.6)
TrueFISP	177.0 (91.8)	88.7 (95.7)	92.5 (23.9)	59.1 (19.1)	140.7 (46.3)	9.7 (1.7)	15.5 (3.4)	61.4 (23.4)	8.2 (2.6)
Difference	15.6 (15.1)	13.8 (12.2)	0.6 (10.6)	4.3 (3.8)	23.2 (11.2)	1.5 (0.7)	2.5 (1.1)	−1.6 (11.6)	0.7 (0.8)
p value	<0.0001	<0.0001	0.775	<0.0001	<0.000	<0.0001	<0.0001	0.532	<0.0001

31. Comparison of TrueFISP and FLASH in Valve Disease

Anna John,[1] Philip Kilner,[1] Raad Mohiaddin,[1] Christine Lorenz,[2] Dudley Pennell.[3] [1]*Royal Brompton Hospital, CMR Unit, London, United Kingdom;* [2]*Royal Brompton Hospital and Siemens Medical Engineering, CMR Unit, London, England United Kingdom;* [3]*Royal Brompton Hospital, CMR Unit, London, England United Kingdom*

Introduction: FLASH cine gradient echo sequences have been used to characterise valve disease. The possible advantages of TrueFISP cine over FLASH cine sequences include shorter acquisition times resulting in shorter breathholds and better blood-tissue contrast (1,2,3). Flow appearances differ between the two sequences, and in this study we set out to compare TrueFISP and FLASH images in a semi-quantitative assessment of diseased mitral and aortic valves.

Methods: 14 patients (9 male, mean age 52, range 19–76 years) were included. 5/14 had mitral regurgitation (MR), 6 had aortic stenosis (AS), and 7 aortic regurgitation (AR), including 4 patients with mixed aortic valve disease. Exclusion criteria were more than one regurgitant lesion, patients having undergone valve surgery and general contraindications for magnetic resonance. Scans were performed on a 1.5T Siemens Sonata scanner using TrueFISP- (TE 1.6 ms, TR 3.2 ms) and FLASH- (TE 6.1 ms, TR 112 ms, echo shared, effective temporal resolution 56 ms)sequences. Images were assessed for valve and jet morphology (in- and through-plane). Jet size was estimated in four- and two-chamber views (MR only), LVOT view (AS, AR, MR), oblique coronal LVOT view (AS and AR only) as well as in cross-section.

Results: Overall image quality of TrueFISP was excellent in 9 patients, good in 4 and satisfactory in 1. For FLASH, image quality was excellent in 4, good in 5, and satisfactory in 5 patients. Jets in TrueFISP images appeared smaller than in FLASH images in all patients. Average jet sizes in TrueFISP images expressed as a percentage of FLASH jet size were 51% in LVOT- and two-chamber orientation, 44% in oblique coronal LVOT view, 28% in four-chamber view and 61% in cross-sectional planes. The number of valve leaflets was detected correctly in all patients in both techniques. Visibility of the cusps was rated good on 7 of the TrueFISP and 4 of the FLASH studies, moderate in 6 TrueFISP and 7 FLASH studies and poor in 1 TrueFISP and 3 FLASH

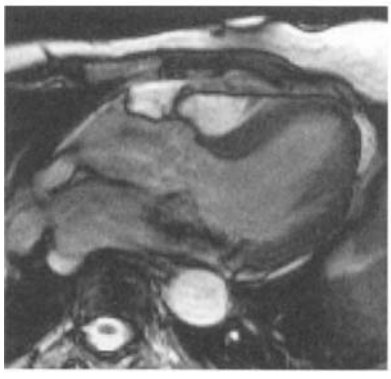

Figure 1. Shows a TrueFISP image of the mitral valve in an LVOT plane.

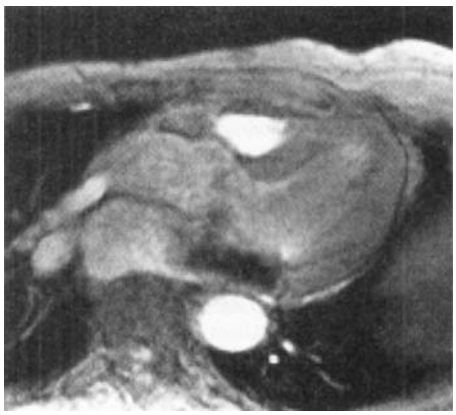

Figure 2. Shows the corresponding FLASH image in the same orientation.

Figure 3. Is a TrueFISP long axis view depicting the mitral valve and its suspensory apparatus.

Table 1

Summarizes the Comparison of Qualitative Lesion Grading for TrueFISP and FLASH

		Mild	Moderate	Severe	Grading Impossible
AR	TrueFISP	2	3	0	2
	FLASH	2	1	3	0
AS	TrueFISP	0	3	0	3
	FLASH	0	3	3	0
MR	TrueFISP	2	2	1	0
	FLASH	2	1	2	0

studies. Agreement between the techniques was good, but severe AR/AS lesions were harder to evaluate by TrueFISP. MR jets were well depicted with both techniques.

Conclusions: Jets appear smaller in TrueFISP than in FLASH images. Severe aortic valve lesions were difficult to grade on TrueFISP, possibly due to a combination of lack of sensitivity for turbulence and additional artefacts caused by flow acceleration. Cusp visibility was similar for both techniques, but the mitral suspensory apparatus was more clearly seen on TrueFISP images due to better blood-tissue contrast. The results of this study demonstrate that there are important differences between TrueFISP and FLASH in visualisation of jets resulting from valvular lesions, which should be taken into consideration when using TrueFISP for functional evaluation of the heart.

32. Pre-Clinical Evaluation of a New Blood Pool Agent B-22956/1 for Myocardial Perfusion and Coronary MRA In a Stenosis Porcine Model

Jie Zheng,[1] Friedrich Cavagna,[2] Debiao LI,[3] Fabio Maggioni,[4] Francis KLOCKE,[5] Dana Abendschein,[6] Orlando Simonetti,[7] Gerhardt Laub,[8] John Finn.[9] [1]*Washington University, Cardiovascular Imaging Lab, St. Louis, Missouri United States;* [2]*Bracco, S.p.A., Bracco, Imaging Department, Milano, Milano Italy;* [3]*Northwestern University, Department of Radiology, Chicago, IL USA;* [4]*Bracco, S.p.A., Bracco, Milano, Milano Italy;* [5]*Northwestern University, Northwestern University Medical School, Chicago, Illinois United States;* [6]*Washington University, Mailstop 8086, St. Louis, Missouri United States;* [7]*Siemens Medical Systems, Ontario Center East Tower, Chicago, IL USA;* [8]*Siemens Medical Systems, 448 E. Ontario Street, Chicago, IL USA;* [9]*Northwestern University, Morton Building 5-681310 E. Superior Street, Chicago, Illinois United States*

Purpose: The blood pool agent B-22956/1 (Bracco, S.p.A., Milan, Italy) is a low molecular weight gadolinium chelate with unprecedented binding to serum proteins. The T1-relaxivity of the agent is 27 mM-1 sec-1. The aim of this work is to assess the feasibility of detecting myocardial perfusion abnormality and coronary artery stenosis in a stenosis swine model by using this agent.

Materials and Methods: Animal Preparation: Six male Yucatan miniswine weighing 15 to 18 kg were fed an atherogenic diet for 2 weeks before vessel injury. A balloon angioplasty procedure was then performed in 2 or 3 coronary arteries of each animal. After the coronary artery injury, the animals were recovered and fed the diet for another 6–8 weeks. X-ray angiography was performed to detect atherosclerotic stenosis.

MR Imaging: All measurements were performed on a Siemens Sonata 1.5 T MR scanner with a high-speed gradient. Several pre-contrast 3D breath-hold and navigator-echo (NE) gated FLASH scans (TR/TE = 4 msec/1.6 msec, FOV = 15 × 20 × 24 cm, imaging matrix = 147 × 256 × 16 for breath-hold and 231 × 256 × 32 for NE, flip-angle = 15°) were performed along the prescribed coronary artery orientations. Adenosine was then infused i.v. at a rate of 1ml/min. After 4 min of infusion, the perfusion imaging, acquired by a IR-prepared TrueFISP 2D sequence, started simultaneously with a bolus injection i.v. of 0.015 mmol/kg B-22956/1 (TR/TE = 3 msec/1.5msec, TI = 374 msec, FOV = 20 × 27 cm, image matrix = 96 × 256, slice thickness = 5 mm). There were 60 single-slice images acquired with one image per heartbeat on the short-axis of left ventricle. After completion of perfusion scan, a dose of 0.085 (total dose 0.1, n = 3) or 0.135 (total dose of 0.15, n = 3) mmol/kg of B-22956/1 was injected. Several 3D breath-hold postcontrast coronary artery scans were then performed by a IR-prepared FLASH sequence (TI = 200 msec, flip-angle = 25°).

Results: Four animals had reduced or no perfusion at stress in the stenosis vessel territories. The post-contrast coronary artery images qualitatively show the same location and degree of the stenosis with the findings from x-ray angiography. A typical perfusion and coronary artery image are demonstrated in the figure (a) and (b), respectively.

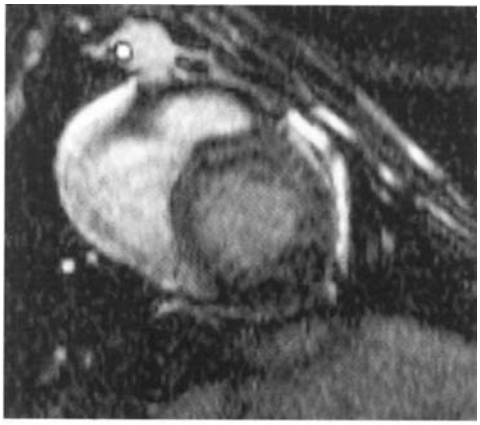

Figure (a).

Figure (b).

Conclusion: B-22956/1 demonstrated the ability for detecting myocardial perfusion abnormality and coronary stenosis in one setting.

33. Regional Blood Flow Variability in Healthy Human Myocardium Assessed with Quantitative Magnetic Resonance First-Pass Perfusion Imaging

Olaf Muehling,[1] Fan Zhao,[2] Prasad Panse,[2] Andrey Zenovich,[2] Betsy Wilson,[4] Robert Wilson,[5] Inderjit Anand,[6] Michael Jerosch-Herold,[7] Norbert Wilke.[7] [1]*University of Minnesota, 420 Delaware St, Minneapolis, Minnesota United States;* [2]*University of Minnesota, 420 Delaware St, Minneapolis, Minnesota USA;* [3]*University of Minnesota, 420 Dealware St, Minneapolis, Minnesota USA;* [4]*Division of Cardiology Department of Medicine University of Minnesota, 401 E River Rd, Minneapolis, Minnesota USA;* [5]*University of Minnesota, 401 E River Rd, Minneapolis, Minnesota United States;* [6]*VA Medical Center, One Veterans Dr, Minneapolis, Minnesota USA;* [7]*University of Minnesota, 420 Delaware St SE, Minneapolis, Minnesota United States*

Background: The knowledge of the distribution of regional myocardial blood flow (MBF) during rest and hyperemia in healthy volunteers is fundamental for the evaluation of patients and their underlying disease. A considerable variability of regional myocardial perfusion has been previously demonstrated in animal studies using radioactive microspheres (1) and in humans (2) with positron emission tomography (PET). We conducted this study to evaluate the regional blood flow variability with Magnetic Resonance First-Pass Perfusion (MRFP) imaging (3). This will also serve as a database of normal MBF values for future studies using MRFP imaging.

Methods: Thirteen healthy volunteers (mean age 34, range 20–47 yrs., 2 females) underwent MRFP imaging in a 1.5T MR Scanner (Vision, Siemens/Germany) during rest and adenosine induced hyperemia (140µg/kg/min i.v.) using a multi-slice saturation recovery turbo-FLASH sequence with a TR, TE and a flip angle of 2.4 ms, 1.2 ms and 18°, a spatial resolution of 2–3 mm, a temporal resolution of 120–200 ms/image at 1 image/slice /heart beat. A contrast bolus of Gd-DTPA 0.02 mmol/l was given during image acquisition. The perfusion studies were analyzed using the ARGUS Software (Siemens Medical Systems, Iselin, NJ) to create regional signal intensity (SI) curves. MBF (ml/g/min) was estimated by using a previously validated Fermi-model of constrained deconvolution (4). MBF was determined in four myocardial regions (anterior, lateral, posterior, septal) in a mid left ventricular short axis position. MBF was corrected for the pressure-rate product (PRP) using the formula MBF × mean patients PRP/ individual patient PRP. The perfusion reserve (PR) was determined by hyperemic/rest MBF for each myocardial region. The variability of flow between regions in individual patients was calculated as coefficient of variation (CV = standard deviation/mean MBF of the individual patient). CV is given as mean ± standard deviation (Std) and range over all volunteers.

Results: Rest and hyperemic MBF, PR and CV are shown in the table below. There was a considerable range of resting, hyperemic MBF and PR over all patients within each region. The regional in-patient variability of MBF was 22% for rest, 23% for hyperemic MBF and 35% for PR, with a maximal variability of up to 40% for rest and hyperemic MBF and up to 65% for PR. Resting MBF was significantly higher in the septal vs. the posterior region in individual patients ($p < 0.03$, paired t-test). Hyperemic MBF and PR were reduced in the septal region vs. the anterior and lateral region in individual patients ($p < 0.05$, paired t-test). In agreement with the literature, resting MBF was significantly higher ($p < 0.04$) in women; however, the number of females in our group of volunteers was small.

Conclusion: The regional blood flow variability in healthy human myocardium assessed with Magnetic Resonance First-Pass Perfusion Imaging is in agreement with previous studies using alternative techniques. Our rest and hyperemic blood flow estimates and perfusion reserve values are in excellent numerical agreement with the data derived from PET (2,5), today's gold standard of non-invasive blood flow quantification. Myocardial perfusion has a physiologic regional variability of about 20% at rest and hyperemia. In the septal wall perfusion reserve is decreased as a result of an increased resting perfusion and a decreased hyperemic perfusion.

Table

	Rest MBF		Hyperemic MBF		Perfusion Reserve	
Region (n = 52)	Mean ± Std	Range	Mean ± Std	Range	Mean ± Std	Range
Anterior	1.03 ± 0.48	0.62–2.12	4.14 ± 1.79	2.20–8.43	4.23 ± 1.15	1.74–6.16
Lateral	0.97 ± 0.40	0.51–1.97	4.29 ± 1.80	2.57–8.59	4.59 ± 1.19	2.86–6.38
Posterior	0.89 ± 0.36	0.42–1.74	3.67 ± 1.70	1.86–7.36	3.93 ± 1.16	2.37–6.81
Septal	1.05 ± 0.39§	0.66–1.75	3.42 ± 1.51#	1.74–7.66	3.50 ± 1.41#	1.25–6.98
Mean	0.98 ± 0.23		3.90 ± 0.8		4.08 ± 1.37	
CV (n = 13)	22 ± 8%	14–40%	21 ± 10%	8–39%	35 ± 18%	9–65%
Male (n = 44)	0.95 ± 0.33		3.79 ± 1.47		4.13 ± 1.34	
Female (n = 8)	1.15 ± 0.73*		4.53 ± 1.33		3.91 ± 1.63	

*$p < 0.05$ vs. male, §$p < 0.03$ vs. posterior, #$p < 0.05$ vs. anterior and lateral

34. Follow-Up of Cardiac Geometric and Functional Changes in Mice with Pressure Overload Hypertrophy by Serial In Vivo Magnetic Resonance Imaging

Frank Wiesmann,[1] Christian Ritter,[2] Charlotte Dienesch,[2] Andrea Leupold,[2] Ralf Illinger,[3] Eberhard Rommel,[4] Axel Haase,[4] Stefan Neubauer.[5] [1]*Department of Medicine, University of Wuerzburg, Wuerzburg, Germany Germany;* [2]*Department of Medicine, University of Wuerzburg, Wuerzburg, Germany Germany;* [3]*Department of Medicine, University of Wuerzburg, Wuerzburg, Germany Germany;* [4]*Institute of Physics (EP5), University of Wuerzburg, Wuerzburg, Germany Germany;* [5]*Department of Cardiovascular Medicine, John Radcliffe Hospital, Oxford, Oxford UK*

The surgical procedure of transverse aortic banding (AoB) has been used to study the consequences of pressure overload-induced left ventricular (LV) hypertrophy in transgenic mice. The purpose of this study was to investigate the morphologic and functional effects of AoB and the exact time course of ventricular remodeling processes in mice by serially performed in vivo magnetic resonance imaging (MRI).

Table

	1 week	2 weeks	4 weeks	7 weeks	13 weeks	27 weeks
LVMI Aob (mg/g)	4.9 ± 0.3*	5.5 ± 0.2*	5.8 + 0.3*	6.2 ± 0.4*	5.6 ± 0.5*	5.4 ± 0.5*
LVMI sham (mg/g)	**4.0 ± 0. 1**	**3.9 ± 0. 2**	**4,3 ± 0. 1**	**4.3 ± 0. 2**	**4.0 ± 0. 1**	**3.6 ± 0.2**
EF AoB (%)	61 ± 2	61 + 4	1 ± 5	50 ± 6*	39 ± 5*	38 ± 4*
EF sham (%)	63 ± 5	62 ± 4	60 ± 2	62 ± 3	57 ± 2	56 ± 2
ESV AoB (µl)	19.0 ± 1. 3	19.9 ± 2. 4	29.4 ± 5. 4	38.8 ± 8.8*	51.6 ± 9.1*	54.5 ± 7.5*
ESV sham (µl)	18.6 ± 2. 3	20.6 ± 2. 1	25.6 ± 2. 1	24.2 ± 1. 9	28.3 ± 1. 9	27.8 ± 2.2

Mean ± SEM; *p < 0.05 vs. sham; n = 8 for each group

C57BL/6 mice underwent transverse aortic restriction (AoB, n = 8) or were sham-operated (sham, n = 8). Changes of LV geometry and function were examined by serial MRI at 6 time points (from 1 week to 27 weeks after surgery) (see table above).

From 1 week there was progressive increase of LV mass index (LVMI) in AoB. At 13 weeks, however, LVMI decreased compared to 7 weeks, possibly indicating apoptosis and cell replacement by fibrosis. Early after AoB, concentric LV hypertrophy occurred, indicated by unchanged end-systolic volume (ESV) and increased LVMI. However, after 13 weeks a significant decrease of LV ejection fraction (EF) was found in AoB, representing heart failure.

Aortic banding in mice results in early LV concentric hypertrophy with preservation of global function over several weeks. Due to remodeling processes, however, the LV is gradually dilating, resulting in excentric hypertrophy with concomittant heart failure.

35. Altered Myocardial High Energy Phosphate Metabolism in Transgenic Mice Lacking Mitochondrial Creatine Kinase

Matthias Spindler,[1] Reinhard Niebler,[2] Michael Horn,[2] Stefan Neubauer.[3] *[1]University Wuerzburg, Medizinische Klinik, Wuerzburg, Germany Germany; [2]Medizinische Klinik, Josef-Schneider-Str. 2, Wuerzburg, Germany Germany; [3]John Radcliffe Hospital, Dept of Cardiovascular Medicine, Oxford, England England, UK*

The creatine kinase (CK) enzyme system exists as a family of four isoenzymes, three located in the cytoplasm (MM-, MB- and BB-CK) and one in the mitochondria (Mito-CK). CK catalyzes the reversible transfer of the phosphoryl group between the energy reserve compound phosphocreatine (PCr) and ATP. In various animal models of heart failure as well as failure in human myocardium, alterations in the PCr/CK system have been described.

We have previously shown that in hearts of transgenic mice lacking the M-isoform of CK, the high-energy phosphate profile remained unchanged, whereas in hearts lacking both M-CK and Mito-CK (remaining total CK activity 3%) PCr/ATP ratios were significantly reduced.

To address the question whether this reduction in PCr/ATP is due to a decrease in total CK activity below a critical threshold or due to the specific loss of Mito-CK, we studied hearts with selective loss of Mito-CK (Mito-/-, remaining total CK activity 79%) using 31P NMR spectroscopy in isolated perfused hearts.

Left ventricular performance in Mito-/- hearts (n = 10) (assessed as rate-pressure product, 103 mmHg/min) was similar during baseline perfusion (34.7 ± 1.2 vs 34.8 ± 1.6), during increased workload (52.4 ± 2.9 vs 51.5 ± 3.1) and recovery (26.3 ± 2.9 vs 27.1 ± 1.2) when compared to wildtype (WT)(n = 13). PCr/ATP, however, was significantly reduced in Mito-/- compared to WT (0.91 ± 0.04* vs 1.37 ± 0.06, *p < 0.05). In parallel, there was an increase in inorganic phosphate (Pi) (Pi/ATP 0.35 ± 0.03* for Mito-/- vs 0.22 ± 0.03 for WT). Calculated free ADP concentration was also higher in Mito-/- compared to WT (174.3 ± 13.0* vs 86.9 ± 7.9 mM), whereas free energy release for ATP hydrolysis (ΔG0) was similar in both groups. Increasing workload resulted in a 25% decrease in PCr/ATP in WT as well as in Mito-/-.

Altered cardiac energetics in Mito-/- hearts demonstrate that the remaining isoenzymes MM-, MB- and BB-CK are unable to completely substitute for the loss of Mito-CK. It is therefore concluded that Mito-CK (in contrast to M-CK or a certain amount of remaining total CK activity) is critically necessary to maintain a normal high-energy phosphate profile.

36. TrueFISP Imaging of the Heart Improves the Success Rate of Automatic Contour Detection

Sven Plein,[1] Timothy Bloomer,[2] Mohan Sivananthan.[2] *[1]Leeds General Infirmary, Cardiac MRI Unit, Leeds, West Yorkshire United Kingdom; [2]Leeds General Infirmary, Cardiac MRI Unit, Leeds, West Yorkshire United Kingdom*

Introduction: With the use of cardiac MRI expected to increase in clinical practice, rapid and reliable automatic contour segmentation and calculation of basic parameters of cardiac function, such as left ventricular volumes and mass, is becoming more important. Several algorithms have been proposed for automatic contour detection of cine MRI scans and have been implemented on commercial analysis packages [1,2]. However, these algorithms remain unreliable in analysing conventional gradient echo images, in particular when image quality and blood/myocardial contrast is poor. Recently, new steady state gradient echo sequences with balanced gradients (generally known as TrueFISP or Balanced Fast Field Echo Imaging = BFFE) have been introduced for cardiac imaging. These sequences provide substantially improved blood-myocardial contrast than conventional gradient echo techniques and are less susceptible to slow blood flow artefacts. The resulting better delineation of the endocardial borders might improve the accuracy of automatic contour detection algorithms. This study compares the success rate of a commercially available automatic contour detection software in images acquired with a TrueFISP and a conventional turbo gradient echo technique.

Methods: Data sets from 16 consecutive patients were analysed. 6 had left ventricular hypertrophy, 5 had left ventricular dilatation and 5 had normal ventricular dimensions. Studies were performed on a 1.5T Philips ACS NT system with Master gradients (Philips Medical Systems, Best, The Netherlands). ECG gated, breath-hold multi-slice multiphase data sets covering the left ventricle in 10–12 short axis slices were acquired using a Turbo Gradient Echo sequence (Turbo Field Echo = TFE: TR 8.1, TE 4.9, Flip angle 35°) and a TrueFISP equivalent sequence (BFFE: TR 3.34, TE 1.67, Flip angle 55°). Slice locations

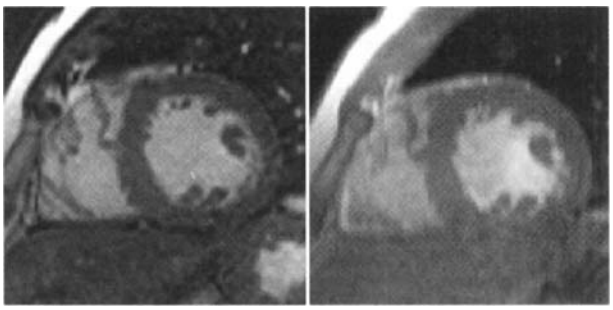

Figure 1.

and slice thickness (6mm, 4mm slice gap) were identical for both scans. All data sets were analysed offline with commercially available software and an automated contour detection option (MASS, Medis, Leiden, The Netherlands). Enddiastolic and endsystolic phases were analysed. A centre point was manually placed in the ventricular cavity and the automatic contour detection function activated to detect endo- and epicardial contours. Each image was then reviewed by an experienced observer and the contours manually corrected where they diverted from the correct position. The number of contours requiring manual correction and the extent of correction required on each contour (expressed as percentage of the circumference of the contour) was recorded and compared between the two acquisition methods.

Results: Figure 1 shows an example of corresponding short axis slices acquired with TrueFISP and TFE acquisition. A significantly lower number of endocardial contours required manual correction on the TrueFISP images (Table 1: Endo = endocardial contour, Epi = epicardial contour, ED = enddiasole, ES = endsystole). The extent of correction required was less for endocardial contours of TrueFISP images (Table 2). Epicardial contours required similar manual correction and differences between TrueFISP and TFE were not statistically significant. For both sequences, an average of almost 50% manual correction of epicardial contours was required.

Discussion: The higher blood/myocardial contrast of TrueFISP images improves automatic detection of endocardial but not epicardial contours. Less than 10% of endocardial contours required manual correction. This is acceptable for clinical practice. Epicardial contour detection was not improved and was unsuccessful in almost 50% of all epicardial contours. This indicates that contrast improvements with TrueFISP affect the epicardial contours to a lesser extent than the endocardial contours, a finding that was expected. The results further suggest that improvements in the algorithms for automatic contour detection of epicardial borders are required for routine clinical use.

Table 1

Number of Contours Requiring Manual Correction

	Endo ED (n = 119)	Epi ED (n = 119)	Endo ES (n = 96)	Epi ES (n = 96)
TrueFISP	25	90	29	84
TFE	51	95	45	82
Difference	24	5	16	2
p value	<0.0001	0.19	<0.0001	0.30

Table 2

Extent of Manual Correction per Contour (Mean in % of Contour and SD)

	Endo ED	Epi ED	Endo ES	Epi ES
TrueFISP	7.4 (19.1)	38.7 (33.6)	11.3 (21.1)	46.2 (30.2)
TFE	17.1 (25.6)	43.4 (35.3)	24.7 (31.2)	42.8 (32.3)
Difference	9.6	4.6	13.3	−3.4
p value	<0.001	0.17	<0.001	0.38

37. Development of a Canine Model of Hibernating Myocardium and Its Use to Validate Corresponding MRI Methods

Katie Lekx,[1] Frank Prato,[1] Jane Sykes,[2] Gerald Wisenberg.[3]
[1]*University of Western Ontario, Lawson Health Research Institute, London, Ontario Canada;* [2]*Lawson Health Research Institute, 268 Grosvenor St., London, Ontario Canada;* [3]*University of Western Ontario, Division of Cardiology, London, Ontario Canada*

Introduction: Coronary artery disease is the leading cause of morbidity and mortality in developed countries and extent of left ventricular dysfunction the most important prognosis determinant (1). Left ventricular dysfunction could be caused by several pathologies including myocardial infarction (MI), hibernating myocardium (HM), and stunned myocardium. Because stunned tissue has normal blood flow and will recover function, and infarcted tissue cannot be revived, these two pathologies, although important to identify, do not require intervention. However, because hibernating myocardium is defined as chronically underperfused myocardium with matched downregualation of cardiac function (2) that returns following restoration of blood flow (3), the identification of this diseased state is clinically relevant as it guides patient treatment. Since HM has been documented in patients with angina, acute MI, and congestive heart failure, a specific and sensitive means of distinguishing HM from other pathological conditions is extremely important in the clinical setting. The development of a diagnostic imaging test for HM using MRI is extremely important as the spatial resolution that is attainable is much greater with MR than the current imaging techniques.Partition coefficient (λ) of Gd-DTPA has been shown to be an accurate indicator of viable vs. infarcted myocardium (4). Infarcted regions, have increased λ compared to viable tissue due to the entry of Gd-DTPA into the once intracellular space, which is manifested as increased signal intensity on T_1-weighted MR images. Since hibernating myocytes are still viable, our hypothesis is that λ and signal intensity in these regions should be the same as normal tissue. In this preliminary study we discuss the development of a canine model of chronic hibernating myocardium and test this hypothesis.The development of our model includes stenosis of a coronary artery to the extent of causing hibernation without infarction. Then, using MRI, analyze wall motion in the LAD region, as well as a remote region, to support the presence of HM. Radioactively labeled microspheres are used to confirm reduction of blood flow at the tissue level and Gd-DTPA infused to measure *in vivo* λ.

Methods: Five female beagles were used for the initial stages of this study. Two died prematurely, two were used for selection of balloon occluders/inflation necessary and correlation of flow probe measurements to microsphere blood flow measurements, and the other studied for 1 week before sacrifice. Two sections of the left anterior descending (LAD) coronary artery were dissected free and a Transonic Doppler ultrasound flow probe and balloon occluder were placed around these regions of the vessel. Prior to inflation of the balloon, microspheres were injected into the atrium for baseline measurement of regional myocardial blood flow. The balloon occluder was then inflated until blood flow (measured by the flow probe) was reduced to about 20% of baseline blood flow. Microspheres were injected again 15 minutes after the stenosis. All imaging was performed on a whole-body Siemens Vision 1.5T MR system (Siemens, Germany). Baseline imaging was performed

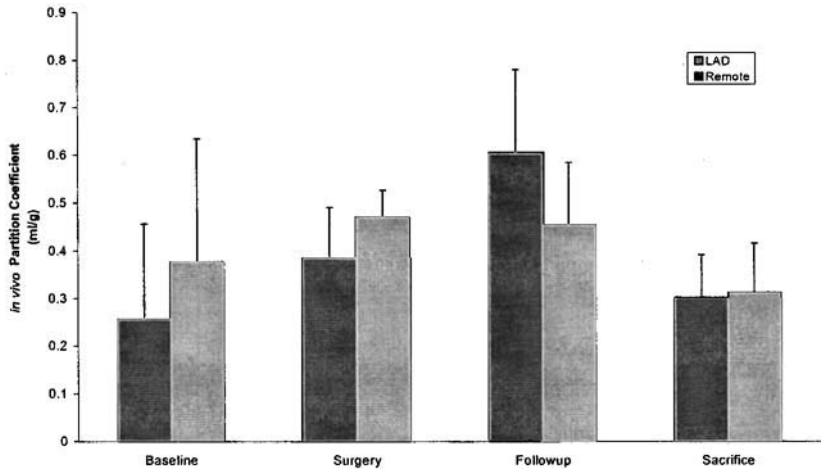

Figure 1. *In vivo* partition coefficient (mean ± SD) of Gd-DTPA in anterior and remote tissue at each time point during the experiment. No significant difference seen between the different tissue types at any time point.

prior to, day of, 2 days after and 7 days after surgery. At each imaging session Gd-DTPA was administered using a bolus followed by a constant infusion (5). Saturation recovery turboFLASH images of 4–6 image positions (srTFL) were acquired pre- and post-contrast in order to quantify λ *in vivo* (4,6). Cine MR images were obtained as a measure of wall thickening (WT) index [WT end systole minus WT end diastole normalized by WT end diastole] and ejection fraction (EF). Regional blood flow (using microspheres) was measured just prior to sacrifice, then the animals were sacrificed and the heart excised. The myocardial tissue was then sectioned and counted for radioactivity to determine myocardial blood flow.

Results: Initial experiments determined an 80% reduction in blood flow necessary to cause contractility dysfunction/HM. Flow, measured by the flow probe, at baseline was 12 ml/min, and was reduced to 3 ml/min. An immediate hyperemic effect was noted, where blood flow increased by 225%. This hyperemic response subsided within seconds after reaching peak, and settled back down to approximately baseline or slightly higher. Microsphere blood flow measurements revealed increased blood flow 15 min. after stenosis and severely reduced blood flow in LAD regions at sacrifice as compared to baseline.Partition coefficient values at each time point in anterior and remote tissues are shown in Fig. 1. No significance difference was seen between the separate tissue types at each time point.In the region of the LAD, there was a 4.6% decrease in WTI following surgery, 34.8% decrease after 2 days, and 81.3% decrease after 1 week compared to baseline WT. In remote regions, there was a 231.2% increase following surgery, 38.9% increase after 2 days, and 32.16% increase after 1 week. EF values were 45.4%, 53.1%, 42.4%, and 23.5% at baseline, surgery, follow-up, and sacrifice, respectively.

Discussion: Although only preliminary data, the results found thus far in this study suggest we have developed a canine HM model in which the extent of coronary artery occlusion is guided by an US flow probe. A progressive decrease in WTI after surgery compared to baseline, as well as a decline in EF at follow-up and sacrifice indicate contractility abnormalities. Further, λ was not increased in the LAD region compared to normal tissue, consistent with our hypothesis that this tissue is viable. In future studies we will use coronary MR to quantify stenosis degree throughout the experiment as well as extend experiment length to further evaluate possible changes in λ, which might accompany cellular remodeling. This canine model of HM will finally allow determination of the specificity of viability imaging studies in MR, as well as examining the role of MR in contractility and tissue blood flow imaging.

38. Comparison of Interstudy Reproducibility of Cardiovascular Magnetic Resonance and 2D-Echocardiography in Normals, Patients with Congestive Heart Failure and in Patients with Left Ventricular Hypertrophy

Frank Grothues,[1] Gillian Smith,[2] Nick Bellenger,[2] Peter Collins,[3] Helmut Klein,[1] Dudley Pennell.[4] [1]*Division of Cardiology, Otto-von-Guericke University, Leipziger Strasse 44, Magdeburg, Magdeburg Germany;* [2]*Cardiovascular Magnetic Resonance Unit, Royal Brompton Hospital, Sydney Street, London, London United Kingdom;* [3]*Imperial College of Science, Technology and Medicine, University of London, South Kensington, London, London United Kingdom;* [4]*Cardiovascular Magnetic Resonance Unit, Royal Brompton Hospital and Imperial College of Science, Technology and Medicine, University of London, Sydney Street, London, London United Kingdom*

Background: Fast breath-hold Cardiovascular Magnetic Resonance (CMR) is considered the gold standard in assessing left ventricular (LV) volumes, ejection fraction (EF) and mass. Excellent results for accuracy and interstudy reproducibility the latter being the most important value for serial measurement- of CMR measurements have been reported and are superior to results achieved with Echocardiography (echo), an established and clinically commonly used method for the assessment of LV function and mass. However, a direct comparison of the interstudy reproducibility of both methods in the same subjects has not to our knowledge been previously reported. We therefore investigated 60 subjects in total (20 normal volunteers, 20 patients with congestive heart failure (CHF) of ischemic or dilated cardiomyopathy origin, and 20 patients with left ventricular hypertrophy [LVH]) for comparison of interstudy reproducibility of CMR and 2D-Echocardiography.

Methods: All 60 subjects (47 male, mean age 51 ± 18 yrs) underwent two CMR and 2 echo studies with a short interval between each study and between each technique. For CMR, a stack of contiguous cine gradient echo short axis cines was acquired and end-diastolic/end-systolic epicardial and endocardial borders were traced for calculation of LV mass, LV end-diastolic volume (EDV) and LV end-systolic vol-

Table

		Interstudy Variability ± SD			% Variability ± SD		
		Normals	CHF	LVH	Normals	CHF	LVH
EDV	CMR	2.2 ± 4.3 ml	−2.3 ± 7.6 ml	0.4 ± 7.3 ml	2.8 ± 1.9*	3.0 ± 1.9*	3.8 ± 2.4*
	Echo	2.8 ± 6.4 ml	−2.7 ± 17.6 ml	2.6 ± 13.9 ml	4.8 ± 4. 0	6.1 ± 5. 6	6.3 ± 6.0
ESV	*CMR*	1.5 ± 2.8 ml	−1.6 ± 7.4 ml	−0.7 ± 4.6 ml	6.3 ± 4.9**	4.1 ± 4.0*	7.7 ± 5.3*
	Echo	0.6 ± 7.0 ml	−2.6 ± 19.7 ml	4.6 ± 12.2 ml	12.7 ± 9. 2	10.6 ± 9. 9	13.5 ± 10.3
EF	*CMR*	−0.5 ± 1.7%	0.1 ± 2.4%	0.7 ± 2.2%	2.2 ± 1.0***	6.0 ± 4.5*	3.0 ± 1.7**
	Echo	0.5 ± 5.6%	0.1 ± 7.0%	−1.5 ± 5.9%	7.2 ± 5. 6	12.7 ± 12. 7	8.4 ± 6.5
Mass	*CMR*	−1.1 ± 4.2 g	0.7 ± 9.6 g	−2.4 ± 8.4 g	2.3 ± 1.7***	3.8 ± 2.7**	2.8 ± 2.4**
	Echo	11.6 ± 15.9 g	4.1 ± 30.4 g	10.5 ± 26.9 g	10.7 ± 9. 2	11.3 ± 9. 9	10.5 ± 9.0

ume (ESV), from which LV stroke volume and LVEF could be derived. For echo, the epicardial and endocardial boundaries of the left ventricle at end-diastole were traced in a short axis view at mid-papillary muscle level to obtain epicardial and endocardial area. From this LV mass was calculated using the previously described 5/6 (area × length) method. Left ventricular volumes were calculated according to biplane Simpson's rule after tracing the end-diastolic and end-systolic endocardial boundaries in the apical 4- and 2-chamber view.

Results: The interstudy variability (mean difference between measurements) and percentage variability of the measured parameters for CMR and Echo for each subgroup are shown in the table above. For all the investigated parameters in each subgroup, the interstudy percentage variability was significantly lower with CMR compared to Echocardiography (*$p < 0.05$, **$p < 0.01$, ***$p < 0.001$). The smaller standard deviation (SD) of the interstudy variability with CMR results in considerably lower sample sizes required by CMR versus Echo. Based on these data, to show a 10 ml change in EDV and ESV and a 3% absolute change in EF in a study population with heart failure would require 13/12/14 patients with CMR versus 66/82/115 patients with echo (power of 90%, alpha error of 0.05). To show a 10 g change in mass in patients with LVH one would only need 15 patients with CMR versus 152 patients with echo (same power/alpha error). The percentage reduction in sample size for these examples varies from 80 to 90%.

Conclusion: In a direct head to head comparison, CMR showed excellent interstudy reproducibility in normal subjects, and in patients with congestive heart failure and LVH with significantly lower percentage variation, but also lower SD of the differences compared with 2D-echo. The latter determines sample size in studies. These results have important implications for longitudinal follow-up in individual patients as well as for the planning of clinical trials, in which serial measurements of left ventricular function and mass are desired, as smaller sample sizes can be used with CMR for the same study power.

39. Real-Time Magnetic Resonance Image Acquisition During Dobutamine Stress for the Detection of Left Ventricular Wall Motion Abnormalities in Patients with Coronary Artery Disease

Simon Schalla,[1] Christoph Klein,[1] Eckart Fleck,[1] Axel Bornstedt,[1] Ingo Paetsch,[1] Bernhard Schnackenburg,[2] Hans Lehmkuhl,[1] Eike Nagel.[1] [1]*German Heart Institute and Charité Campus Virchow, Augustenburger Platz 1, Berlin, Berlin Germany;* [2]*Philips Medical Systems, Hamburg, Hamburg, Germany*

Background: Magnetic resonance (MR) imaging has been shown to be superior to dobutamine stress echocardiography for the detection of left ventricular wall motion abnormalities. A shortcoming of magnetic resonance imaging in comparison with echocardiography is the need to acquire images during several cardiac cycles which prohibits the assessment of new onset of wall motion abnormalities in real-time and requires breath holding. Purpose of this study was to compare real-time imaging with standard MR imaging for the detection of wall motion abnormalities.

Methods: In 22 patients with coronary artery disease left ventricular wall motion was examined at rest and during increasing doses of dobutamine (up to 40μg/kg + atropine) using echo planar imaging (TE 5.6 ms; TR 1 heartbeat; Flip angle 30; spatial resolution 1.3 × 2.6 mm; temporal resolution 30ms) and a new real-time imaging technique (TE 6.8 ms; TR 16.5 ms; Flip angle 20; spatial resolution 2.2 × 4.4 mm; temporal resolution 62 ms). Wall motion abnormalities for each perfusion territory were determined visually. Coronary angiography was performed after dobutamine stress MR examinations in all patients.

Results: Sensitivity and specificity for real-time in comparison with breath-hold MR imaging were 100%/98% at rest and 97%/97% at maximum dobutamine stress. In comparison with coronary angiography sensitivity and specificity were 87.5%/83.3% for echo planar imaging and 81.3%/83.3% for real-time MR imaging.

Conclusions: Real-time imaging of left ventricular wall motion is possible under stress conditions and allows an accurate detection of wall motion abnormalities. This technique can be used for an online analysis of wall motion at pharmacological or physical stress.

40. Magnetization Transfer Contrast of In Vivo Normal and Infarcted Myocardium of Sheep

Qing Yuan,[1] James Pilla,[2] Daniel Brockman,[3] Victor Ferrari,[3] Robert Greenman,[3] Michael Acker,[3] Leon Axel.[4] [1]*University of Pennsylvania, 213 Jackson Ave, Lamsdowne, PA USA;* [2]*University of Pennsylvania, Philadelphia, PA USA;* [3]*University of Pennsylvania, Philadelphia, PA USA;* [4]*University of Pennsylvania, Department of Radiology, Philadelphia, PA USA*

Introduction: Magnetization transfer (MT) imaging offers a unique quantitative method for tissue characterization of myocardium [1]. The MT contrast of myocardium may reveal ischemic or infarcted region in animals and in humans [2,3]. However, most previous animal studies have been ex vivo. In this study, we examined the normal and infarcted myocardium in a sheep infarct model in vivo, using an MT-weighted fast gradient-echo technique.

Methods: A cardiac- and respiratory-gated segmented k-space fast gradient-echo (FGRE) sequence with an MT conditioning pulse was developed and implemented on a 1.5T whole-body MRI scanner (Signa, GE Medical Systems). The non-selective MT pulse (a 14 ms long sinc pulse with 1500 degree flip angle) was applied at every cardiac phase to reach a steady state of MT saturation. The pulse sequence was trig-

gered by the cardiac signal but data acquisition was only allowed during expiration, as determined by a selected threshold.

Four sheep with chronic infarct (two months after the ligation of the diagonal branches of the left anterior descending coronary artery) were studied with cardiac phased-array coils. The left ventricular pressure was monitored and sent to a custom-built cardiac gating system [4] to provide the cardiac trigger. A respiratory signal was generated using a bellows. Short-axis cardiac images were acquired without MT contrast as a reference. Imaging with MT contrast was then repeated with the off-resonance frequency of the MT pulse varied over a range of 0 to 50 kHz. MT contrast of two myocardial regions, septum at basal-LV (normal) and infarct at mid-LV, were measured as the percentage ratio of the signal intensity of the saturation image (Ms) over the intensity of the reference image (Mo). MT ratio (Ms/Mo) was then plotted versus the offset frequency of the MT pulse to obtain the magnetization transfer Z spectrum. A non-exchanging two-pool system model consisting of free water and macromolecule-associated water components was proposed as a sum of two Lorentzian functions to analyze the MT effect:

$$Ms/Mo = Na * f^2/(f^2 + Wa^2) + Nb * f^2/(f^2 + Wb^2)$$

where f is the frequency offset of the MT pulse, Wa and Wb are the widths at half maximum of the A-pool and B-pool, and Na and Nb are the population fractions of the A-pool and B-pool, respectively. Magnetization transfer Z spectra obtained from MRI measurements were fitted to the above model using a non-linear least-square fitting routine in IDL (RSI, Boulder, CO). All statistical analyses of the fitted parameters were conducted using a repeated measures ANOVA with the SuperANOVA software package (Abacus Concepts, Inc., Berkeley, CA).

Results: The chronic infarct (2 months) demonstrates greater signal intensity, i.e., a decreased MT suppression on the MT contrast image (Figure). The ex vivo heart tissue specimen corresponding to the MR image shows scar tissue at the same region. The chronic infarct also exhibits a greater Ms/Mo and narrower line width of the MT Z spectrum compared to the remote normal myocardium. Theoretical analysis of the Z spectrum has revealed a relative increase of free water pool (Na) and a decrease of macromolecule water pool (Nb) in the infarct region. The narrower line widths of both components (Wa and Wb) are due to the corresponding decrease of T1/T2 in infarct (see Table).

Discussion/Conclusion: Using an in vivo sheep model of myocardial infarction, we have demonstrated an increase of Ms/Mo in chronic infarct (2 months) compared to normal myocardium. This result is consistent with other studies of chronic infarct (4 weeks) of ex vivo rat myocardium [2] and human myocardial scar [3]. Future correlation study with histopathology will give us more insight as to the mechanism of the MT characterization changes and a better understanding of the evolution of myocardial infarction.

In conclusion, MT technique can aid in chararcterizing chronic infarctions in vivo, which may be a useful tool for clinical diagnosis of myocardial infarction.

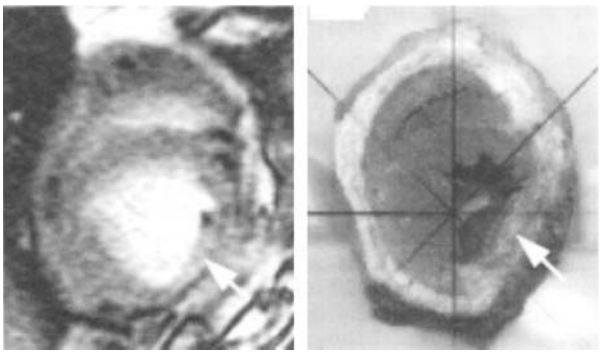

Figure. MT image obtained from a sheep with a 2-month old infarct (left) and the corresponding scanned image of heart tissue specimen (right).

Table

Fitting Parameters of MT Z Spectra Using a Two-Pool Model

	Na	Nb	Wa(kHz)	Wb(kHz)
Normal	0.54 ± 0.02	0.43 ± 0.04	0.37 ± 0.09+	8.41 ± 2.05
Infarct	0.60 ± 0.05	0.29 ± 0.07	0.21 ± 0.04+	4.58 ± 1.44
p value	0.051	0.055	0.017	0.093

References

1. Wolff SD, Balaban RS. Radiology, 1994; 192:593–599.
2. Scholz TD, et al. MRM, 1995; 33:178–184.
3. Buchthal SD, et al. J Cardiovascular MR. 1999; 1:97.
4. Pilla JJ et al. ASAIO J. 1999; 45:131.

41. Gender Differences in Left Ventricular Anatomy: The Framingham Heart Pilot MRI Study

Carol Salton,[1] Christopher O'Donnell,[2] Michael Chuang,[1] Kraig Kissinger,[1] Martin Larson,[2] Robert Edelman,[3] Daniel Levy,[2] Warren Manning.[4] *[1]Beth Israel Deaconess Medical Center, 330 Brookline Ave, Boston, MA USA; [2]NHLBI's Framingham Heart Study, 5 Thurber St, Framingham, MA USA; [3]Beth Israel Deaconess Medical Center, 330 Brookline Ave AN-234, Boston, Massachusetts United States; [4]Beth Israel Deaconess Medical Center, 330 Brookline Avenue, Boston, Massachusetts United States*

Purpose: Elevated left ventricular mass (LVM) is an independent predictor of morbidity and mortality. Similarly, LV end-diastolic volume (EDV) provides important prognostic information and may be useful for assessing the effect of therapy. MRI allows noninvasive determination of cardiac anatomy with high accuracy, but normal adult values have not been reported in a longitudinally followed cohort of both genders.

Methods and Subjects: 247 adult participants from the offspring cohort of the Framingham Heart Study who were free of symptomatic cardiovascular disease were recruited based on equal distribution of gender (119M, 128F), decade age, and quintile of Framingham Coronary Risk Score. The mean (±SD) age of the subjects was 59.5 ± 9.0 years (range 36–78 years).

Imaging and Analysis: MRI was performed on a 1.5-T system (Gyroscan ACS/NT, Philips Medical Systems, Best, NL) using a TFE-EPI breathhold cine sequence with a cardiac array coil for RF signal reception. Eight to 10 contiguous slices in the cardiac short-axis orientation were used to encompass the left ventricle during end-tidal breathholds. Image analysis was performed on an EasyScil workstation (Philips) by a single expert observer. Endocardial and epicardial borders were manually segmented from end-diastolic images and volumes were computed using a summation of disks method. LV EDV and LVM were also indexed by height (m) and body surface area (BSA, m2) using subject-reported height and weight. Simple t-tests were used for comparison between genders within each age group.

Results: Unless otherwise specified, results are summarized as mean ± SD. Height and weight did not differ between age groups within the same gender, but men were taller (1.77 ± 0.06 vs 1.62 ± 0.06 m) and heavier (88 ± 13 vs 70 ± 15 kg) women, $p < 0.001$ both.

Table

	LVM (g)	LVM/Ht (g/m)	LVM/BSA (g/m^2)	EDV (ml)	EDV/Ht (ml/m)	EDV/BSA (ml/m^2)
F:36–49	119 ± 14**	73 ± 8**	67 ± 5*	96 ± 13*	59 ± 8	54 ± 6
M:36–49	167 ± 38	94 ± 21	81 ± 17	118 ± 21	66 ± 12	57 ± 10
F:50–59	107 ± 18**	66 ± 10**	62 ± 7**	85 ± 14**	53 ± 8**	49 ± 7**
M:50–59	156 ± 23	88 ± 13	76 ± 11	117 ± 23	66 ± 12	56 ± 11
F:60–69	110 ± 26**	68 ± 16**	63 ± 13**	84 ± 23**	52 ± 14**	48 ± 11*
M:60–69	153 ± 26	86 ± 14	75 ± 12	108 ± 18	60 ± 10	53 ± 9
F:70–79	103 ± 17**	65 ± 11**	60 ± 10**	77 ± 16**	48 ± 10**	45 ± 10
M:70–79	153 ± 31	87 ± 18	76 ± 14	101 ± 22	58 ± 12	50 ± 9

**$p < 0.01$ vs men, *$p < 0.05$ vs men

LVM was significantly greater in men (157 ± 28 g) than women (108 ± 21 g), $p < 0.001$; this difference was seen in each age group (see table above) and persisted when LV was indexed to height or BSA.

EDV was significantly greater in men (112 ± 22 ml) than women (84 ± 18 ml), $p < 0.001$. Greater EDV with male sex was seen in all age groups, and persisted when indexed to height or BSA.

Conclusion: In this large series from a closely followed cohort, we defined the normal range of LV anatomy based on gender and age, normalized by height and BSA.

42. Clinical Myocardial 31P MRS Studies at 4.1T

William Evanochko,[1] Jan A. den Hollander,[2] Steven D. Buchthal,[3] Ronald M. Razmi,[4] Gerald Pohost.[5] *[1]University of Alabama at Birmingham, 828 8th Court S.CNIR(205) 934-9450, Birmingham, Alabama United States; [2]UAB, Birmingham, AL USA; [3]UAB, 828 8th Ct S, Birmingham, AL USA; [4]UAB, CVMR, Birmingham, AL USA; [5]University of Alabama at Birmingham, 828 8th Court South, Birmingham, Alabama United States*

The use of 31P MRS as a clinical tool to assess myocardial energetics is becoming a reality. For example, studies have shown the importance of the 31P MRS stress test in MI patients, women's ischemia syndrome, and heart transplantation [1–3]. To date, all of these studies have been conducted at 1.5T. We report here for the first time results obtained at the ultra-high field of 4.1T involving cardiac patients. Patient are being studied from two populations, those whom have had a recent MI and those with congestive heart failure. The 4.1T interrogates much smaller voxels than those reported at 1.5T (14 vs. ~50cc). The 31P MRS examination was conducted on a 1 m bore, 4.1T research magnet equipped with a new Bruker AVANCE console. Proton scout images were obtained using a 20 cm surface coil tuned to 174.86 MHz placed on the chest of the supine subject. Two orthogonal vials of "doped" water are taped in place in the middle of this coil for alignment purposes for the subsequent placement of a 10 cm 31P receive-only surface coil tuned to 70.79 MHz for 31P data acquisition. A dedicated birdcage body coil tuned to 70.79 MHz driven in the linear mode is used for RF excitation. The 3D 31P MRSI data sets were acquired with a TR = 75 ms; a flip angle of 12 degrees, a matrix size = 22 × 22 × 22 and a FOV of 243 cm. Rewinder gradients and a crusher gradient were used with RF phase spoiling. A total of 10,648 phase encodes were collected in 50¼ minutes with spherical gaussian weighting in k-space (FWHM = 10). This approach corresponded to an actual voxel size of 13.8 cc. The maximum number of acquisitions is 32 for the k = 0 profile. The 4D data set is processed without windowing in k-space, but with Lorentz-gauss windowing in the time domain. The data sets are divided into 10 slices for display purposes. Quantitation is done by fitting in the time-domain, after Fourier transformation in k-space only. Recent myocardial infarction displayed decreases in PCr/ATP compared to nonischemic regions of the same heart (PCr/ATP 0.76 vs. 1.60). In summary, the data collected at 4.1T are superior to those at 1.5T and should provide added advantage when interrogating transmural distributions of P-31 metabolites and performing the P-31 MRS stress test.

43. Impact of Navigator Timing on Image Quality in Navigator-Gated and Real-Time Motion Corrected Free-Breathing 3D Sub-millimeter Coronary MRA

Elmar Spuentrup,[1] Rene M Botnar,[1] Kraig V Kissinger,[1] Warren Manning,[2] Matthias Stuber.[3] *[1]Beth Israel Deaconess Medical Center, 330 Brookline Avenue, Boston, MA USA; [2]Beth Israel Deaconess Medical Center, Cardiovascular Division, Boston, Massachusetts United States; [3]Beth Israel Deaconess Medical Center, 330 Brookline Ave, Boston, Massachusetts United States*

Introduction: Three-dimensional free-breathing coronary MRA has been successfully acquired using navigator technology and real-time motion correction for the suppression of respiratory motion artifacts. While studies of navigator gating window and navigator localization have been reported, the impact of navigator timing, remains to be defined. Recently, increased image spatial resolution in the sub-millimeter range became feasible (1,2) and may require improved navigator accuracy. We therefore sought to investigate the impact of navigator timing (time delay between navigator and imaging part of the sequence = navigator time delay) on variable image spatial resolution including new ultra-fast navigator technology.

Materials and Methods: Navigator-gated and real-time motion corrected free-breathing double-oblique 3D coronary MRA was applied in 10 healthy adult subjects on a 1.5T ACS-NT scanner (Philips, Best, The Netherlands) using a 5-element cardiac synergy-coil and vector-ECG triggering. The sequence parameters of the segmented k-space 3D sequence included 8 excitation/R-R interval, TR 7.9 ms, TE 2.2 ms, five 3.0 mm thick slices interpolated (zero-filling) to 10 1.5 mm slices. A T2 magnetization preparation (3) and a fat saturation was used for contrast enhancement. Identical images of the RCA with variable image spatial resolutions (in-plane 1.4 × 1.4 mm and 0.7 × 0.7 mm) were acquired. For each of those acquisitions two different navigator timings, one with a minimal (20ms) navigator time delay and one with a prolonged (100ms) navigator time delay, resulting in 4 sequences in each volunteer. A diaphragmatic navigator with an 8mm gating window and with real-time motion correction (1) was used for all sequences. Objective image quality parameters including vessel sharpness (2) and con-

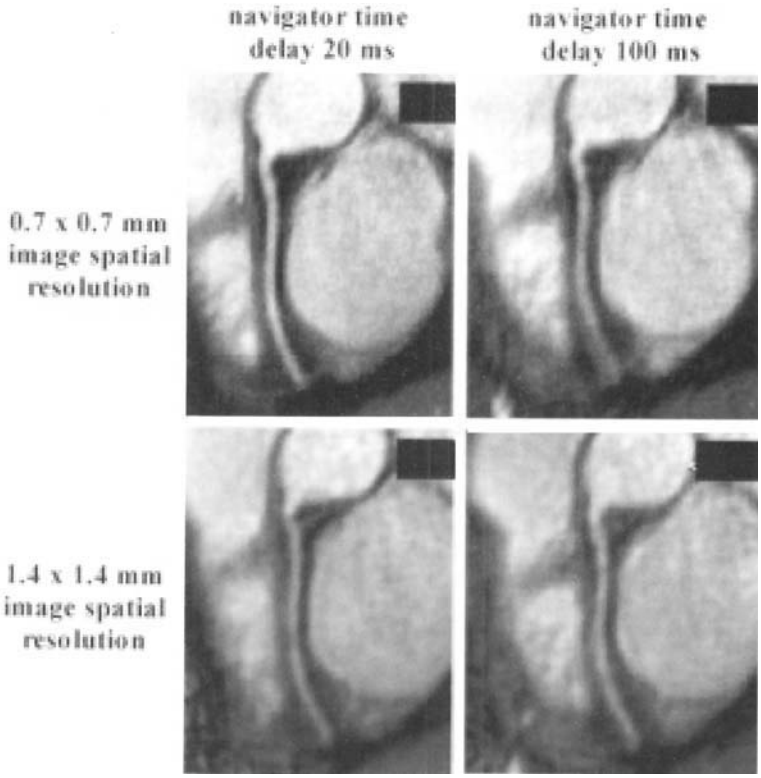

Figure 1. Free-breathing 3D coronary MRA in a healthy adult subject. In the sub-millimeter image spatial resolution (0.7 × 0.7 mm), superior image quality is seen in the images acquired with the minimal (20ms) navigator time delay.

Table

Vessel Sharpness (VS), CNR and Image Quality Score for the Two Investigated Image Spatial Resolutions (in-plane 0.7 × 0.7 and 1.4 × 1.4 mm), Each Acquired with a Minimally Short (20ms) and a Prolonged (100ms) Navigator Time Delay

	VS 20ms	VS 100ms	CNR 20ms	CNR 100ms	Quality 20ms	Quality 100ms	p-value
0.7 × 0.7 mm	0.55 ± 0.05	0.42 ± 0.08	6.7 ± 1.3	4.2 ± 1.2	3.9 ± 1.3	2.7 ± 1.1	<0.01
1.4 × 1.4 mm	0.39 ± 0.06	0.39 ± 0.08	6.1 ± 1.6	5.6 ± 1.4	2.5 ± 0.81	2.4 ± 0.66	n.s.

trast-to-noise ratio (CNR) as well as subjective image quality scores (1 (coronary non visible)–6 (excellent image quality), by two blinded observers) were subsequently assessed and compared.

Results: In navigator-gated and real-time motion corrected submillimeter coronary MRA (in-plane 0.7x0.7mm) superior image quality was found using a minimal (20ms) navigator time delay when compared with images acquired with a prolonged (100ms) navigator time delay. This was consistently found for the objective parameters vessel sharpness and CNR as well as for the image quality score (Table and Figure, $p < 0.01$). For the lower spatial image resolution (in-plane 1.4 × 1.4 mm) no significant differences were found (Table and Figure, p = n.s. in any parameter).

Conclusion: In navigator-gated and real-time motion corrected free-breathing 3D sub-millimeter coronary MRA, a minimal navigator time delay (20ms) is of importance. This has to be taken into account for sequence design and the relative position of the navigator with respect to the pre-pulses and the imaging part of the sequence. For lower image spatial resolution, navigator timing had only minor impact on image quality.

44. Improved Accuracy of Inflow Independent Functional Cardiac MR Imaging for the Quantification of Left Ventricular Volumes and Function Using Geometric Models

Holger Thiele,[1] Ingo Paetsch,[2] Axel Bornstedt,[2] Bernhard Schnackenburg,[3] Olaf Grebe,[2] Eike Nagel,[2] Eckart Fleck.[2] [1]*University of Leipzig, Heart Center Leipzig, Russenstr. 19, Leipzig, Saxonia Germany;* [2]*German Heart Institute and Charité, Augustenburger Platz 1, Berlin, Berlin Germany;* [3]*Philips Medical Systems, Augustenburger Platz 1, Berlin, Berlin Germany*

Background: Using 3-dimensional data sets MRI is an excellent method for evaluation of ventricular volumes and ejection fraction (EF). How-

Table

	TFE	TFE	SSFP	SSFP
	r	MD (%)	r	MD (%)
MSR	0.98	7.2	0.98	7.0
HCM	0.96	7.9	0.98	7.0
BPEM	0.75	20.6	0.97	8.2
SPEM (4-CH)	0.76	30.2	0.96	11.4
SPEM (2-CH)	0.71	15.9	0.94	11.3
TM	0.82	26.6	0.88	16.2

ever, data acquisition and processing is time-consuming and could be reduced using geometric models. The accuracy of these models is highly dependent on the determination of the endocardial border, which can be significantly improved by the use of steady-state free precession (SSFP) techniques in comparison to standard turbo gradient echo techniques (TFE).

Methods: In 25 patients cardiac cine loops of the heart in 3-dimensional short and horizontal long axis planes were acquired during single breath hold using TFE (TE/TR/flip: 1.9, 5.0, 25) and compared with SSFP (TE/TR/flip: 1.2, 3.2, 60) using a 1.5 Tesla MR tomograph (ACS NT, Philips, The Netherlands). Left ventricular volumes and ejection fractions were calculated with various geometric models for TFE and SSFP.

Results: Correlation (r) and mean relative difference (MD) of EF for various geometric models in comparison to a 3-dimensional data set are shown in the Table.

MSR = modified Simpson Rule; HCM = hemisphere cylinder model; BPEM = biplane ellipsoid model; SPEM = single plane ellipsoid model; TM = Teichholz model; CH = chamber

Conclusions: Significant differences between models using the long axes in comparison with the 3-dimensional data set were found for TFE but not for SSFP. The improved endocardial border delineation of SSFP in comparison with TFE allows a more accurate and reproducible use of geometric models. This may increase clinical utility of MR imaging by shorter acquisition and processing times.

45. Patient-Specific Diastolic Acquisition Is Required for Right Coronary MR Vessel Wall Imaging

Won Yong Kim,[1] Rene M. Botnar,[2] Matthias Stuber,[3] Kraig V. Kissinger,[2] Warren Manning.[4] [1]*MR-Center, Department of Cardiology and Institute of Experimental Clinical Research, Skejby Hospital, Aarhus, Denmark, Beth Israel Deaconess Medical Center, Boston, MA USA;* [2]*Beth Israel Deaconess Medical Center, Division of Cardiology, Boston, MA USA;* [3]*Beth Israel Deaconess Medical Center, Division of Cardiology, Boston, Massachusetts United States;* [4]*Beth Israel Deaconess Medical Center, Division of Cardiology, Boston, MA USA*

Introduction: Magnetic resonance(MR) offers great potential for diagnosis of coronary artery disease (1). Recently, MR coronary vessel wall imaging has been reported (2–4), which could potentially assess local atherosclerotic plaque burden and composition. One major challenge for coronary wall imaging is to minimize artifacts due to intrinsic cardiac motion. During middiastolic diastasis coronary artery motion is minimal. The right coronary artery (RCA) shows the most extensive motion and has a shorter rest period compared to the left coronary artery (5,6). The purpose of this study was to investigate the importance of optimal/patient-specific timing of MR acquisition for RCA vessel wall imaging and angiograms.

Methods: Fifteen healthy adults (age 21–55 years) subjects were studied. The MRI examination was performed on a 1.5 Tesla system (Gyroscan ACS-NT 15, Philips Medical Systems, Best, The Netherlands). RCA motion was assessed using breathhold cine acquisition oriented perpendicular to the proximal portion of the vessel. RCA imaging was subsequently performed during the visually apparent middiastolic rest period (defined by inplane motion <4cm/s) and during early diastole using a previously reported algorithm ((R-R interval-350 ms) × 0.3 + 350 ms) (7).

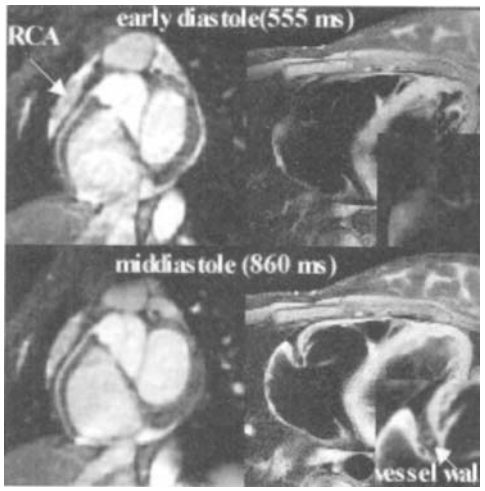

Figure 1. Middiastolic image acquisition (lower row) results in sharper vessel definition in comparison to early diastolic acquisition (upper row). RCA wall was not visible for early diastolic image acquisition.

MR angiography of the RCA was performed with a free-breathing, navigator gated 3D TFE/EPI scan (TR = 16 ms, TE = 5.1 ms, flip angle = 40°, EPI factor = 7, 1 NSA, FOV = 340 mm, scan matrix = 256 × 177, inplane resolution = 1.3 × 1.9 mm, slice thickness 3 mm) (8). RCA vessel wall imaging was planned perpendicular to the proximal RCA. A dual inversion recovery (Dual IR) prepulse suppressed signal from coronary blood flow.To enhance definition of the outer RCA wall, a frequency selective fat suppression prepulse was applied. Fast spin echo (TSE) was used for wall imaging (TR = 2 RR intervals, 4 NSA, TE 25 ms, echo train length 8, echo spacing 6.4 ms,acquisition window 51 ms, slice thickness 5 mm, FOV 340 × 170 mm, acquisition matrix 512 × 256, inplane resolution 0.66 × 0.66 mm).

Results: The center of the middiastolic rest period was linearly related to the cardiac R-R interval ($y = 0.58x + 181.94$, $R^2 = 0.87$). The duration of the rest period was dependent of the R-R interval showing a sigmoidal shape. For heart rates lower than 60 beats/minute, the duration of the rest period was >200 ms, which was wider than the 95% confidence intervals for the linear prediction. In the MR angiogram (see figure, left panels), vessel definition was improved ($p < 0.001$) with the optimal mid-diastolic image acquisition in comparison to early diastolic image acquisition. The optimal diastolic image acquisition showed a well-defined RCA vessel wall (see figure,right panels) in 11 out of the 15 subjects (73%), while none were seen with early diastolic imaging.

Conclusions: Elimination of cardiac motion is of critical importance for submillimeter vessel wall imaging using a Dual IR TSE sequence. For successful imaging of the RCA wall, a cardiac cine scan perpendicular to the proximal RCA is recommended to locate the patient specific optimal middiastolic rest period. For heart rates lower than 60 beats/minute rest periods are relatively long and allow the optimal timing to be linearly predicted.

References
1. Manning WJ. NEJM 1993; 328:828–832
2. Meyer CH. ISMRM 1998:15
3. Fayad ZA. Circ 2000; 102:506–510
4. Botnar RM. Circ (in press)
5. Hofman MB. JMRI 1998; 8:568–576
6. Wang Y. Radiology 1999; 213:751–8
7. Stuber M. Radiology 1999; 212:579–587
8. Botnar RM. JMRI 1999; 10:821–5

46. Contrast-Enhanced 3D Coronary Artery Angiography Capable of 1.0 × 1.0 × 2.0 mm³ Resolution Within a Single Breath-Hold

Steven Shea,[1] Richard McCarthy,[2] Gerhard Laub,[3] Vibhas Deshpande,[4] John Finn,[5] Debiao Li.[6] [1]*Northwestern University, Department of Radiology, Chicago, IL United States;* [2]*Northwestern University, Department of Radiology, Chicago, IL United States of America;* [3]*Siemens Medical Systems, 448 E. Ontario Street, Chicago, IL United States;* [4]*Northwestern University, Department of Radiology, Chicago, Illinois United States;* [5]*Northwestern University, Morton Building\5-681\310 E. Superior Street, Chicago, Illinois United States;* [6]*Northwestern University, Department of Radiology, Chicago, IL United States*

Introduction: Contrast-enhanced, volume targeted breath-hold imaging has been shown to be an effective technique to image the coronary arteries [1]. One of the major problems of 3D breath-hold coronary artery imaging is the limited spatial resolution because of the constraint of the imaging time. The voxel sizes of previous studies with 3D breath-hold coronary imaging ranged between 1.6 × 1.0 × 4.0 and 1.9 × 1.2 × 2.0 mm³ [1–5]. It is necessary to improve the resolution for the reliable clinical application of the technique. The goal of the current work was to achieve a spatial resolution of 1.0 × 1.0 × 2.0 mm³ within a single breath-hold by taking various measures. The question was whether there is adequate signal-to-noise ratio (SNR) and contrast-to-noise (CNR).

Methods: The basic data acquisition sequence was an inversion recovery (IR) prepared, segmented 3D FLASH. Several measures were taken to improve the spatial resolution. Partial k-space coverage (75%) and asymmetric sampling (1:2 between data on one side of the echo to the other side) [1] was used in both the readout and phase encoding directions to reduce the TR and the number of lines collected, respectively. The minimal TR/TE available on the high-performance gradient sub-system (Sonata, Siemens Medical Systems, 40 mT/m, slew rate: 200 mT/m/ms) was used to maximize the speed of data acquisition. The data acquisition window per cardiac cycle was maximized by observing the cardiac motion in images collected using a True-FISP cine sequence with a temporal resolution of 21 ms [6].

Normal volunteers (n = 5) were studied using the technique. For each subject, a segmented echo-planar volume localizer was used to cover the entire heart in a single breath-hold. Multi-planar reconstructions (MPR) of this data were used to determine the optimal imaging plane for the left or right proximal coronary arteries. 40 ml MR contrast agent (Prohance, Bracco) was injected, followed by a first-pass, 3D breath-hold, IR-FLASH scan to cover either the left or right coronary artery.

Imaging parameters included: TR/TE = 2.9/1.7 ms, inversion time = 300 ms, flip angle = 20°, FOV = 163–225 × 260–300 mm² number of lines per cardiac cycle = 41–51, matrix size = 136–204 × 256, slab thickness = 20–24 mm, number of partitions = 10–12 (20–24 with sinc-interpolation), imaging time = 24–36 heartbeats.

Results: The SNR and CNR were 9.0 ± 2.5 and 6.3 ± 3.0, respectively, in post-contrast images, and represented 37% and 98% improvements over pre-contrast images that did not have IR-preparation. Long segments of the left and right coronary arteries were clearly depicted. The boundary definition was clearly improved as compared to previous studies with lower resolutions. The SNR in distal portions of coronary arteries was relatively low, hindered their reliable definition.

Conclusion: A contrast-enhanced 3D targeted imaging technique capable of 1.0 × 1.0 × 2.0 mm³ resolution (1.0 × 1.0 × 1.0 mm³ with interpolation) within a single breath-hold was evaluated. The resolution represents an improvement of a factor of 2–3 over previous investigations with 3D breath-hold coronary imaging. Proximal portions of coronary arteries were well defined but further improvements in SNR and CNR are required to better define distal portions. This may be possible with first-pass imaging with newly developed intravascular contrast agents.

47. Comparison of the Metabolic and Functional Effects of Isoflurane and Propofol Anaesthesia in a Canine Ischaemia/Reperfusion Model

Kerry Thompson,[1] R. Thompson,[1] Jane Sykes,[2] Gerald Wisenberg.[3] [1]*University of Western Ontario, Lawson Health Research Institute, London, Ontario Canada;* [2]*Lawson Health Research Institute, 268 Grosvenor Street, London, ON Canada;* [3]*Lawson Health Research Institute, Department of Cardiology, London, Ontario Canada*

Introduction: Using ^{31}P 2D-Chemical Shift Imaging (CSI) MRS for *in vivo* monitoring of the cardiac high-energy phosphates throughout ischaemia and reperfusion, our lab has been able to show the benefits of various drug therapies to moderate the final infarct size (1). Our current work includes the comparison of two different anaesthetics, inhalational isoflurane and intravenously infused propofol. It has been proposed that isoflurane is a cardioprotective agent during a reperfused myocardial infarction and therefore would mitigate the degree of reperfusion injury during cardiac surgery and transplantation (2). Propofol, although much more controversial, is also thought to have potential cardioprotective effects (3). To assess both metabolic and functional effects, ^{31}P CSI MRS was combined with ^{1}H cine MR imaging.

Methods: In a group of 13 dogs, general anaesthesia was induced intravenously with propofol and maintained with a constant infusion of propofol at a rate of 0.6–1.0 ml/min/kg. A second group of 10 dogs were also induced with propofol, however anaesthesia was maintained with isoflurane 1–2% prior to any data collection. Each dog was then subjected to a 2-hour occlusion of the left anterior descending coronary artery, followed by 10 days of reperfusion before sacrifice. The same anaesthetic procedure was followed for each dog at all of the experiments: days 1, 3 and 10. The animals were placed in a Siemens Vision MRI/MRS 1.5T system. Cardiac gated ^{1}H spin echo transverse images were obtained to facilitate positioning on the dual tuned ^{1}H/^{31}P rf transmit/receive surface coil. Multivoxel (16 × 16) ^{31}P 2D-CSI were acquired from a 3cm transverse slab, proximal to the apex of the heart. Spectra were collected at baseline, twice each during occlusion and reperfusion and once each at days 3 and 10 post-occlusion. Interleaved with the CSI were the collection of cine cardiac images. The dogs were placed prone in a rigid ^{1}H rf transmit/receive coil and a transverse image was used to localise the desired short axis plane. Cine images were acquired using cardiac gating before, during and immediately following the ischaemic insult as well as at days 3 and 10. Using the Siemens software package ARGUS, end diastole and end systole images were identified and endocardial contours drawn for each slice through the heart. The ejection fraction (EF) was determined, and the results were compared using a repeated measures ANOVA ($p < 0.05$ considered significant). Prior to sacrifice the dogs received a bolus followed by a one-hour constant infusion of Magnevist™ (Gd-DTPA). The heart was then excised and imaged using a T_1-weighted 3D FLASH sequence.

Table 1

Infarct Sizes, Regions at Risk, Damage Ratios, and Corresponding p-Values for Both Groups, Mean (±SEM)

	Infarct Sizes (% LV)	Regions at Risk (% LV)	Damage Ratios
Isoflurane (n = 10)	13.1 (2.2)	29.5 (1.3)	0.562 (0.103)
Propofol (n = 12)	14.9 (2.8)	27.7 (2.8)	0.611 (0.059)
p-values	0.62	0.60	0.67

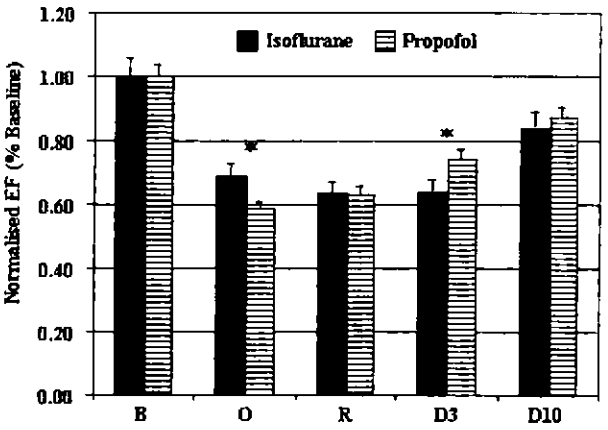

Figure 1. Baseline normalised EF values (error bars are SEM) for both isoflurane and propofol where significance *($p < 0.05$) is between the two groups.

The *ex vivo* images were analysed using the software package ANALYZE (4). Left ventricular and infarct volumes were measured, to determine the percent of infarcted left ventricle (1,5). To monitor the degree and extent of the occlusion and reperfusion, blood flow was measured using radioactively labelled microspheres injected into the left atrium at baseline, during the occlusion, at reperfusion and just prior to sacrifice (1,5,6).

Results: There were no intracellular pH differences noted between the two groups. The high-energy phosphate ratios also followed a similar pattern in both anaesthetic groups. The mean (±SEM) final infarct size for the isoflurane group was 14.9% (±2.8%) and 13.1% (±2.2%) for the propofol group (NS). Normalising these infarct sizes by the regions at risk (as determined by the volume of reduced blood flow) determines the damage ratios, which were also insignificant ($p = 0.67$). (Table 1). However, the EF normalised by the baseline, was significantly different throughout the occlusion as well as at day 3 (Figure 1).

Discussion: The differences between isoflurane and propofol anaesthesia during a reperfused ischaemic insult are seen only in terms of cardiac function. The final infarct sizes and damage ratios at day 10 were not significantly different between the two groups suggesting no differences in the degree of protection with the use of either anaesthetic. The speed of the recovery of intracellular pH following the occlusion, which we have previously shown to correlate with final infarct size, was similar in both groups (1). During the occlusion there was less of a negative inotropic effect in the isoflurane group, indicating better preservation of cardiac function; however by day 3 it was apparent that propofol promoted a faster recovery of function following reperfusion. Further studies are required to determine the mechanisms of this protection and how to best use these anaesthetics in the setting of cardiac surgery and also in the acute myocardial infarction/reperfusion setting.

Acknowledgements: Supported by a grant from HSFO(NA3774). An OGSST and the Department of Medicine and Dentistry, UWO funded KT. We would also like to thank Siemens Canada for technical support and Berlex Canada for their donation of Magnevist™. Finally, we thank Drs. Bartha and Pereira for technical assistance.

48. Dobutamine Magnetic Resonance Tagging in Ischemic Cardiomyopathy: Comparison to Left Ventricular Electromechanical Mapping

C. Joon Choi,[1] Habib Samady,[2] Michael Ragosta,[3] Joseph DiMaria,[4] Jennifer Hunter,[5] Frederick Epstein,[6] Christopher Kramer.[7]
[1]*University of Virginia, Cardiovascular Division P.O. Box 800662, Charlottesville, VA U.S.A.;* [2]*University of Virginia, Dept. of Cardiology–Box 158-22, Charlottesville, Virginia United States;* [3]*University of Virginia, P.O. Box 158\5th Floor Private Clinics, Charlottesville, Virginia United States;* [4]*University of Virginia, Lane Rd. Building MR4, Rm 1157, Charlottesville, VA U.S.A.;* [5]*University of Virginia, Heart Center P.O. Box 800697, Charlottesville, VA U.S.A.;* [6]*University of Virginia, Radiology Department, Charlottesville, Virginia United States;* [7]*University of Virginia, Departments of Radiology and Medicine, Charlottesville, Virginia United States*

Background: MRI measures of wall thickness and wall thickening have been validated as measures of viable myocardium in ischemic cardiomyopathy. The quantitative response to low dose dobutamine by MR tagging is a new method to evaluate viability in this setting, as is LV electromechanical mapping (NOGA) in the catheterization laboratory. We hypothesized that NOGA-derived voltage would identify segments with MR tagging-defined contractile reserve.

Methods: 17 patients (12 men, age 63 ± 9, mean ± SD), with LV dysfunction and multivessel CAD underwent NOGA and MRI within 24 hours of each other. Linear local shortening (LLS) and unipolar voltage (UpV) were assessed by NOGA. UpV ≥6.0 mV is considered a marker of viability. Breathhold short-axis cine MRI (TR 100 msec, TE 5 msec, 7 mm thick slices, FOV 300 mm, matrix 128 × 256, phase duration 50 msec) from apex to base was used to measure LV mass, end-diastolic and end-systolic volumes, EF, end-diastolic wall thickness, and systolic wall thickening. Breathhold short-axis tagged cine MRI (TR 90 msec, TE 4 msec, pixel size same as for cine, phase duration 45 msec) assessed subendocardial and transmural% circumferential shortening (%S) at baseline and at peak response to low-dose dobuta-

Table

	UpV < 6 mV	UpV ≥ 6 mV	P value
Wall thickness (mm)	11.6 ± 3.1	13.1 ± 3.1	0.003
Wall thickening (mm)	2.0 ± 2.5	3.3 ± 2.9	0.007
Transmural baseline %S	5.0 ± 10.3	9.5 ± 8.7	0.002
Transmural peak dob %S	8.1 ± 9.5	14.3 ± 9.1	<0.001
Subendocardial peak dob %S	10.1 ± 10.0	18.0 ± 10.9	<0.001

mine (dob) (5 and 10 μg/kg/min). Both imaging modalities were divided into 12 segments per patient (4 apical, 4 mid, 4 basal) and matched by short axis location.

Results: By MRI, LV mass was 268 ± 81 g, end-diastolic volume 160 ± 56 ml, end-systolic volume 109 ± 54 ml, and EF 34 ± 14%. Of 204 myocardial segments measured, 193 had adequate NOGA points for analysis. For all myocardial segments, LLS was 7.6 ± 6.6% and UpV 9.6 ± 4.7 mV. LLS correlated with MRI wall thickening ($r = 0.32$, $p < 0.001$). UpV correlated with endocardial peak dob %S ($r = 0.32$, $p < 0.001$). Segments with UpV ≥6 mV by NOGA demonstrated greater wall thickness, wall thickening, and %S at baseline and peak dob, especially in the subendocardium, compared to segments with UpV <6 mV. (See table).

Conclusion: In patients with ischemic cardiomyopathy, myocardial segments with preserved voltage by electromechanical mapping demonstrate greater wall thickness, wall thickening and quantitative response to dobutamine, especially in the subendocardium. Thus, both contractile reserve by low dose dobutamine MR tagging and NOGA-derived voltage may identify viable myocardium in patients with ischemic cardiomyopathy.

49. The Radial Long Axis Balanced FFE Method Can Be Recommended to Evaluate Left Ventricular Volume, Function and Mass

Timothy Bloomer,[1] Sven Plein,[1] Sasha Radjenovic,[2] David Higgins,[2] Mohan Sivanathan.[2] [1]*Leeds General Infirmary, Cardiac MRI Unit, Leeds, W Yorks United Kingdom;* [2]*Leeds General Infirmary, Cardiac MRI Unit, Leeds, W Yorks UK*

Introduction: Cardiac Magnetic Resonance Imaging has become established as the most accurate measure of left ventricular volume and mass. Conventionally a series of short axis slices are obtained in the left ventricular short axis orientation and endocardial and epicardial contours are drawn either manually or using automatic edge detection. The main source of observer variability is the determination and treatment of the most basal slice of the left ventricle. This slice usually moves through the imaging plane during systole and there is no clear agreement on conventions for contour drawing. Other sources of variability include the treatment of the papillary muscles and trabeculations of the left ventricle which tend to exaggerate systolic thickening. An alternative strategy is to acquire slices orientated radially around the left ventricular long axis. This has the advantage that the mitral valve plane can be identified easily in all orientations and phases of the cardiac cycle. We have assessed the use of Turbo Field Echo (TFE) and balanced Fast Field Echo (FFE, "True FISP") as imaging techniques for radial volume measurement compared with short axis acquisitions using the same imaging modalities.

Method: Five normal volunteers and ten patients underwent cardiac MRI on a Philips 1.5T Intera MRI system using a five element surface coil. Two series of left ventricular short axis slices were acquired using TFE and balanced FFE during breatholding. Two radial series using ten long axis slices orientated radially around the left ventricular long axis were also acquired using TFE and balanced FFE. Imaging parameters were as follows: TFE: TE ~4.8 ms, TR ~8ms, Flip Angle 35 degrees, Balanced FFE: TE ~1.6 ms TR ~3.2 ms, Flip Angle 55 degrees.

Endocardial and epicardial contours were drawn manually on both short axis and radial images using MASS (MR analytical system, Medis, Leiden). Short axis volumes were computed by the MASS software to give left ventricular end diastolic volume (LV EDV), left ventricular end systolic volume (LV ESV), left ventricular stroke volume (LV SV), left ventricular ejection fraction (LV EF) and left ventricular mass. Radial contours from MASS were analysed on a programme developed in our unit (PlotContours004). For the purposes of comparison, papillary muscles were excluded from left ventricular mass and included as endocardial volume. Differences between TFE and balanced FFE sequences have been assessed as well as the agreement between two experienced observers.

Table

Left Ventricular Volumes by Short Axis and Radial Long Axis Using TFE and Balanced FFE

	TFE Short Axis	TFE Radial	BFFE Short Axis	BFFE Radial
LV EDV	190.5ml	184.9ml	208.6ml	213.6ml
LV ESV	98.5ml	106.1ml	112.6ml	115.5ml
LV SV	91.9ml	78.9ml	96.7ml	98.1ml
LV EF	57.6%	50.3%	54.9%	53.7%
LV Mass	158.2g	173.2g	140.9g	151.6g

Results: Image quality at end diastole was comparable between TFE and balanced FFE for contour drawing. Image quality at end systole was better in all cases for balanced FFE than TFE. In both the short axis and radial orientations, LV EDV, LV ESV and LV SV were greater for balanced FFE than for TFE, while left ventricular mass was reduced for balanced FFE compared to TFE. However LV EDV was higher for TFE short axis compared with radial, but lower for balanced FFE short axis compared with radial. LV ESV was higher for radial than short axis for both TFE and balanced FFE. LV Mass was higher for radial than short axis in TFE and balanced FFE. The mean values for short axis versus radial orientation were much closer for balanced FFE than TFE. Interobserver agreement for left ventricular volumes was close with correlation coefficients of >0.98 for TFE and >0.99 for BFFE in the short axis orientation and >.99 for TFE and BFFE in the radial orientation. Interobserver correlation was >0.98 for LV Mass in both TFE, BFFE short axis and radial orientations. Mean differences between observers in the balanced FFE radial orientation were 1% for EDV, 4% for ESV, 2% for SV, 2% for EF and <0.5% for Mass. There were no statistically significant differences between EDV or Mass between the observers in any combination of orientation or acquisition type. There were significant but clinically small differences between observers for ESV, SV and EF in radial BFFE and larger differences in radial TFE.

Conclusion: Radial balanced FFE provides satisfactory image quality for assessment of left ventricular volumes and mass with good interobserver agreement. Radial TFE is satisfactory for assessment of LV Mass and end diastolic volume but not for systolic function due to the loss of contrast at end systole. A large normal data set is required to put radial BFFE into clinical practice as overall values differ significantly from short axis measurements.

50. Severe Coronary Stenosis Reduces Myocardial Perfusion Reserve Equally in Ischemic and Remote Myocardium

Olaf Muehling,[1] Fan Zhao,[2] Yimei Huang,[2] Prasad Panse,[2] Andrey Zenovich,[2] M. Jerosch-Herold,[3] Norbert Wilke.[4] [1]*Department of Radiology of the University of Minnesota, 420 Delaware St. SE, Minneapolis, Minnesota United States;* [2]*University of Minnesota, 420 Delaware St. SE, Minneapolis, Minnesota USA;* [3]*University of Minnesota, 420 Delaware St. SE, Minneapolis, Minnesota United States;* [4]*University of Minnesota, CMRR, Minneapolis, Minnesota United States*

Background: It has been shown that, the perfusion reserve is reduced in the myocardium affected by a severe coronary artery stenosis as well as in the remote myocardium supplied by a normal coronary artery in the same heart (1). Thus, the regional myocardial perfusion reserve

Table

	Group	Rest		Hyperemia§		Perfusion Reserve	
		A	B	A	B	A	B
MBF	LCx (ischemic)	0.9 ± 0.2	1.1 ± 0.2†	1.2 ± 0.3	3.1 ± 1.2†	1.5 ± 0.3	2.4 ± 0.7†
FMV	LAD (remote)	1.5 ± 0.3*	1.2 ± 0.3†	2.0 ± 0.8*	3.4 ± 1.3†	1.2 ± 0.3	2.9 ± 0.9†
	LCx (ischemic)	121 ± 71	122 ± 25	70 ± 24	45 ± 16†		
MVR	LAD (remote)	62 ± 18*	123 ± 41†	44 ± 9*	43 ± 21		
MBP (mmHg)		85 ± 6	133 ± 7†	78 ± 11	124 ± 16†		
HR (1/min)		102 ± 25	114 ± 13	136 ± 34	138 ± 27		
PRP (mmHg/s)		140 ± 30	250 ± 30†	180 ± 50	290 ± 90†		

* $p < 0.02$ vs. Ischemic Myocardium.
† $p < 0.04$ vs. Group A.
§ $p < 0.05$, *n.s.* vs. Rest.

alone might not allow differentiating between ischemic and remote myocardium. The hypothesis is, that resting and hyperemic perfusion causing the reduction of regional myocardial perfusion reserve is different in ischemic and remote zone.

We determined regional blood flow at rest and hyperemia non-invasively with magnetic resonance first-pass perfusion (MRFP) imaging (2) in a group of animals with a severe coronary artery stenosis and a control group with normal coronary arteries to study the perfusion of ischemic and remote myocardium.

Methods: A total of 24 pigs (mean body weight 21 ± 7 kg; range: 13–29 kg) were divided in two groups A and B. In group A ($n = 12$) a stenosis of the proximal left circumflex artery (LCx) was created by catheter-guided hollow bead embolization. The control group B was left with normal coronary arteries. Both groups underwent MRFP imaging, one week after bead placement in group A. MRFP-imaging was performed on a 1.5T MR Scanner (Siemens Vision, Germany) using a multi-slice saturation recovery turboFLASH sequence with a TR, TE and flip angle of 2.4ms, 1.2ms and 18°, a spatial resolution of 2–3mm, a temporal resolution of 120–200 ms/image at 1 image/slice/heartbeat. A Gd-DTPA-bolus of 0.02 mmol/l was given during image acquisition. Regional signal intensity (SI) time curves were generated using the ARGUS software (Siemens, Medical Systems, Iselin, NJ). Myocardial blood flow estimates (MBF, ml/g/min) were calculated from the SI-curves using a previously validated Fermi-model of constrained deconvolution (3). Myocardial perfusion reserve (MPR) was calculated as the ratio of hyperemic/rest MBF. Myocardial vascular resistance (MVR) was calculated as the ratio of mean blood pressure (MBP)/MBF (mmHg*g*min/ml). MBF and MVR were determined at rest and hyperemia in the stenosis-dependent and the antero-septal (remote) myocardium of group A and the corresponding LCx- and LAD-supplied region of the healthy group B. Hyperemia was induced by a maximal vasodilating dose of adenosine. MBF was normalized by the pressure rate product (PRP) using the formula MBF × mean group PRP/individual animal PRP.

Results: MBF, MPR, MVR, MBP, PRP and heart rate (HR) are shown in the table above.

MPR was significantly ($p < 0.01$) reduced in stenosis-dependent as well remote myocardium of group A compared to the control group B. MPR in ischemic and remote myocardium of group A were not significantly different ($p = 0.1$).

Resting MBF was significantly elevated ($p < 0.03$) in remote myocardium and significantly ($p < 0.04$) decreased in ischemic myocardium when compared to the corresponding region of group B. Resting MBF was significantly ($p < 0.02$) higher in remote compared to ischemic myocardium of group A. The reduced resting MBF in the remote region was caused by a significantly ($p < 0.02$) lower MVR compared to the corresponding region in group B.

Hyperemic MBF was significantly decreased in remote and ischemic myocardium of group A compared to the corresponding region of group B. Hyperemic MBF in the ischemic region was significantly ($p < 0.02$) lower compared to the remote region of group A. This was the result of a higher MVR in the ischemic region. A significantly ($p < 0.01$) lower MBP in group A was the reason for a reduced hyperemic MBF in the remote zone of group A compared to the corresponding region in B.

Conclusion: 1) The resting perfusion in the remote region was increased compared to the ischemic zone because of a low resting MVR. An increased workload and mechanical tethering (4) with a higher metabolic demand in the remote myocardium might explain the reduced resting MVR. 2) The hyperemic perfusion in the ischemic region was decreased compared to the remote zone. This is caused by a stenosis-limited drop in vascular resistance in the ischemic region.

Resulting from 1) and 2) the myocardial perfusion reserve is equally reduced in remote and ischemic myocardium in a group of animals with severe coronary artery stenosis. Thus, MPR alone does not allow distinguishing between these two regions.

51. Impaired Left Ventricular Filling due to Right Ventricular Pressure Overload in Primary Pulmonary Hypertension: Non-invasive Monitoring by MRI

J. Tim Marcus,[1] Anton Vonk Noordegraaf,[2] Roald Rocleveld,[3] Pieter Postmus,[3] Albert van Rossum,[4] Robert Heethaar,[5] Anco Boonstra.[3]
[1]*Dept of Clinical Physics & Informatics, University Hospital Vrije Universiteit, P.O. Box 7057, Amsterdam, The Netherlands The Netherlands;* [2]*Dept. of Pulmonary Medicine, University Hospital Vrije Universiteit, P.O. Box 7057, Amsterdam, Netherlands Netherlands;* [3]*University Hospital Vrije Universiteit, P.O. Box 7057, Amsterdam, Netherlands Netherlands;* [4]*Dept. of Cardiology, University Hospital Vrije Universiteit, P.O. Box 7057, Amsterdam, Netherlands Netherlands;* [5]*University Hospital Vrije Universiteit, Dept. Clinical Physics, Amsterdam, Netherlands Netherlands*

Objective: This study aims to analyze the effect of Primary Pulmonary Hypertension (PPH) on the cardiac function by MRI.

Methods: In 12 patients (9 female, age 30–56 y) the diagnosis PPH had been established by catheterization (mean pulmonary artery pressure (PAP) was 56 ± 8 mmHg). With breathhold cine MRI, a series of short-axis images was acquired covering the whole left ventricle (LV) and right ventricle (RV). The curvature, defined as 1 divided by

the radius of curvature in cm, was calculated for the septum and the LV free wall in early diastole. Leftward ventricular septal bowing (LVSB) is denoted by a negative curvature. For LV and RV, the end-diastolic volume (EDV), stroke volume (SV) and volumetric filling rate were calculated. Control subjects (n = 14, 11 female) were all healthy, aged 20–57 y.

Results: In the patients, LVSB was quantified in early diastole by the negative septal curvature of -0.14 ± 0.07 cm^{-1}, and the septal to free wall curvature ratio of -0.42 ± 0.21 LV-EDV and LV-SV correlated negatively with diastolic PAP ($p = 0.004$ and $p = 0.04$ respectively). In the patients versus controls, RV-SV was reduced (52 ± 12 vs. 82 ± 11 ml, $p < 0.0001$); LV peak filling rate was smaller (2.2 ± 0.7 EDV/s, vs. 3.3 ± 0.5 EDV/s, $p < 0.001$); LV-EDV was smaller (81 ± 23 vs. 117 ± 19 ml, $p = 0.001$); and LV-SV was smaller (49 ± 18 vs. 83 ± 13 ml, $p < 0.0001$).

Conclusion: In PPH, RV pressure overload leads to leftward ventricular septal bowing and reduced RV output. By decreased blood delivery, LV filling is reduced which results in further loss of LV stroke volume by the Frank Starling mechanism.

52. Transmyocardial Laser Revascularisation Improves Perfusion but Enhances Left Ventricular Remodeling in Rats After Myocardial Infarction

Karl-Heinz Hiller,[1] Matthias Nahrendorf,[2] Dirk Theisen,[3] Kai Hu,[4] Christiane Waller,[5] Ralf Kaiser,[6] Axel Haase,[7] Georg Ertl,[8] Ralf Brinkmann,[9] Wolfgang Bauer.[10] [1]*Wuerzburg University, EP5, Am Hubland, Wuerzburg, Germany Germany;* [2]*Wuerzburg University, Uni Wuerzburg/EP5, Wuerzburg, Germany Germany;* [3]*Laserzentrum Luebeck, Medical Laser Center Luebeck, Luebeck, Germany Germany;* [4]*Wuerzburg University, Cardiology Department, Medizinische Klinik, Wuerzburg, Germany Germany;* [5]*Wuerzburg University/Cardiology Department, Medizinische Klinik, Wuerzburg, Germany Germany;* [6]*Wuerzburg University, Cardiology Department, Medizinische Klinik, Wuerzburg, Germany Germany;* [7]*Wuerzburg University/ EP 5, Am Hubland, Würzburg, Germany Germany;* [8]*Wuerzburg University, Cardiology Department, Direktor Medizinische Klinik, Wuerzburg, Germany Germany;* [9]*Medical Laser Center Luebeck, Medizinisches Laserzentrum Luebeck, Luebeck, Germany Germany;* [10]*Wuerzburg University, Cardiology Department, Medizinische Klinik, Wuerzburg, Germany Germany*

Hypertrophy following MI causes diffuse hypoperfusion of the remote myocardium. We therefore used the MI rat model for assessment of transmyocardial laser revascularisation (TMR).

Methods: 8 weeks after coronary artery ligation rats had Cine-MRI using a 7 Tesla magnet; thereafter TMR was done. A self-designed Holmium: Yag laser system emitting a wavelength at 2.1μm (pulse energy 4J, pulse duration 1 ms, 365μm fiber diameter) was placed in soft contact to the remote myocardium. 4 weeks after TMR a second Cine-MRI including dobutamine-stress (10 μg/kg/min via tail vein) was followed by high resolution spin labeling perfusion imaging (pixel size 140μm) of the isolated retrogradly perfused heart using an 11 Tesla magnet in 12 Wistar rats. To locate laser areas histology was used.

Table

	Control	TMR
Delta EDV (μl)	24.6 ± 16.7	81.7 ± 15.7*
Delta LV mass (mg)	54.5 ± 19.2	124.1 ± 30.7*
EF at 12 weeks (%)	40 ± 2	38 ± 2
CI at 12 weeks (ml/kg/min)	232.2 ± 12.8	242.4 ± 12.8
EF at 12 weeks stress (%)	49.6 ± 5. 3	54.4 ± 4.9

Results: MI-size measured by Cine-MRI was equal ($27 \pm 2\%$ both groups). Lased areas were better perfused than nonlased myocardium (Δlased vs. control region $+3.89 \pm 0.83$ ml/min/g at rest and $+2.29 \pm 1.06$ ml/min/g during nitro stress, $p < 0.05$ both).

Conclusion: Using high resolution perfusion imaging, improvement of perfusion within the TMR regions and their vicinity was visualized. Due to the retrograde perfusion setting and application of the spin labeling technique this improvement can not be caused by flow from inside the LV cavity via open channels. TMR should be used with caution in patients undergoing LV remodeling after MI, because dilation and hypertrophy was enhanced.

53. The Benefit of TrueFISP Versus FLASH Cine Imaging in Patients with Poor Left Ventricular Function

Jane Francis,[1] James Moon,[2] Gillian Smith,[3] Christine Lorenz,[4] Dudley Pennell.[5] [1]*The Royal Brompton Hospital, Magnetic Resonance Unit, London, England UK;* [2]*Royal Brompton Hospital, Sydney St, London, UK UK;* [3]*Royal Brompton Hospital, Sydney St, London, England UK;* [4]*Royal Brompton Hospital, CMR Unit, London, England UK;* [5]*Imperial College of Science, Technology and Medicine, University of London, South Kensington, London, England UK*

Background: The accuracy of analysis of left ventricular mass and volume, calculated by cardiovascular magnetic resonance techniques (CMR) is dependent on contrast between the endocardium and the blood pool. Conventional imaging techniques such as FLASH rely on blood flow for delineation of the endocardial border. However, contrast may be reduced in patients with impaired left ventricular (LV) function due to slow flow, particularly at the apex. Image contrast in TrueFISP is independent of flow as the signal is inversely proportional to T1/T2 at TR ≪ T2 and therefore has the potential to overcome this problem. 1 2 3

Method: 6 patients (13 males, 3 females aged 19–84, mean 62) with either ischaemic cardiomyopathy or dilated cardiomyopathy (DCM) which was idiopathic or as a result of valvular disease, were referred for follow-up assessment of LV mass and volumes. Ejection fraction calculated by previous CMR studies within the last two years was 25–69%, mean 43%. Imaging was performed on a 1.5T Sonata scanner (Siemens AG, Erlangen, Germany) using a conventional breath-hold FLASH technique and a single slice breath-hold TrueFISP technique.

The FLASH imaging parameters were TE 6.1 ms/TR 56 ms, slice thickness 7 mm, gap 3 mm, in plane pixel size 2.08 × 1.37 mm, temporal resolution 56 ms, flip angle 20, acquired in 15 heartbeats. The TrueFISP imaging parameters were, TE 1.6 ms/TR 3.2 ms, slice thickness 7 mm, gap 3 mm, in plane pixel size 2.27 × 1.37 mm, temporal resolution 48 ms, flip angle 60 acquired in approximately 12–15 heartbeats.

Real time TrueFISP imaging was also carried out with 14 slices acquired (7 slices in each of two breath-holds), slice thickness 7 mm, gap 3 mm, TE 1.1 ms/TR 2.2 ms, 77 ms temporal resolution, flip angle 47–55, in plane pixel size approximately 2.8 × 3.8 mm. Each breath-hold was approximately 15 seconds. Images were acquired in the horizontal long axis (HLA), vertical long axis (VLA) and short axis (SA) projections.

Data Analysis: Image quality in all three techniques was assessed using contrast-to-noise (CNR) and signal-to-noise (SNR) ratios. Signal intensity of the images was measured in the septum for the myocardium and in the mid ventricular cavity for the blood signal in systole. Regions of interest (ROI's) were placed in a systolic frame in all cases to avoid thinned myocardium at end diastole due to infarction. The septum was chosen for myocardial ROI's to avoid any epicardial fat.

CNR was calculated as (Signal Intensity blood − Signal Intensity myocardium)/background noise.

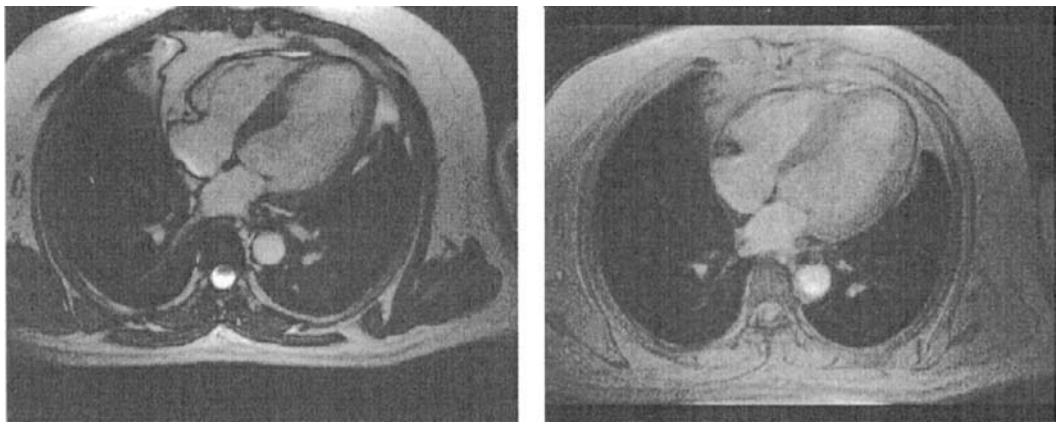

Figure 1.

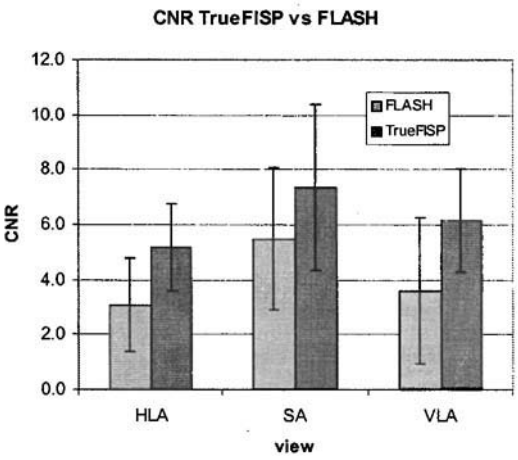

Figure 2.

SNR = Signal Intensity/background noise for both blood and myocardium. Background noise was measured drawing a region of interest within the field of view, but outside the patients' body in the phase-encode direction. CNR and SNR were compared between techniques using a paired student's t-test.

Results: Figure 1 shows example horizontal long axis views for FLASH (left) and TrueFISP (right).

CNR between blood and myocardium was higher for TrueFISP than FLASH for all three views acquired (HLA $p = 0.015$, VLA $p = 0.0004$, SA $p = 0.015$).

SNR for blood was not significantly different between FLASH and TrueFISP. However SNR of the myocardium was significantly higher for FLASH compared to TrueFISP. ($p < 0.001$ for all three views). These results are consistent with those reported by Carr et al. 4

For the real time TrueFISP (rt TrueFISP) sequence the CNR was better with rt TrueFISP than FLASH ($p = 0.003$), the SNR in the myocardium showed no significant difference between the two techniques, but SNR in blood was better in rt TrueFISP than FLASH ($p = 0.035$).

Conclusion: TrueFISP provides better blood-myocardial contrast than FLASH in patients with poor ventricular function and is associated with a modest drop in SNR of the myocardium. Real time TrueFISP is an alternative to multislice TrueFISP cine imaging in patients who cannot tolerate multiple breath-holds.

54. Susceptibility to Ischemia/Reperfusion Injury in Chronically Infarcted Rat Hearts

Michael Horn,[1] Stephanie Hügel,[2] Kai Hu,[2] Stefan Neubauer.[3]
[1]*Medizinische Universitaetsklinik, Josef-Schneider-Str. 2, Wuerzburg, Germany;* [2]*Medizinische Klinik, Josef-Schneider-Str. 2, Würzburg, Germany;* [3]*Oxford University, John Radcliffe Hospital, Headley Way, Oxford, UK*

Introduction: Ventricular remodeling, with depression of the mechanical function, as well as alterations of the creatine kinase system is reported in chronically infarcted hearts (Neubauer S et al., J Clin Invest 1995). It is unknown whether this process increases susceptibility to a second subsequent ischemic event. Therefore, we tested the susceptibility of chronically infarcted rat hearts to ischemia/reperfusion injury.

Methods: Male Wistar rats underwent chronic myocardial infarction (MI) by LAD ligation or were sham (SH) operated. Eight weeks later, in vivo end-diastolic pressure (EDP) was measured. Next, hearts were excised and perfused with Krebs-Henseleit buffer in Langendorff mode at a constant pressure of 100 mmHg. LV pressures and heart rate were monitored via a LV balloon. Balloon volume was adjusted to EDP = 10 mmHg in SH ($n = 11$) and MI1 ($n = 9$) hearts (to much EDP of sham hearts); MI2 ($n = 5$) hearts were set to in vivo EDP (20 ± 2 mmHg, to match in vivo EDP). 31P-NMR spectra at 7.05 T were recorded throughout the protocol. Briefly, 152 FIDs (TR 1.93 sec, pulse angle 45°) were averaged over 5 min intervals, then Fourier transformed, phased individually, resonance areas integrated (NMRi software) and corrected for partial saturation.

Protocol: 15 min of baseline perfusion, 15 min of total global ischemia and 30 min of reperfusion.

Results: During baseline perfusion, mechanical function was comparable in SH and MI2 hearts, while MI1 hearts showed depressed function. The content of ATP and inorganic phosphate (Pi) was equal in all groups. Phosphocreatine (PCr) was reduced in MI hearts (see table).

During ischemia, all hearts were arrested and PCr as well as ATP

Table

		Baseline			End of Ischemia			End of Reperfusion		
		SH	MI1	MI2	SH	MI1	MK2	SH	MI1	MI2
EDP	mmHg	10 ± 0	10 ± 0	20 ± 2[bc]	28 ± 6	9 ± 1[a]	15 ± 1[a]	46 ± 6	17 ± 1[a]	39 ± 7[c]
LVDP	mmHg	89 ± 5	66 ± 7	96 ± 11	0	0	0	37 ± 10	72 ± 5[a]	55 ± 16
PCr	mM	16 ± 0	13 ± 1[a]	10 ± 1[bc]	0	0	0	11 ± 1	14 ± 1	12 ± 2
ATP	mM	11 ± 0	11 ± 0	11 ± 0	4 ± 0	5.0 ± 0	4 ± 0	4 ± 0	4 ± 1[a]	5 ± 1
Pi	mM	4 ± 0	4 ± 0	5 ± 0[b]	7 ± 1	7 ± 1	8 ± 1	5 ± 1	3 ± 1	2 ± 1

[a] $p < 0.05$ SH vs. MI1, [b]$p < 0.05$ SH vs. MI2, [c]$p < 0.05$ MI1 vs. MI2.

contents declined, while Pi content increased approx. 5-fold. At the end of ischemia, PCr content was highest in MI1 hearts.

Hearts resumed sinus rhythm during the first few minutes of reperfusion. Recovery of function (LVDP, RPP) at the end of reperfusion was highest in MI1 hearts. PCr levels recovered to pre-ischemic values, while ATP levels returned to approx. 50% of pre-ischemic values. Again, MI1 hearts showed higher ATP levels than SH hearts and a trend for higher values compared to MI2 hearts.

Conclusion: At baseline perfusion, depression of LV function and high energy phosphate metabolism was seen in MI hearts. During reperfusion, hearts with lowered pre-ischemic workload (MI1) showed the best recovery.

Mi hearts with in vivo preload did not show reduced recovery compared to SH. We conclude that the remodeled post-MI heart does not exhibit increased susceptibility to a second ischemic event.

55. Noninvasive Imaging of Coronary Vasodilation

Brian Keeffe,[1] Craig Meyer,[2] Dwight Nishimura,[3] Michael McConnell.[4] [1]*Stanford University, 300 Pasteur Drive, Stanford, CA USA;* [2]*Stanford University, Packard 216, Stanford, California United States;* [3]*Stanford University, Department of Electrical Engineering, Stanford, California United States;* [4]*Stanford University, Cardiovascular Medicine, Stanford, CA United States*

Introduction: Coronary artery vasodilation plays a critical role in the ability of the heart to respond to varying demand and can be impaired in atherosclerosis. Previous methods of assessing coronary artery vasodilation have required invasive coronary angiography. Coronary MR angiography is a non-invasive method of imaging the coronary arteries with high resolution. The purpose of this study is to determine whether MRI can detect changes in coronary artery diameter in response to a vasodilator.

Methods: Ten healthy volunteers (8M, 2F, age 27–40) without evidence of cardiovascular disease or contraindication to MRI were scanned. Heart rate and blood pressure were monitored throughout the study. Informed consent was obtained under a protocol approved by the Stanford University Human Subjects Committee. A 1.5 T GE Signa scanner was used, equipped with a cardiac gradient set (40 mT/m, 150 mT/m/msec) and a specially developed workstation for real-time interactive imaging. A standard 5-inch surface coil was used for signal reception and pulse cardiac gating was employed.

The real-time imaging system was used to prescribe in-plane and through-plane (cross-sectional) images of the right and left coronary arteries (1). To allow accurate analysis, careful attention was paid to prescribing the right coronary artery (RCA) cross-section at a relatively linear segment of the vessel, which was typically in the mid RCA. Then, high-resolution coronary MR angiography was performed using a breath-held, cardiac-gated, multi-slice, interleaved-spiral sequence described previously (1): FOV 20–24 cm, 14–20 interleaves, spatial resolution 0.5–0.8 mm, slice thickness 5 mm, flip angle 60. Nitroglycerin (NTG, 0.4 mg sl) was given while subjects remained in the magnet. High-resolution coronary MRA was repeated 3 minutes after NTG.

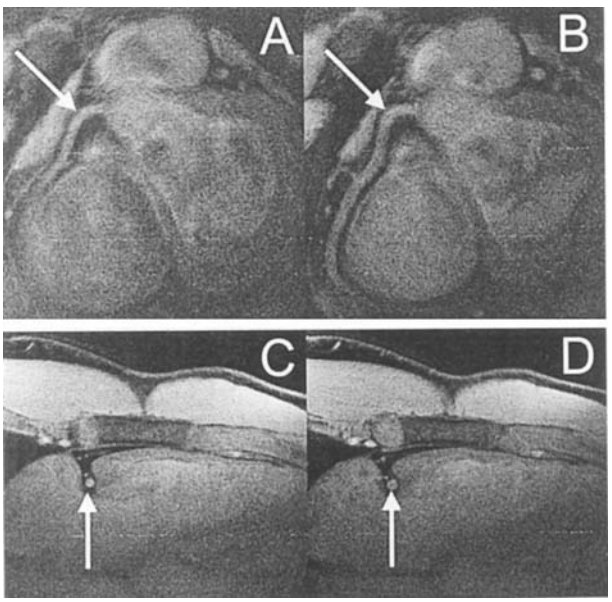

Figure 1. Through-plane images of the proximal RCA before (A) and after NTG (B). An increase in vessel size is also clearly seen on RCA cross-sectional images (C: pre-NTG, D: post-NTG).

The primary analysis was the comparison of RCA cross-sectional area before and after NTG. One subject had a non-dominant RCA and was excluded from analysis. Pre- and post-images were mixed and analyzed in random order by an observer blinded to identifying data. Scion Image (Scion Corporation, Frederick, MD) was used to trace a region-of-interest around the RCA to calculate vessel area. Data were analyzed using a two-sided paired t test.

Results: Coronary vasodilation in response to NTG was clearly visible on in-plane and through-plane images of the both the right and left coronary arteries (Figure 1). Quantitative analysis demonstrated a 31% increase in RCA cross-sectional area following NTG (from 14.0 ± 1.1 mm^2 to 18.4 ± 1.3 mm^2), which was highly statistically significant ($p = 0.002$).

Conclusions: Coronary MRA can noninvasively detect and quantify coronary artery vasodilation and is a promising technique to study coronary function.

56. Comparison of Stress Myocardial Perfusion MRI and Myocardial Perfusion SPECT Using Receiver Operating Characteristics Analysis

Nanaka Kawada,[1] Hajime Sakuma,[2] Munenobu Motoyasu,[3] Takeshi Nakano,[4] Kan Takeda,[5] Atsushi Nozaki.[6] *[1]Mie University Hospital, Department of Radiology, Tsu, Mie Japan; [2]Department of Radiology, Mie University Hospital, 2-174 Edobashi, Tsu, Mie Japan; [3]Department of Cardiology, Mie University Hospital, 2-174 Edobashi, Tsu, Mie Japan; [4]Department of Cardiology, Mie Unviersity Hospital, 2-174 Edobashi, Tsu, Mie Japan; [5]Department of Radiology, Mie University Hospital, 2-174 Edobashi, Tsu, Mie Japan; [6]GE Medical Systems, 4-7-127 Asahigaoka, Hino, Tokyo Japan*

Introduction: Regional myocardial perfusion in ischemic heart disease has been evaluated with stress nuclear perfusion imaging. A dynamic MR sequence using short echoplanar readouts and interleaved notched saturation can provide first-pass myocardial perfusion imaging covering the entire left ventricular myocardium with sufficient temporal resolution and good T1 contrast. Recent clinical studies using this technique demonstrated that myocardial perfusion MR imaging after pharmacological stress can detect perfusion abnormalities in patients with coronary artery disease. The purpose of the current study was to evaluate the accuracy of first-pass myocardial perfusion MR imaging with combined dipyridamole injection and handgrip exercise for the detection of myocardial ischemia by using X-ray angiography as a gold standard. Receiver operator characteristic (ROC) analysis was used to assess diagnostic performances of stress myocardial perfusion MR imaging and stress myocardial perfusion SPECT.

Subjects and Methods: Thirty-nine patients with known or suspected coronary artery disease were evaluated. All patients underwent both selective coronary angiography and myocardial perfusion SPECT within two weeks of the MR study. Patients with electrocardiographic evidence of Q wave myocardial infarction were no included in this study protocol. Myocardial perfusion was assessed with a 1.5 T cardiac MR imager (Signa CV/i, GE Medical Systems, Milwaukee, WI) equipped with gradients that had a maximum slew rate of 150T/m/sec and a gradient strength of 40 mT/m. Seven short axis MR images of the left ventricle were acquired every other heartbeats by using a gradient-echo sequence with echo-planar readouts (Fastcard echo-train, TR of 6–7ms, number of echo trains of 4, receiver bandwidth of ±125 kHz, field of view of 32 cm, matrix of 128 × 128, slice thickness of 10 mm). Interleaved notched saturation was used to obtain optimal T1 contrast and SNR without reducing slice coverage. After acquiring scout MR images, dipyridamole (0.56 mg/kg) was injected intravenously for 4 minutes. All patients performed isometric handgrip exercise in addition to the pharmacological stress. Stress perfusion MR images were acquired by injecting 0.075 mmol/kg of gadolinium contrast medium into antecubital vein followed by 20 ml of saline flush at a rate of 4ml/sec with a power injector. Immediately after perfusion MR study, breath-hold ultra-fast cine MR images were acquired with a gradient-echo cine MR sequence with echo-planar readouts to evaluate LV function during stress. After inravenous injection of aminophyline and 15 minutes delay time, perfusion MR images and cine MR images were obtained in the resting state. Myocardial perfusion MR and SPECT images were evaluated without knowing the results on X-ray coronary angiography. A 70% or larger diameter stenosis in the coronary artery was considered to be significant. ROC curve analysis was performed to compare the diagnostic performances of stress perfusion MRI and SPECT for the detection of myocardial ischemia. MR images were read by two readers who had cardiac MR experience of 11 years and 4 years. Myocardial perfusion SPECT images were interpreted by two readers who had nuclear cardiology experience of 21 years and 4 years. The LV myocardium was divided into 3 segments corresponding to the major coronary arteries. The readers assigned one of five confidence levels as follows: 1, definitely absent; 2, probably absent; 3, equivocal; 4, probably present; 5, definitely present. The diagnostic accuracy of each imaging modality was estimated by calculating the area under the ROC curve (Az) using the ROKIT 0.9B software. The statistical significance of the difference between the areas under the ROC curves was evaluated with an univariate z score test. Two-tailed P values of less than .05 was considered to be significant.

Results: Diagnostic perfusion MR images were obtained during stress and at rest in all patients. On X-ray angiography, significant stenosis in the coronary artery was found in 52 of the 117 major coronary arteries (18 in the left anterior descending artery, 19 in the circumflex artery, 15 in the right coronary artery). The sensitivity of MRI with combined dipyridamole injection and handgrip exercise for detecting >70% diameter stenosis was 84.6% (44/52, 77.8% in the left anterior descending artery, 84.2% in the circumflex artery, 93.3% in the right coronary artery), which was higher than that with stress SPECT (63.5%, 33/52). The specificity for detecting coronary arterial stenosis was 90.8% (59/65) with MRI and 78.5% (51/65) with SPECT. The area under ROC curve, which indicates the diagnostic accuracy for predicting coronary arterial stenosis, was significantly higher with myocardial perfusion MRI after combined dipyridamole injection and handgrip exercise (the mean Az = 0.898) than with exercise stress myocardial SPECT (the mean Az = 0.670, $p < 0.01$). When the subjects were divided into two groups based on tracers used in myocardial perfusion SPECT, the area under ROC curve with MRI was significantly higher than that with Tc-99m-tetrofosmin SPECT and that with Tl-201 SPECT ($p < 0.05$, and $p < 0.01$, respectively).

Conclusion: The results in this study using ROC analysis indicated that first-pass myocardial perfusion MRI with combined dipyridamole and handgrip exercise demonstrates significantly better diagnostic performance for detecting myocardial ischemia when compared with stress myocardial perfusion SPECT.

57. A Comparison of Rectilinear Reduced FOV TrueFISP Cine Imaging Techniques

Andrew Larson,[1] Orlando Simonetti.[2] *[1]Dept. of Radiology, Northwestern University, 448 East Ontario Ave Suite 700, Chicago, IL USA; [2]Siemens Medical Systems, 448 East Ontario Ave Suite 700, Chicago, IL USA*

Discussion: Several recently introduced cine imaging techniques, UNFOLD [1], rFOV [2], and SLAM [3], involve acquiring a reduced subset of k-space lines for each cine frame that if reconstructed separately would produce images with spatial aliasing. For a decrease in acquisition time or an increase in temporal resolution by a factor of 2, these techniques involve collecting only the odd or the even phase encode lines at each cardiac phase. Full FOV images are reconstructed by either filtering the temporal dimension of the cine series [1], performing complex interpolation between neighboring k-space frames to derive the unsampled odd or even phase encode lines [3], or interpolating the change between undersampled cardiac phases to allow transfer of sparsely sampled lines to the frame being reconstructed [2]. To evaluate the effectiveness of these methods, raw data was acquired from which cardiac cine images were reconstructed using each technique allowing subsequent comparison.

Methods: The raw data was acquired from a healthy volunteer using a constant RF trueFISP [4] cardiac breath-hold cine sequence with linephase segmentation of 10, 280mm square FOV, 780ms acquisition window, TE/TR 1.5/3.0, Fl 56°, 6mm slice thickness and matrix size 120 × 256. Examination was performed on a 1.5T scanner (Magnetom Sonata, Siemens Medical Engineering, Erlangen, Germany). The methods under comparison used only the odd or even lines acquired at each cardiac phase for reconstruction. Such techniques would require half of the acquisition time necessary for the 10 line/phase segmented acquisition.

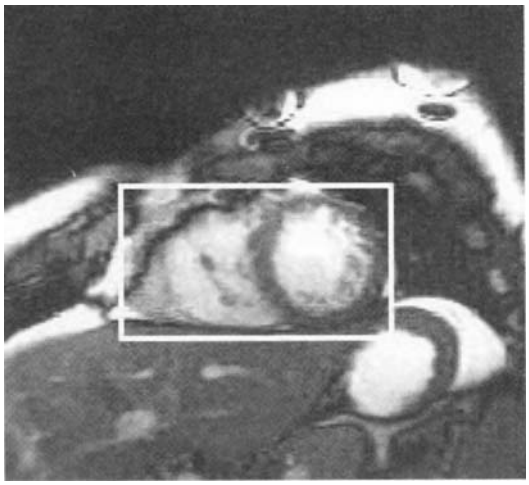

Figure 1. TrueFISP Cardiac Cine Image ROI.

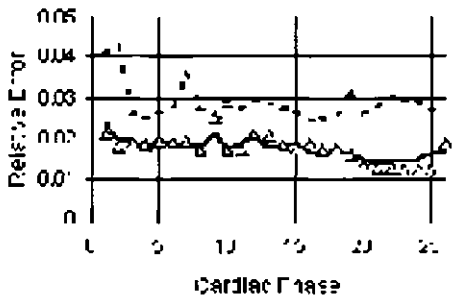

Figure 2. Reconstruction Error Comparison UNFOLD (solid) SLAM(^) rFOV(- -).

Error was calculated for each cine frame by averaging the summed differences between the normalized images reconstructed using the various reduced FOV techniques and those reconstructed using conventional 10 line/phase segmentation in the ROI shown in Figure 1. SNR for each cine frame was measured as the difference between mean blood signal intensity and mean myocardial signal intensity, normalized by the standard deviation of the null signal intensity.

Results: The UNFOLD [1] and SLAM [3] methods reconstructed images with comparable relative error, both significantly less than the relative error of those images reconstructed using the rFOV [2] method. See Figure 2. The mean SNR (across all cine frames) for the SLAM, UNFOLD, and rFOV techniques were measured to be 58.36, 46.30, and 33.87 respectively.

Conclusion: On the basis of achieving minimal relative error, the UNFOLD and SLAM techniques performed quite similarly and proved superior to the rFOV technique. The SLAM technique theoretically improves SNR rather than decreasing SNR as does UNFOLD [1,3]. The reconstructed cine images in this comparison did show that on average the SLAM images had 26% greater SNR than those reconstructed using the UNFOLD technique. When considering these SNR differences as well as the significantly greater computational complexity of the UNFOLD technique, SLAM appears the better method for reconstruction. Further studies are required to evaluate the consistency of the superiority of this technique in more volunteers and at other slice orientations and temporal resolutions.

58. Transmural Late Enhancement by Contrast-Enhanced MR Predicts No Functional Recovery After Acute Myocardial Infarction

Anna John,[1] Thorsten Dill,[2] Matthias Rau,[3] Wolfgang RICKEN,[4] Georg Bachmann,[5] Christian Hamm,[6] Christine Lorenz.[7] [1]*Royal Brompton Hospital, Sydney Street, London, United Kingdom;* [2]*Kerckhoff Clinic, Dept. of Cardiovascular MR, Benekestr. 2-8, Bad Nauheim, Germany;* [3]*Kerckhoff Clinic, Dept of Cardiology, Benekestr. 2-8, Bad Nauheim, Germany;* [4]*Kerckhoff Clinic, Dept. of Cardiology, Benekestr. 2-8, Bad Nauheim, Germany;* [5]*Kerckhoff Clinic, Dept. of Radiology, Benekestr. 2-8, Bad Nauheim, Germany;* [6]*Kerckhoff Clinic, Benekestr. 2-8, Bad Nauheim, Germany;* [7]*Royal Brompton Hospital, CMR Unit, London, England, UK*

Background: Contrast-enhanced MR has been shown to clearly depict the site of acute myocardial infarction. The aim of this study was to determine whether late enhancement could be used to predict functional recovery after acute myocardial infarction (AMI).

Methods: 11 patients underwent emergency PTCA with or without stent implantation for AMI. Mean age was 53 (range 44–71) years. Exclusion criteria were cardiac rhythm other than sinus, previous myocardial infarction, intervention to more than one coronary lesion and general MR contraindications. MR scans were performed on days 1, 3, 7 and 28 post-AMI using a Siemens Magnetom Sonata 1.5 T scanner. TrueFISP cine sequences were used for volume studies and detection of wall motion abnormalities. A 3D-inversion recovery sequence was used 10 min after Gd-DTPA administration (0.2 ml per kg bodyweight) to visualise infarcted (bright) myocardium (defined as late enhancement). Observers were blinded to the angiography reports.

Results: Late enhancement was present in all patients at all time points. Localisation of late enhancement areas allowed correct definition of the infarct related artery in all cases. 6/11 patients had transmural infarctions as detected by contrast-enhanced MR. These 6/11 had persistent wall motion abnormalities at 28 days. 5/11 patients showed non-transmural late enhancement. Of these, 4 had normal wall motion at 28 days. In the 5th, wall motion abnormalities persisted. In this patient, the infarction was non-transmural, but had a large extent throughout the subendocardium of the inferior and inferolateral wall.

Conclusions: Transmural late enhancement is associated with lack of functional recovery after AMI, and non-transmural late enhancement in this small patient group was associated with functional recovery. These results are consistent with those presented by Kim RJ et al. (ACC 2000, NEJM in press). Larger patient numbers are required to further validate the role of late enhancement as a predictor of functional recovery after AMI.

59. Inter and Intra-Observer Variability of Global Ventricular Function in Cardiac MRI(CMR) Core Lab

Prasad Panse,[1] Cory Swingen,[2] Yimei Huang,[2] Ravi Seethamraju,[2] Andrey Zenovich,[2] Olaf Muehling,[3] Neeta Panse,[2] M. Jerosch-Herold,[4] I. Anand,[5] Norbert Wilke.[6] [1]*University of Minnesota, Cardiac MRI Core Lab, Mayo mail code 292,420 Delaware Sreet, Minneapolis, MN USA;* [2]*University of Minnesota, Cardiac MRI Core Lab, Department of Radiology, Minneapolis, MN USA;* [3]*University of Minnesota, Cardiac MRI Core Lab, Department of Radiology, Minneapolis, Minnesota United States;* [4]*University of Minnesota, Cardiac MRI Core Lab, Department of Radiology, Minneapolis, MN United States;* [5]*VA Medical Center, Division of Cardiology, Minneapolis, MN United States;* [6]*University of Minnesota, Cardiac MRI Core Lab, Department of Radiology, Minneapolis, Minnesota United States*

High degree of reproducibility is desired in Cine MRI, for drug monitoring and follow up in Ongoing Clinical trials. Reproducibility of Cine

Table

	Interobs. RD(%)	Interobs. σ(%)	Intraobs. RD(%)	Intraobs. σ(%)
LVEDV	3.53	3.17	1.7	3.0
LVESV	0.62	4.83	0.89	6.54
LVmass	2.42	3.0	1.4	2.54
EF	2.49	3.75	0.54	2.93
SV	6.02	5.29	2.24	2.28

MRI,has been either reported in normal subjects (1) or patients with myocardial infarction (2). However,Inter and Intra observer reproducibility has not been validated for Cine MRI in clinical setting, over a wide range of ejection fractions, encountered in the CMR core lab. This variability is very important to assess the significance of a change of Left Ventricular (LV) parameter in follow up examination. We hypothesize: Over a wide range of ejection fractions, Cine MRI in core lab is highly reproducible and reliable.

Methods: Two independent experienced observers manually traced contours of subjects (n = 24) who underwent multiple short axis cine MRI. Patients were selected from a wide range of clinical spectrum from low (heart failure) to high ejection fractions (hypertrophic cardiomyopathy patients). The entire heart was covered from base to apex from ED and ES phases. Analysis was done using customized software (MASS version 4.0) to determine the left ventricular end diastolic volume (LVEDV), End systolic volume (LVESV), stroke volume (LVSV) and ejection fraction (LVEF). One observer repeated the tracings after two weeks. The correlation coefficient (r), mean difference (RD) and standard deviation of difference (ó) were determined.

Results: The LVEF in the present study ranged from 14 to 80%. There was good Inter and Intra Observer reproducibility (Table). The Intra Observer results were better than the Inter Observer results. The Correlation Coefficient ranged from 0.985 to 0.999 ($p < 0.001$) for the InterObserver study and 0.996 to 0.999 ($p < 0.001$) for Intraobserver study.

Conclusion: For the first time, we have demonstrated that experienced Observers in CMR core lab can yield excellent reproducibility over a wide range of ejection fractions (14–80%). Cine MRI is thus an effective and reproducible tool for follow up assessment of global ventricular function.

60. Fully Automatic Detection of Right- and Left Ventricular Contours in Short-Axis Cardiac MR Images Using Active Appearance Models

Boudewijn Lelieveldt,[1] Rob van der Geest,[2] Steve Mitchell,[3] Milan Sonka,[4] Johan Reiber.[5] *[1]Div. of Image Processing, Dept. Radiology, LUMC, P.O. Box 9600, Leiden, ZH Netherlands; [2]Leiden University Medical Center, P.O. Box 9600, Leiden, ZH The Netherlands; [3]Dept. Electrical Eng., University of Iowa, Dept. Electrical Engineering, Iowa City, IA USA; [4]University of Iowa, 3404B EB, Iowa City, Iowa United States; [5]Div. Image Processing, LUMC, P.O. Box 9600, Leiden, ZH Netherlands*

Background: To quantitatively evaluate global and regional Left Ventricular (LV) and Right Ventricular (RV) function from short-axis cardiac MR images, the contours of the LV endocardium (ENDO), LV epicardium (EPI) and RV need to be traced in the images. In clinical studies typically consisting of 200–300 images, this is mainly performed manually, which is time-consuming and sensitive to inter- and intra-observer variations.

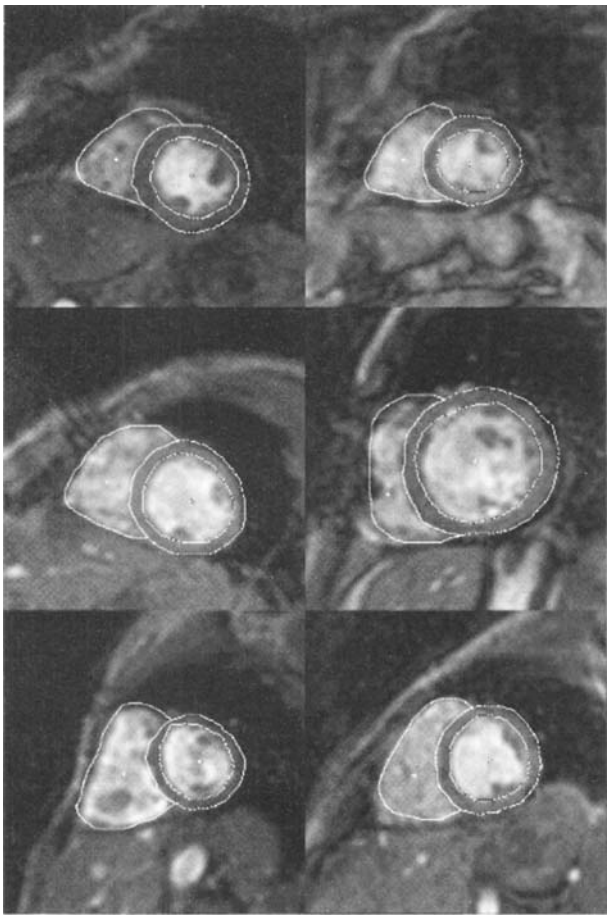

Figure 1.

Aim: To develop and validate a robust, automated contour detection technique for tracing the ENDO, EPI and RV contours in short-axis cardiac MR images.

Methods: Previous experience has shown, that a robust contour detection method requires a mathematical description of prior knowledge about typical organ shape, typical organ appearance and anatomical or pathological shape variations. In this work, a trainable statistical model named 'Active Appearance Model' (AAM) is applied, which consists of two components: a statistical model of the shape of the heart, which is combined with a statistical model of the image appearance of the heart in a set of example cardiac MR images. The combined model is trained to learn the shape and image structure of the LV and RV from a representative set of cardiac MR images from 11 patients and 23 normal subjects. The AAM can be automatically matched to a new study image, yielding the locations of the ENDO, EPI and RV contours. The AAM technique was evaluated on a separate set of 60 end-diastolic mid-ventricular cardiac MR images from 9 patients and 11 normal subjects.

Results: Examples of fully automatically detected contours are provided in Figure 1. The results of the current evaluation study demonstrated:

1) an excellent correspondence between the automatically and manually derived area measures such as LV cavity area ($r = 0.96$, $N = 60$), LV epicardial area ($r = 0.96$, $N = 60$) and RV cavity area ($r = 0.90$, $N = 60$). The slopes and intercepts of the LV and RV cavity area regression lines did not differ significantly from one and zero respec-

tively. The average paired differences between the automatic/manual measurement pairs was -0.4 ± 1.6 cm^2 for the LV cavity area, and 0.5 ± 3 cm^2 for the RV cavity area, which is comparable to inter- and intra-observer variabilities in manual measurements,

2) a high degree of robustness of the AAM contour detection with respect to noise and image artifacts, even in low-fidelity, routinely acquired cardiac MR images from sometimes severely deformed patient hearts (in 60 out of 60 images, the automated method delivered visually correct ENDO, EPI and RV contours),

3) the ability of the AAM method to generate LV contours according to observer preference, which exclude papillary muscles and epicardial fat.

Conclusions: Active Appearance Models have demonstrated to be a highly robust contour detection method for RV, ENDO and EPI contours, and may potentially reduce analysis time for cardiac MR examinations to a minimum.

61. Visualization of Left Ventricular Function Under Physically Induced Stress by Interactive Real-Time MRI

Oliver Weber,[1] Markus Oelhafen,[2] Holger Eggers,[3] Peter Börnert,[4] Peter Boesiger.[2] [1]*Institute of Biomedical Engineering, University of Zurich and ETH Zurich, Zurich, CH Switzerland;* [2]*Institute of Biomedical Engineering, University of Zurich and ETH Zurich, Zurich, CH Switzerland;* [3]*Philips Research, Division Technical Systems, Hamburg, D Germany;* [4]*Philips Research Laboratories, Technical Systems, Hamburg, Hamburg, D Germany*

The aim of the present work was to demonstrate the applicability of an interactive, real-time capable MR system for the visualization of left-ventricular function under rest as well as under physically induced stress.

Introduction: Stress tests are an approved method to detect deficits in myocardial perfusion at an early stage. The current imaging method of choice for routine diagnosis is ultrasound echocardiography. Despite the development of novel techniques, such as second harmonic imaging, image quality is still frequently unsatisfactory. In contrast, MRI has been shown to provide improved consistency in image quality [1]. Furthermore, real-time interactive MRI has recently been presented. The MR systems involved mimic ultrasound with respect to interactive geometry definition capability as well as to image acquisition and display speed [2,3]. We extended the usage of such a system to the visualization of LV function under physically induced stress.

Methods: Equipment: A Philips Gyroscan-NT 1.5 Tesla system, equipped with PT6000 gradients and a dedicated real-time reconstruction unit [4], was used. Images were acquired continuously and displayed immediately on the screen. An interactive user interface allowed interactive scan plane definition during the scan by means of computer-mouse manipulation.

Imaging: Measurements were performed using either a spiral imaging sequence [5] or an echo planar imaging (EPI) sequence [3]. For spiral imaging, a binomial 1331 spectral-spatial excitation was used, followed by an 18 ms spiral readout with an effective TE of 4.8 ms. For an entire image, four interleaves were acquired at a TR of 29 ms. A 128×128 matrix was acquired, and images were reconstructed to a 256×256 matrix. Gradient EPI was performed acquiring six readouts per excitation with an effective TE of 5.3 ms. Eight interleaves were acquired with a TR of 15 ms. A 256×128 matrix was acquired using half scan and a 60% rectangular field of view (FOV). Images were reconstructed to a 256×256 matrix. With both sequences, a FOV of 256 mm was imaged using an array of two circular receive coils. Images were acquired in a free-run mode, without cardiac triggering or respiratory control. Images were displayed after sliding window reconstruction, resulting in a frame rate of 33 images per second for both acquisition schemes.

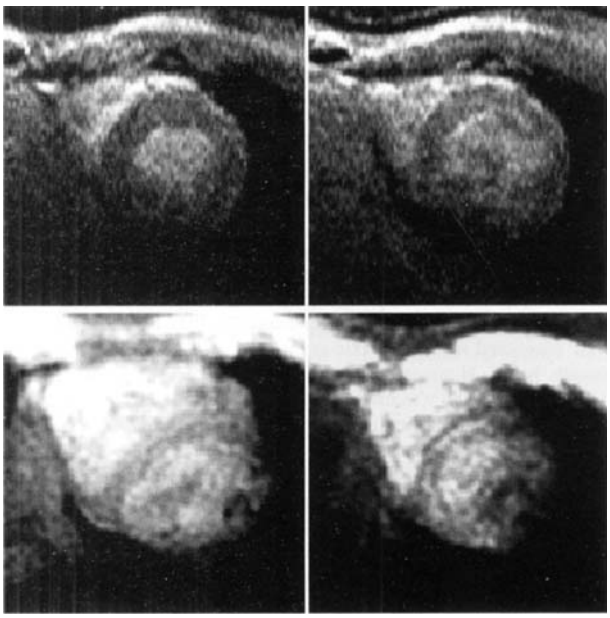

Figure.

Healthy volunteers were examined in supine position during rest, as well as at various stages of physically induced stress. Stress was applied within the magnet bore by means of a bicycle ergometer. Four-chamber views and short axis views at various levels of the left ventricle were acquired and visually evaluated.

Results and Discussion: The figure shows short axis views acquired with EPI (top) and spiral readout (bottom) under rest (left) and during physically induced stress (right). When seen during real-time acquisition, the high frame rate of 33 frames per second allowed smooth display of heart motion in all acquired views. In rest, image contrast between myocardium and blood was good for EPI, and sufficient for spiral imaging. During stress, contrast was enhanced due to increased blood flow. On the other hand, the images suffered from increased motion artifacts due to increased breathing motion as well as body motion because of the cycling. Due to its inherently reduced motion sensitivity, spiral imaging was found to suffer to a smaller extent from motion artifacts than EPI. This was particularly well recognized in the four-chamber views.

Conclusion: The interactive, real-time capable MR system has successfully been used for the visualization of LV function both under rest and during physically induced stress. To increase the contrast between blood and myocardium, magnetization preparation (e.g., T2-preparation [6]) may be useful [3].

62. Three-Dimensional Diastolic Strain Analysis in the Normal Left Ventricle

Joost Kuijer,[1] J. Tim Marcus,[2] Marco Gotte,[3] Albert van Rossum,[3] Robert Heethaar.[4] [1]*University Hospital Vrije Universiteit, Dept. Clinical Physics & Informatics, Amsterdam, NL Netherlands;* [2]*University Hospital Vrije Universiteit;* [3]*University Hospital Vrije Universiteit, Dept. of Cardiology;* [4]*University Hospital Vrije*

Universiteit, Dept. of Clinical Physics & Informatics, Amsterdam, NL Netherlands

Introduction: Abnormalities in diastolic function may precede systolic dysfunction in patiens with hypertension [De Simone et al., 2000], aortic stenosis [Stuber et al, 1999] and coronary artery disease [Bruch et al, 1999]. In this study, MR tagging and three-dimensional (3D) strain analysis were used to assess the time evolution of local wall mechanics in the left-ventricular heart wall. Because diastolic function is known to alter with age, we also investigated age-related effects of strains.

Methods: Ten healthy volunteers aged between 28 and 61 years were subjected to cine MR tagging with a time resolution of 30 ms. A 7-mm tagging grid was applied at end diastole (ED); five to seven short-axis slices and three long-axis slices were imaged in multiple short breath holds. Homogeneous strain analysis of small tetrahedrons [Kuijer et al, 2000] was used to calculate the local deformation over a time span of 300 ms, starting at end systole (ES). The ES image was defined to be the last image of the cine before reversal of the motion, determined by visual inspection. To assess regional differences, the tetrahedrons were pooled into six circumferential and three longitudinal segments. Axial strains were expressed as a relative change in length, while the shear strains were expressed as the change in angle between two initially orthogonal line segments.

Results: ES was established at 346 ± 19 ms (mean ± SD) after the R-wave. ES radial strain was larger at the base (34 ± 4%) than at the apex (28 ± 7%, $P < .01$), while the circumferential shortening was stronger at the apex (24 ± 1%) compared to the base (19 ± 1%). There was no significant difference between longitudinal levels in the *cl*-shear strain (mean 7.3 ± 1.5°), indicating a homogeneous contribution to LV torsion.

To compare the temporal evolution of the three axial strains and the *cl*-shear strain we normalized the strains to their ES value (the ED strain equals zero by definition). The plot of the normalized strains is given in Figure 1 (below). The 50% recovery time ($t_{50\%}$) was defined as the time at which the normalized strain crossed the 0.5-level. For the *cl*-shear, $t_{50\%}$ was 122 ± 35 ms. The radial strain recovered 26 ± 25 ms ($P < .05$) after *cl*-shear. Circumferential strain recovered 62 ± 25 ms ($P < .001$) and longitudinal strain 57 ± 29 ms ($P < .001$) after *cl*-shear. No significant effect of age on heart rate or on ES strains was found. However, the maximum normalized strain rate decreased significantly with age. The regression plot is shown in Figure 2 (above), the slope of the regression line was −0.07 ($P < .001$).

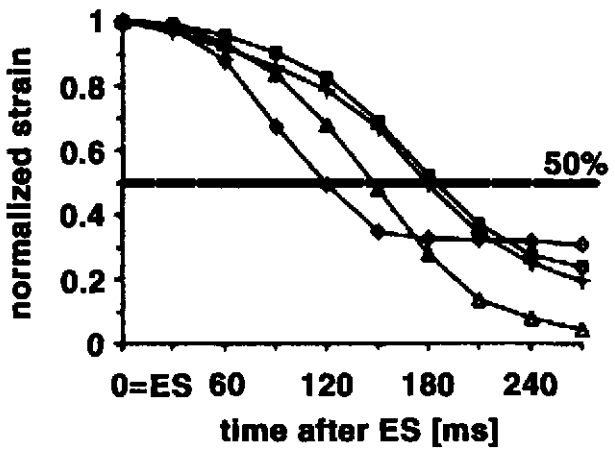

Figure 1. Temporal evolution of normalized strain during diastole. Legend: triangle = radial, square = circumferential, cross eq longitudinal and diamond = *cl*-shear strain.

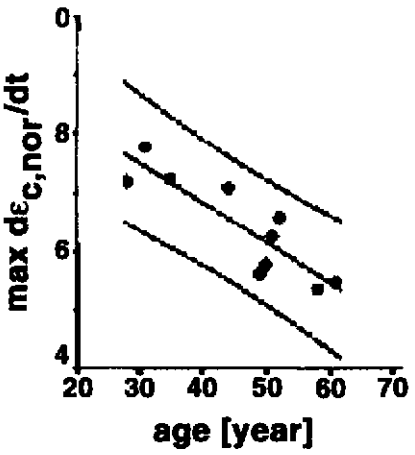

Figure 2. Regression line and 95% prediction interval for the effect of age on maximum normalized circumferential strain rate.

Discussion: The relaxation of the axial strains is related to filling of the LV, while the *cl*-shear strain is related to torsion of the LV. The relative timing of the relaxation curves in Figure 1 are in agreement with the untwisting of the LV before filling.

This study shows that the local wall mechanics of the LV can be assessed during diastole. Diastolic strain analysis may allow differentiation between normal and abnormal diastolic mechanics, offering the prospect of early detection of local diastolic dysfunction and local compensatory hyperfunction. The effect of age on diastolic strains indicate that control groups should be age-matched.

63. Evaluation of Cardiac Function Within 30 Seconds: Comparison of MRI and MDCT

Seiki Hamada,[1] Takashi Ueguchi,[2] Shuji Yamamoto,[2] Hiroaki Naito,[3] Hironobu Nakamura[4] [1]*Osaka University, 2-2 Yamadaoka, Suita, Osaka Japan;* [2]*Osaka University Hospital, 2-15 Yamadaoka, Suita, Osaka Japan;* [3]*Osaka University, 1-7 Yamadaoka, Suita, Osaka Japan;* [4]*Osaka University Medical School, 2-2 Yamadaoka, Suita, Osaka Japan*

Purpose: Our goal is the reduction of examination time in estimating left ventricular function. We compared a single shot fast spin-echo MR sequence, HASTE-method, and retrospective ECG-gating multidetector-row CT (MDCT).

Materials and Methods: Twelve patients (mean age 53 y.o.) with heart disease were studied. Short axial HASTE images covering the entire heart were obtained within single breath holding using a 1.5 T MRI (Siemens). Scan parameters were effective TE 43 msec, slice thickness 6mm, slice gap 1.5, slice number 15, and matrix 175 × 256. A double inversion recovery preparation near R wave was used to obtain a high black blood contrast. A time delay (Td) was kept between the IR pulses and the echo center. The Td of end-diastole was set to one RR interval. The acquision time of each slice was 2 times RR interval. A phase of end-systole (Tes) from R wave was determined with use of the short axial single-slice segmented FLASH. The Td of end-systole was adjusted as (RR interval + Tes). Each imaging time covering the entire heart was 30 times RR interval. Within 2 weeks, MDCT was

performed in the same group. With a single breath-hold (approximate 30 seconds), the entire heart was scanned with ECG-gating by MDCT (Toshiba). Scan parameters were 2mm-thick detector-row, pitch 0.9–1.3, and 0.5 sec per rotation. Forty-percent phase data of RR interval was retrospectively reconstructed as end-systole, and 0% phase data as end-diastole. Calculation of volume was performed by slice summation. We compared cardiac parameters of both methods.

Results: HASTE-defined values were not statistically different from MDCT-defined value ($p < 0.05$).

Conclusion: LV volume is quantified in a time-efficient manner with use of MRI and MDCT. We prefer HASTE method, because the disadvantages of MDCT are increased radiation dose due to overlap scanning, and administration of iodinated contrast media.

64. MR Cine Assessment of Transmyocardial Laser Revascularization

Miia Torvinen,[1] Jarmo Simpanen,[2] Kirsi Lauerma,[3] Hannu Aronen,[4] Helena Hänninen,[5] Kalervo Verkkala.[6] *[1]Helsinki University Central Hospital, Radiology, Haartmaninkatu 4 PL 340 00029 HUS, Helsinki, Helsinki Finland; [2]Department of Cardiovascular Surgery, Helsinki University Hospital, Helsinki, Finland Finland; [3]Helsinki University Hospital, Dept. of Radiology, Meilahti, Helsinki, Helsinki Finland; [4]Department of Radiology, Helsinki University, Helsinki, Helsinki Finland; [5]Bio-Mag Laboratory, Helsinki University of Technology, Helsinki, Helsinki Finland; [6]Department of Cardiovascular Surgery, Helsinki University Hospital, Helsinki, Helsinki Finland*

Introduction: Transmyocardial laser revascularization (TMR) is a technique in which Holmium-YAG (Eclipse®) laser is used to drill 1 mm channels endo-or epicardially into beating heart after thoracotomy. TMR aims to improve myocardial blood supply by creating transmural ventricular channels into ischemic areas of the myocardium. Via these channels blood supply to the heart is delivered from the ventricular cavity directly into the myocardium. Animal studies have shown that TMR improves regional perfusion and myocardial function in the ischemic (treated) segments and also in remote zones. We evaluated results of transmyocardial laser revascularization in eight patients with cine MRI.

Materials and Methods: Eight patients (all male, age 57–72) with three vessel coronary artery disease were studied. These patients did not respond to any available form of medical management and were not candidates for (new) conventional bypass procedure. Therefore they were treated with transmyocardial laser revascularization. MR imaging was performed on a 1.5 Tesla Siemens Vision Scanner and body coil before and six months after transmyocardial laser revascularization. Short axis cine images (TR 80.0 ms, TE 6.1 ms and FA 20 deg) were obtained for the assesment of left ventricular function and systolic wall thickening. Eight consecutive 1 cm sections with no gap were imaged during free breathing. Left ventricular diastolic and systolic volumes were assessed according to Simpsons rule. Diastolic and systolic wall thickness was assessed at lateral wall (treated region) and at septum (remote region).

Results: There was no change in diastolic volumes, ejection fractions or wall thickness six months after TMR (Table 1).

Table 1

Mean (±SD) Diastolic Volumes and Ejection Fractions Before Transmyocardial Laser Revascularization and Six Months After Treatment

	Before	After	P =
Diastolic volume (ml)	158 ± 37	166 ± 61	0.622
Ejection fraction (%)	53 ± 12	50 ± 17	0.367

Conclusions: Cine-magnetic resonance imaging is a good diagnostic tool to assess function of left ventricle after treatment with TMR. Transmyocardial laser revascularization did not improve global or regional left ventricular function in our small patient group.

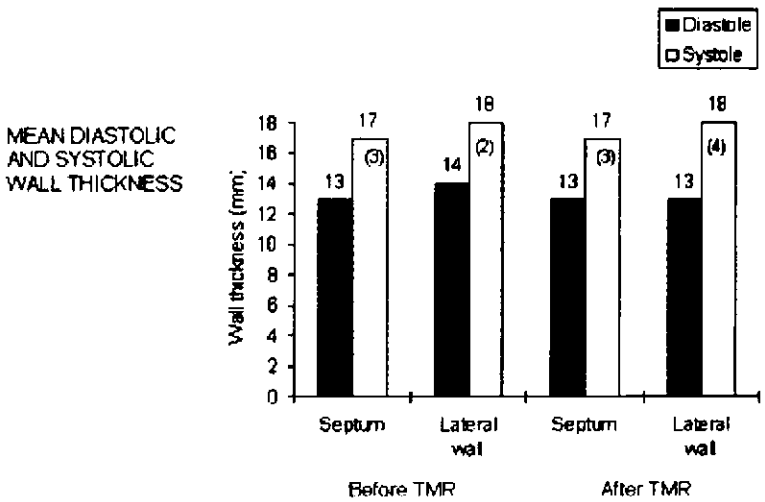

Figure 1. Wall thickness before and six months after transmyocardial laser revcascularization in eight patients. Wall thickness was measured at lateral wall (treated region) and septum (remote region). Mean diastolic and systolic wall thickness is shown in millimetres (SD inside the column). There was no change in diastolic wall thickness or systolic wall thickening after TMR.

65. Cardiac MRI Demonstrates Changes in Right Ventricular Function After Inferior Myocardial Infarction

Timothy Bloomer,[1] John Ridgway,[2] Mohan Sivanathan.[3] [1]*Leeds General Infirmary, Cardiac MRI Unit, Leeds, W Yorks United Kingdom;* [2]*Leeds General Infirmary, Cardiac MRI Unit, Leeds, W. Yorks UK;* [3]*Leeds General Infirmary, Cardiac MRI Unit, Leeds, W Yorks UK*

Introduction: Inferior myocardial infarction is primarily due to right coronary artery occlusion. Proximal lesions can cause extension to the right ventricle which worsens the outcome. Right ventricular extension is diagnosed by ST elevation in leads V3R and V4R on electrocardiography. Anatomical imaging of the right ventricle is limited however by the right ventricular geometry. Cardiac Magnetic Resonance Imaging (MRI) can assess left and right ventricular function non-invasively without geometric assumptions.

Method: Twenty-five patients with acute inferior myocardial infarction were recruited from the Coronary Care Unit (CCU). All patients had standard twelve lead electrocardiography withh additional right ventricular leads on arrival at CCU. Cardiac MRI was performed on the third or fourth day after myocardial infarction on a Philips 1.5T Intera MRI scanner using a five element phased array cardiac surface coil. Gradient echo sequences were acquired in the axial plane from the diaphragm to the pulmonary bifurcation and in the left ventricular short axis orientation from the apex to the atria. Volumetric analysis was performed using MASS software (MR analytical software system, Medis, Leiden). Follow up cardiac MRI has been performed at eight weeks after myocardial infarction in fifteen patients.

Results: Seven patients had electrocardiographic evidence of right ventricular extension. All patients had inferior left ventricular wall motion abnormalities on cardiac MRI. Mean left ventricular ejection fraction was reduced at 53%. Inferior right ventricular wall motion abnormalities were seen in 17/25 patients. At follow up there were reductions in right ventricular end diastolic volume (p = NS), right ventricular end systolic volume ($p < 0.001$) and an increase in right ventricular ejection fraction ($p < 0.001$) compared with the initial scan (Table).

Right Ventricular Volumes After Myocardial Infarction

	3 Days	2 Months	Difference	p value
RVEDV	107.2 ml	101.5 ml	5.7 ml	p = 0.25
RVESV	49.4 ml	39.8 ml	9.6 ml	p = 0.001
RVStroke	57.9 ml	60.4 ml	2.6 ml	p = 0.48
RV EF	54.7%	61.3%	6.5%	p = 0.001

Right ventricular wall motion had improved in 6/15 patients and worsened in 2/15 patients. There were however no significant differences in left ventricular volumes, ejection fraction or mass.

Conclusion: Cardiac MRI is more sensitive than electrocardiography in the diagnosis of right ventricular extension of inferior MI and can assess left and right ventricular recovery and remodelling. Right ventricular function is impaired immediately after inferior myocardial infarction and shows improvement after two months. This supports the view that the right ventricle is resistant to true infarction but that its function is acutely impaired by right coronary occlusion.

66. Left Ventricular Outflow Tract Area as Assessed by Magnetic Resonance Imaging—Findings in Different Forms of Left Ventricular Hypertrophy

Jeanette Schulz-Menger,[1] Oliver Strohm,[1] Rainer Dietz,[2] Matthias Friedrich.[3] [1]*Franz-Volhard-Klinik; Charite, Humboldt-Universitaet zu Berlin, Wiltbergstr.50, Berlin, Berlin Germany;* [2]*Franz-Volhard-Klinik; Charite, Campus Buch; Humboldt-Universität zu Berlin, Wiltbergstraßbe 50, Berlin, Berlin Germany;* [3]*Franz-Volhard-Klinik, Charite, Humboldt-Universitaet zu Berlin, Wiltbergstr.50, Berlin, Berlin Germany*

The dimensions of the left ventricular outflow tract in different forms of hypertrophy are not well studied. The degree of left ventricular outflow tract (LVOT) obstruction, however, determines the hemodynamic relevance of hypertrophic obstructive cardiomyopathy (HOCM).

Using gradient-echo sequences, we directly measured the minimal orifice area of the left ventricular outflow tract (LVOT) during systole. The studies were performed on conventional MRI scanners (Siemens Expert 1.0T and GE Signa CV/i 1.5T).

We compared 7 mildly symptomatic patients with HOCM,11 patients with HOCM after septal artery embolization (SAE) during a follow up over 3 years, 18 patients with symptomatic aortic stenosis (AS), 8 patients with arterial hypertension (AH), and 10 volunteers (V).

Results: Three independent cardiologists, experienced in cardiac MRI and not aware of other results or the clinical status, performed the planimetry of LVOT in 11 cases. Intra-observer variability and inter-observer variability were 10.7% and 12.8%, respectively. In HOCM patients after SAE, the LVOT area increased by 135 ± 33% during the subsequent 3 years. The increase of the LVOT area correlated closely to the improvement of the clinical outcome (R = 0.9). However, the LVOT area after 3 years (2.6 ± 0.6/SE cm2) remained significantly smaller to that of volunteers (5.3 ± 0.3 cm2), patients with AS (4.6 ± 0.2 cm2), and patients with hypertension (5.2 ± 0.3 cm2, $p < 0.01$ for all). On the other hand, there was no difference to asymptomatic or only mildly symptomatic HOCM patients (2.6 ± 0.3 cm2, p = ns, see fig. 1)

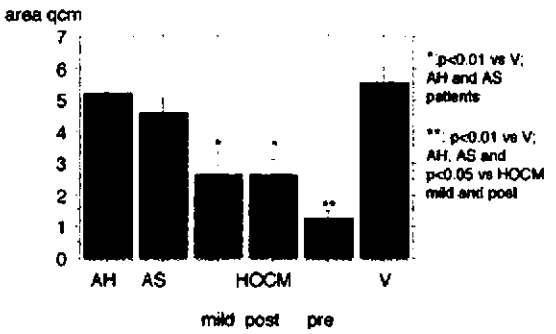

Figure 1. Comparison of the LVOT-area.

Conclusion: In conclusion, the left ventricular outflow tract area increases significantly after septal artery embolization and is similar to that of asymptomatic or only mildly symptomatic HOCM patients. However, it remains significantly smaller than that of controls or patients with hypertrophy due to other reasons.

Planimetry of the LVOT-area by MRI is a reliable method to assess the LVOT obstruction in patients and may be helpful in clinical decision-making.

67. Is Cardiac Gating Beneficial for Myocardial Perfusion Imaging? A Non ECG-Gated Model and Diagnostic Performance Evaluation in Patients with Coronary Artery Disease (CAD)

Penelope Sensky,[1] Mark Horsfield,[2] Nilesh Samani,[3] Graham Cherryman.[4] [1]*Glenfield Hospital, Department of Cardiology, Leicester, Leics England, UK;* [2]*Leicester Royal Infirmary, Department of Medical Physics, Leicester, Leics UK;* [3]*Glenfield Hospital, Department of Cardiology, Leicester, Leics UK;* [4]*Leicester*

Table 1

	ECG-Gated		Non ECG-Gated		Gating vs Non-Gating	
Data Set	No Images	RR(ms) mean ± SD	F mean ± SD	No Images	F mean ± SD	p(F)
i SR	53	982 ± 27	0.31 ± 0.03	97	0.51 ± 0.29	<0.001
ii SR	44	828 ± 176	0.58 ± 0.23	104	0.50 ± 0.28	ns
iii error	65	575 ± 250	0.55 ± 0.30	103	0.48 ± 0.28	ns
iv AF	65	626 ± 124	0.38 ± 0.31	96	0.52 ± 0.29	ns
v MVEs	65	806 ± 245	0.40 ± 0.26	102	0.52 ± 0.29	ns

Royal Infirmary, Department of Radiology, Leicester, Leics United Kingdom

Introduction: ECG-gating for myocardial perfusion imaging is traditionally employed. However, insertion of a sequence trigger delay (TD) increases image acquisition (IA) time, reducing signal intensity time curve temporal resolution. When changes in longitudinal myocardial relaxation rate (R_1) are measured, the correction of magnetization saturation error relies on a constant total repetition time (TR_0) and is only effective with a constant heart rate. Accurate ECG-gating requires repeated, precise R wave recognition. The MRI ECG trace is subject to artefact distortion, e.g. gradient switching, radiofrequency pulsing, patient motion, low voltage R waves, high amplitude T waves, aberrant conduction, and large vessel flow. In addition to natural heart rate variability (HRV), arrhythmias are common in CAD. Varying R-R intervals cause difficulty in TD selection, with inconsistencies of scan placement within the cardiac cycle and inaccuracies in the calculation of R_1. Constant TR_0 IA, i.e. non ECG-gated IA could overcome many of these difficulties.

Methods: Five extracts from continuous ambulatory ECG recordings containing consecutive R-R interval data (Pathfinder 700, Reynolds, UK) were selected at random from patients with (i) sinus rhythm (SR) with low HRV, (ii) SR with high HRV, (iii) SR with episodic high amplitude T waves misinterpreted as R-waves (iv) atrial fibrillation (AF), and (v) multiple ventricular ectopics (MVEs). The point of the cardiac cycle (F)at which the mid line of k-space is acquired for each image during a 2 minute single slice T1-weighted inversion recovery-snapshot FLASH sequence (1.5 Tesla Vision (Siemens, Erlangen), TI_{eff} = 516ms, TI = 300ms, TR = 4.5ms, TR0 = 1080ms, matrix = 96 × 128, IA = 432ms (n_k * TR), dead time = 348ms (c)) was calculated for both ECG-gated and constant TR_0 IA. For ECG-gating, TD was calculated from the first R-R interval (R_0) of the data set, i.e. TD = (1.3 * R_0)-TI_{eff}. After triggering, F is a fraction of the current R-R interval (R_t): $F = (TD + TI_{eff})-R_{t-1})/R_t$, where R_{t-1} is the preceding R interval. If TI_{eff} + TD is greater than the sum of R_{t-1} and R_t, then $F = ((TD + TI_{eff})-(R_{t-1} + R_{t-2}))/R_t$, where R_{t-2} is the R-R interval preceding R_{t-1}. If TI_{eff} + TD is less than R_t, then $F = (TD + TI_{eff})/R_t$. Where TR_0 is greater than (R_{t-1} + R_t), triggering is on the next R wave (R_{t+1}). $TR_0 = (TD + TI_{eff} + (IA/2) + c)$. For non ECG-gating the time interval prior to IA is constant ($TR_0 = TI_{eff} + IA/2 + c$ = 1080ms). The theoretical number of images acquired was counted and mean ± SD F obtained for each sample of R-R intervals modelled. Seven patients, 2 with normal coronary angiography (group A) and 5 with single vessel CAD (group B), underwent rest/adenosine (140 mcg/kg/min) perfusion imaging with constant TR_0 IA. 3 short axis slices, each divided into 8 radial regions of interest (ROIs) were obtained at basal, mid-papillary and supra-apical levels. With the use of a previously described tracer kinetic model (1), the rest and stress unidirectional transfer constants, K_i, were computed for coronary arterial ROIs, as described by the Green Lane system. CAD was defined as measured reduction in coronary artery (CA) cross-sectional area of >50% (Quantcor, Siemens, Germany). Myocardial perfusion reserve index (MPRI) was defined as the K_i stress: rest ratio. Mean K_i values for ROIs supplied by normal vessels (CA) were compared with those obtained in ROIs supplied by stenosed CAs. A receiver operator characteristic (ROC) curve was constructed for MPRI values.

Results: The theoretical number of images acquired and variance in F is shown in table 1 for the five rhythms studied. Significant variance in F between non ECG-gated and gated acquisitions is only seen in example i ($p < 0.001$). Temporal resolution is higher with non ECG-gated acquisition ($p < 0.005$) in all cases. Image quality was acceptable for signal intensity extraction and K_i calculation in all patients. Mean ± SD MPRI in group A was 3.21 ± 0. 58. MPRI was lower in the normal CA territories in group B, i.e. 2.02 ± 0.94 ($p < 0.001$). MPRI in ROIs supplied by stenosed vessels i.e. 1.51 ± 0.74 was lower than group A ($p < 0.001$), and the normal territories in group B, ($p < 0.001$). The ROC curve demonstrated that a MPRI of 1.8 had the best discriminatory capacity for detecting ROIs supplied by a stenosed coronary artery, i.e. sensitivity of 79% and specificity of 68%.

Conclusion: For dynamic first pass imaging, ECG-gating IA has the theoretical advantage that motion artefact may be reduced. Because of the mandatory duration of IA and dead times, this is only realised for subjects with low heart rates and minimal HRV. In clinical practice, increased HRV, ectopic activity and arrhythmias cause errors in ECG-gating that lead to the same degree of variance in IA placement within the cardiac cycle as those images acquired with a constant TR_0. The temporal resolution of IA using the ECG-gated technique is much less than that of the non ECG-gated method. We have shown that the calculation of regional K_i values from images acquired at a constant TR_0 can provide diagnostic information in patients regarding the presence of coronary artery stenoses of greater than 50% reduction in cross-sectional area and early coronary artery dysfunction.

68. Visualization of Cardiac Involvement in Patients with Systemic Sarcoidosis by Magnetic Resonance Imaging

Jeanette Schulz-Menger,[1] Oliver Strohm,[2] Rainer Dietz,[3] Matthias Friedrich.[4] [1]*Franz-Volhard-Klinik, Charite, Humboldt-Universitaet zu Berlin, Wiltbergstr.50, Berlin, Berlin Germany;* [2]*Franz-Volhard-Klinik; Charite, Humboldt-Universitaet zu Berlin, Wiltbergstr.50, Berlin, Berlin Germany;* [3]*Franz-Volhard-Klinik; Charite, Humboldt-Universität zu Berlin, Wiltbergstr.50, Berlin, Berlin Germany;* [4]*Franz-Volhard-Klinik, Charite, Humboldt-Universitaet zu Berlin, Wiltbergstr. 50, Berlin, Berlin Germany*

The diagnosis of the cardiac involvement in patients with known systemic sarcoidosis is difficult, especially because of the low sensitivity of myocardial biopsy and the low specifity of impaired left ventricular function. Applying contrast-enhanced magnetic resonance imaging (MRI) it is possible to detect tissue changes associated with inflammation.

Patients and Methods: We applied contrast-enhanced MRI in 6 patients with proven systemic sarcoidois and suspected cardiac involvement (carc-cardiac) as defined by the presence of typical symptoms (dyspnea, fatigue) and arrhythmias documented by ECG.

We performed standard T1-weighted multislice spin-echo sequences (TE 30 ms; TR 480-725 ms; slice thickness 6 mm) in an axial and short-axis orientation (before and after application of 0.1 mmol/kg Gd-DTPA (Magnevist®, Schering AG; Berlin, Germany) on conventional MRI systems (1.0 T; Siemens-Expert; Siemens AG, Erlangen, Germany and 1.5 TSigna CV/i; GE; Milwaukee, USA, respectively) using a body coil. The relative signal enhancement of the myocardium as related to the skeletal muscle was calculated. Furthermore we compared the left ventricular ejection fraction (LVEF) as determined by gradient echo sequences. Results were compared to 8 patients with proven systemic sarcoidois but without cardiac symptoms or arrhythmias (sarc), and to 9 healthy volunteers (vol).

Results: We found a patchy accumulation of contrast media in the hearts of the patients with evidence for cardiac involvement, but not in others (see fig. 1). The focal relative signal enhancement was significantly higher in patients with suspected myocardial involvement (7.0 ± 1.7) than in patients without any clinical evidence for cardiac involvement (2.2 ± 0.3, $p < 0.01$). Furthermore, the global myocardial contrast enhancement was also significantly increased (6.3 ± 2.0) as compared to patients without evidence for cardiac involvement (2.2 ± 0.3, $p < 0.01$). The difference between patients without cardiac involvement and controls (1.9 ± 0.2) was not significant (see fig. 2a). Follow-up studies over 2 years (after 1, 6, 12 and 24 months) showed a normalization of the relative enhancement in 5 of 6 affected patients undergoing steroid medication. In one patient there were varying enhancement values with a close relation to the clinical status. The LVEF was within the normal range in all subjects, but showed significant differences between sarc-cardiac and sarc (57.5 ± 5% vs. 69.3 ± 2%; $p > 0.01$), between sarc-cardiac and V (57.5 ± 5.0% vs. 74.2 ± 2.0%; $p > 0.01$), whereas there was no significant difference between sarc und V (see fig. 2b)

Discussion: Contrast-enhanced MRI reveals an increased accumulation of contrast media in patients with systemic sarcoidosis and clinical evidence for cardiac involvement. This was present in focal areas, but also but also when quantified for the whole myocardium. However, also in myocarditis, dilative cardiomyopathy, malignant processes and acute myocardial infarction (AMI) the signal intensity may be increased following contrast media administration. Thus, MRI signal intensity changes as such may–with the exception of hemosiderosis–be not very specific for the disease, but the patient's history, the very patchy contrast distribution, and lacking relation to coronary perfusion areas may be sufficient to make other diseases unlikely.

The LVEF shows signifanct differences between the affected patients (sarc-cardiac) and other groups, but stays within the normal range.

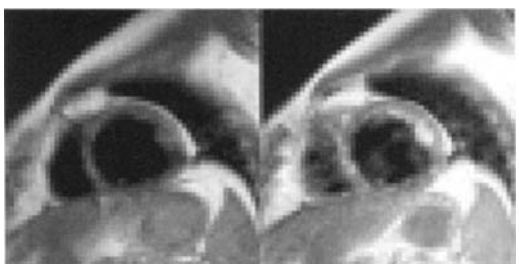

Figure 1. Short axis view before and after application of contrast media with patchy accumulation of contrast medium (follow-up study after 9 months).

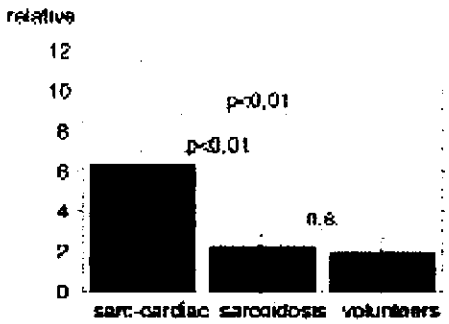

Figure 2a. Relative enhancement of patients with proven systemic sarcoidosis with (sarc-cardiac) and without (sarcoidosis) suspected cardiac involvement, and volunteers (V).

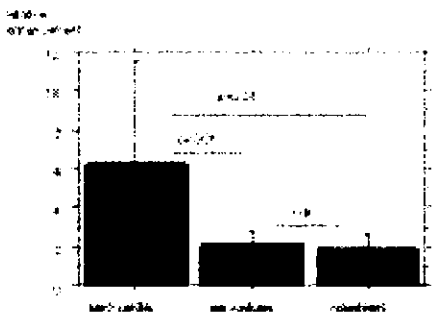

Figure 2b. Comparison of the left ventricular ejection fraction in patients with proven systemic sarcoidosis with (sarc-cardiac) and without (sarcoidosis) suspected cardiac involvement, and volunteers (V).

Conclusion: Contrast-enhanced MRI may serve as a sensitive non-invasive tool for the detection and follow-up of myocardial involvement in patients with systemic sarcoidosis. Further studies in larger patient groups are necessary to assess its' clinical applicability.

69. Visualization of Very Early MRI Signal Changes in Patients

Jeanette Schulz-Menger,[1] Oliver Strohm,[2] Rainer Dietz,[3] Frank Uhlich,[3] Matthias Friedrich.[4] *[1]Franz-Volhard-Klinik, Wiltbergstrasse 50, Berlin, Berlin Germany; [2]Franz-Volhard-Klinik; Charite, Campus Buch; Humboldt-Universität zu Berlin, Wiltbergstr. 50, Berlin, Berlin Germany; [3]Franz-Volhard-Klinik; Charite Campus Buch; Humboldt-Universität zu Berlin, Wiltbergstrasse 50, Berlin, Berlin Germany; [4]Franz-Volhard-Klinik, Charite, Wiltbergstr. 50, Berlin, Berlin Germany*

Background: Acute myocardial infarction following interventional septal artery embolisation in patients with hypertrophic obstructive cardiomyopathy presents an excellent experimental model for the investigation of signal changes.

Methods: We studied 11 patients on days 1,3,7,14, 28 and 90 and a subgroup of 5 patients within 45 min after embolization in a MRI-Scanner (Siemens-Expert 1.0 T resp. GE Signa 1.5T). Necrosis and associated edema were assessed by T2-weighted-spinecho sequences (STIR, TE 64 ms) before and by T1-weighted spinecho-sequences be-

fore and after application of 0.1 mmol/kg Gd-DTPA (Magnevist®, Schering AG; Berlin).

Results: There were no complications in any of the studies.

In T1-weighted images a late signal enhancement in the infarct-associated septal region could be visualized within the first hour after the occlussion of the septal artery. This area shows a contrast enhancement during the whole follow up, with varying size. Remarkably, there was no evidence of myocardial edema. Within the first hour after cessation of the coronary flow. On the other hand, between day 1–28. Edema was visible in all patients After 3 months there was no increase of a signal in the T2-weighted images.

In general, the edema showed a larger extention than the area defined by contrast enhancement.

Conclusion: Myocardial edema is not detectable during the first hour after induced myocardial infarction. For the detection of very early myocardial infarction the assessment of edema is not sufficient.

70. High Frequency of Abnormal Delayed Hyperenhancement

Ralf Wassmuth,[1] Anthony Aletras,[2] David Begley,[3] Karen Bove Bettis,[4] Pat Woltz,[5] Lameh Fananapazir,[6] Andrew Arai.[7] [1]*National Institutes of Health, Bldg 10 B1D161 MSC 1061, Bethesda, Maryland United States;* [2]*National Institutes of Health, Bldg 10, B1D161, MSC 1061, Bethesda, Md USA;* [3]*National Institutes of Health, Bldg 10, B1D161, MSC 1061, Bethesda, Md USA;* [4]*National Institutes of Health, Bldg 10, B1D161 MSC 1061, Bethesda, Md USA;* [5]*National Institutes of Health, Bldg 10, B1D161 MSC 1061, Bethesda, Md USA;* [6]*National Institutes of Health, Bldg 10 B1D161 MSC 1061, Bethesda, Md USA;* [7]*National Institutes of Health, Building 10, Room B1-D161, Bethesda, MD USA*

Background: Delayed hyperenhancement has been described as characteristic for myocardial infarctions using gadolinium enhanced magnetic resonance imaging (MRI). In hypertrophic cardiomyopathy (HCM) focal areas of infarction as well as increased collagen content of the myocardial wall have been described in pathology studies. Fibrosis forms the substrate of arrhythmias with the risk of sudden death. We hypothesized that patients with HCM might have focal irregularities that can be detected using delayed hyperenhancement imaging.

Patients and Methods: 13 consecutive patients with HCM were scanned in a 1.5 T clinical scanner (GE, Milwaukee) using an imaging protocol appropriate for patients with coronary artery disease. An ECG-gated inversion recovery fast gradient echo sequence (TR 8 ms, TE 3.4 ms Flip angle 20, spatial resolution 1.5 × 3 mm) was applied 15–30 minutes after administration of 0.2 mmol/kg Gadolinium-DTPA. The inversion time was chosen to null the signal of normal myocardium. In addition all patients underwent resting, stress and reinjection Thallium-201 SPECT. No patient had significant coronary artery stenosis on coronary angiography.

Results: In 11 out of 13 patients, lesions were detected in the hypertrophied myocardium appearing either as predominantly focal (n = 5) or diffuse (n = 6) enhancement relative to the remaining myocardium. In 4 patients, both focal and diffuse areas of hyperenhancement were found. The focal enhancement had a signal intensity (SI) equal or higher than the blood pool (mean SI 33 vs. 31, arbitrary units). The focal areas of hyperenhancement were between 5 and 19 mm in diameter. The diffusely enhanced areas were less bright than blood (mean SI: 26 vs. 49) but were substantially brighter than the normal myocardium (SI: 7) and covered wide portions of the thickened wall. The diffuse lesions were typically transmural or located in the mid myocardium. The thallium studies revealed reversible defects in all 13 patients in the hypertrophic area but no fixed defects were seen.

Conclusions: In HCM focal areas of delayed hyperenhancement can be found with MRI characteristics similar to myocardial infarction. These MRI abnormalities most likely represent focal infarction or fibrosis, known complications of HCM. As use of contrast enhanced infarct imaging protocols disseminate, it is important to understand other pathological processes that may result in abnormal delayed hyperenhancement.

71. In-Vivo Delineation of Scar Tissue by MR: Hyperenhancing Myocardium is Negative for Glucose Metabolism

Juerg Schwitter,[1] Daniel Nanz,[2] Patrick Knuesel,[3] Christophe Wyss,[4] Philipp Kaufmann,[4] Borut Marincek,[3] Thomas Luescher,[5] Gustav von Schulthess.[4] [1]*University of Zurich, Division of Cardiology, Zurich, ZH Switzerland;* [2]*University Hospital Zurich, Department of Radiology, Zurich, ZH Switzerland;* [3]*University Hospital Zurich, Institute of Diagnostic Radiology, Zurich, ZH Switzerland;* [4]*University Hospital Zurich, Clinic of Nuclear Medicine, Zurich, ZH Switzerland;* [5]*University Hospital Zurich, Division of Cardiology, Zurich, ZH Switzerland*

Background: Differentiation of scar tissue from viable myocardium and quantification of scar is of major importance for risk stratification particularly in patients referred for aorto-coronary bypass surgery.

In experimental studies it was shown that signal enhancement during the equilibrium phase distribution of an extravascular contrast medium (CM) correlates with an increased distribution volume, i.e. loss of cell membrane integrity in the acute phase [1] and/or an increase in extracellular space in the chronic phase [2]. In man myocardial tissue exhibiting signal enhancement following CM administration is less well characterized.

Purpose: To test the hypothesis that myocardial regions exhibiting delayed enhancement are metabolically inactive, i.e. correspond to scar tissue as defined by positron emission tomography.

Material and Methods: Patients with documented coronary artery disease and hypokinetic or akinetic myocardial segments on invasive examination were recruited for this study. All subjects gave written informed consent to participate in the study that was approved by the local ethics committee.

a) MR Imaging and Data Analysis: All subjects were examined in supine position in a 1.5T system (CV/i, GE Medical Systems, Milwaukee, WI) and a four-element phased-array RF coil (GE Medical Systems, Milwaukee, WI) was used for signal reception. Following assessment of resting cardiac function 0.25 mmol/kg of the extravascular CM Gd-DTPA-BMA (Omniscan™ Gadodiamide injection, Nycomed Imaging AS, Norway) was injected. 15 minutes later the zero crossing of blood, normal myocardium and scar tissue was determined by increasing the inversion time (TI) from 50 ms to 275 ms (increments of 25ms) by means of an inversion recovery segmented k space pulse sequence (TR/TE: 6.4/1.6 ms, matrix 160 × 256 with a field of view of 34–40 cm × 34–40 cm) performed during repeated breathholds. The TI nulling normal myocardium was then used to cover the whole left ventricle (slice thickness 8mm) from base to apex.

On all slices left ventricular (LV) endocardial/epicardial borders and areas of hyperenhancement were drawn manually. Each slice was then automatically divided up in 8 equiangular sectors (rotating clockwise and using the anterior septal insertion of the right ventricle as a reference point) and the fraction of enhanced tissue/sector was calculated. In addition polar maps of hyperenhancement in the subendocardial layer and for full wall thickness were generated. Total LV mass and mass of scar was also calculated.

b) PET Imaging and Data Analysis:

PET imaging was performed to assess glycolytic metabolism with 18F-Fluorodeoxyglucose (FDG) by a whole-body scanner

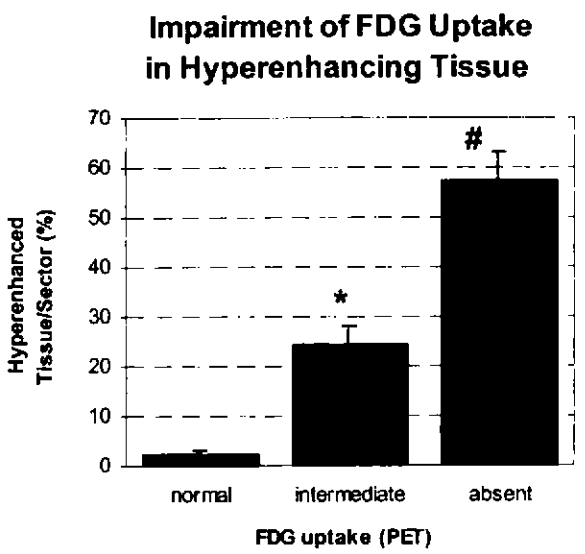

Figure 1. Bar graph showing increasing fraction of hyperenhancing tissue in sectors with intermediate or complete impairment of FDG uptake, respectively. * and #: $p < 0.005$ vs normal and intermediate, respectively.

(Advance, GE Medical Systems, WI). Following oral administration of glucose (50g), measurement of resting myocardial perfusion by means of 13N-ammonia PET was performed and blood sugar was controlled by insulin administration. FDG was then injected (dose: 250 MBq IV) and image acquisition (12 × 5 minutes) was initated 30 minutes later.

On reformated short axis images FDG uptake was evaluated in 8 sectors/slice. Uptake was rated qualitatively as normal, intermediate or absent. Sectors with normal resting perfusion served as reference sectors for normal glucose uptake.

c) Conventional X-ray Coronary Angiography:

LV angiography was performed to document regional myocardial dysfunction and coronary angiography was performed to confirm the ischemic origin of dysfunction.

Statistics: Data are presented as mean value ± SEM. Differences in the fraction of enhancing tissue/sector on MR images with respect to the different PET categories were assessed using a repeated measures ANOVA.

Results: In 7 patients 9 occluded vessels (6 major coronary arteries and 3 side branches) were found that correlated with hypokinetic regions. In one patient a hypokinetic inferior region was supplied by a stenosed right coronary artery. The inferior wall in this patient showed delayed hyperenhancement on MR in agreement with a lack of glucose uptake on PET. 5 of the 9 occluded vessels were collateralized. Mean ejection fraction was 54 ± 13%.

MR Results: Total LV mass was 192 ± 48g with a scar mass of 14.9 ± 11.3 g (7.3 ± 4.1% of LV mass). All myocardial infarctions were correctly identified by hyperenhanced areas on MR even when infarct-related arteries were well collateralized. From the 440 sectors evaluated 123 (28.0%) showed hyperencement, only 52 (42.3%) of those showed transmural hyperenhancement.

Comparison with PET: On PET images 48 sectors demonstrated absence of FDG uptake, 66 additional sectors were graded as demonstrating intermediate FDG uptake. An inverse relationship was observed between extent of hyperenhancing tissue in a given sector and its ability to take up FDG: In sectors lacking FDG uptake the fraction of hyperenhancing tissue was 57.5 ± 5.7%, whereas in sectors with intermediate FDG uptake the fraction of hyperenhancing tissue was 24.1 ± 3.9% ($p < 0.005$, Bonferroni-corrected). In sectors with normal FDG uptake the fraction of hyperenhanced tissue was 2.4 ± 0.7% ($p < 0.005$ vs intermediate sectors, Bonferroni-corrected).

Conclusions: In myocardium that demonstrates delayed signal enhancement uptake of FDG is impaired indicating the presence of scar. The technique enables accurate assessment of distribution of scar tissue, i.e. subendocardial versus transmural scar formation and further allows quantification of scar tissue.

72. Dobutamine/Adenosine Double Stress and Delayed Enhancement (DADS-DE) MRI in Patients with Coronary Artery Disease: Initial Clinical Evaluation

Lieven Van Hoe,[1] Marc Vanderheyden,[2] Luc Janssens,[2] Jan Schillebeeckx.[3] [1]*Imelda Hospital Bonheiden, Imeldalaan 9, Bonheiden, Brabant Belgium;* [2]*Imeldahospital, Imeldalaan 9, Bonheiden, Brabant Belgium;* [3]*Imeldaziekenhuis, Imeldalaan 9, Bonheiden, Brabant Belgium*

Lieven Van Hoe, Marc Vanderheyden1, Luc Janssens1, Jan Schillebeeckx *Departments of Radiology and* [1]*Cardiology, Imelda Hospital, Bonheiden, Belgium*

Background: One of the promises of MRI is that it would offer a noninvasive test to select patients with suspected coronary disease for PTCA or surgery. While much research focuses on direct visualisation of coronary stenoses with MRA, a lot of useful informaton can also be obtained with combined evaluation of global and regional function, pefusion, and delayed enhancement.

Aims: To assess the feasability of the comprehensive DADS-DE MRI protocol in clinical practice and to correlate the results with those obtained with coronary angiography.

Methods: Sixteen patients with suspected coronary artery disease were examined with MRI prior to coronarography. A 1.5T MRI scanner (Siemens Symphony, Germany) was used. Rest perfusion was imaged using an inversion recovery snapshot FLASH sequence with TR 2.4, TE 1.2, TI 200 msec, matrix 48 × 128, 40 measures). Basal, midpapillary and apical short axis planes were acquired after a bolus of 0.025 mmol/kg aspecific contrast medium (Gadolinium). As a next step, basal function was assessed using a breath-hold cine sequence (TR 60 msec, TE 4.8 msec, contiguous short-axis slices covering the entire heart). Next, the perfusion study was repeated after injection of a bolus of 0.05 mmol/kg contrast medium and during adenosine infusion (140 µk/kg/min). Immediately after this study, 0.125 mmol/kg contrast medium was injected in order to allow high-dose delayed contrast-enhanced imaging. If an abnormal regional contractile function was detected on the cine studies, the contractility study was repated during low dose dobutamin infusion (10µ/kg/min). Finally, delayed contrast-enhanced images were obtained using an inversion recovery segmented FLASH sequence (12 heart beats, TR 8, TE4, TA 10 sec, matrix 253 × 256, 180° IR pulse). The TI value was adjusted in every individual patient in order to obtain optimal contrast (TI between 250 and 300 msec). Global cardiac function was assessed after manual contouring of cine images using the ARGUS software. EF, EDV, ESV, SV, and myocardial mass were calculated. For evaluation of perfusion, regional function, and delayed enhancement, each short axis slice was divided radially into 6 segments (anterior, lateral, posterior, inferior, inferoseptal, anteroseptal). Perfusion (rest and stress) was qualitatively assessed per segment by using a three-point score (normal, probably abnormal, abnormal). Segmental contractility was described as follows: normal, hypokinetic, akinetic, dyskinetic. Segmental delayed enhancement was described as absent, subendocardial, or transmural. The total volume of the enhancing myocardium was calculated. The results

obtained with the different tests were compared with those obtained with coronary angiography. Therefore, it was assumed that the anterior-anteroseptal, inferoseptal-inferior, and lateral-posterior segments represented the LAD, right, and Cx coronary perfusion territories, respectively.

Results: There were no serious adverse effects. Average scanning time was 50min. Average time for postprocessing and image evaluation was 35 min. When evaluated per perfusion territory, the sensitivity and specificity for detection of significant coronary artery stenoses were 0.74/0.85 for rest perfusion, 0.7/ 0.73 for contractility during rest, 0.81/ 0.71 for adenosine pefusion. The overall sensitivity for detection of the presence of significant coronary stenoses per patient was 0.9, 0.81, and 1 for rest perfusion, contractility during rest, and stress perfusion, respectively. In 9 patients, delayed enhancement was observed (5 subendocardial, 3 transmural). Eight of these patients had a previously diagnosed myocardial infarction. The total infarcted volume, as calculated with MRI, was not significantly correlated to EF. As expected, there was a significant correlation between recovery during low dose dobutamin stress and presence of delayed segmental subendocardial hyperencancement.

Discussion: The DADS-DE protocol proved to be clinically feasible and provided a huge amount of information in each patient. In most patients, different segments showed either abnormal perfusion, abnormal contractilty, or delayed enhancement, showing that these tests provide complementary information. These data suggest that this protocol offers an adequate assessment of myocardial status (normal, hibernating, nonviable, ischemic during stress) per segment. The imperfect correlation of segmental abnormalities on MRI with the exact location of coronary stenoses may be partially due to anatomic variants in coronary anatomy and presence of collateral circulation. Further studies in patients without coronary disease should be performed to assess the specificity of the different types of abnormalities.

Overall, DADS-DE MRI without coronary MRA holds promise as a noninvasive test that may guide the selection of patients for specific treatment. Delayed high-dose contrast-enhanced MRI represents a simple and robust technique to assess the total infarct burden1 and provides unique information on the exact spatial location of the infarcted tissue (transmural versus subendocardial). Moreover, the total infarcted volume could represent a useful new prognostic parameter.

Reference
1. Kim et al. Circ 1999; 100:1992–2002

73. Evaluation of Short-Axis, Parallel Long-Axis and Radial Long-Axis Measurements of Ventricular Mass in Ex Vivo Pig Hearts

Sven Plein,[1] Timothy Bloomer,[2] Tim Jones,[3] David Higgins,[1] Gavin Bainbridge,[4] Aleksandra Radjenovic,[5] Mohan Sivananthan.[1] [1]*Leeds General Infirmary, Cardiac MRI Unit, Leeds, West Yorkshire United Kingdom;* [2]*Leeds General Infirmary, Clarendon Wing, Leeds, West Yorks United Kingdom;* [3]*Leeds General Infirmary, Cardiac MRI Unit, Leeds, West Yorkshire United Kingdom;* [4]*Leeds General Infirmary, Cardiac MRI Unit, Leeds, W Yorks United Kingdom;* [5]*University of Leeds, Department of Medical Physics, Leeds, West Yorkshire United Kingdom*

Introduction: In clinical practice, short axis is the preferred orientation for measurements of ventricular volumes and mass. This is because contrast in the conventionally used gradient echo sequences depends on blood flow through the imaging plane, and is thus often poor in long-axis images. However, short axis analysis has well known and documented limitations, which are mainly related to the longitudinal contraction of the heart and the resulting change in the position of the basal and apical slices. The inclusion or exclusion of the basal slice in diastole and systole shows large observer variability with a significant effect on volume measurements. With recently introduced new acquisition sequences (TrueFISP and equivalent sequences) long-axis cine images with excellent blood/myocardial contrast can now be acquired as contrast in these sequences depends mainly on the T1/T2 properties of tissue. This might allow the use of long-axis images for measurements of ventricular dimensions. Acquisition of parallel long-axis slices, though, would result in large partial volume effects, but acquisition of slices in a radial orientation along the long axis of the heart might be a useful alternative approach.

This study had four objectives:

1. To compare short-axis, parallel long axis and radial long-axis measurements of left ventricular mass in an ex vivo animal model prior to clinical evaluation of radial long-axis acquisitiom
2. To evaluate a customised analysis software for radial images
3. To define, how many radial slices are required to produce accurate mass estimations
4. To establish, how measurements of mass on an optimal model differ from true ventricular mass.

Methods: Ten whole ex-vivo pig hearts were studied on a 1.5T Philips ACS NT Cardiac MRI system (Philips Medical Systems, Best, The Netherlands). The cardiac chambers were cleaned, stuffed with gauze and the hearts were then placed in the middle of a quadrature receive-only coil with RF mirror. The following scans were acquired:

1. a high resolution T2 weighted 3D Turbo Spin Echo Scan (Slice thickness 1.6mm, with 0.8mm overlap, TR 2.5s, TE 100ms, Flip angle 90, FOV 230mm, 512 × 512 matrix).
2. three T1 weighted Spin Echo EPI scans in short axis, long-axis and a radial long-axis oreintation with 6 slices (6mm slice thickness, 1mm gap, TR 1s, TE 25ms, Flip angle 90, FOV 350mm, 256 × 256 matrix).

The pig hearts were then dissected and the left ventricle isolated. Care was taken to remove the epicardial fat, the right ventricular papillary muscles and the valve aparatus. Left ventricular papillary muscles were left in situ. Following this, the same scans as above were repeated on the isolated ventricle.

The isolated left ventricles were then weighed on a high-precision digital scale (accuracy <0.1mg). The 3D data sets were reconstructed in radial long-axis orientation with 2,4,6,9,12, 24 and 36 radial slices (1mm slice thickness). Endo- and epicardial contours were drawn on all data sets using MASS software (Medis, Leiden, The Netherlands). Left ventricular papillary muscles were included in the contours, right ventricular attachments at the septum were excluded. Mass measurements were performed with the MASS software for short-axis and parallel long-axis images. For radial data sets, a customised software that was developed at this institution was used (PlotContour004).

All data sets were measured independently by two experienced observers.

Results: Mesurements of left ventricular mass based on the whole hearts differed significantly from the true weight in all acquisition orientations (Table 1). Differences were lowest for short axis orientation and largest for radial long axis acquisition. Measurements of the isolated left ventricle were more accurate (Table 2), with measurements of the 3D data sets less than 0.5% different from the true weight. Of the other sequences, measurements on short axis images was most accurate and long-axis measurements were least accurate. The radially reconstructed 3D images showed excellent agreement with the true mass for all slice numbers, except for 2 and 4 slices (no table). All interobserver variabilities were within 5%, with lowest variabilities on the 3D measurements.

Discussion: Even in an optimised model of non-beating ex-vivo pig hearts and high resolution scans, left ventricular mass was consistently overestimated by two experienced observers and in 3 different slice orientations. This suggest cardiac tissue outside the left ventricle was systematically included in left ventricular contours. Some of the oversti-

Table 1

Differences of Mass Estimates on Whole Hearts from True Mass (Mean = 184.03g)

	Short Axis	Long Axis	Radial	3D
Mass estimate (mean)	195.6g	196.7g	203.5g	192.4g
Difference to true weight	11.6g	12.6g	19.5g	8.4g
p value	0.001	<0.0001	<0.0001	0.013

Table 2

Differences of Mass Estimates on Isolated Ventricles from True Mass (Mean = 184.03g)

	Short Axis	Long Axis	Radial	3D
Mass estimate (mean)	188.4g	192.3g	195.8g	184.7g
Difference to true weight	4.3g	8.3g	11.7g	0.7g
p value	0.089	0.1	0.001	0.565

mation could be due to partial volume effects. The measurements of the isolated ventricles were closer to the true mass with the 3D measurements differing by less than 0.5%. This validates the analysis methods used. The fact that the 2D measurements of isolated ventricles also showed some overestimation of mass is probably due to partial volume effects in view of the larger slice thickness. Radial acquisition produced similar results to the other orientations. This validates our customised radial analysis software and suggests that radial acquisition can be used for clinical evaluation. 6 or more radial slices provide good agreement with true mass.

74. Assessment of Patients with Left Bundle Branch Block and Septal Defects on Nuclear Scintigraphy Using Cardiovascular Magnetic Resonance

Jane Mccrohon Dr,[1] Shelley Rahman,[2] Nicholas Bunce,[3] Dudley Pennell.[4] [1]*Royal Brompton Hospital CMR Unit, Sydney St, London, London UK;* [2]*Royal Brompton Hospital, Department of Nuclear Medicine, London, London United Kingdom;* [3]*Royal Brompton MRI Unit, Sydney Street, London, London United Kingdom;* [4]*Royal Brompton and Harefield NHS Trust, Sydney Street, London, London United Kingdom*

Background: The non-invasive assessment of left bundle branch block (LBBB) remains an area of significant diagnostic limitation. Exercise scintigraphy shows septal defects in many of these patients who have subsequently been shown not to have significant epicardial coronary artery stenoses. The mechanism of these defects is poorly understood and has not previously been evaluated by cardiovascular magnetic resonance (CMR).

Methods: We performed magnetic resonance first pass myocardial perfusion imaging using a 2D Turbo FLASH technique and wall motion assessment using CMR in 26 patients with LBBB noted to have perfusion defects on stress scintigraphy. First-pass perfusion was performed on a Picker Edge 1.5T scanner using a phased array coil and a FLASH gradient-echo sequence with a 180° inversion pulse for T1-weighting and parameters of; TE 1.9ms, TR 4ms, TI 450ms, SLT 10mm, FOV 50mm × 50mm and matrix size of 64 × 128.

Results: In the 14 patients who underwent coronary angiography, 6 had normal epicardial coronaries, 5 had minor LAD lesions (<50%), and 3 had occluded LAD arteries. With CMR, all 26 patients had incoordinate septal wall motion and 24/26 had reduced systolic thickening of the septum. In these 24 patients, myocardial perfusion reserve (MPR) was significantly reduced in the septum when compared to other left ventricular walls with normal systolic function. In the patients with normal coronaries (n = 6), MPR of the septum was significantly lower than in the lateral wall (septum 1.29 ± 0.58 vs lateral wall 2.3 ± 0.9, p = 0.002). In the patients with known coronary disease (n = 8), MPR in the septum was 0.85 ± 0.19 versus 2.09 ± 0.35 (p = 0.003) in remote myocardium with normal contractility, and in the 12 patients of unknown coronary status MPR in the septum was 1.26 ± 0.45 versus 2.21 ± 0.92 (p = 0.004) in remote myocardium. The 2 patients with well preserved systolic thickening of the septum, had better septal perfusion reserve than seen in the 24 patients with impaired septal systolic function (2.3 ± 0.01 versus 1.07 ± 0.39, p = 0.002) suggesting a possible threshold before functional loss is evident.

Conclusion: CMR confirms that scintigraphic septal defects in LBBB are associated with a reduced septal MPR and with reduced systolic thickening. Further studies using new CMR techniques to assess previous infarction in these septal regions may be useful to differentiate between ischaemic and non-ischaemic etiologies of LBBB.

References

1. Skalidis et al; JACC 1999; 33(5):1338–1346.
2. Sugihara et al; J Nucl Med 1997; 38:545–547.

75. Detection of Viable Myocardium in Patients with Severely Reduced Left Ventricular Function by Late Gadolinium-DPTA Kinetics: A Comparison with Positron Emission Tomography

Christoph Klein,[1] Stephan Nekolla,[1] Bernhard Schnackenburg,[2] Felix Haas,[3] Frank Bengel,[4] Andrea Sammer,[5] Markus Schwaiger.[5]

[1]*Nuklearmedizinische Klinik, Klinikum rechts der Isar der TU Muenchen, Ismaningerstr. 22, Muenchen, Bayern Germany;* [2]*Philips Medical Systems Germany, Berlin, Berlin Germany;* [3]*Department of Cardiovascular surgery, German Heart Institute Muenchen, Muenchen, Bayern Germany;* [4]*Nuklearmedizinische Klinik, Klinkum rechts der Isar der TU Muenchen, Muenchen, Bayern Germany;* [5]*Nuklearmedizinische Klinik, Klinikum rechts der Isar der TU Muenchen, Muenchen, Bayern Germany*

Introduction: Patients with severely reduced left ventricular function due to coronary artery disease (CAD) have an increased incidence of perioperative mortality when undergoing operative revascularisation. However, if dysfunctional segments contain enough viable myocardial cells (hibernating myocardium) which exhibit the potential for functional recovery prognosis increases considerably after successful revascularisation. Thus, the need for preoperative evaluation for hibernating myocardium of these patients is well appreciated. Currently the gold standard for the detection of hibernating myocardium is positron emission tomography (PET).

Late Gadolinium-DPTA (Gd-DPTA) kinetics have shown to be able to differentiate between dyskinetic myocardium which has the potential to recover or not recover after revascularisation.

The aim of the study was to compare results obtained by magnetic resonance imaging (MRI) with those by PET.

Method: 14 patients with severely reduced left ventricular function due to CAD who had an indication for a PET examination for the assessment of viable myocardium were included into the study. They were examined with a 1.5 Tesla whole body scanner (ACS NT, INCA, Philips, The Netherlands) in the supine position using a phased array surface coil. After a rapid survey the short axis of the heart was identified. For the evaluation of regional and global LV-function short axis views, covering the entire heart were obtained. Fifteen to twenty minutes after the administration of GD-DPTA (0.2 mmol/kg bw) short axis slices in late diastole covering the entire heart using a 2D inversion recovery gradient echo technique (TE/TR 3.8/7.5 ms, flip angle 15°, prepulse delay 225 to 300 ms, spatial resolution 1.3 × 1.3 mm, slice thickness 8 mm) were acquired. For analysis the heart was divided into 17 segments (apex, 4 apical and 6 equatorial and 6 basal). Segments with hyperenhancement were visually delineated. Additionally myocardial mass and the mass of the hyperenhanced areas were calculated. For the PET examination the routine protocol for viabilty assessing rest myocardial blood flow using the tracer 13N-ammonia and myocardial metabolism using 18F-2-fluoro-2-deoxyglucose (18FDG) were used. Seventeen segments, identical to the MRI were visually classified as normal, mismatched and scared. Ratios compared to normal tissue were calculated using the Munich Heart software.

Results: All 14 patients were successfully examined with both imaging modalities. The mean left ventricular ejection fraction assessed by MRI was 34 ± 11%. All 238 segments had sufficient image quality in both modalities to be evaluated. With PET, 43 segments were classified as scared and 5 as mismatched. The sensitivity and specificity for MRI identifying scar tissue was 91% and 94% respectively. Nine of 12 false positive segments had subendocardial enhancement only. Of the 5 segments showing mismatch only one showed hyperenhancement. The mean percent scar tissue were 14% ± 17 for PET and 15% ± 13 for MRI ($p = 0.76$).

Summary: Patients with reduced LV-function due to CAD who had an indication for an PET examination could also successfully examined with MRI. The amount and location of scar tissue identified by PET could also be identified by hyperenhancement with MRI with good sensitivity and specificity. All segments of mismatch but one did not show hyperenhancement. Spatial resolution is sufficient to detect subendocardial scarring which might not be detected by PET.

Conclusion: With MRI and the late enhancement technique patients with reduced LV-function can be examined to detect the amount and location of scar and viable tissue. Thus MRI is an easy, relative inexpensive and readily available method for a preoperative assessment.

76. Real Time TrueFISP Cardiac Cine Using Radial Sampling

Ajit Shankaranarayanan,[1] Orlando Simonetti,[2] Gerhard LAUB,[3] Oliver Heid,[4] Jonathan Lewin,[5] Jeffrey Duerk.[6] [1]*Case Western Reserve University, B100, Bolwell Building, Cleveland, Ohio United States;* [2]*Siemens Medical Systems, Ontario Center East Tower, Chicago, IL USA;* [3]*Siemens Medical Systems, Inc., Cardiovascular MR Program Manager, Chicago, Illinois United States;* [4]*Siemens Medical Engineering, Siemens AG, Med MRZ, Erlangen, Bavaria Germany;* [5]*Case Western Reserve University, University Hospitals of Cleveland, Cleveland, Ohio United States;* [6]*Case Western Reserve University, University Hospitals of Cleveland, Cleveland, Ohio United States*

Purpose: Cardiac MRI is primarily driven by the conflicting requirements of high spatial and temporal resolution and short acqusition times. The recently reintroduced TrueFISP [1], with its exceedingly high signal yield at short TR, high inherent blood/myocardium contrast, and motion insensitivity, has shown to be an excellent technique for rapid (current temporal resolution of 77 ms) cine imaging of the heart [2,3,4]. Radial sampling techniques (also known as Projection Reconstruction or PR) offer a different set of tradeoffs than encountered in standard Fourier imaging; undersampling give rise to primarily reduced signal-to-noise (SNR) and to a lesser extent a decrease in resolution, and reduced FOV does not give rise to aliasing but again only to reduced SNR. Our hypothesis was that these tradeoffs of radial acquisitions would offer advantages in temporal and spatial resolution when combined with the high SNR and contrast of the TrueFISP cine technique.

Material and Methods: Real time TrueFISP sequences using radial trajectories were implemented on a 1.5T Magnetom Sonata (Siemens Medical Systems, Erlangen, Germany) with a high performance gradient system (maximum gradient strengths of 40mT/m and maximum slew rate of 200mT/m/msec). Online reconstruction was implemented using a variant of recently described regridding method [5]. The sequence was tested on three normal volunteers.

Real Time Radial TrueFISP: The sequence is based on a real time ungated 2DFT TrueFISP sequence with echo sharing [6] to improve the temporal resolution. View sharing, as it will be called here, was done for 50% of the views. Theoretically two different sharing methods can be implemented. Continuous, where the shared views are adjacent, and interleaved, where the shared views cover the entire k-space. Both of these methods were implemented and compared. The imaging parameters used were 50 views to reconstruct image on 128 × 128 matrix and an FOV of 320mm × 320mm. The basic TrueFISP timing module used had TR/TE = 2.2ms/1.1ms which gave an effective temporal resolution of 55ms. A Circularly Polarized (CP) 4-channel body array was used for signal reception.

Results: Figure 1 shows the short axis views obtained with the real time ungated PR cine sequence. Images from both continuous and interleaved sharing are shown. Images shown are temporal snapshots extracted from a time series during continuous scanning. Motion of the heart appeared to be asynchronous in continuous sharing method and smooth in interleaved sharing. However, a slight increase in radial streaks was observed with the interleaved sharing method.

Discussion: In radial sampling techniques, the image resolution is primarily dependent on the number of samples in the read direction and less on the number of views acquired. This results in a higher resolution per unit time than Fourier imaging, at the expense of SNR. This is advantageous in cardiac cine imaging where temporal resolution and

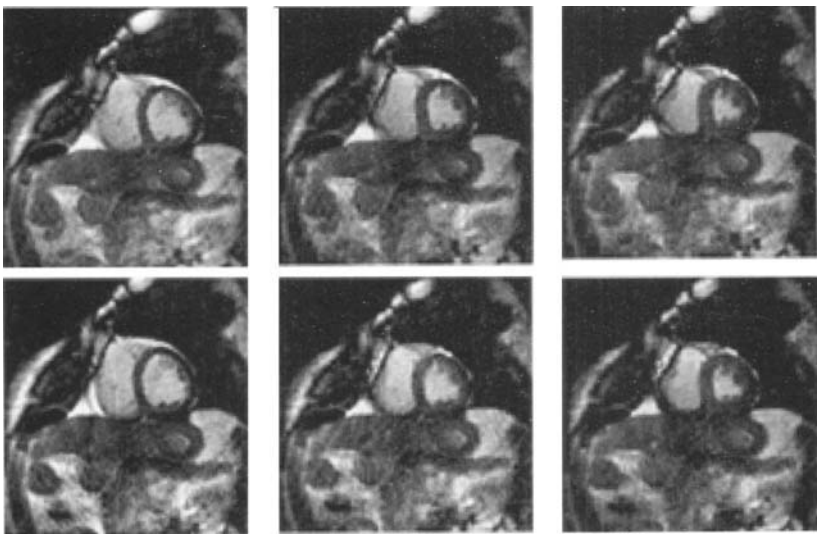

Figure 1. The images from real time radial cine sequence are shown here, at different time points. The upper row shows images from continuous sharing and lower ones from interleaved sharing.

scan time are critical parameters, and also advantageous for TrueFISP which has inherently high SNR. The number of projections can be optimized for SNR and minimization of the streak artifacts. The results from the implementation of the real time radial sequence show that interleaved sharing is better suited for cardiac cine studies. Continuous sharing, which is analogous to the sliding window reconstruction previously described [7], results in alternating updating of data in horizontal and vertical directions. This causes the motion of the heart to appear discontinuous and asynchronous. In a short-axis view, the radial motion of the heart is such that k-space must be continuously updated in all directions, as is done in the interleaved sharing approach. Moreover temporal resolutions achieved here were significantly higher than those currently used, without degrading the image quality. Combining the advantages of TrueFISP and that of undersampled radial techniques for application in real-time cardiac cine imaging is therefore feasible and appears to be very promising.

77. Flow-Related Signal Loss on TrueFISP Images Due to Shear Rather than Turbulence

Philip Kilner,[1] Anna John,[2] Christine Lorenz,[3] David Firmin,[4] Dudley Pennell.[5] [1]*Royal Brompton Hospital, CMR Unit, London, London, United Kingdom;* [2]*Royal Brompton Hospital, Sydney Street, London, London United Kingdom;* [3]*Royal Brompton Hospital, CMR Unit, London, London England, UK;* [4]*Imperial College of Science, Technology and Medicine, Royal Brompton Hospital, London, London UK;* [5]*Imperial College of Science, Technology and Medicine, University of London, South Kensington, London, London United Kingdom*

Introduction: TrueFISP cine imaging allows good blood-tissue contrast to be achieved in short breathhold acquisitions. With an echo time of less than 2ms, we expected TrueFISP images to show little signal loss from turbulent flow. Using theoretical understanding of jet flow dynamics, we set out to interpret appearances on TrueFISP images in the regions of jets in patients.

Methods: We acquired TrueFISP breathhold cines (TE 1.8 ms, TR 3.2, flip angle 60, 285 × 380 pixels in 120 × 256 × 6 mm slice, temporal resolution 56ms, acquired in 10 to 15 heartbeats) on a 1.5T Siemens Sonata system (Siemens AG, Erlangen, Germany), in planes aligned with and transecting jets in patients with aortic stenosis (n = 6), aortic regurgitation (n = 7), mitral regurgitation (n = 5) and repaired aortic coarctation (n = 3). We also acquired non-breathhold, velocity compensated gradient echo cine images aligned with the jets, TE = 14ms.

Results: The images in the figure on the next page show systolic frames from coronal (A and B) and trans-jet (C) slices in a patient with moderate stenosis of a bicuspid aortic valve. In this as in other cases, we found that while TrueFISP images recovered signal from most of the area of turbulent jet flow, as represented by signal loss on TE14 images (asterisks), there were more limited, often clearly defined lines of signal loss on True FISP images (arrowed). Their location appeared to correspond to high shear layers immediately adjacent to jets. Signal loss was also observed in True FISP images in regions of convergent flow immediately upstream of narrow orifices. In cases where the slice appeared to have been aligned accurately with the core of a jet, the edges of the jet were clearly seen (panel B). In cases where the slice transected the jet immediately down-stream of the orifice, a line of signal void, which allowed clear delineation of the cross-sectional area of the jet, surrounded a bright jet core (panel C). Jet boundaries were less clear in some examples, possibly where the slice cut a shear layer tangentially, or where a narrow, high velocity jet lacked a coherent core.

Discussion: These patterns of signal loss may be explained as follows. Phase dispersion associated with turbulent flow, which caused signal loss on velocity-compensated TE14 images, was probably mainly due to fluctuations of velocity or higher orders of motion as turbulent eddies were carried through voxels between excitation and read-out. This effect would have been minimized by the very short echo time of TrueFISP imaging. Using this non-velocity-compensated sequence, however, phase dispersion in regions of high shear or convergent flow could have been caused by steep instantaneous gradients of velocity–across streamlines in the case of shear, and in the direction of streamlines in the case of convergent flow. These gradients may be present in a voxel, regardless of echo time.

Conclusion: While TrueFISP images did not depict the extent of turbulence, the signal loss confined to the shear layer allowed clear

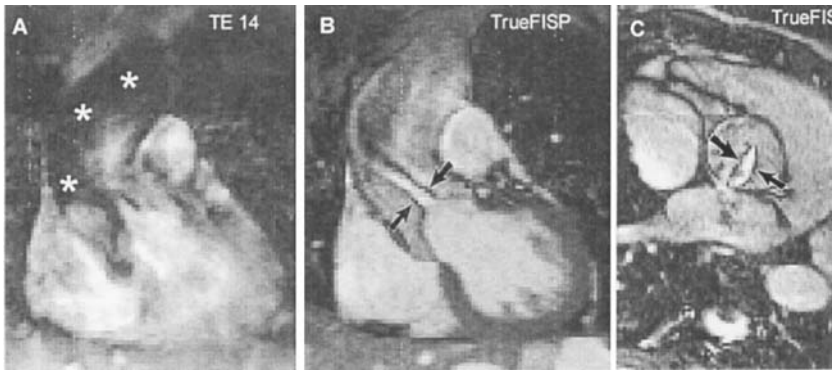

Figure.

delineation of the jet core. This suggests potential usefulness of TrueFISP imaging in assessment of jet lesions, but the choice of slice location, and the use of shear layer signal loss for orifice area measurement need further investigation.

78. Cardiac Magnetic Resonance for the Early Diagnosis of Myocardial Iron Overload

Lisa Anderson,[1] Sally Holden,[2] Clare Charrier,[1] Emma Prescott,[3] Bernard Davis,[2] David Firmin,[4] Malcolm Walker,[2] John Porter,[2] Beatrix Wonke,[3] Dudley Pennell.[5] [1]*Royal Brompton Hospital, Sydney Street, London, London UK;* [2]*University College Hospital, Grafton Way, London, London UK;* [3]*The Whittington Hospital, Highgate Hill, London, London UK;* [4]*Imperial College of Science, Technology and Medicine, University of London, Magnetic Resonance Unit, London, London United Kingdom;* [5]*Imperial College of Science, Technology and Medicine, University of London, South Kensington, London, London United Kingdom*

Background: Heart failure caused by myocardial iron overload is the commonest cause of death in thalassemia major. In the UK, 50% of patients still die before reaching the age of 35. Although the cardiomyopathy is reversible in its early stages, once heart failure develops it is difficult to treat and carries a high mortality. A direct measurement of myocardial iron would allow earlier diagnosis and earlier treatment, but no established technique currently exists.

Methods: We have assessed myocardial iron and function using CMR in 106 patients with thalassemia major. Myocardial iron concentrations were measured using T2* values, which, we have shown, are inversely related to tissue iron concentration. We have also performed multivariate analysis of clinical, cardiological and iron parameters in order to identify the best predictor for the requirement for cardiac medication for ventricular dysfunction.

Results: Despite long-term iron-chelation therapy, 60% of patients had excess myocardial iron deposition (T2* < 20ms). In these patients there was a progressive decline in ventricular function with increasing myocardial iron, but significant ventricular abnormalities were detectable in only 10 patients (9.4%), all of whom had severe myocardial iron overload (<11ms). Multivariate analysis of cardiological and iron parameters for prediction of requirement for cardiac medication identified myocardial T2* as the most significant variable (odds ratio 0.79, $p < 0.002$).

Conclusions: Using this technique, myocardial iron deposition can be detected before ventricular dysfunction occurs. Increasing myocardial iron (<20ms) is related to a gradual linear increase in ventricular impairment. Conventional assessments of cardiac function can only detect those with advanced disease. Myocardial T2* is the most significant variable for predicting a requirement for treatment of ventricular dysfunction in thalassemic patients. This technique will allow early identification of myocardial iron deposition and is likely to reduce mortality from this reversible cardiomyopathy.

79. Age-Associated LV Shape Change in Normal Women and Men

Paul Hees Ph.D.,[1] Jerome Fleg,[2] Edward Shapiro.[3] [1]*Johns Hopkins University, Cardiology Division, Baltimore, MD USA;* [2]*Gerontology Research Center, NIA, 4940 Eastern Avenue, Baltimore, MD USA;* [3]*Johns Hopkins University, Bayview Medical Center, Baltimore, Maryland United States*

Introduction: Structural remodeling of the left ventricle is part of the normal cardiovascular aging process, even in the absence of disease. Most cross-sectional studies have shown an increase in wall thickness with advancing age. Remodeling of the LV may also result in change of overall geometry. The LV has been reported to become less prolate and more hemispherical in a variety of cardiac conditions, mitral regurgitation, [1] aortic regurgitation, [2] coronary artery disease, [3] and myocardial infarction. [4] Abnormal geometry was found to be associated with poorer survival in patients with idiopathic dilated cardiomyopathy, [5] and to improve with successful treatment. [6] Despite a growing body of literature describing LV shape change in multiple cardiovascular conditions, the effect of age per se on LV geometry is unknown.

Methods: We studied 3D structural changes of the LV with aging using spin-echo MRI, in 228 normal subjects (142 female and 86 male, ages 21–93) in the Baltimore Longitudinal Study of Aging, carefully screened for the absence of hypertension and coronary disease. In each subject, LV apex-to-base cavity length (L), wall thickness (WT), basal septum-to-lateral-wall diameter (D) were measured from end-diastolic images; linear measures were indexed to height. Sphericity index (Si) was the L/D ratio, and ED cavity volume (V) was calculated using the 3 principal LV dimensions assuming ellipsoid geometry. LV mass (M) was determined from a separate series of short-axis slices using Simpson's rule; Mi and Vi were indexed to BSA. Statistical significance of correlations with age were determined by Fischer's r-to-z.

Results: Overall, the average Si in 20-year-olds was 1.46, which becomes 1.32 by the age of 90 ($p < 0.002$). In women, Si goes from 1.47 to 1.33 ($p < 0.03$), and in men, 1.45 to 1.31 ($p < 0.03$) over the 7 decades. In women, WTi increased by 14% ($p < .02$), but was unchanged in men; Di was unchanged. However, Li decreased by 9.2% women ($p < .0006$) and by 10.6% in men ($p < .003$). Decreased Li

was probably the main cause for an 11% decrease in Vi in women ($p < .007$) and 14% in men ($p < .01$), as well as a 10% decrease in Mi in men only ($p < .03$).

Conclusions: We have observed for the first time a remodeling of left ventricular structure with age, in both genders, characterized by increased sphericity in both genders, largely via shortening of the LV long axis. Moreover, this remodeling is reflected in decreased ED volume, and, in men, reduced LV mass. Whether geometric changes directly impact function, or merely parallel actual causes of functional deficit, requires further study.

80. The Assessment of Coronary Artery Disease by Combined Magnetic Resonance Coronary Angiography and Perfusion

Nicholas Bunce,[1] Shelley Rahman,[1] Permi Jhooti,[1] Christine Lorenz,[1] Dudley Pennell.[1] [1]*Royal Brompton Hospital, Sydney Street, London, London UK*

Background: The current gold-standard for the diagnosis of significant coronary artery disease is cardiac catheterisation. However this technique is invasive and does not provide functional information about myocardial ischaemia or infarction. Magnetic resonance can detect coronary artery stenoses with reasonable accuracy but is limited to proximal segments and can be affected by motion artefacts (1,2). First-pass gadolinium myocardial perfusion imaging has been used to detect significant coronary stenoses (>75% luminal diameter reduction) with high accuracy (3). Combining magnetic resonance coronary angiography with myocardial perfusion might improve the detection of coronary artery stenoses, and provide additional functional information about the stenosed artery.

Purpose: a) To determine whether magnetic resonance coronary angiography (MRCA) or gadolinium myocardial perfusion are accurate for the detection of coronary artery disease.

b) To determine whether the combination of MRCA and myocardial perfusion can improve the accuracy of detection of coronary artery disease.

Methods: 34 patients (26 men, 8 women, mean age 56 yrs,) with angina were studied using a 1.5T Picker Edge scanner and 4-channel phased array coil. MRCA was performed using a navigator respiratory-gated 3D Turbo-FLASH gradient echo sequence with Hybrid Ordered Phase Encoding (HOPE) (4,5). Images were acquired in mid to late diastole after a fat suppression pulse. Imaging was performed using the following parameters: TE 4.3ms, TR 12.9ms, incremental flip angle 20–90°, voxel dimensions 1.02 × 1.35 × 2.5 mm, 8 slices per slab, navigator acceptance window 10mm. Positioning a double oblique volume slab from the right anterior sinus of Valsalva down the right atrio-ventricular groove imaged the right coronary artery. The left and circumflex arteries were imaged in an oblique transverse volume slab positioned from at left sinus of Valsalva along the inter-ventricular groove.

For the myocardial perfusion, two short axis slices were positioned through the left ventricle, and acquired with an ultra-fast gradient-echo sequence: repetition time/echo time 2.0/3.0 ms, flip angle 18°, pre-saturation flip angle 90°, voxel dimensions of 1.95 × 7.81 × 10 mm. With the patient performing shallow respiration, 50 images were obtained with both slices acquired during the same R-R interval. A baseline myocardial perfusion study was performed using 0.05 mmol/kg gadolinium (Magnevist®, Schering AG, Germany) injected with a power injector into an ante-cubital vein. After allowing 10 minutes for gadolinium to washout, adenosine 140μg/kg/min was infused via a separate cannula for 6 minutes and a stress myocardial perfusion scan was acquired using the same parameters and slice set-up.

Cardiac catheterisation was performed using standard methods and assessed for the presence of significant stenoses (>50 percent luminal diameter reduction).

Table 1

	MRCA	Perfusion	Combined
Sensitivity	88%	81%	100%
Specificity	72%	78%	83%

Analysis: For the MRCA scans two observers blinded to patient identity assessed each coronary artery and a consensus was reached for the presence or absence of a significant stenosis (as determined by vessel narrowing or signal loss). Blinded to the results from MRCA and angiography the two observers then assessed myocardial perfusion by reviewing the images played back as a cine-loop. Delayed myocardial signal intensity increase was indicative of a myocardial ischaemia. Each short axis slice was divided into three arterial territories (left anterior descending, circumflex and right coronary arteries) without consideration of dominance. The results from MRCA and myocardial perfusion were then reviewed together and if the two tests disagreed, then the study with the better image quality was given preference and a final diagnosis decided.

Results: All studies were performed within 3 months of cardiac catheterisation with no documented cardiovascular events between the MR and cardiac catheterisation. The mean magnetic resonance scan duration was 60 minutes and no adverse events occurred during adenosine stress. 16 patients had significant coronary artery disease on cardiac catheterisation with 33 stenosed arterial segments. Sensitivity and specificity were calculated for the 94 arterial segments assessed on cardiac catheterisation and MRCA. Vessel segments not seen on MRCA were excluded. The detection of coronary artery disease was improved with the combined approach as illustrated in Table 1.

Discussion: The combined study was well tolerated and time efficient. The performance of the 3D respiratory gated MRCA and myocardial perfusion acquisitions were similar to those reported in other published studies (1,2,3). The accuracy of MRCA can be affected by residual motion artefact and distal vessel stenoses outside the imaging volume slab. Visual assessment of myocardial perfusion may be affected by multi-vessel disease and vessel collaterals. The combined assessment of MRCA and myocardial perfusion increased the sensitivity to 100% and the specificity to 83%, when using cardiac catheterisation as the reference investigation. In addition the negative predictive value for the combined assessment was 100% which would potentially allow for this technique to be used for screening patients with suspected coronary disease without the need to proceed to invasive cardiac catherisation.

It is possible that a combined approach may enable targeting of revascularisation to stenosed arteries that produce myocardial ischaemia.

81. Delayed Cardiac Recovery from Physical Exercise in Patients after Mustard or Senning Operation for Transposition of the Great Arteries Assessed by Ultra-Fast MRI

Arno Roest,[1] Patrik Kunz,[2] Willem Helbing,[3] Hildo Lamb,[2] Albert deRoos,[2] Ernst VanderWall.[4] [1]*LUMC Dept. Pediatric Cardiology, Albinusdreef 2, Leiden, Z-H The Netherlands;* [2]*LUMC, Dept. Radiology, Leiden, ZH The Netherlands;* [3]*LUMC, Albinusrdeef 2, Leiden, ZH The Netherlands;* [4]*LUMC, Dept. of Cardiology, Leiden, ZH The Netherlands*

Background: Assessment of recovery from physical exercise may reveal cardiac dysfunction in patients with acquired or congenital heart

disease. In specific patient groups the decline in heart rate during recovery from physical exercise serves as a direct predictor of mortality (1). The purpose of the present study was to monitor changes in aortic flow during recovery from sub-maximal bicycle exercise in patients after Mustard or Senning repair for transposition of the great arteries (M/S patients) and healthy controls by using ultra-fast MRI.

Methods: 8 M/S patients (26 ± 5 years) and 10 healthy controls (25 ± 5 years) were studied using a Philips ACS/NT 1.5 T system and a MR-compatible bicycle ergometer (Lode BV, The Netherlands). MR-workload was based on 60% of peak-oxygen, measured during a graded maximal exercise examination, which was performed prior to MR examination. Flow in the ascending aorta was measured at rest, with exercise and each 30 seconds after exercise during a period of 8 minutes. Flow measurements were performed during a breath hold of 8 heart beats at end-expiration using a turbo field echo planar imaging (TFEPI) MR sequence. Parameters of TFEPI sequence: echo time: 3.4ms, repetition time: 6.7ms, flip angle: 30°, EPIfactor: 3, turbo factor: 3, shots: 4, matrix: 128 × 36, field of view: 420 × 210mm. During the entire examination heart rate of the subjects was recorded. Images were quantitatively analysed using the FLOW software package (MEDIS, The Netherlands)

Results: From rest to exercise percentage increase in heart rate and aortic flow was significantly lower in the M/S patients: Heart rate: M/S patients +64 ± 11% vs controls +91 ± 21% ($p < 0.05$); Aortic flow: M/S patients +9 ± 13% vs controls +20 ± 7% ($p < 0.05$).

During the recovery period heart rate exponentially decreased. No difference in heart rate recovery was observed between both groups. Both patients and healthy controls showed an initial increase in aortic flow immediately after exercise. In the healthy subjects aortic flow decreased thereafter. In the M/S patients, however, aortic flow (expressed as % difference from rest) remained significantly higher at 4 to 6 minutes after exercise (table 1, *$p < 0.05$). Subsequently cardiac output of the M/S patients also remained significantly higher 4 to 6 minutes after exercise (table 2, *$p < 0.05$).

Conclusion: Heart rate recovery after physical exercise was normal in M/S patients. Evaluation of cardiac function during recovery from sub-maximal exercise revealed delayed recovery of aortic flow and cardiac output in M/S patients. Furthermore, near real-time MR flow assessment of cardiac recovery after physical exercise may provide an additional clinical tool for the evaluation myocardial function in patients with congenital as well as acquired heart disease.

Table 1

Aortic Flow Recovery

	M/S Patients	Controls
4 min recovery	+15 ± 16%*	+4 ± 3%
4.5 min recovery	+18 ± 18%*	+1 ± 6%
5 min recovery	+17 ± 17%*	+1 ± 4%
5.5 min recovery	+19 ± 18%*	+0 ± 5%
6 min recovery	+19 ± 22%*	+0 ± 4%

Table 2

Cardiac Output Recovery

	M/S Patients	Controls
4.5 min recovery	+30 ± 14%*	+13 ± 11%
5 min recovery	+34 ± 14%*	+16 ± 11%
5.5 min recovery	+31 ± 10%*	+14 ± 8%
6 min recovery	+29 ± 15%*	+13 ± 10%

82. Quantification of Right Ventricular Morphology and Function in Mice by High-Resolution Magnetic Resonance Imaging

Frank Wiesmann,[1] Ralf Illinger,[1] Alex Frydrychowicz,[1] Eberhard Rommel,[2] Axel Haase,[3] Stefan Neubauer.[4] [1]*Department of Medicine, University of Wuerzburg, Wuerzburg, Germany Germany;* [2]*Institute of Physics, University of Wuerzburg, Wuerzburg, Germany Germany;* [3]*Institute of Physics, University of Wuerzburg, Würzburg, Germany Germany;* [4]*John Radcliffe Hospital, Dept of Cardiovascular Medicine, Oxford, England England, UK*

High resolution magnetic resonance imaging (MRI) has proved highly accurate for the quantification of left ventricular (LV) volumes and function in mice. However, assessment of right ventricular (RV) morphology and volumes is by far more difficult due to the complex geometry of the RV. As transgenic mouse models of cardiomyopathy may involve morphologic and functional changes of the right heart, purpose of this study was to test for the feasibility of MRI for in vivo quantification of RV function.

12 mice of various age (body weight range 29–50 g) were studied by ECG-triggered FLASH-Cine MRI at 7 T. Imaging was performed in multiple contiguous slices orthogonal to the ventricular septum to encompass the entire right and left heart. Mice were anesthetized with Isoflurane via a nose cone, allowing to maintain heart rate at 454 ± 13 bpm. Total RV and LV volumes were calculated applying Simpson's rule.

MR measurements of RV cavity volume was feasible in all mice studied. MRI revealed close correlations betwen RV and LV stroke volume (SV) ($r = 0.90$, $p < 0.0001$) and hence, cardiac output (CO) ($r = 0.94$, $p < 0.0001$). Consistent with human physiology, RV EDV and ESV were significantly higher compared to LV volumes ($p < 0.05$ each). In parallel, RV ejection fraction (EF) tended to be lower than

Table

	EDV (µl)	ESV (µl)	SV (µl)	CO (ml/min)	EF (%)
RV	88.3 ± 3.5*	38.1 ± 3.0*	50.2 ± 2.1	22.6 ± 1.3	57.2 ± 2.3
LV	77.3 ± 3.7	27.7 ± 3.4	49.5 ± 2.0	22.4 ± 1.2	65.1 ± 3.1

mean SEM; * $p < 0.05$ vs LV; n = 12

LV EF ($p = 0.06$). Bland-Altman analysis revealed a mean difference of 1.8 ul between RV and LV SV with close limits of agreement (±1.3 ul). Intraobserver variability of MRI-determined RV SV was 4.6%.

MR-microimaging provides sufficient temporal and spatial resolution to quantify cardiac morphology and function of the RV. MRI should therefore be of high relevance in the evaluation of the cardiac phenotype in transgenic mouse models with geometric and functional changes of the RV.

83. Quality Control in the Cardiac MR Laboratory

Arvind Bakhru,[1] David Bluemke,[2] John Paul Finn,[3] Antoinette S. Gomes,[4] W. Gregory Hundley,[5] Michael Jerosch-Herold,[6] Joao Lima,[7] Rola Saouaf,[8] Shantanu Sinha.[9] [1]Johns Hopkins University Department of Radiology, Yale University Department of Epidemiology & Public Health, 367 Cedar St., New Haven, Connecticut USA; [2]*Johns Hopkins University Department of Radiology, MRI 143–Nelson Basement, Baltimore, Maryland USA;* [3]*Northwestern University Medical School, Division of Radiology, 448 E. Ontario St Suite 700, Chicago, Illinois USA;* [4]*UCLA School of Medicine, Department of Radiology, CHS BL-141, Los Angeles, California USA;* [5]*Wake Forest University School of Medicine,*

Section of Cardiology, Winston-Salem, North Carolina USA; [b]University of Minnesota, Department of Radiology, J1-356 Mayo, Radiology Box 292, Minneapolis, Minnesota USA; [3]Johns Hopkins University Department of Cardiology, Johns Hopkins Hospital, School of Medicine, Baltimore, Maryland USA; [4]Columbia University, Department of Radiology, MHB2-121, New York, New York USA; [5]UCLA School of Medicine, Department of Radiological Sciences, Box 951721, Los Angeles, California USA

Purpose: To examine the variation and comparability of quantitative cardiovascular data of cardiac MR from multiple MR centers.

Methods: Six cardiac MR centers performed cardiac cine MR studies with protocols designed to achieve comparable time and spatial resolution as part of the multi-center Multi-Ethnic Study of Atherosclerosis (MESA) study. Data were transmitted to a central MR reading center and imported into a platform-independent FileMaker Pro (version 5, FileMaker, Inc.) relational database developed to store, clinically evaluate, and perform quality assurance measures on cardiac MR reports. Cardiac MR studies were analyzed using MASS and FLOW software packages (Medis, The Netherlands). Fifty-six volunteer participants underwent cardiac MR testing at six sites. 1.5 T GE LX scanners were used at 4 sites, 1.5 T Siemens Vision scanners were used at 2 sites and a 1.5 T Symphony scanner was used at 1 site. Quantitative cardiac MR reports were completed on the fifty-six subjects using MASS; quantitative cardiac MR reports using FLOW were completed on fifty-two of those subjects. The following left-ventricular cardiac function parameters were analyzed: end-diastolic mass, end-diastolic volume, ejection fraction, stroke volume, and cardiac output. Flow data provided for analysis of aortic peak velocities, cardiac output, peak positive area change, normalized peak positive area change, and distensibility. Cardiac MR reports were generated by two technologist readers randomly assigned to generate original, inter-observer, and intra-observer readings for each subject for a total of 168 Mass and 156 Flow readings. Analysis of reader variability, comparability of MASS and FLOW cardiac output data, and center-by-center variation utilized these reports. Additionally, scanner variability was evaluated using paired data from seven subjects who underwent testing in both GE and Siemens scanner.

Results: : Cardiac measurements were performed over a two-month period and were imported into the quantitative cardiac MR database system. Inter-observer and intra-observer percent variation between quantitative readers was assessed for end-diastolic mass (inter-observer variation 0.98% ± 8.1%, intra-observer variation 2.59% ± 6.18%), end-diastolic volume (inter-observer 1.04% ± 5.83%, intra-observer 1.78% ± 5.08%), ejection fraction (inter-observer 0.43% ± 6.84%, intra-observer 1.52% ± 3.79%), and stroke volume (inter-observer 0.64% ± 8.43%, intra-observer 0.21% ± 5.85%). Mass and Flow cardiac output was also compared through a center-by-center analysis. Multi-factorial, paired analysis by MR scanner manufacturer showed significant differences in cardiac output difference ($F = 6.41$, $p < 0.0001$) and variation (110% variation, $p < 0.0001$) as determined by phase contrast flow methods for the aorta versus contour outlining of short axis cardiac cine images. Seven subjects were imaged using both GE and Siemens scanners; paired difference testing revealed no significant difference in end-diastolic mass (difference = 1.75g, $p = 0.54$), end-systolic mass (2.96g, $p = 0.073$), end-diastolic volume (2.52mL, $p = 0.42$), end-systolic volume (0.42mL, $p = 0.76$), ejection fraction (0.04%, $p = 0.97$), stroke volume (2.10mL, $p = 0.54$), or cardiac output (0.32 L/min, $p = 0.38$).

Table

Variability in Left Ventricular Cardiac MR Readings

	Original Values		% Variation	
	Value	s.d.	Inter-variation (%)*	Intra-variation (%)*
End-diastolic mass (g)	121.5	31.6	0.98 (8.10)	2.59 (6.18)
End-diastolic volume (mL)	110.3	28.2	1.04 (5.83)	1.78 (5.08)
Ejection fraction (%)	74.2	6.9	0.43 (6.84)	1.52 (3.79)
Stroke volume (mL)	81.1	19.0	0.64 (8.43)	0.21 (5.85)
Cardiac output (l/min)	5.38	1.54	0.64 (8.43)	0.21 (5.85)

* Variation (s.d.).

Values include all 56 participants.

Conclusion: This relational database enabled with a quality control system to associate multiple quantitative readings was useful for assessing inter-observer and intra-observer reader variability of cardiac functional parameters from individuals undergoing cardiac MR testing. The approach is useful for clinical evaluation and reporting, assessing variation between technologist readers, as well as comparing different MR scanning centers. General Electric and Siemens 1.5 T MR scanners show similar results for cardiac MR functional analysis.

Sponsored by NIH NHBLI grant N01-HC-95168.

84. Black-Blood Dual-Contrast Fast Spin Echo of the Heart/Aorta

Agus Priatna.[1] [1]*Marconi Medical System, Inc., 595 Miner Road, Cleveland, Ohio United States*

Introduction: Black-blood imaging using double inversion recovery (IR) fast spin echo (FSE) has been used for imaging of the heart and the vasculature [1,2]. Recently, the applications of double-IR FSE sequences have been extended for vessel wall imaging [3] and plaque characterization studies [4,5]. For these applications, proton density and T2-weighted images are usually acquired for characterizing the plaque/tissue. However, separate acquisitions are performed to obtain proton density and T2-weighted images that might result in misregistration of the object being imaged. The technique described here provides both proton density and T2-weighted images simultaneously in a single acquisition using double-IR dual-contrast fast spin echo sequence.

Method: Black blood preparation was implemented with dual-contrast FSE sequences on 1.5T Eclipse whole body scanner system (Marconi Medical System, Inc., Cleveland, Ohio) with a high performance gradient system (27 mT/m with a slew rate of 72 T/m/s). The black-blood preparation consisted of a non-selective adiabatic inversion pulse followed immediately by a selective inversion pulse (double-IR). The inversion time from the first inversion pulse to the imaging acquisition was set to 500 msec for nulling the blood. The dual-contrast fast spin echo sequence used a split echo train lengths (ETL). A total of 16 ETL was used for the sequence. The first group of echoes (8 ETL) formed the proton density weighted image of which the first echo signal was arranged to the center of k-space. The second group of ETL (8 ETL) formed the T2-weighted image of which the middle echo signal (ETL/2) was placed to the center of k-space. The inter-echo spacing was 6.5 msec. The first echo time was 6.5 msec for proton density imaging and the second echo time was 104 msec for heavily T2-weighted imaging.

Images of the heart and the aortic vessel of a normal volunteer were obtained with ECG triggered double-IR dual-contrast FSE sequence each within a single breathold period. The acquisition was acquired every R-R interval. The matrix size = 256 × 256, thickness = 4 mm, number of averages = 1 for imaging the heart and 2 for the aortic vessel. A rectangular field of view was applied for imaging the aortic vessel to shorten the scan time.

Results: Figure 1A. shows the proton density weighted image of the short axis of the heart of the volunteer and Figure 1B. shows the corresponding T2-weighted image. Note that the blood is completely darkened on both proton density and T2-weighted images. The myocardium shown in the proton density image is brighter than the correspond-

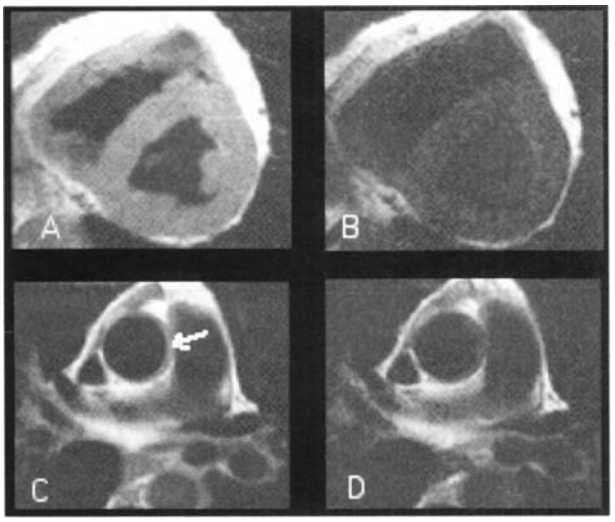

Figure 1. (A) Black-blood proton density weighted image of the heart and (B) the corresponding T2-weighted image. (C) Black-blood proton density weighted image of the aortic vessel and (D) the corresponding T2-weighted image.

ing T2-weighted image. Figure 1C shows the proton density weighted image of the aortic vessel and Figure 1D shows the corresponding T2-weighted image. There are some wall thickening in the aortic vessel as seen on the proton density image (indicated with arrow). These tissues are not seen on the T2-weighted image.

Conclusion: We have shown the feasibility for acquiring simultaneous proton density and T2-weighted images using double-IR dual-contrast FSE for imaging the heart as well as the aortic vessel in a single acquisition within a breathold period. This feature is important for cardiovascular imaging especially for plaque characterization studies in which both proton density and T2-weighted images are needed to image the same location of the plaque/tissue.

85. A Novel Approach for Non-Invasive Detection of Cardiac Allograft Rejection with Multi-Dimensional Cardiac MRI

Yi-Jen WU,[1] Shinichi Kanno,[1] Chien HO.[2] [1]*Carnegie Mellon University, NMR Center for Biomedical Research, Pittsburgh, PA USA;* [2]*Carnegie Mellon University, 4400 Fifth Avenue, Pittsburgh, Pennsylvania United States*

Introduction: The ability to maintain the cardiac graft after heart transplantation depends greatly on timely and proper evaluation of the rejection progression as well as managing the cardiac dysfunction accompanying rejection. However, the clinical procedure such as endomyocardial biopsy is not only invasive, but also prone to mis-sampling. Early detection of cardiac allograft rejection remains an outstanding clinical issue. The motivation of this study is to establish reliable and practical MRI parameters for non-invasive detection of acute rejection and accompanied cardiac dysfunction.

We have probed the detection of cardiac graft rejection with two approaches: A. detection of the accumulation of immune cells at the rejection sites by monitoring ultra-small superparamagnetic iron oxide (USPIO) labeled immune cells, and B. detection of dysfunction of the transplanted hearts by multi-dimensional functional cardiac MRI. We have developed a new rat model of heterotopic heart and lung transplantation to the inguinal region as our model system.

Results: I. Detection of rejection with MRI by monitoring the accumulation of USPIO-labeled immune cells

Allogeneic cardiac grafts (DA to BN rats) developed a grade 3 or 4 rejection pathologically at post-operation day (POD) 6. A significant decrease in MR signal intensity was seen after USPIO injection; whereas the syngeneic (BN to BN rats) counterparts showed no significant intensity changes after USPIO injection. Immunohistochemistry and iron staining in the allografts revealed that USPIO was residing mainly in the infiltrating ED1+ macrophages that accumulated at the rejecting site. Allogeneic transplants treated with immuno-suppressant cyclosporin A (CsA) exhibited less severe rejection, which is correlated with attenuated MRI signal decrease after USPIO injection. These data demonstrated that the MRI signal changes resulting from USPIO-labeled immune cells infiltrated at the rejection sites correlated with the site and the degree of rejection.

II. Detection of rejection by multi-dimensional functional cardiac MRI

Multiple cardiac functional parameters, both systolic and diastolic, were established with MRI in order to detect cardiac dysfunction resulting from acute rejection. For systolic functions, stroke volume (SV) and ejection fraction (EF) were derived from cine images, and the contractility of myocardium was evaluated by myocardial tagging. For diastolic functions, the compliance of the heart was evaluated by the ability for left ventricular (LV) wall to relax in the diastolic phase, and the relative timing of the diastolic phase was measured by fast MRI sequences.

At POD 5–6 when moderate to severe rejection occurred, EF and myocardium contractility of allogeneic transplants decreased to less than 30% of the controls, while that of the syngeneic controls remained the same. On the other hand, at POD 4–5 when mild to moderate rejection occurred, allogeneic transplants still preserved 60% of its systolic functions, but have already lost most of its diastolic functions. The LV wall of allogeneic transplants lost 70% of its ability to relax during diastolic phase, and the time spent in the isovolumic relaxation is about 1.5 times longer in allogeneic grafts than in the control hearts. This is indicative that the diastolic functions degrade faster than the systolic functions.

Conclusion: We have demonstrated a novel approach for detecting acute cardiac allograft rejection using MRI coupled with USPIO injection. In addition, acute rejection of transplanted hearts could be detected by multi-dimensional MRI. Our data suggested that the diastolic dysfunction precedes systolic dysfunction. Simultaneous combination of multiple MRI parameters makes non-invasive diagnosis of rejection possible.

86. High-Speed Cardiac MRI Using the Selective Line Acquisition Mode—Theory and Clinical Application

Wolfgang Rehwald,[1] Raymond Kim,[2] Orlando Simonetti,[3] Gerhard Laub,[4] Robert Judd.[5] [1]*Northwestern University, Tarry 12-703, Chicago, Illinois United States;* [2]*Northwestern University Medical School, Tarry 12-703, Chicago, IL USA;* [3]*Siemens Medical Systems, 448 E. Ontario St., Chicago, IL USA;* [4]*Siemens Medical Systems, Onterie Bldg., Suite 700, Chicago, IL USA;* [5]*Northwestern University, Northwestern University, Chicago, Illinois United States*

Introduction: Constant cardiac motion and the need for breath hold are specific problems of cardiac MRI. Fast imaging can alleviate these problems but comes with a penalty either in signal-to-noise ratio (SNR), spatial resolution, temporal resolution, fold-in artifacts, or any combination thereof. To minimize this penalty for the specific case of cardiac MRI we developed SLAM (Selective Line Acquisition Mode).

Theory: Every nth line per cardiac frame is acquired cutting acquisi-

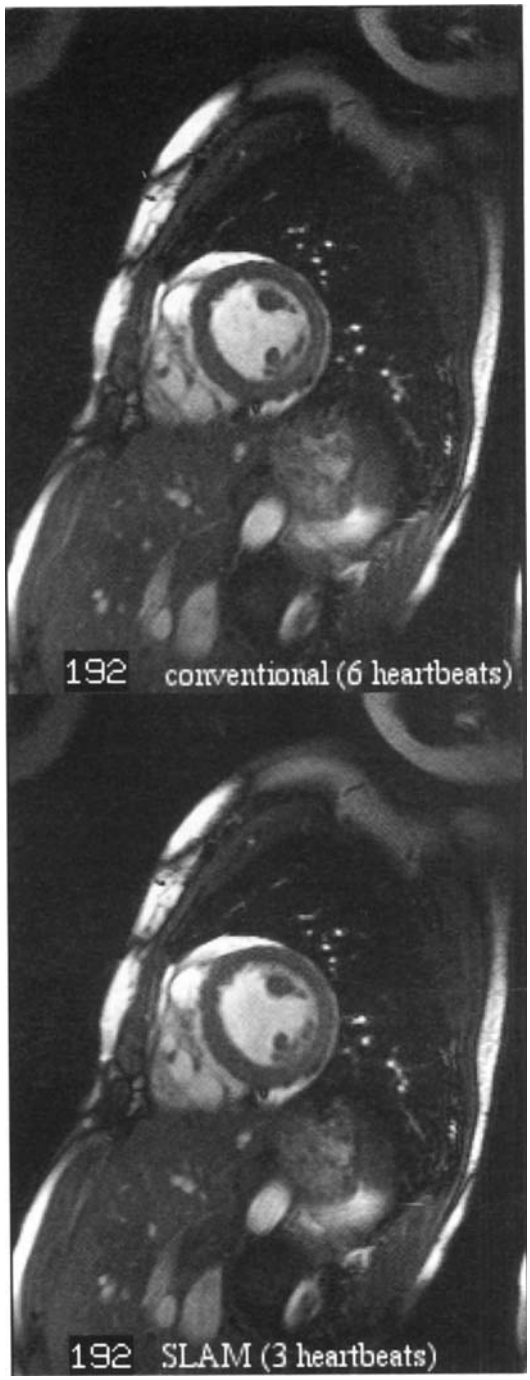

Figure.

tion time by factor n. Lines not acquired are calculated from previous and consecutive frames using assumptions about location and speed of the contracting heart.

Materials and Methods: SLAM was tested clinically on twenty patients with advanced forms of cardiac disease and compared to conventional two-frame interpolation (2FI). We determined SLAM and 2FI error for each heart pixel.

Results: SLAM is very well suited for imaging moving objects confined to 1/n of the fov such as the heart. On average, 2FI exhibited 52 ± 5% ($p < 0.001$) larger errors than SLAM. Images reconstructed with SLAM were sharper than 2FI and showed well-defined endocardial borders and papillary muscles. The figure shows one frame of a series of cine images acquired with SLAM ($n = 2$) during a total scan time of three heartbeats. The conventional acquisition took six heartbeats.

Conclusion: SLAM can be used clinically for dynamic imaging, cine-MRI or perfusion. It is a fast, accurate, and robust alternative to conventional cardiac imaging.

87. Inflow Independent Functional MR Imaging with Steady-State Free Precession (SSFP) Significantly Improves Endocardial Border Delineation Without Contrast Agents

Holger Thiele,[1] Ingo Paetsch,[2] Bernhard Schnackenburg,[3] Axel Bornstedt,[2] Andreas Wahl,[2] Gerhard Schuler,[4] Eike Nagel,[2] Eckart Fleck.[2] [1]*University of Leipzig, Heart Center Leipzig, Russenstr. 19, Leipzig, Saxonia Germany;* [2]*German Heart Institute and Charité, Augustenburger Platz 1, Berlin, Berlin Germany;* [3]*Philips Medical Systems, Augustenburger Platz 1, Berlin, Berlin Germany;* [4]*University of Leipzig, Russenstr. 19, Leipzig, Saxonia Germany*

Background: The contrast between blood and myocardium in MR imaging with standard turbo gradient echo techniques (TFE) is mainly determined by contrast from inflowing blood, which is low in long axis views especially in patients with impaired left ventricular function. Better contrast allows an easier and more reproducible detection of the endocardial border. SSFP is a new inflow independent technique.

Methods: In 45 patients functional images of the heart in 2 long axis projections (2- and 4-chamber) were acquired using standard TFE (TE/TR/flip: 1.9, 5.0, 25) compared with SSFP (TE/TR/flip: 1.2, 3.2, 60) on a 1.5 Tesla MR tomograph (ACS NT, Philips, The Netherlands). Acquisition was performed during a single breath hold for each scan. A visual score for endocardial border delineation ranging from 0 (worst)–6 (best) for 6 myocardial segments in 2 long axis views during the systolic and enddiastolic phase (=24 segments/patient) was assigned by 2 independent observers.

Results: Endocardial border delineation score for standard TFE was 50 ± 15 and 100 ± 13 ($p < 0.0001$) for the SSFP sequence. Signal intensity blood/signal intensity myocardium was 1.5 ± 0.4 during systolic and 1.4 ± 0.3 during diastolic phase for standard TFE and 3.5 ± 1.1 ($p < 0.0001$) and 3.2 ± 1.3 ($p < 0.0001$) for SSFP, respectively. The determination of the score and the contrast was highly reproducible ($r = 0.86$–0.96) between 2 independent observers.

Conclusion: Contrast between blood and myocardium is increased by a factor of almost 2.5 by use of SSFP. This is similar to the expected effects of intravascular contrast agents and may further improve diagnostic accuracy for stress MR imaging and reduce variability for the determination of cardiac volumes and ejection fraction.

88. Myocardial Tagging with 3D CSPAMM

Salome Ryf,[1] Marcus Spiegel,[1] Oliver Weber,[2] Peter Boesiger.[1] [1]*Swiss Federal Institute of Technology, Institute of Biomedical*

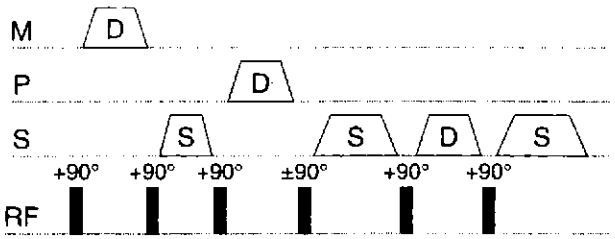

Figure 1.

Engineering, Zurich, ZH Switzerland; [3]Swiss Federal Insitute of Technology, Institute of Biomedical Engineering, Zurich, ZH Switzerland

Introduction: Analysis of myocardial motion is essential for the understanding of the heart mechanics and consequently, the estimation of heart condition. Myocardial tagging enables to assess accurately tissue deformations. However, conventional tagging sequences such as SPAMM [1] or CSPAMM [2] allow for registration of the spatial displacement of the myocardium mere as a two dimensional projection. Thus, analysis of the effective 3D motion trajectories is only possible in a limited way. Former methods for 3D motion tracking combined for example a 2D tagged short axis view with a 2D tagged long axis view or with a 1D velocity map. A novel myocardial tagging technique is presented allowing demonstration of true three-dimensional motion and overcoming the limitations known from 2D tagging methods.

Methods: The 3D CSPAMM (Complementary Spatial Modulation of Magnetization) tagging preparation (Fig. 1) is an extension of the 2D CSPAMM sequence.

CSPAMM is based on the subtraction of two images with complementary signed tagging modulation. It delays tagline intensity fading and consequently allows observing the heart motion throughout the whole heart cycle. Two 90° block pulses, interspersed by a dephasing gradient, produce a sinusoidal modulation of z-magnetization and thus a line shaped tag pattern. For the second image one 90° pulse has to be inverted to get the complementary signed modulation. To generate a three-dimensional tagging lattice the modulation is repeated in all three spatial directions. Each modulation is followed by a spoiler of different size in order to destroy remaining transversal magnetization and to avoid phase coherence. The whole tagging preparation takes 7.6ms. A tagline distance of 10mm was chosen.

After tagging preparation, a 3D flow compensated, interleaved gradient EPI sequence (EPI factor 9, flip angle = 16°, TE = 7.1ms) was used for imaging. A volume of 256 × 256 × 40mm3 was imaged with a spatial resolution of 2 × 2 × 2mm3. Fourteen heart phases were achieved with a frame to frame resolution of 35ms.

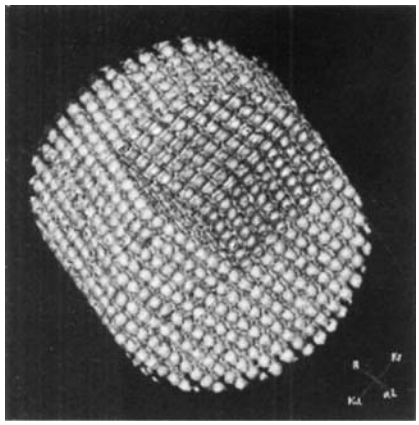

Figure 3.

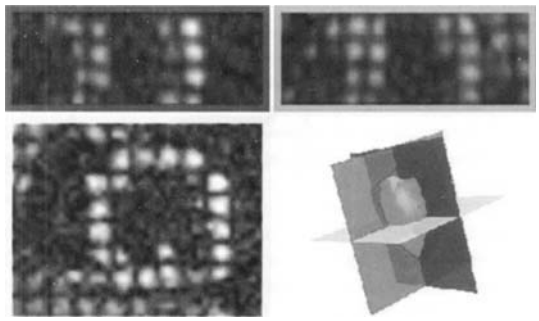

Figure 4.

To avoid respiratory motion the scan duration was split into several breath holds of 10s. In order to guarantee the same diaphragm position throughout the whole scan, a novel navigator guided breath hold technique was introduced. The excursion of the diaphragm was tracked in real time (100ms time resolution), allowing the operator to guide the subject to the correct breath hold position (Fig. 2). During the breath hold, navigator gating was applied.

All measurements were performed on a Philips Gyroscan ACS/NT 1.5T whole body scanner equipped with PowerTrak 6000 gradient system.

Results: The 3D tagging measurements were successfully accomplished in phantom and in 16 healthy volunteers.

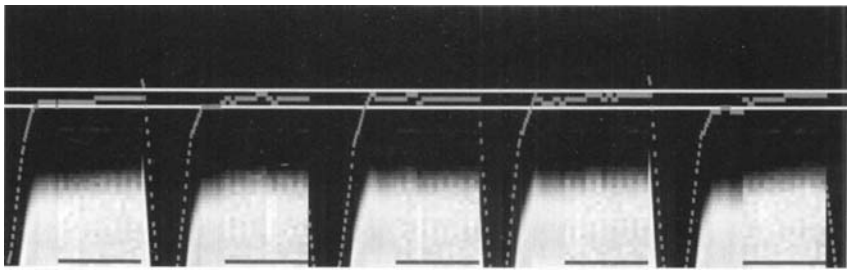

Figure 2.

Fig. 3 shows a rendered 3D tagging image of a phantom after segmentation by thresholding.

On the in vivo images, the saturation lattice and its deformation during the heart contraction can be observed throughout the cardiac cycle. In Fig. 4 cuts in all three spatial directions through a 3D tagged human left ventricle are shown.

Discussion: A new 3D myocardial tagging technique has been demonstrated. It allows true 3D motion tracking with high temporal and spatial resolution, allowing a better understanding of heart mechanics.

89. Multi-Slice Dual Inversion Black Blood Aortic Imaging

René Botnar,[1] Matthias Stuber,[2] Kraig Kissinger,[3] Lois Goepfert,[3] Warren Manning.[4] *[1]Beth Israel Deaconess Medical Center, 330 Brookline Avenue, Boston, MA USA; [2]Beth Israel Deaconess Medical Center, 330 Brookline Ave, Boston, Massachusetts United States; [3]Beth Israel Deaconess Medical Center, 330 Brookline Ave, Boston, MA USA; [4]Beth Israel Deaconess Medical Center, 330 Brookline Ave, Boston, MA USA*

Introduction: Turbo spin echo (TSE) black blood imaging is heavily dependent on blood flow during the acquisition period. Slow flowing blood can mimic signal from the vessel wall, plaque, and thrombus. To achieve consistent signal nulling from blood in the great vessels, imaging is usually performed during systole, a period of rapid blood flow. During systole, ventricular blood flow and cardiac motion is are maximal, thereby often causing blurring of the thoracic aorta. A dual inversion (Dual-IR) fast spin echo technique [1,2] is less dependent on blood flow during the acquisition period, but rather on flow exchange in-between the Dual-IR pre-pulse and the imaging sequence. This approach would allow for imaging of the thoracic aorta during diastole, when cardiac motion is minimal, and therefore minimize artifacts due to cardiac motion while preserving the black blood properties. As current Dual-IR approaches are implemented as single slice techniques, imaging of the whole aorta would lead to extremely long measurement times. We therefore thought to develop an interleaved multi-slice (MS) Dual-IR sequence that allows imaging of the entire aorta in a reasonable scanning time.

Purpose: The purpose of this study was to develop a fast interleaved multi-slice Dual-IR technique for aortic vessel wall imaging.

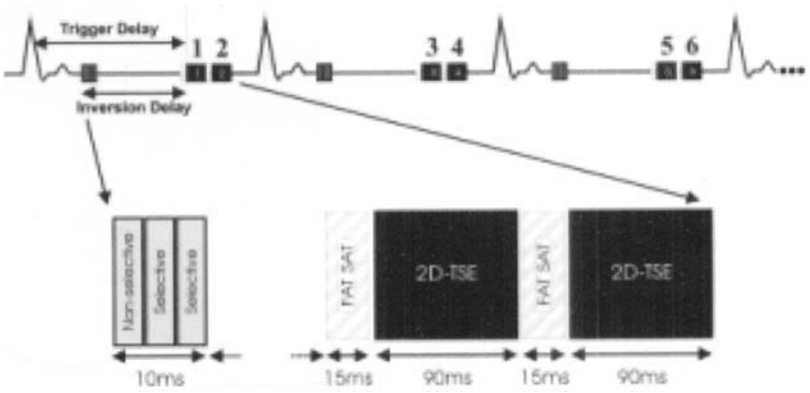

Figure 1. Schematic of a multi-slice Dual-IR imaging sequence with a repetition time of TR of 3 heartbeats.

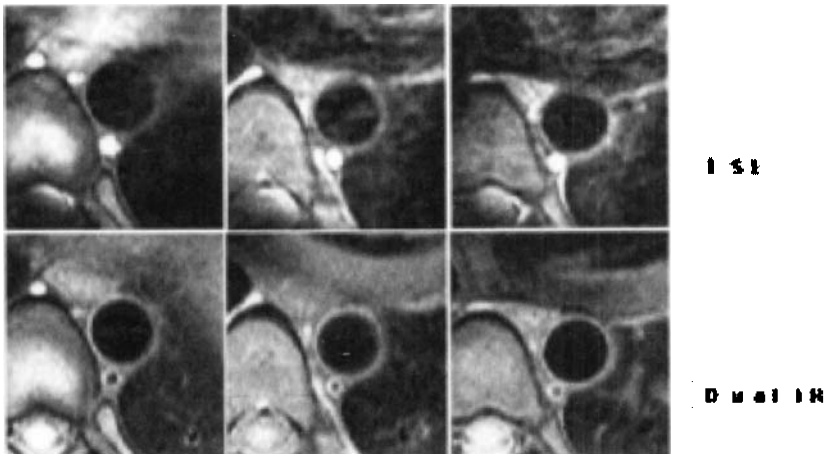

Figure 2. Images of the thoracic aorta acquired with an ECG triggered MS TSE (upper row) and a MS Dual-IR sequence (lower row).

Methods: Three healthy adult subjects without clinical history of vascular disease were examined in supine position with a Philips Gyroscan ACS-NT MR scanner (Philips Medical Systems, Best, NL) using a commercial 5-element cardiac synergy coil and an interactive cardiac software package (INCA2). Six cross-sectional slices (2 slices per RR-interval) of the thoracic aorta were acquired using an ECG triggered suppressed T2 weighted (linear profile order) multi-slice TSE and an interleaved multi-slice Dual-IR TSE sequence. In-plane resolution was 0.6 * 1.3mm and slice thickness was 5mm with a slice gap of 10mm. Imaging parameters were TE = 45ms, TR = 3 heartbeats, ETL = 14 echoes, ESP = 6.0ms, NSA = 4, scan time = 2:33 min (HB = 60bpm), and acquisition window = 90ms. Systolic data acquisition (75ms) was used for the TSE and diastolic for the MS Dual-IR sequence. The inversion delay was calculated using a TR of 1 according to TI = T1 * ln 2-T1 * ln(1 + exp(-TR/T1) [3] and was approximately 400ms for a heart rate of 60bpm. To achieve a diastolic data acquisition, the Dual-IR pre-pulse was applied approximately 250ms after the R-wave and imaging was performed 650ms after the R-wave. To compensate for cardiac motion, the labeled slice was 2.5 times thicker than the imaged slice. Figure 1 shows a schematic of the Dual-IR imaging sequence.

Results: In all subjects the thoracic aorta could be successfully visualized (Figure 2). In the TSE images, however, artifacts from systolic ventricular blood flow and cardiac motion can be observed, which degrade the delineation of the aortic vessel wall. In images acquired with the MS Dual-IR technique, these artifacts were minimized, thus allowing for a better delineation of the aortic vessel wall. Fat suppression using a water selective spectral spatial pulse (1331) allowed for better vessel wall definition than with a chemical shift (CHESS) prepulse, but also seemed to be more sensitive to proper shimming.

Conclusions: We demonstrated the feasibility of interleaved multi-slice Dual-IR imaging of the thoracic aorta and the great cardiac chambers. Image quality was superior when compared to a multi-slice TSE sequence, which sometimes suffered from blood flow and motion artifacts due to rapid systolic ventricular flow and cardiac motion. This technique allows for artifact free thoracic aortic imaging without a penalty in measurement time and also seems to have to potential for artifact free morphologic cardiac imaging.

90. Evidence of Myocardial Iron Deposition by MRI in Patients with Iron Overload from Different Causes: Preliminary Results

Guillem Pons-Lladó,[1] Sandra Pujadas,[2] Francesc Carreras,[2] Xavier Borrás,[2] Jaume Llauger,[2] Jaume Palmer,[2] Albert Altés,[2] Angel Remacha.[2] [1]*Hospital Sant Pau, Barcelona, SPAIN, P. Claret 167, Barcelona, Barcelona Spain;* [2]*Hospital Sant Pau, P. Claret 167, Barcelona, Barcelona Spain*

Introduction: Patients with iron overload present with increased deposition of the metal in liver, heart, pancreas, and other organs. As the principal responsible for storage and detoxification of iron, the liver is the first organ damaged by iron overload. An increase in hepatic iron concentration decreases relaxation time leading to a reduced signal intensity in MR images, this making the liver appear tipically dark on spin-echo sequences. The liver-to-muscle signal intensity ratio has been shown to inversely correlate with hepatic iron concentration at liver biopsy (1). Although also recognized as a potential target for iron deposition, heart muscle has not been so extensively studied by MRI (2), most reports dealing on anecdotal cases (3). The present investigation is aimed to detect the presence of myocardial iron deposition in a series of patients with iron overload by means of MRI.

Patients and Methods: 9 patients diagnosed of iron overload by the Hematology Dept. have been consecutively included in the study up to date. Primary hemochromatosis was present in 4 of them, while in the remaining 5 iron overload was secondary to another cause. Three patients had been treated by phlebotomy at the time of the study. None of them had clinical data indicative of heart disease.

All patients were prospectively studied with a 1.0 T Siemens Magnetom system using a standard protocol including: 1) a multi-slice transverse T1-weighted spin-echo sequence encompassing the heart and the upper half of the liver; and 2) a multi-phase cine-MR sequence oriented on a single horizontal long-axis plane of the left ventricle. Mean signal intensity of left ventricular myocardium was obtained averaging the values at 3 preselected sites (i.e.: septum, apex and free wall) on the spin-echo images. Myocardial signal intensity was normalized to the signal intensity from skeletal muscle (paraspinal) obtained in the same image. This heart-to-muscle ratio (HMR) was compared with that obtained in a control group of 16 individuals without iron overload or any other cardiac condition. Additionally, signal intensity from the liver and its ratio to skeletal muscle (LMR) was also calculated in both patients and control subjects. In all patients with iron overload, left ventricular dimensions, mass, and ejection fraction were also obtained from the cine gradient-echo sequences.

Results: In cardiac images, mean HMR was significantly lower in patients (0.91 ± 0.17) than in control subjects (1.03 ± 0.09) ($p = 0.029$). In 3 of the 9 patients (33%) the HMR was below 0.85, the lower normal limit (95% confidence established from the control group). Of note, the 3 patients treated by phlebotomy had the highest values of HMR (1.08, 1.08, and 1.15), well within the normal range.

In liver images, a large difference was observed in mean LMR between patients and controls (0.46 ± 0.37 vs. 1.47 ± 0.2, respectively; $p < 0.001$). Eight out of the 9 patients (89%) showed an LMR under the lower normal limit (1.07) established from the control group.

Data on left ventricular structure and function from the cine-MR sequences showed a mildly dilated left ventricle with increased left ventricular mass in 3 patients, ejection fraction being within normal limits in all cases. Only 1 out of these 3 patients had an abnormally low HMR on spin-echo images.

Conclusions:

1) An abnormally decreased signal intensity from the left ventricular myocardium consistent with iron deposition can be detected by spin-echo MRI in up to 33% of patients with iron overload, particularly in those not treated by phlebotomy.

2) The demostration of myocardial deposits by MRI is not necessarily related to the presence of detectable structural or functional left ventricular abnormalities.

3) The confirmation of these preliminary results will reinforce the role of MRI in clinical practice for the study of cardiac involvement in patients with iron overload.

91. Characterization and Reduction of Stent Artifacts in Cardiac MRI

Andrew Powell,[1] Gerald Greil,[2] Robert Mulkern,[3] Kee Chung,[3] Tal Geva.[4] [1]*Children's Hospital of Boston, Department of Cardiology, Boston, MA USA;* [2]*Children's Hospital, Department of Cardiology, Boston, MA USA;* [3]*Children's Hospital, Department of Radiology, Boston, MA USA;* [4]*Department of Cardiology, Children's Hospital, Boston, MA USA*

Background: Technical advances in cardiac MRI have greatly expanded its role in non-invasive imaging of patients with congenital heart disease. Concurrently, the use of endovascular stents has grown creating a potential source of image artifact in this patient group. This study sought to characterize the effects of stents on MR imaging of nearby structures and evaluate techniques to minimize their impact.

Methods: Imaging was performed using 1.5 T scanner on a phantom

consisting of a stent expanded in a plastic tube (OD × ID, 18 × 13 mm) suspended in a doped fluid bath and in-line with a flow circuit and pump. A Palmaz 40 mm stainless steel stent (Johnson & Johnson) and a Cheatham 39 mm platinum/iridium stent (NuMED) were examined under static and pulsatile flow conditions. Long and short-axis images of the stent and tubing were acquired using ECG-gated spin echo (SE), fast spin echo (FSE), double inversion recovery (DIR) FSE, and fast gradient echo (FGE) sequences; and with gadolinium-enhanced 3D MR angiography (MRA).

Results: The Palmaz stent induced a relatively small susceptibility artifact in the frequency encode direction secondary to alterations in the local magnetic field. This artifact was largest with SE, FGE, and MRA sequences where it distorted the stented vessel and surrounding region within 4 mm of the stent. FSE and DIR FSE imaging reduced the artifact to the surrounding 1 mm. An increase in SE receiver bandwidth from 3.9 to 15.9 kHz decreased the artifact area by 45%. Unlike the Palmaz stent, the Cheatham stent did not create appreciable artifact outside the stent with any sequence; consequently, the tube wall could be clearly imaged. Both stent types caused severe signal loss within the stent lumen on all imaging sequences consistent with a Faraday cage effect.

Conclusion: Palmaz stents induce a relatively small susceptibility artifact such that structures >5 mm from the stent are unaffected. The impact of this artifact can be reduced by appropriate selection of the frequency encode direction, maximizing receiver bandwidth, employing FSE sequences, and using platinum stents. Imaging of both platinum and stainless steel stent lumens is limited by signal loss due to a Faraday cage effect.

92. Value of Flow Velocity Measurements in Contrast Enhanced Magnetic Resonance Angiography to Improve the Quantification of Stenosis

Gesine Doerr,[1] Ernst Wellnhofer,[2] Holger Langreck,[2] Olaf Grebe,[3] Johannes Schwab,[4] Ingo Paetsch,[2] Bernhard Schnackenburg,[2] Axel Bornstedt,[2] Eike Nagel,[2] Eckart Fleck.[2] [1]*Internal Medicine/Cardiology, German Heart Institute and Charite, Campus Virchow, Humboldt University, Berlin, Augustenburger Platz 1, Berlin, Germany;* [2]*Internal Medicine/Cardiology, German Heart Institute and Charite, Campus Virchow, Humboldt University, Augustenburger Platz 1, Berlin, Germany;* [3]*Department of Internal Medicine, Division of Cardiology, College of Medicine, University of Ulm, Robert-Koch-Str. 8, Ulm, Germany;* [4]*Medizinische Klinik 8 (Kardiologie), Städtisches Klinikum Nürnberg-Süd, Breslauer Str. 201, Nuernberg, Germany*

Background: Contrast enhanced magnetic resonance angiography (CE-MRA) in patients with peripheral artery disease is an established diagnostic procedure. The measurement of maximum peak velocity (MPV) as routinely performed with Doppler technique is an additional technique which may improve the quantification of stenoses. However intrastenotic turbulent flow may limit the use of MR flow techniques. This study was aimed at evaluating the feasibility of flow velocity measurements by magnetic resonance in vitro and in vivo for the quantification of stenoses.

Methods: Magnetic resonance MPV (MR-MPV) and Doppler MPV (PW-MPV) were determined with a flow model, which simulated physiological circulation. Three morphological different models of stenoses (asymmetrical 75%, symmetrical 75% and concentric 90%) were evaluated in the phantom. For the assessment of PW-MPV an intraluminal Doppler guide wire (0.014″) was used. Both MR-MPV and PW-MPV were performed 1,5 cm proximal, within and 5 cm distal to stenoses.

Then, 10 healthy subjects were examined by CEMRA and transcutaneous Doppler ultrasound in the Aa. femorales communes, Aa. femorales superficialis and Aa. poplitea. The results were correlated between MR-MPV and PW-MPV and intraindividual correlations between the left and right side were calculated.

MR measurements were performed on a 1.5T whole body scanner (ACS NT, Philips Medical Systems, Best, The Netherlands) with Power Track 6000 gradients (slew rate 103 T/m/s, amplitude 23 mT/m), cardiac software package INCA 2B. An inflow MR angiography using a T1 weighted segmented gradient echo sequence was performed to determine vessel positions. Only in the control group a high-resolution 3D-angiography scan was performed after the injection of a 20 ml bolus of Gd-DTPA administered with a power injector (flow 4ml/s) into a peripheral vein. The arrival of the contrast agent bolus was monitored by real time imaging of the more proximal vessels (Bolus Trak), thus timing was optimal for the interactively started high resolution scan. Scan parameters were: matrix 512 × 90, resolution 1 mm × 4 mm × 2 (4) mm, TE 1.2 ms, TR 3.8 ms, flip angle 40°. A maximum intensity projection was performed online and used for further planning of the quantitative flow measurements. A segmented gradient echo quantitative flow (phase contrast) scan was used (matrix 128 × 115 with 256 pixel reconstruction, slice thickness 4 mm, TE 3.6 ms, TR 5.9 ms, Flip angle 15°, velocity encoding intrastenotic 20% over the reference Doppler values for the segments). The field of view was adjusted to the flow model (about 300–350 mm) and patients.

MR-MPV and PW-MPV were compared. Individual correlations between left and right sided measurements in patients were performed. In addition, MR-MPV was calculated from the prestenotic flow velocitiy (1.5 cm proximal) and the prestenotic and intrastenotic diameters.

Results: The measurement of the intrastenotic MR-MPV was not possible, if the peak flow velocity was higher than 80 cm/sec (see Bland-Altman Plot #1) In contrast, a good aggreement between MR and Doppler were found for the measurements 1.5 cm proximal and 5 cm distal to the stenoses in the phantom. The calculated intrastenotic MR-MPV showed a good agreement with the Doppler flow measurements in vitro (see Bland-Altman Plot #2).

In vivo, a close correlation ($r = 0.839$ $p < 0.01$) between MR-MPV and PW-MPV was found, however no patient had a maximum flow velocity over 80 cm/sec. The intraindividual comparison of MR-MPV on right and left side shows a high correlation ($r = 0.894$ $p < 0.01$).

Conclusion: In the present in vivo and in vitro examinations there was a satisfying correlation between MR-MPV and PW-MPV up to a maximum flow velocity of 80 cm/sec. With higher flow velocities, which produce more turbulence within the stenoses MR-MPV could not be adequately assessed. If intrastenotic MR-MPV is calculated from the prestenotic flow velocity and the prestenotic and intrastenotic diameters a close correlation can be achieved. This approach allows to determine the functional sifgnificance of stenoses by means of the combined diameter and flow measurement in CEMRA. A clinical important indication could be the assessment of pelvic stenoses, which cannot be adequately assessed with trans(see Bland-Altman Plot #2) cutaneous Doppler ultrasound technique.

93. Magnetic Resonance Flow Mapping Versus Intracoronary Doppler Guide Wire in the Assessment of Coronary Flow Reserve in Patients with Coronary Artery Disease

Willemijn Bedaux,[1] Mark Hofman,[2] Martin Stoel,[3] Carel Cock de,[4] Cees Visser,[5] Albert Rossum.[5] [1]*Academic Hospital Vrije Universiteit, Dept. Cardiology, Amsterdam, The Netherlands;* [2]*Univ Hospital Vrije Universiteit, Clinical Physics & Engineering, Amsterdam, Netherlands;* [3]*Academic Hospital Vrije Universiteit, Dept.*

Cardiology, Amsterdam, The Netherlands; [4]Academic Hospital Vrije Universiteit, Amsterdam, The Netherlands; [5]Academic Hospital Vrije Universiteit, Dept. Cardiology, Amsterdam, The Netherlands

Purpose: Numerous studies have demonstrated the value of Coronary Flow Velocity Reserve (CFVR) as a marker of physiologic significance of a given coronary obstruction, especially in the assessment of an intermediate luminal obstruction. CFVR is defined as the ratio of the maximal hyperemic flow velocity to baseline flow velocity. Doppler guide wire measurements during catheterization allow quantifying Averaged Peak Flow Velocity (APFV) distal from the stenosis in coronary arteries at baseline and during maximal hyperemia. With magnetic resonance (MR) flow mapping it is possible to quantify coronary flow velocity reserve noninvasively. The purpose of this study was to compare CFVR, acquired with the noninvasive MR technique to the Doppler guide wire measurements in a group of patients with ischemic heart disease.

Methods: The study included 16 patients all referred for elective coronary angioplasty because of one or two vessel disease. Before angioplasty was performed, APFV was measured with a Doppler guide wire (DGW) distal from the stenosis and in a healthy reference artery. The same measurement was repeated after an intracoronary bolus of adenosine [18 microg for left anterior descending artery (LAD), 12 microg right coronary artery (RCA)]. Within the same week all individuals underwent MRI. From series of anatomic images the LAD and RCA were visualized. Perpendicular to the vessel MR phase contrast velocity quantification was performed within a breath-hold at the same location as the Doppler guide wire measurement. A segmented k-space technique was used to obtain 5 phase-encoding steps for each frame within the cardiac cycle, resulting in an acquisition window of 105 ms. Other imaging parameters included a temporal resolution of 125 msec, a flip angle of 300, a field of view of 200 × 200 mm2, an echo time of 5 msec, a spatial resolution of 0.9 × 1.5 × 6 mm3 and a scan duration of 27 heart beats. Prior to every frame a fat saturation pre-pulse was applied. The encoding velocity was set to 75 cm/s, resulting in a velocity window of −75 to 75 cm/s. Heart rate and systemic arterial pressure were recorded. Measurements in the coronary arteries were repeated after intravenous administration of adenosine (140 microg/kgmin). A region of interest was drawn around the vessel and nearby located myocardial tissue, to analyze the flow velocity data and correct for myocardial motion.

Results: Flow reserve measurements were acquired with both techniques in 23 segments (RCA n = 10, LAD n = 13), 35% of the segments were stenosed (n = 8). Mean CFVR-MRI in the groups with stenosed and healthy reference arteries was 1.7 ± 0.7 (range 0.9–3.1) and 3.1 ± 2.0 (range 1.1–7.2) (p = 0.02), respectively. Mean CFVR-DGW in the groups with stenosed and healthy reference arteries was 1.97 ± 0.8 (range 1.15–3.4) and 2.95 ± 0.52 (range 2.2–4.1) (p = 0.001), respectively. Bland-Altman analysis showed a mean difference between the invasive Doppler guide wire technique and MRI of 0.2 ± 1.5. Location of the segments did not significantly influence the comparison.

Conclusion: Assessment of CFVR can be used as a marker of physiologic significance of coronary artery stenosis. MR flow velocity quantification in stable patients with coronary artery stenosis in the LAD and RCA provides equivalent noninvasive data to those acquired with Doppler guide wire measurements. No systematic difference between the two techniques was found. However, variability in both the MR and Doppler ultrasound measurement resulted in significant scatter of the data.

94. An In Vitro Evaluation of Ultra-Fast Segmented Space MR Velocity Mapping

Haosen Zhang,[1] Sandra S. Halliburton,[2] James R. Moore,[3] Orlando P. Simonetti,[4] Paulo Schvartzman,[5] Richard D. White,[5] George P. Chatzimavroudis.[6] *[1]Cleveland State University, Department of Chemical Engineering, Cleveland, OH USA; [2]The Cleveland Clinic Foundation, Section of Cardiovascular Imaging, Cleveland, OH USA; [3]Siemens Medical Systems, 1705 West Le Moyne Street, #E, Chicago, IL USA; [4]Siemens Medical Systems, Ontario Center East Tower, Chicago, IL USA; [5]The Cleveland Clinic Foundation, Section of Cardiovascular Imaging, Cleveland, OH USA; [6]Cleveland State University, Department of Chemical Engineering, Cleveland, OH USA*

Introduction and Aim: Traditional MR phase velocity mapping (MRPVM) involves a gradient-echo sequence with velocity-encoding gradients, and acquires one line of k-space (non-segmented) for each time phase per heart beat. This results in an acquisition of several minutes. Considering that new approaches in cardiovascular disease diagnosis have started to involve multi-slice and multi-directional velocity acquisitions, the non-segmented technique becomes less practical clinically. With the development of rapid imaging sequences, it has become possible to implement MRPVM much faster. Echo-planar techniques are very rapid, but show low resolution and frequent flow-related artifacts. Turbo gradient-echo shows higher resolution and generally good flow behavior. A number of excitations per time phase are performed, so multiple lines of k-space (segmented) are acquired for each time phase per beat. This shortens the total acquisition by a factor equal to the number of lines corresponding to a time phase. The aim of this study was to evaluate the turbo gradient-echo technique, and in particular to study the effect of increasing the number of k-space lines per time phase and beat on the accuracy of the flow measurements.

Methods: In vitro studies were performed in a 1.5 Tesla Siemens Sonata MRI scanner, under steady and pulsatile flow (with water), using 4 straight tubes (diameters 5.6, 14.7, 20.2, and 26.2 mm). The range of flow rates used in steady flow was 1.67–200 ml/s. (Reynolds number ~400–10,000). The true flow rates were known via rotameters. A computer-controlled piston pump was used for pulsatile flow. The range of piston stroke volumes studied was 6-90 ml/cycle, under a rate of 60 cycles/min. A sinusoidal flow waveform was downloaded to the pump. The true flow waveform, and thus the true flow volume were known via an MRI-compatible flowprobe. After the scout images, a slice was placed perpendicular to the long axis of the tube under study. Four MRPVM acquisitions of the through-plane velocity were performed for each flow condition: (a) non-segmented; (b) segmented with 5 k-space lines per phase and cycle; (c) segmented with 7 lines per phase and cycle; and (d) segmented with 9 lines per phase and cycle (slice thickness 5 and 3 mm; field of view 200 and 300 mm; in-plane resolution 0.8x0.8 mm and 1.2 × 1.2 mm; TE and TR shortest). A TTL signal, synchronized with the flow waveform, triggered the scanner to acquire a number of phases throughout the cycle. The duration of sequence (a) was 3.2 minutes and that of sequences (b), (c), and (d) was 28, 20, and 16 seconds, respectively. Using echo view-sharing, the temporal resolution increased, providing 25, 25, 19, and 15 phases per cycle for sequence (a), (b), (c), and (d), respectively. The phase was converted to velocity, and the velocity was integrated over the tube area to find the flow rate (ml/s). In pulsatile flow, integration of the flow curve over the cycle provided the flow volume (ml/cycle). Regression analysis and non-parametric statistical tests were performed to compare the flow data between the segmented and non-segmented techniques and between the segmented techniques and the true flow values.

Results: Fig. 1 and Fig. 2 show the comparison between the measured and true flow rates for steady and pulsatile flow, respectively, and for all sequences (5 mm slice thickness). Very good correlations were found between the measured and the true flow rates ($R^2 > 0.996$) and volumes ($R^2 > 0.981$), as well as between the non-segmented and segmented flow data ($R^2 > 0.988$). The regression analysis results for

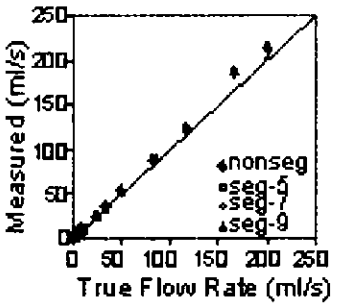

Figure 1. Steady flow results.

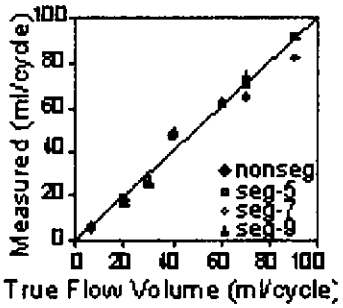

Figure 2. Pulsatile flow results.

the "segmented-9 lines" sequence were: (i) steady flow: "seg-9" = 1.08 "true" −0.38 ml/s, R^2 = 0.996; "seg-9" = 0.989 "non-seg" +0.35 ml/s, R^2 = 0.998); (ii) pulsatile flow: "seg-9" = 1.06 "true"-1.01 ml/cycle, R^2 = 0.981; "seg-9" = 1.13 "non-seg" −2.44 ml/cycle, R^2 = 0.988). Mann-Whitney analysis showed no significant difference (all p-values > 0.85) comparing the measured flow rates and volumes for all techniques with the true values, and between the segmented techniques and the non-segmented technique. No significant differences (p > 0.85) were found between the 3 mm and the 5 mm slice thickness data.

Discussion: The results from all segmented sequences agreed with the true flow values and with the non-segmented flow data in both steady and pulsatile flow cases. Increasing the number of lines to 9 did not show any negative effect on the accuracy of the measured flow. The number of phases per cycle decreased, but were still adequate (>10/cycle) for flow quantification. Although MRI is traditionally very susceptible to turbulent flow, measurements at high Reynolds numbers (~10,000) were accurate, especially in the larger tubes (diameter of 20.2 and 26.2 mm), by using a short TE (2.3 ms). In conclusion, the accuracy of the 9-line technique, in combination to its short duration (important in breath-hold protocols), promises great potential for in vivo flow quantification

95. Contributing Factors to the Development of Atherosclerotic Plaques in Thoracic and Abdominal Aorta, Assessed by Magnetic Resonance Imaging

Hiroaki Taniguchi,[1] *Yukihiko Momiyama,*[1] Reiko Hirano,[1] Akiko Hara,[2] Noboru Kameyama,[2] Atsushi Nozaki,[2] Kiyoshi Nagasawa,[3] Kumiko Noya,[2] Masayoshi Nagata,[2] Fumitaka Ohsuzu.[1] [1]*National Defense Medical College, 3-2 Namiki, Tokorozawa, Saitama Japan;* [2]*Iruma Heart Hospital, 1258-1 Kotanida, Iruma, Saitama Japan;* [3]*GE Yokogawa Medical Systems, 4-7-127 Asahigaoka, Hino, Tokyo Japan*

Background: Recently, it was reported that MRI can detect atherosclerotic plaques in aorta (Ao). Using MRI, we investigated the associations of atherosclerotic risk factors with plaques in thoracic descending and abdominal Ao.

Methods: We performed MRI on GE Signa 1.5T CVi scanner using ECG-gated, breath-hold double inversion recovery fast spin echo sequence in 42 patients (pts) who had elective coronary angiography for suspected CAD. T2 weighted images (TR of 2 RR intervals, TE of 50–60 ms, 20-cm FOV, and 256 × 256 matrix) of Ao were obtained every 12 mm with 4 mm slice thickness. In each pt, we assessed 9 slices of thoracic descending Ao and 9 slices of abdominal Ao which covered about 10-cm portions of thoracic and abdominal Ao. Each slice was scored (0 to 4 point) by plaque extent in Ao wall.

Results: Of the 42 pts, 29 (69%) had CAD (>50% stenosis). In MRI, plaques in thoracic and abdominal Ao were found in 15 (36%) and 34 (81%) pts, respectively. Plaque extents (the sum of scores of all slices) in both thoracic and abdominal Ao were significantly associated with age and blood pressure. Plaques were more prevalent in abdominal Ao than in thoracic Ao (32% of slices vs 12%, $p < 0.001$). However, hyperlipidemia was related to plaque extent in thoracic Ao ($p < 0.025$) but not in abdominal Ao. Notably, serum total cholesterol ($r = 0.56$) and LDL ($r = 0.47$) levels were associated with plaque extent in thoracic Ao ($p < 0.005$). In contrast, smoking was related to plaque extent in abdominal Ao ($p < 0.025$). Plaque extent in abdominal Ao was also associated with the number of stenotic coronary arteries ($r = 0.32$, $p < 0.025$). MRI detected complex plaques (irregular ones extending >5 mm into Ao lumen) in 9 pts (21%) and 16 slices (2%). Of the 16 slices with complex plaques, 15 were in abdominal Ao. Compared with pts without complex plaques, pts with complex plaques had more extensive plaques in both thoracic and abdominal Ao ($p < 0.001$). Moreover, pts with complex plaques were found to have higher blood pressure and higher Lp(a) level. Conclusions: MRI is useful to evaluate plaques in both thoracic and abdominal Ao noninvasively. Plaque extents in both Ao are associated with age and blood pressure. However, smoking is related to plaques in abdominal Ao, but hyperlipidemia is related to plaques in thoracic Ao. MRI can detect complex plaques which are related to high blood pressure and high Lp(a) level.

96. Comparison of Gated Positron Emission Tomography and Cardiac Magnetic Resonance for Left Ventricular Volume and Function Assessment

Kim Rajappan,[1] Lefteris Livieratos,[2] Paolo Camici,[3] Dudley Pennell.[4] [1]*Cardiovascular MR Unit, Royal Brompton Hospital, Sydney Street, London, London United Kingdom;* [2]*MRC Cyclotron Unit, Du Cane Road, London, London United Kingdom;* [3]*MRC Clinical Sciences Centre–Cyclotron Unit, Du Cane Road, London, London United Kingdom;* [4]*Cardiovascular MR Unit, Royal Brompton Hospital, London, London United Kingdom*

Background: Accurate and reproducible assessment of left ventricular (LV) volumes and function is important in various cardiac conditions, and has been shown to be indicative of prognosis. Cardiac magnetic resonance (CMR) is recognised as the reference standard for non-invasive measurement of these parameters. Positron emission tomography (PET) is another non-invasive technique used for assessment of various aspects of myocardial function, but is limited by the use of radioisotopes

Table of Results

	EDV (ml)	ESV (ml)	SV (ml)	EF (%)
CMR	100.2 ± 25.8	36.8 ± 23.0	± 16.8	65.0 ± 14.8
PET	90.7 ± 25.8	40.5 ± 24.3	50.2 ± 13.1	57.8 ± 15.8
Correlation R^2	0.93	0.96	0.78	0.95

and therefore exposure to ionising radiation. However, if a patient is undergoing a PET scan, it would be helpful if volume and function data could be acquired simultaneously. The aim of this pilot study was to determine whether results using PET correlate with those of CMR.

Methods: 6 patients undergoing PET scans were recruited. As part of the PET protocol, each patient was scanned using a high sensitivity PET scanner (EXACT 3D, 4.5mm resolution FWHM) and inhaled $C^{15}O$. Data was retrospectively ECG gated into 8 gates (the first being end diastolic), and off-line analysis using a singular value decomposition and thresholding method was performed to measure end-diastolic volume (EDV), end-systolic volume (ESV), stroke volume (SV) and ejection fraction (EF). A Picker Edge 1.5T MR scanner was used to obtain contiguous 10mm short-axis slices covering the entire LV and EDV, ESV, SV and EF were calculated as described previously.[1]

Results: See table.

Conclusion: In this pilot study, there was good agreement between CMR and PET for all the measured parameters, although CMR still has the advantage of being free from ionising radiation exposure. If a patient is undergoing a $C^{15}O$ PET scan for other reasons, useful functional and volumetric data may be acquired without further scanning.

97. Dobutamine-Induced Increase of Right Ventricular Contractility Without Increased Stroke Volume in Adolescent Patients with Transposition of the Great Arteries

Igor Tulevski,[1] Peter Lee,[2] Maarten Groenink,[3] Ernst van der Wall,[4] Jaap Stoker,[5] Hans Romkes,[6] Alexander Hirsch,[5] Barbara Mulder.[7]
[1]Academisch Medisch Centrum, Department of Cardiology, Amsterdam, Noord Holland The Netherlands; [2]Academisch Medisch Centrum, Meibergdreef 9, Amsterdam, N Holland The Netherlands; [3]Academisch Medisch Centrum, Meibergdreef 9, Amsterdam, N. Holland The Netherlands; [4]Leiden University Medical Center, Street 78, Leiden, N.H. The Netherlands; [5]Academisch Medisch Centrum, Meibergdreef 9, Amsterdam, N.H. The Netherlands; [6]Acedemisch Medisch Centrum, Meibergdreef 9, Amsterdam, N.H. The Netherlands; [7]Academisch Medisch Centrum, Meibergdreef 9, Amsterdam, N.H. The Netherlands

Objective: Prognosis in patients with surgically corrected (Senning or Mustard) transposition of the great arteries (TGA) depends mainly on right ventricular (RV) function and RV functional reserve. We examined the role of dobutamine stress in the early detection of RV dysfunction in asymptomatic or slightly symptomatic patients with TGA using magnetic resonance imaging (MRI).

Design and Patients: Twelve asymptomatic or slightly symptomatic patients with chronic RV pressure overload, surgically corrected (Mustard or Senning) TGA (age 22.8 (3.4) years; NYHA class I/II) and nine age matched healthy volunteers (age 27.3 (4.4) years) were included. MRI was applied both at baseline and during dobutamine stress (start dose 5 g/kg/min to maximum dose 15 g/kg/min) to determine RV and left ventricular (LV) stroke volumes (SV) and ejection fraction (EF).

Results: At baseline only RVEF was significantly higher in controls than in patients (71(9) v 57(10)%, $p < 0.001$), other RV parameters were not significantly different between the two examined groups: RVSV (86(21) v 72(27)ml, p = ns), RV end-diastolic volume (EDV) (123(37) v 123(33)ml, p = ns), and heart rate (61(10) v 69(14)bpm, p = ns), respectively. During dobutamine stress RVEF increased significantly both in controls and patients (20(16) v 17(18)%, $p < 0.01$ and $p < 0.02$ v rest, respectively), but stress RVEF was significantly higher in controls than in patients (85(3) v 66(7)%, $p < 0.0001$). RVSV increased significantly in controls (22(19)%, $p < 0.02$), and there was no significant increase in RVSV in patients (−10(28)%, p = ns). The controls showed no change in RVEDV (2(17)%, p = ns), but in patients a significant decrease in RVEDV (−24(15)%, $p < 0.001$) was observed. Maximal heart rate was significantly higher in patients than in controls (122(20) v 101(14)bpm, $p < 0.02$).

Conclusion: In asymptomatic or slightly symptomatic patients with surgically corrected TGA dobutamine had a positive inotropic effect on RV, but the increased contractility was not accompanied by an appropriate increase in SV. Our data suggest inadequate RV filling in this category of patients, possibly due to rigid atrial baffles and compromised atrial function or decreased compliance due to RV hypertrophy.

98. Evaluation and Follow-up of Patients with Left Ventricular Apical to Aortic Conduits Using Two and Three-Dimensional Magnetic Resonance Imaging and Doppler Echocardiography: A New Look at an Old Operation

Mark Fogel,[1] Jack Rychik,[2] Anne Hubbard,[3] Alvin Chin,[3] Paul Weinberg.[4] *[1]The Children's Hospital of Philadelphia, CHOP–Division of Cardiology, Philadelphia, Pennsylvania United States; [2]The Children's Hospital of Phildelphia, 34th St and Civic Center Blvd, Philadelphia, PA USA; [3]The Children's Hospital of Philadelphia, 34th St and Civic Center Blvd, Philadelphia, PA USA; [4]Children's Hospital of Philadelphia, 34th & Civic Center, Philadelphia, Pennsylvania United States*

Objectives: Although the interposition of left ventricular apical to descending aorta conduits (AAC) has diminished with the advent of the Ross-Konno operation, it remains a useful option particularly in very young infants. We reviewed our institutional experience imaging AACs and tested the hypothesis that the gradient across the native left ventricular outflow tract (LVOT) by echocardiography (echo) correlated with the AAC gradient by cardiac catheterization (cath). In a patient with an unobstructed AAC, no gradient should exist across the native LVOT.

Methods: A retrospective review of the echo, cath, magnetic resonance imaging (MRI) data and history of 9 patients with AACs over

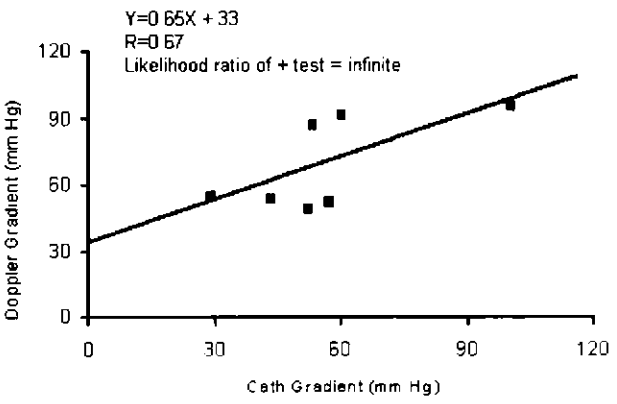

Graph. Correlation between Doppler and Cath Gradients.

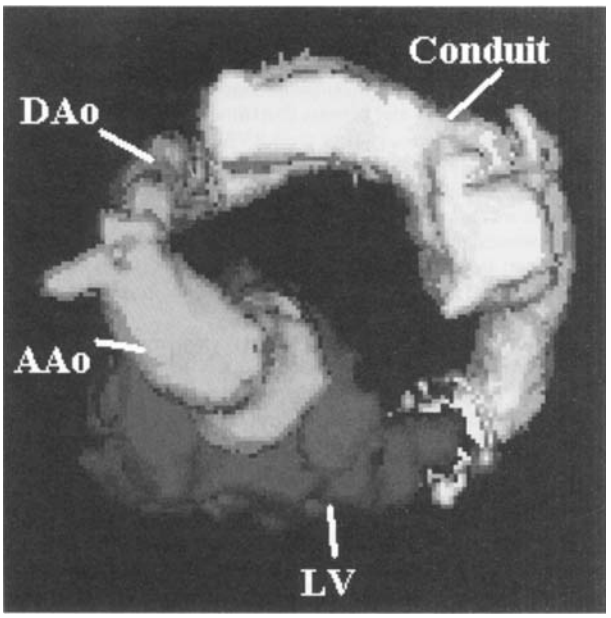

Figure. 3-Dimensional MRI of AAC.

an 8 year period. In 7/9 patients, 8 AAC obstruction events were assessed by Doppler interrogation of the native LVOT and by cath. 5 patients underwent 6 MRI scans.

Results: In all cases of obstruction diagnosed by cath (56.3 ± 21.9 mm Hg), Doppler echo demonstrated gradients across the native LVOT (69.3 ± 21.2 mm Hg, r = 0.67, see graph).

Since 2-D echo could not visualize the entire AAC in any patient, 2- & 3-D MRI was used successfully to evaluate anatomy and identify the site of obstruction (see figure).

All patients manifested AAC obstruction. Four of 9 (44%) patients have died, three underwent the Ross operation, one continues to live with his original AAC and one was lost to follow-up.

Conclusion: A gradient by Doppler interrogation of the native left ventricular outflow tract is an indirect means of assessing AAC obstruction. MRI is a useful tool to complement anatomic diagnosis by echo. AAC obstruction is common, and late mortality appears to be high.

99. Gadolinium-Enhanced 3-Dimensional MR Angiography Evaluation of Systemic and Pulmonary Venous Anomalies: A New Reference Standard?

Gerald GREIL,[1] Andrew POWELL,[2] Tal GEVA.[3] [1]*Cardiology, 300 Longwood Avenue, Boston, Massachusetts United States;* [2]*Cardiology, Children's Hospital, Boston, Massachusetts United States;* [3]*Children's Hospital Boston, 300 Longwood Avenue, Boston, MA USA*

Background: Echocardiographic (Echo) imaging of pulmonary and systemic venous anomalies (PulV and SysV, respectively) is limited by acoustic windows and patient size. Cardiac catheterisation with x-ray angiography (Cath) is invasive and expensive. The goal of this study was to evaluate the diagnostic utility of Gadolinium-enhanced 3-dimensional magnetic resonance angiography (Gd-enhanced 3D MRA) in these anomalies.

Methods: The MRA studies of 50 consecutive patients whose median age was 15.8 years (range 1 day to 60 years) with SysV and PulV anomalies diagnosed by MRI were compared to Echo, Cath, surgery, and autopsy data, when available. Two sequential Gd-enhanced (0.2 mmol/kg) 3D MRA datasets were acquired. The data were reviewed offline using maximal intensity projection and multiplanar reconstruction (MIP/ MPR).

Results: The most common indication for MRA was failure of Echo to establish a diagnosis (n = 36). All MRA studies (n = 54) were technically successful without adverse effects. The mean acquisition time of a MRA dataset was 27.3 ± 5.7 sec. MIP/MPR produced multiple user-defined angiographic-like images that clearly defined both vascular anatomy as well as its relationships with nonvascular structures. Thirty patients had PulV anomalies: PulV stenosis (n = 12), partial anomalous PulV drainage (n = 14), total anomalous PulV connection (n = 1), other (n = 3). Twenty patients had SysV anomalies: Mustard pathway obstruction (n = 4), LSVC (n = 6), multiple SysV anomalies in heterotaxy (n = 3), SVC obstruction (n = 3), other (n = 4). Seven patients had both SysV and PulV anomalies. The MRA diagnoses were concordant with Cath (n = 16), surgery (n = 7), pathology (n = 3), transesophageal Echo (n = 1) or a combination of both (n = 4). The MRA diagnosis proved to be accurate in all patients who had confirmation by other imaging studies or intraoperative inspection. Nine interventional Cath procedures were based on MRI findings alone as well as 11 operations. MRA provided information on spatial relationship of vascular and non vascular structures that was not available by Cath. In one patient the abnormal drainage of the right upper pulmonary vein was only found by 3D MRA and not seen by Cath. 3D MRA helped to delineate PulV stenosis in 3 patients as Cath was not able to define the anatomy clearly.

Conclusions: Gd-enhanced 3D MRA is an accurate and rapid noninvasive method to delineate PulV and SysV anomalies. Its diagnostic utility may surpass that of catheterisation.

100. Left Ventricular (LV) Dysfunction: Inter-Study Reproducibility of Global LV Structure and Function Assessed in Cardiac MRI(CMR) Core Lab

Prasad Panse,[1] Olaf Muehling,[2] Andrey Zenovich,[3] Neeta Panse,[3] Ravi Seethamraju,[4] Yimei Huang,[4] M. Jerosch-Herold,[5] I. Anand,[6] Norbert Wilke.[7] [1]*University of Minnesota,Cardiac MRI Core Lab, Mayo mail code 292, Minneapolis, MN USA;* [2]*University of Minnesota, Cardiac MRI Core Lab, Department of Radiology, Minneapolis, Minnesota United States;* [3]*University of Minnesota, Cardiac MRI Core Lab, Department of Radiology, Minneapolis, Minnesota USA;* [4]*University of Minnesota,Cardiac MRI Core Lab, Department of Radiology, Minneapolis, MN USA;* [5]*University of Minnesota,Cardiac MRI Core Lab, Department of Radiology, Minneapolis, MN United States;* [6]*VA Medical Center, Division of Cardiology, Minneapolis, MN United States;* [7]*University of Minnesota, Cardiac MRI Core Lab, Department of Radiology, Minneapolis, Minnesota United States*

Background: Serial measurement of ventricular mass, volume and function is important for assessing new drugs considered to attenuate ventricular remodeling. It has been reported that Cine MR produces highly reproducible data in normal hearts (1). In patients with LV dysfunction, low cardiac output and distorted ventricles, the resolution between anatomic structures remains poor. Values for Inter-study reproducibility in such sick patients are not available.These values are however important in cardiac core lab data analysis for calculating sample size in drug studies in the CHF trials (Val-HeFT, Renaissance). We report reproducibility data of LV structure and function in patients with a wide range of LV dysfunction obtained in the cardiac core lab setting.

Methods: Eight subjects underwent MRI of the heart, with a 1.5T Siemens scanner on two occassions, one week apart using the same

Table

	% Variability	Std. dev.	Correlation Coefficient
LVEDV	3.79	3.1	0.99
LVESV	8.79	4.72	0.98
LVmass	3.33	2.76	0.99
EF	7.46	3.9	0.94
SV	7.97	3.31	0.84

breath-hold protocol. The entire heart was covered from base to apex with 8mm slices and 15–20 phases including the end-diastolic (ED) and end-systolic (ES) phases. An experienced observer manually traced the RV and LV contours using MASS analysis software version to determine the ED volume (EDV), ES volume (ESV), Stroke volume (SV), Ejection fraction (EF) and LV mass. Standard deviation, correlation coefficient and percent variability was determined. Percent variability was calculated as the absolute value of the difference between the two measurements over the mean of the two measurements.

Results: The average EDV was 183 ± 52 ml and EF was 46%. The standard deviation, correlation-coefficient, and percent variability for the LV mass, volume, EF and SV are shown in the table. The data are very similar to those described for subjects with normal hearts. In normal subjects, (average EDV 113 ± 14.6 ml and EF 65%) 3.6% to 3.8% variability for LV mass, 3.9 to 5.2% variability for end-diastolic volume and 9.0 to 9.7% for end systolic volume has been reported (1).

Conclusion: For the first time, in the core lab setting, we determined Interstudy reproducibility for the assessment of LV remodeling in heart failure patients by CMR.

Assessment of LV remodeling by CMR in heart failure patients is highly reproducible when assessed in a core lab with standardized analysis procedure. Cine MR is thus capable of assessing a given change in LV structure and function with a much smaller sample size as compared with the other non-invasive imaging techniques such as echocardiography.

101. Assessment of Regional Differences in Myocardial Blood Flow Using MR True FISP BOLD Imaging

Debiao LI,[1] Kara Wright,[2] Francis Klocke.[3] [1]*Northwestern University, Department of Radiology, Chicago, IL USA;* [2]*Northwestern University, Suite 700, 448 E. Ontario St., Chicago, IL USA;* [3]*Northwestern University, Northwestern University Medical School, Chicago, Illinois United States*

Introduction: The blood oxygen level dependent (BOLD) effect uses the intrinsic properties of paramagnetic deoxyhemoglobin in the blood as an endogenous contrast agent. With stimulated blood flow, changes in venous oxygenation reflect changes in blood flow to the myocardium which in turn changes the T2 and T2* of the myocardium. The purpose of this study was to evaluate the use of the T2/T1-weighted 2D True FISP (fast imaging with steady-state free precession) sequence (1) to detect regional differences in myocardial blood flow based on the BOLD effect.

Materials and Methods: Six dogs were imaged on a 1.5T Siemens Symphony system. Surgical preparations were performed to create regional differences in blood flow to the myocardium surrounding the left ventricle. A catheter was placed in the left circumflex artery (LCX) through which adenosine was infused to increase the blood flow in the LCX. Adenosine is a vasodilator that would allow for increased blood flow in coronary arteries with little effect on myocardial oxygen consumption. MR measurements were obtained before and during adenosine administration. Fluorescent microspheres were injected through a catheter placed in the left atrium to determine the relative myocardial blood flow on a regional basis.

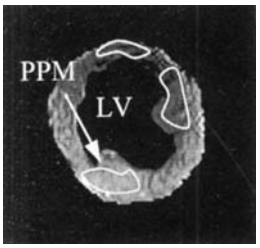

Figure 1. Normalized BOLD image shows the higher signal intensity in the posterior myocardial region near the posterior papillary muscle (PPM) compared to the rest of the myocardium surrounding the left ventricle (LV). The other two circled regions were supplied by the left anterior descending artery and were relatively unaffected by adenosine.

The BOLD imaging sequence was a 2D True FISP cine sequence (TR/TE = 3.0/1.5 ms, flip angle = 60˚, slice thickness = 6 mm, 4 signal averages, acquisition time ≫30 s). The True FISP sequence maintains steady-state magnetization by rewinding the applied gradients in all three directions after the readout during each TR. It is T2/T1-weighted and has much greater signal-to-noise ratio than the conventional steady-state incoherence gradient-echo sequence in which the transverse magnetization is spoiled after the readout. Each cardiac cycle included acquisition of 10 phase encoding lines. The ventilator was turned off during imaging to freeze respiratory motion.

Results: Figure 1 shows a normalized BOLD image, which was created by subtracting the baseline image from the adenosine image. This subtracted image was then divided by the baseline image. Note the high signal intensity in the posterior region near the posterior papillary muscle (PPM), which represents the area of the myocardium affected by the adenosine administration. The rest of the myocardium was relatively unaffected.

The regional difference in normalized signals between the focal region and one of the remote regions in Fig. 1 was then correlated to the normalized myocardial blood flow difference as measured using the fluorescent microspheres (Fig. 2). A significant correlation ($R = 0.73$) was found. A 100% flow increase resulted in a 5% BOLD signal increase.

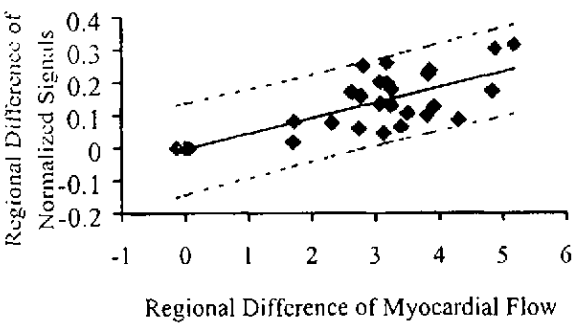

Figure 2. The correlation between the regional signal difference from the MR BOLD images and the regional myocardial flow difference. The 95% confidence interval for the MR BOLD signal difference caused by the flow difference is shown by dotted lines.

Discussion and Conclusion: Our preliminary studies showed the feasibility of detecting regional differences in myocardial blood flow using the T2/T1-weighted True FISP sequence based on the BOLD effect. The technique needs to be tested in a clinically relevant setting where the coronary artery flow is reduced in a myocardial region as compared to other parts of the heart.

Reference

1. Oppelt A et al. Electromedica, 54, 15–18, 1986.

102. Edge Voxel Detection in MR Phase-Velocity Imaging: Theoretical Considerations

John Wood.[1] [1]*University of Southern California, CHLA, Cardiology, Mailstop 34, Los Angeles, CA USA*

Magnetic resonance phase-velocity imaging has become an accepted tool for flow quantitation. Unfortunately, this technique often requires laboriously tracing vessel boundaries manually through multiple cardiac phases (2). Although automated vessel boundary detection algorithms exist, none are universally accepted (1). Typically, vessel segmentation has been performed using simple thresholds adjusted to compensate for partial volume effects (3). We examined optimal thresholding criteria for detection of circular or elliptical vessels in a uniform, noisy background. The problem may be cast into a degenerate ternary hypothesis-testing problem, which may be described using classic Receiver Operator Characteristic (ROC) statistics.

$$P_D = \int_t^{\infty} \left[\frac{P_1^* PR_{|H_1}(R|H_1) + P_2^* P_{|H_2}(R|H_2)}{P_1 + P_2} \right] dx$$

$$P_t = \int_t^{\infty} \frac{1}{\sqrt{2\pi}\sigma} e\left(\frac{1 - B}{\sqrt{2}\sigma} \right)^2 dx$$

Equation 1.

Where PD and PF represent the true positive and false positive detection rates, P1 and P2 are apriori probabilities of partial volume and intralumenal pixels, Pr|H1(R|H1) and Pr|H2(R|H2) are the corresponding conditional probability density functions, sigma is the

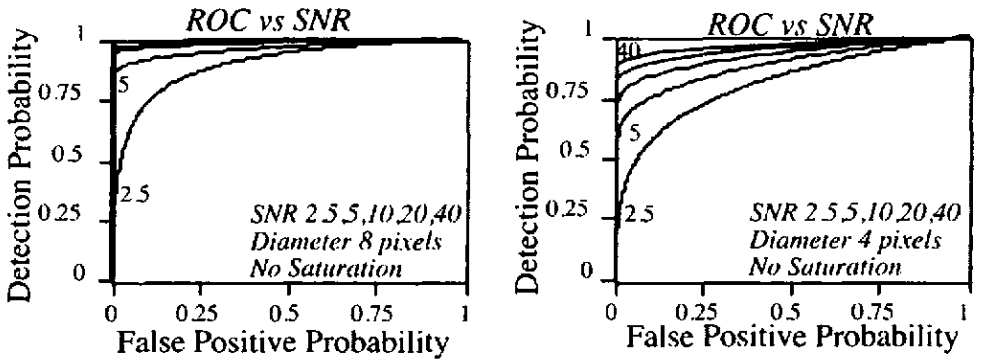

Figure 1. Vessel pixel ROC curves as a function of SNR for 8 pixel and 4 pixel diameter vessels. Pixel detection is relatively noise insensitive for large vessels.

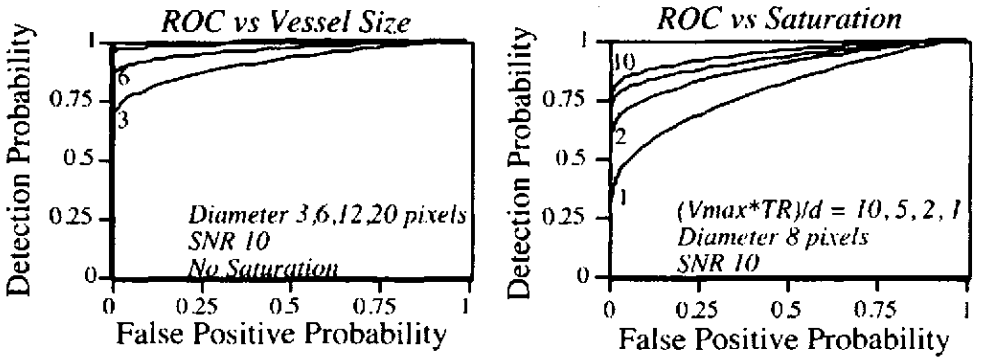

Figure 2. A. Vessel pixel ROC curves as a function of vessel size for an SNR of 10. Detection efficacy falls dramatically for vessel diameters <6 pixels. B. ROC curves as a function of blood saturation for parabolic flow in a simulated 2D, gradient echo, 90 degree flip, having through-plane velocity encoding. Increasing flow-related enhancement, indexed by maximum blood velocity * TR/slice thickness, markedly decreases pixel detectability as V^*_{max} TR/d approaches 1. Minimum error threshold criteria, although "optimal" when the conditional density functions can be accurately estimated, fails in the presence of significant saturation modulation and in the presence of Rician noise. Fixed false positive error thresholds have comparable performance but are more robust to nonidealities and parameter estimation.

Gaussian noise variance, B is the background level, and t is the threshold. Monte Carlo simulations demonstrated simple relationships for the necessary apriori probabilities as a function of vessel radius, r, and the number of pixels in the region of interest (Eq. 2).

$$P_1 = \frac{\pi r\sqrt{2\pi}}{\#\ ROI} \quad P_2 = \frac{\left(r\sqrt{\pi} - \frac{\sqrt{2\pi}}{2}\right)^2}{\#\ ROI}$$

Equation 2.

Partial-volumed conditional probability functions were nearly uniform for large vessels, but became skewed toward lower intensities for vessels <4 pixel diameter. Vessel pixel detectability, described by the area under the ROC curve, decreases for smaller vessels, Rician noise, and vessel saturation, as well as for poorer SNR (see Figures 1 and 2 on previous page).

References

1. Burkart D, Felmlee J, Johnson C, Wolf R, Weaver A, Ehman R. Cine phase-contrast MR flow measurements: improved precision using an automated method of vessel detection. JCAT 1994; 18:469–475.
2. Oyre S, Ringgaard S, Kezerke S, Paaske W, Erlandsen M, Boesiger P, Pedersen E. Accurate noninvasive quantitation of blood flow, cross-sectional lumen vessel area and wall stress by three-dimensional paraboloid modeling of magnetic resonance imaging velocity data. JACC 1998; 32:128–134.
3. Tang C, Blatter DD, Parker DL. Accuracy of phase-contrast flow measurements in the presence of partialvolume effects. JMRI 1993; 3: 377–385.

103. Accurate Determination of Acute Infarct Size with Delayed Hyperenhancement Requires Imaging at a Specific Time After Gd-DTPA Injection

John Oshinski,[1] Jeffery Jones,[2] Zequan Yang,[3] Brent French.[4] [1]*Emory University, Department of Radiology, Atlanta, Georgia United States;* [2]*University of Virginia, Box 801332, Charlottesville, VA USA;* [3]*University of Virginia, Stacey Hall, Charlottesville, Virginia United States;* [4]*University of Virginia, 300 Park Place, MR4 Room 5021, Charlottesville, Virginia United States*

Introduction: In patients with acute MI, hyperenhancement 5–7 min after Gd-DTPA injection has been reported in regions that later show recovery of mechanical function. In a canine model of acute MI, it has been reported that hyperenhancement 20–30 min after Gd-DTPA injection occurs only in necrotic regions and not in surrounding reversibly-injured regions of myocardium. The objective of this study was to determine if the size of the hyperenhanced region varies with time after Gd-DTPA injection or duration of ischemia.

Methods: The left coronary artery was occluded in 10 Lewis rats for 30 min (n = 5) or 2 hr (n = 5) followed by 48 ± 2.4 hours of reperfusion. MRI scans were performed post-MI in a 1.5 T MR scanner with a quadrature wrist coil. An ECG-triggered, spin echo sequence with a non-selective inversion pre-pulse was used to obtain mid-ventricular short axis images (TE = 20, TI = 225, TD adjusted for data collection every third RR interval). Images were acquired continuously for 40 minutes (13–20 images) following Gd-DTPA injection (0.3 mmol/kg). The sizes of hyperenhanced regions at each time point were obtained by threshold analysis and compared with TTC-stained sections of the excised rat heart to determine the relation between the size of the hyperenhancement zone and the infarct size.

Results and Conclusion: Immediately after Gd-DTPA injection (3 min), the hyperenhanced zone region overestimated the TTC-determined infarct size by 28 ± 6%. The hyperenhanced zone receded over time to match infarct size. An example from one animal is shown in figure 1. The time required for the hyperenhancement zone to accurately determine infarct size was significantly different for animals undergoing a 2 hour occlusion (16 ± 2 min) compared to animals undergoing a 30 minute occlusion (26 ± 4 min). Correspondence time was longer in the 30 minute occlusion group, despite the smaller infarct size in the 30 minute group (24 ± 9%) versus the 2 hour occlusion group (33 ± 11%). Although the time required for the delayed enhancement zone to match the true infarct size varied considerably between animals, correspondence was always observed within 32 min of Gd-DTPA injection.

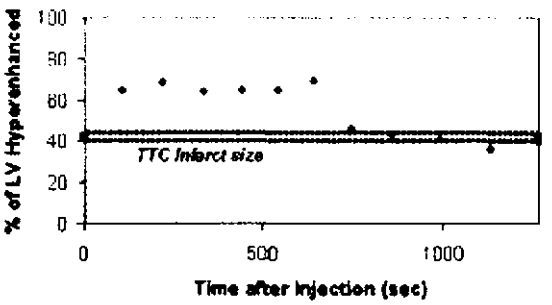

Figure 1. Size of hyperenhancement zone versus time after injection

104. Cardiovascular MRI in a Clinical Cardiology Setting—A Single-Center Experience in 2513 Cases

Matthias Friedrich,[1] Jeanette Schulz-Menger,[2] Oliver Strohm,[3] Thomas Poetsch,[2] Wolfgang Lankes,[2] Rainer Dietz.[2] [1]*Franz-Volhard-Klinik, Charite, Wiltbergstr. 50, Berlin, Berlin Germany;* [2]*Franz-Volhard-Klinik, Charite, Humboldt-Universitaet zu Berlin, Wiltbergstr. 50, Berlin, Berlin Germany;* [3]*Franz-Volhard-Klinik; Charite, Campus Buch; Humboldt-Universität zu Berlin, Wiltbergstr. 50, Berlin, Berlin Germany*

Cardiovascular magnetic resonance imaging (CMRI) is widely accepted as the noninvasive gold standard for many parameters used for cardiologic diagnosis. However, the impact of CMRI results on daily clinical decision-making is widely unknown.

In our cardiology department, equipped with standard technology including nuclear medicine facilities, echocardiography and catheterization labs we assessed the impact of a CMRI study on the final diagnosis of the referring physicians (from our hospital and from others) between January 1996 and March 2000. All MRI studies were requested due to clinical reasons. A cardiologist (W.L.), experienced in echocardiography and cardiac catheterization and not related to the MRI department, compared the CMRI findings to the final diagnosis as based on all clinical and other criteria. The cases were classified into three categories, depending on the impact of the CMRI diagnosis on the diagnostic decision (no impact, confirmation only, decisive).

The most frequent questions were related to myocardial disease such as cardiomyopathies or myocardial involvement in systemic disease (63%) and vascular disorders (12%).

From a total of 2513 requested studies 156 (6.2%) could not be performed because of contraindications (n = 48, 1.9%) or claustrophobia (n = 108, 4.3%). One of 58 studies (1.8%) with dobutamine or adenosine stress had to be stopped due to severe angina. There was one unspecific systemic reaction on contrast media in 1507 studies with Gd-DTPA (0.07%). No other complications were observed.

In 241 cases we were not able to get information on the final diagnosis. Of the remaining 2116 studies the impact was decisive for establishing the diagnosis in 1013 cases (47.9%), in 37.6% CMRI only confirmed the diagnosis. In 307 (14.5%) cases CMRI had no impact on the final diagnosis of the referring physician (other diagnoses, mostly due to conflicting results of other methods).

We conclude that in a clinical cardiology setting CMRI has a strong impact on decision-making. Detailed analyses of the impact on prognosis and costs have to be awaited.

105. RELIF for Cardiac Cine MRI: A Rapid Acquisition Scheme Cuts Imaging Time by Six

Wolfgang Rehwald,[1] Raymond Kim,[2] Robert Judd.[3] [1]*Northwestern University, Tarry 12-703, Chicago, Illinois United States;* [2]*Northwestern University, Division of Cardiology, Northwestern University Medical School, Chicago, Illinois United States;* [3]*Northwestern University, Northwestern University, Chicago, Illinois United States*

Introduction: To overcome the need for long breath holds in cardiac cine MRI we have previously developed the SLAM sequence (Selective Line Acquisition Mode). Twofold savings in scan time are possible, however it is unlikely that further improvements will come from this technique alone. Therefore we developed the RELIF technique (Reconstruction by Estimation of Lines and Inhibition of Fold-In) that combines the advantages of SLAM with those of another reduced field of view method yielding a six-fold reduction in scan time.

Theory: Every sixth k-space line per cardiac frame is acquired: lines 1, 7, 13, for odd cardiac phases and lines 4, 10, 16, for even cardiac phases. Lines 1, 4, 7, 10, 13 not acquired during the time window of the respective cardiac phase are reconstructed using line estimation by SLAM. Transforming the partially filled k-spaces into image space yields images with one-third the fov. The non-moving sides are folded into the center third. Therefore the side parts can be recorded once as reference and then be subtracted from the image with artifacts. This restores an artifact-free image of the center fov.

Materials and Methods: We tested RELIF clinically on ten cardiac patients with various forms of cardiac disease. We acquired full data sets with a trueFISP sequence, discarded five out of every six lines and used the reduced data sets as input for the RELIF algorithm.

Results: Figure 1a shows a typical example of a cine-scan by RELIF. Within the equivalent of two heartbeats a series of twenty-four images was acquired of which six are shown. The conventional acquisition took twelve heartbeats (figure 1b). For all patients SNR in the two-heartbeat case was measured as 52 ± 7% of the twelve-heartbeat case (in myocardium). This SNR is more than adequate (SNR = 22.3 ± 7.0 in cavity, SNR = 10.5 ± 3.3 in myocardium), because the underlying trueFISP sequence has intrinsically high SNR. Spatial resolution is preserved.

Conclusion: RELIF allows a six-fold reduction in scan time and comes with an affordable penalty in SNR. The technique optimizes image quality by distributing losses inevitable when reducing scan time. Thus RELIF can be used clinically for extremely fast imaging of the heart.

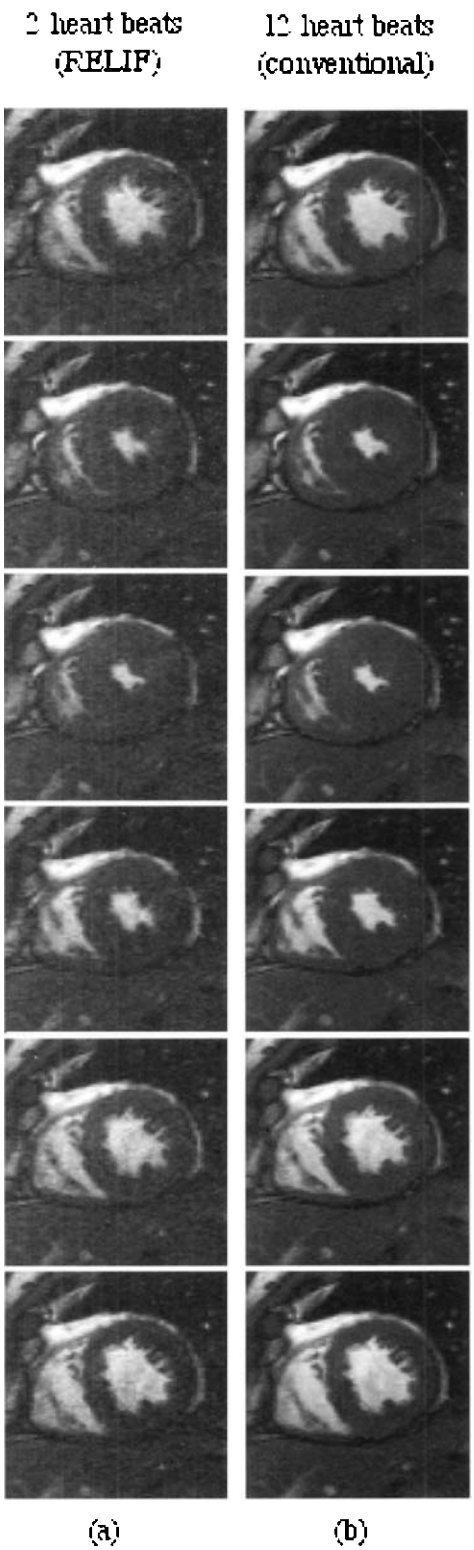

Figure 1.

106. Transmural Infarct Extent Correlate with Left Ventricle Regional Contractile Function One Year After Myocardial Infarction

Carlos Rochitte,[1] Paulo Oliveira,[2] José Parga,[1] Luis Ávila,[4] Rosa Maria Piva,[5] José Nicolau,[3] Roberto Kalil,[6] Claudio Castro,[3] Giovanni Cerri,[3] José Ramires.[3] [1]*Heart Institute–InCor–University of*

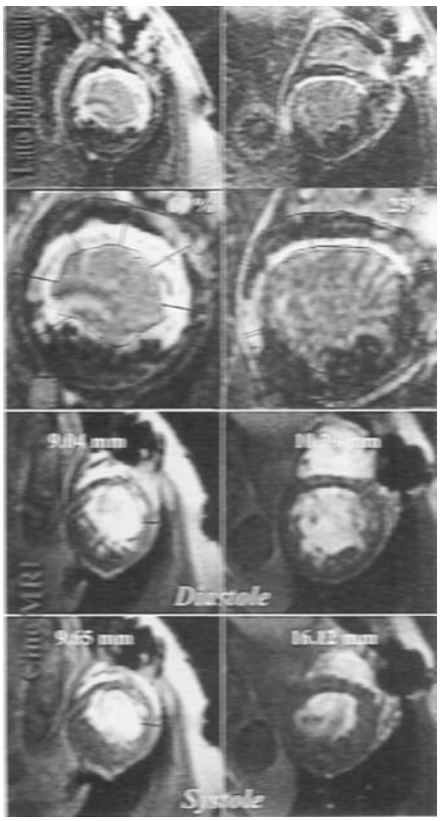

Figure 1.

São Paulo Medical School, Av. Dr. Enéas de Carvalho Aguiar, 44, São Paulo, SP Brazil; [2]Heart Institute–InCor–University of São Paulo Medical School, Av. Dr. Enéas de Carvalho Aguiar,44, São Paulo, SP BRAZIL; [3]Heart Institute (InCor)–University of São Paulo Medical School, Av. Dr. Enéas de Carvalho Aguiar, 44, São Paulo, SP BRAZIL; [4]Heart Institute (InCor)–University of São Paulo Medical SchoolUniversity of São Paulo Medical School, Av. Dr. Enéas de Carvalho Aguiar, 44, São Paulo, SP BRAZIL; [5]Heart Institute–InCor–University of Sao Paulo Medical School, Av. Dr. Eneas Carvalho de Aguiar, Sao Paulo, Sao Paulo Brazil; [6]Heart Institute (InCor)–University of São Paulo Medical School, Av. Dr. Enéas de Carvalho Aguiar, 44, São Paulo, SP BRAZIL

Background: Myocardial viability is crucial to clinical decision-making. MRI delayed enhancement techniques have recently been shown to delineate infarct size precisely. It is still unclear how the myocardial infarction (MI) transmurality relates to contractility in chronic infarcts.

Methods: We studied 10 patients with approximately 12 months old MI that underwent CABG during the MI acute phase. MRI studies were performed in a 1.5T GE CV/i magnet using a cardiac phased-array surface coil. We used a contrast-enhanced MRI (ceMRI) pulse sequence (fcardvt), specially designed for infarct sizing and myocardial viability evaluation, after 10–20 minutes of 0.2 mmol/kg of Gd-DTPA bolus. Cine-MRI was used to assess contractility as wall thickening. We acquired 6–10 short-axis slices and 4 radial long-axis slices of the left ventricle. To assess transmurality we divided short-axis slices in 8 radial segments. We measured the total myocardial area and the enhanced myocardial area within each segment. The ratio of infarcted/normal myocardial for each segment was defined as an index of infarct transmurality. Figure 1 shows examples of a 60% (left column) and a 23% (right column) infarct transmuralilty index. First 2 rows show the delayed enhanced images and last 2 rows the cine MRI. The second row is a zoomed version of the first row and demonstrates the delineation of myocardial segments for the infarct transmurality index measurements. Two observers blinded to ceMRI delineated epicardial and endocardial contours and automated software calculated the wall thickening ((systolic–diastolic)/diastolic wall thickness) at each 15 degrees (24 measurements, 3 for each radial segment) around the circumference of 8–10 LV short axis slices. The mean of 3 wall thickness measurements was compared with each transmural index.

Results: Infarcted regions were significantly thinner than remote normal regions ($p < 0.01$) and had decreased thickening (18 ± 7 vs. $40 \pm 4\%$, $p < 0.01$) for the entire group. Wall thickening correlated with infarct transmurality ($r = 0.6$), circumferential extent($r = 0.86$) and even more with the infarct size/circumferential extent ratio ($r = 0.90$, $p < 0.05$). LV ejection fraction and volumes also correlated with infarct size ($r = 0.8$). Note on the figure the correlation of the infarct transmurality index and the wall thickening. Myocardial regions with transmural indexes greater than 50% had a mean wall thickening of $6.9 \pm 3.1\%$ while regions with indexes less than or equal to 50% had $22.8 \pm 2.2\%$ ($p < 0.002$). Regions with transmural indexes less than 25% and those between 25 and 50% had no significant differences in wall thickening (23.8 ± 3.9 vs. 22.5 ± 2.7, p NS). We observed in our population of patients that underwent CABG during acute phase of MI, not only late enhanced regions corresponding to infarcted related artery territory, but also several regions of subendocardial enhancement not related to the previous myocardial infarction in 8 of our 10 patients. The causes of this new observation unknown. Several hypotheses can be made, as for instance, that they have been caused by cardiopulmonary bypass and inadequate myocardial protection during CABG. However, these hypotheses will require further pathophysiological investigations. It is important to note that LV regions with subendocardial enhancement did not show decreased wall thickening, and therefore impossible to be detected by methods assessing wall motion.

Conclusion: Wall motion late after myocardial infarction is related to the transmural and circumferential infarct extent and can be precisely determined by contrast-enhanced MRI. Delayed enhancement MRI can accurately delineated one-year-old myocardial infarction. The possibility of detecting small subendocardial areas of enhancement opens a window of opportunity to use this technique to monitor and diagnose small myocardial injuries after procedures, such as CABG, and more importantly to evaluate new techniques of myocardial protection and to assess myocardial salvage after therapy.

107. Application of Spatial Modulation of Magnetization to Children: The Effect of Image Resolution on Tagging Pattern

John Haselgrove,[1] Mark Fogel.[2] *[1]The Children's Hospital of Philadelphia, Department of Radiology, Philadelphia, Pennsylvania United States; [2]The Children's Hospital of Philadelphia, CHOP–Division of Cardiology, Philadelphia, Pennsylvania United States*

Background and Objective: Spatial modulation of magnetization (SPAMM) is a valuable magnetic resonance imaging technique for studying ventricular biomechanics. In order to track the intersection points of the stripes to calculate regional wall motion and strain, the stripe spacing should be at most half the wall thickness, yet sufficiently larger than the image pixel size in order that the stripes be well resolved. These conflicting requirements, that the grid spacing be much smaller than the wall thickness yet much larger than the pixel size, are relatively

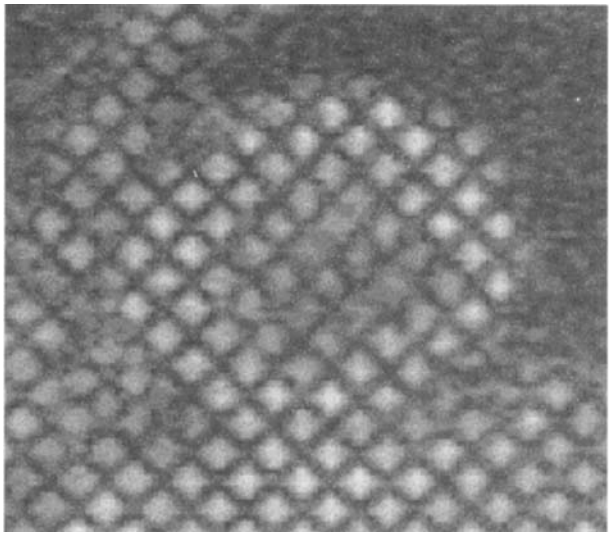

Figure 1. High ratio of pixel size to grid spacing SPAMM imaging.

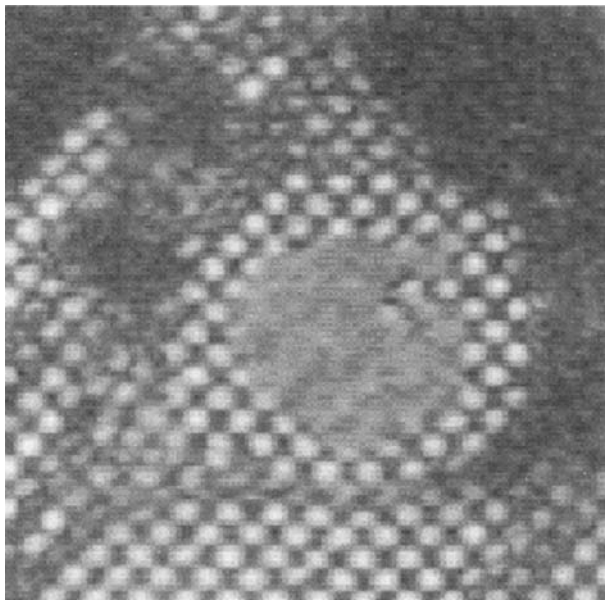

Figure 2. Low ratio of pixel size to grid spacing SPAMM imaging.

easy to meet in adult subjects but are difficult in children because of their small size. The purpose of this study was to delineate the effect of pixel size relative to SPAMM grid spacing on the stripe pattern produced by SPAMM with application towards its use in children.

Methods: We performed SPAMM imaging on a 1.5 Telsa Siemen's Vision and SP-63 on a phantom, using an artificial ECG (R-R interval = 450 ms for triggering), holding the pixel size constant and varying the degree of stripe spacing (4, 6, 8, 32 mm). We used both square (1 mm) and rectangular (1 mm by 2 mm) pixels. We express the ratio of pixel size:grid size as the ratio of the horizontal pixel size:the center-center spacing of the grid lines. We then performed SPAMM imaging in 3 children with differing pixel:grid spacing.

Results: In a phantom, the effect of decreasing the separation between stripes while keeping the resolution of the image constant changed the stripe pattern from a series of 2 parallel lines perpendicular to each other to a "checkerboard" pattern. With a relative pixel:grid ratio of 1:8 as used with adult studies, the dark bands and the crossing points are well defined. As the ratio decreases from 1:8 to 1:6, the black band is less well resolved. With a pixel resolution of 1 by 2 mm, the image becomes a series of white dots superimposed on a black background. When the resolution is reduced further to a pixel:grid ratio of 1:4 the image appears to be a checkerboard of white and dark squares. This progressive loss of definition of the sharp black line is to be expected because signal intensity is averaged over the area of each pixel. The pixel can therefore be thought of as a smoothing and sampling filter. The smoothing operation spreads any sharp features (the grid lines) in space and makes them appear broader. As the pixel becomes a larger fraction of the object (the unit cell of the grid), the broadening of the sharp lines becomes greater.

The effect in-vivo is similar. When the ratio is approximately 1:8, as in the patient in figure 1 with single left ventricle, the stripe pattern is a set of parallel lines perpendicular to each other.

When the ratio is approximately 1:4, as in the patient in figure 2 also with single left ventricle, the stripe pattern is "checkerboard".

Conclusion: With decreasing ratio of pixel size to grid spacing, SPAMM stripe patterns change from a set of parallel lines perpendicular to each other to a "checkboard" pattern. This effect has implications for tracking techniques to determine strain and wall motion. At smaller ratios, as is needed sometimes in children, it may be preferable to track the signal intense regions rather than the "intersection" points of the stripes.

108. Low Dose Ramiprilate Treatment Improves Wall Thickening After Myocardial Ischemia and Reperfusion

Steffen Petersen,[1] Georg Horstick,[1] Dietmar Becker,[1] Thomas Voigtländer,[1] Wolfgang Schreiber,[2] Manfred Thelen,[3] Oliver Kempski,[4] Jürgen Meyer.[1] *[1]2nd Medical Clinic, University Hospital Mainz, Langenbeckstr. 1, Mainz, Germany Germany; [2]Department of Radiology, University Hospital Mainz, Langenbeckstr. 1, Mainz, Germany Germany; [3]Department of Radiology, Langenbeckstr. 1, Mainz, Germany Germany; [4]Institute for neurosurgical pathophysiology, University Hospital Mainz, Langenbeckstr. 1, Mainz, Germany Germany*

Background: Reperfusion of a previously ischemic area results in an inflammatory response leading to additional damage of myocytes which are still viable at the end of the ischemic period. There is evidence in the literature that the local renin-angiotensin-aldosterone-system (RAAS) is activated by reperfusion. To prove the concept of local RAAS activation we examined the effect of low dose ramiprilate administration (preventing ACE-inhibitor dependent afterload reduction) on infarct size and regional myocardial function.

Methods: After anaesthesia with chloralhydrate, intubation and mechanical ventilation, left lateral thoracotomy was performed. The left coronary artery (LCA) was occluded for 30 minutes. 5 minutes prior to reperfusion an arterial blood gas was drawn and either ramiprilate (10 mcg/kg, n = 6) or NaCl 0.9% (n = 6) were infused into the left atrium under normoxic conditions and 6-lead-ECG control. Rats were extubated after reperfusion and reintubated 24 hours later for final examinations. Evans-Blue was injected after reocclusion of the LCA to determine the area at risk (AR) followed by a vital staining with TTC. The left ventricle (LV), the area at risk (AR) and the zone of myocardial infarction (MI) were determined by planimetry. Examinations of myo-

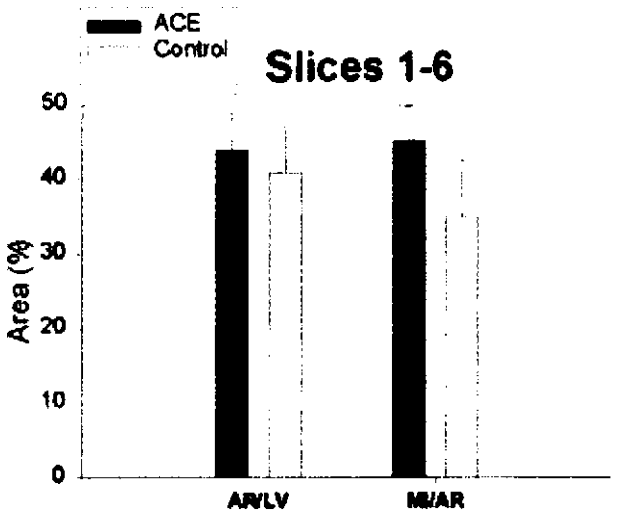

Figure 1.

cardial wall motion were performed on a conventional 1.5 T Siemens Vision system using a small eye coil. The ECG-triggered spin-echo sequences (TR/TE = 600 ms/14 ms, FOV 85 mm, MA = 192 × 256, slice thickness 2 mm) had an in-plane resolution of 0.3 × 0.3 mm. Images were recorded at 20ms increments following the R-wave of the ECG acquiring a basal and an apical slice. Maximum diastolic relaxation and systolic contraction were used for off-line analysis of regional wall thickening.

Results: The area at risk was similar in both groups (ramiprilate: 44 ± 5% vs. NaCl 0.9%: 41 ± 6%). Areas of MI/AR were not different between both groups (ramiprilate: 45 ± 11.7% vs NaCl 0.9%: 35 ± 15%) (Figure 1). Concerning regional wall motion analysis apical slices demonstrated significantly improved wall thickening of the reperfused lateral wall after treatment with ramiprilate (Figure 2).

Conclusion: The study clearly demonstrated improved regional wall thickening after ischemia and reperfusion with low dose ramiprilate treatment despite equivalent infarct sizes in both groups. We conclude that low dose ACE-inhibitor administration might reduce myocardial stunning after a brief period of ischemia. This effect could be demonstrated with a clinical 1.5 T scanner.

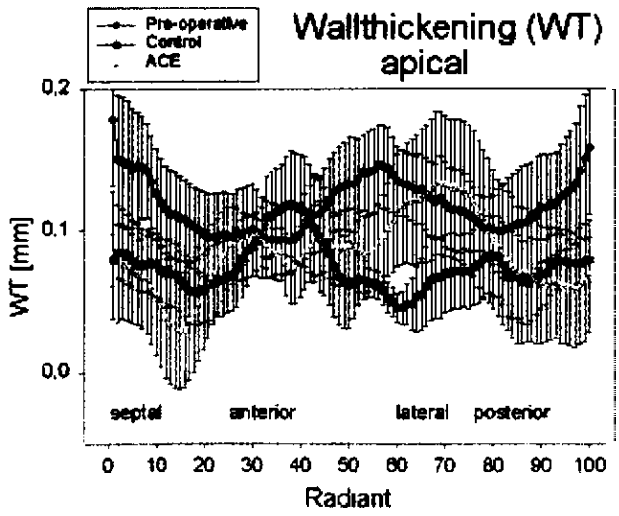

Figure 2.

109. TrueFISP Imaging of the Heart May Provide Information About Myocardial Viability in Patients with Chronic Myocardial Ischaemia—First Observations

Sven Plein,[1] John Ridgway,[1] Timothy Bloomer,[1] Mohan Sivananthan.[1] [1]*Leeds General Infirmary, Cardiac MRI Unit, Leeds, West Yorkshire United Kingdom*

Introduction: Delayed MRI imaging after injection of an intravenous contrast agent delineates acute and chronic myocardial ischaemia as areas of hyperenhancement. In acute ischaemia, this is probably the result of "entrapment" of contrast in interstitial oedema. The mechanisms of delayed enhancement in chronic ischaemia are not yet clear, but could be related to differences in the extracellular matrix of scar tissue. Steady state gradient echo MRI with balanced gradients (TrueFISP or BFFE = Balanced Fast Field Echo) is increasingly used in cardiac MRI. Like other gradient echo sequences, TrueFISP imaging is susceptible to chemical shift artefacts, visible as black bands, most prominent at the interfaces of tissues with different fat and liquid contents [1]. In the heart, these generally occur at the epicardial borders. At field strengths of 1.5T and echo times of less than 2ms, as generally used in TrueFISP imaging, water and fat protons precess out of phase, so that substantial artefacts can occur.

We report first observations of an apparent match of black bands within the myocardium on TrueFISP images, presumed to be chemical misregistration artefacts, with areas of hyperenhancement in patients with chronic ischaemia.

Methods: Ten patients with fixed perfusion defect on SPECT scans were studied on a 1.5T Philips ACS NT system with Master gradients (Philips Medical Systems, Best, The Netherlands). 10–15 minutes after injection of 0.5 mmol/kg gadolinium, a scan optimised to delineate delayed enhancement (TR 7.5, TE 3.8, Flip angle 15°, TD 600 ms, FOV 300 mm, 6 short axis slices) was acquired followed by a multi-phase TrueFISP equivalent scan (BFFE: TR 3.34, TE 1.67, Flip angle 55°, FOV 360 mm). Areas of hyperenhancement were compared with black bands on corresponding TrueFISP images and their size was measured.

Results: One patient (Pat 6) could not be analysed because of poor image quality on TrueFISP (Table 1). Four of the nine remaining patients showed areas of hyperenhancement and in three of these, black bands were observed in the TrueFISP images which exactly matched the areas of hyperenhancement (Figure 1). The total size of hyperenhancement on these three patients was 1200mm2 versus 1070mm2 of black bands on the TrueFISP images. The black bands were observed in all phases of the TrueFISP scan. One patient (Pat 10) showed no matching black band on TrueFISP.

Five patients showed no delayed hyperenhancement. One of these (Pat 2) showed an area of signal loss in the inferior wall on the TrueFISP scans. All other TrueFISP scans showed no black bands within the myocardium.

Discussion: In 7 of 9 patients that were analysed, we have observed a match between delayed hyperenhancement after Gadolinium injection and black bands on TrueFISP, while two patients showed a mismatch. A possible explanation for these observations is that chemical misregistration artefacts could occur in TrueFISP imaging at borders between scar tissue, normal myocardium and blood pool, giving rise to the observed black bands. The components and the structure of scar tissue may vary, explaining the one "false negative" TrueFISP scan in this study. In other MRI applications, chemical shift artefacts have been

Table 1

	Pat 1	Pat 2	Pat 3	Pat 4	Pat 5	Pat 6	Pat 7	Pat 8	Pat 9	Pat 10
Delayed enhancement	yes	no	yes	no	yes	yes	no	no	no	yes
Black band on TrueFISP	yes	yes	yes	no	yes	n/a	no	no	no	no

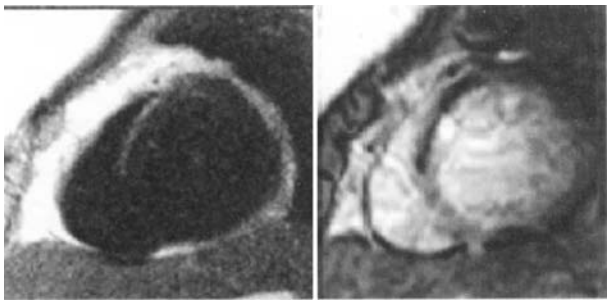

Figure 1.

exploited for diagnostic imaging to improve delineation of organs and demonstrate differences in fat contents of tissue. It is possible, that the phenomenon we have observed could be used in a similar way. It has been demonstated that the conspicuity of chemical shift artefacts is greater after injection of gadolinium contrast agents [2]. This might have accentuated the artefacts in our study, but it is possible that similar observations can be made without prior administration of contrast.

The results presented here are only a first observation with important limitations. We have studied only a small number of patients and consequently no statistical analysis could be performed. It is possible, that the observed black bands are specific to the sequence and imaging parameters we have used. The complexity of TrueFISP sequences might also give rise to additional imaging artefacts that could have contributed to our observations. We have used a lower dose of Gadolinium than usual for viability studies. However, we have found our delayed enhancement sequence reliable and we were able to acquire good quality viability images in all patients.

In conclusion, black bands on TrueFISP imaging might be used as indicators of scar tissue. This would have the benefit of adding viability information to multi-phase data-sets, allowing to view the abnormality in combination with wall motion. Further evaluation of our first observations is needed. The possibility of acquiring similar information on non-contrast TrueFISP images should be explored.

110. Quantitative Wall Motion Analysis in Patients with Angiographically Excluded Coronary Artery Disease Using High-Dose-Dobutamine-Stress MR

Ingo Paetsch,[1] Simon Schalla,[2] Nidal Al-Saadi,[2] Agnes Weinhold,[2] Eike Nagel,[2] Eckart Fleck.[2] [1]*German Heart Institute Berlin, Augustenburger Platz 1, Berlin, Berlin Germany;* [2]*German Heart Institute, Augustenburger Platz 1, Berlin, Berlin Germany*

Background: High dose dobutamine stress is widely accepted for the detection of coronary artery disease. The criteria for evaluation are

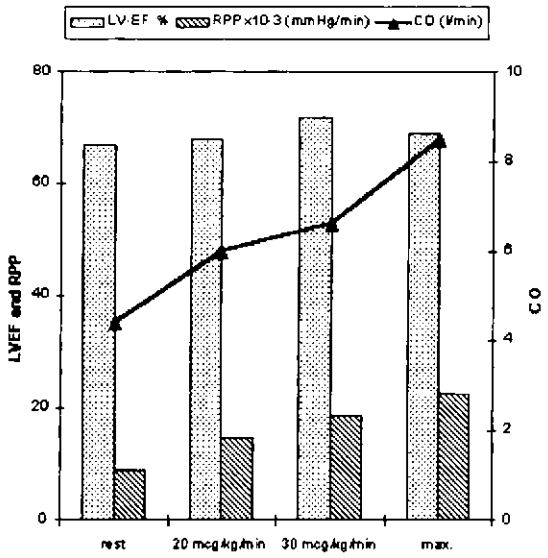

Figure 1.

based on the assumption of a uniform response in myocardial contraction and increasing wall thickening with every stress level in healthy patients. This concept has been questioned by quantitative echocardiographic data (see reference). Using MR imaging an accurate determination of wall thickness under stress conditions is possible.

Methods: 13 patients with angiographically normal coronary arteries were examined with magnetic resonance imaging during increasing doses of up to 40 microgram/kg bodyweight/minute using horizontal (HLA) and vertical (VLA) long axis cine loops (1.5 Tesla MR tomograph, ACS NT, Philips, The Netherlands). Stress was terminated when age predicted heart rate [0.85 × (220-age)] was reached. Parameters of contractile response (wall thickness, WT) were analyzed at endsystole (ES) and enddiastole (ED) for 100 chords per view at all dobutamine levels, wall thickening (WTH%) was calculated as (WTES-WTED)/WTED.

Results: Cardiac output increased significantly under stress conditions as well as heart rate (not shown) and rate pressure product (RPP). However, left ventricular ejection fraction remained nearly constant during stress conditions. The results for wall thickness and thickening are shown in figure 2.

Conclusions: Quantitative analysis of contractile response using high dose dobutamine stress MRI showed a reduction of WTH% at maximal stress due to an concomitant increase of WTED indicating reduced capability for complete left ventricular relaxation. These findings need to be integrated into the criteria used for the diagnosis of coronary artery disease.

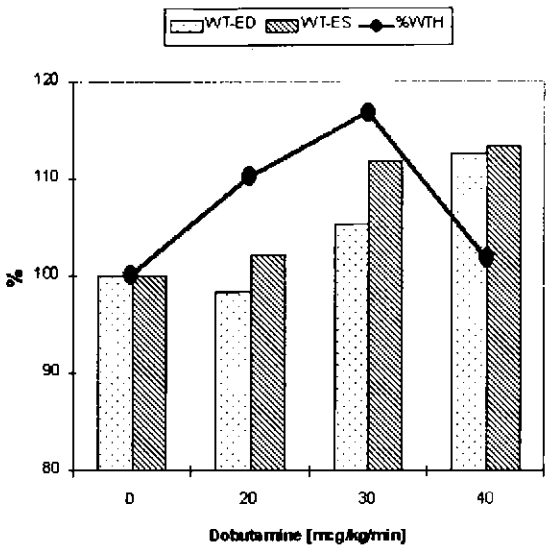

Figure 2.

111. Feasibility of Using High Resolution MR Atherosclerotic Plaque Imaging in an Epidemiological Study

Shaoxiong Zhang,[1] Norman Beauchamp,[2] Chun Yuan.[3] [1]*University of Washington, 1959 NE Pacific, Seattle, Washington United States;* [2]*Johns Hopkins University, JH Medical Institutions E Balt, Baltimore, MD USA;* [3]*University of Washington, Box 357115, Seattle, Washington United States*

Background: We have previously shown that high-resolution magnetic resonance imaging (MRI) is capable of quantifying lesion size and identifying tissue types in carotid atherosclerosis (1,2). The purpose of this research is to demonstrate the feasibility of performing high resolution carotid MRI of atherosclerotic plaque in an epidemiological study.

Methods: MRI scans were performed on 28 (17 female, mean age = 85) members of the Cardiovascular Health Study (CHS) at a participating site using a high resolution carotid plaque imaging protocol on a GE SIGNA scanner. The imaging protocol included 3D time-of-flight, T1-weighted, and proton density-weighted cross sectional images of bilateral carotid arteries centered at the bifurcation. A specially designed phase-array carotid coil was used to obtain images of 3–5 cm. Flow suppression was applied in T1W and PDW images to suppress signals from flowing blood and to generate images with good plaque tissue contrast. An image quality (IQ) rating on a scale of 1–5 was applied to all three series of images with 1 being the poorest and 5 representing the highest based on 1) image information content, 2) image artifacts and 3) overall signal-to-noise level. A singular rating was assigned to each series of images and series with a rating of 2 or less was discard from review. Lumenal and outer wall boundaries at the site of most severe lesion (most stenotic location) were traced and lumenal and outer wall areas were measured. From these areas, a diameter reduction(DR) rate was calculated.

Results: The overall scan time was around 40 minutes (including set up time), and all subjects tolerated the scan. The mean IQ was 3.5 among all subjects and series of images and the IQ was not uniform across different contrast weightings. Of the 56 arteries available for review (28 * 2), all can be reviewed with at least one series of images with different contrast weightings. There were 22 cases with 31–40% DR, 17 cases with 41–50% DR, 1 case with >50% DR, the rest has <30% DR. At these measurement sites, 13 lesions were categorized as complicated lesions with at least two tissue types other than fibrous tissue identified such as calcium, lipid core, and hemorrhage.

Conclusions: This study demonstrated the feasibility of performing high resolution carotid MRI in an large scale epidemiological study. All elderly cohorts tolerated the scanning with resultant characterizable images.

112. Post-Operative Fallot's Tetralogy: MRI Appearances and Quantitative Analysis

Jane Crossin,[1] Naeem Merchant,[2] Gruschen Veldtman.[3] [1]*University Health Network and Mount Sinai Hospital, 200 Elizabeth Street, Toronto, Ontario Canada;* [2]*University Health Network and Mount Sinai Hospital, 200 Elizabeth Street, Toronto, Ontario Canada;* [3]*Toronto General Hospital, 200 Elizabeth Street, Toronto, Ontario Canada*

Purpose: Long term survival of patients after complete surgical repair of tetralogy of Fallot is reduced as compared with the general population. Postoperative complications lead to right ventricular (RV) dysfunction resulting in significant morbidity and premature mortality. This study explores the spectrum and prevalence of intra and extra cardiac complications and the utility of cardiac MRI in the evaluation of post-op adult Fallot patients.

Method and Materials: Thirty-one adult post-op Fallot patients, (13 males, 18 females) mean age 35 years, were studied on a 1.5 T system. The mean post-operative period from primary surgical repair was 24 years (range 3–39 years). Seven patients had pulmonary valve replacement. T1 axial, fast cine/cine PC sequences were performed through the RV, main, right and left pulmonary arteries (PA). The cardiac chambers, valves, aorta and pulmonary arteries were assessed for size, mor-

Figure 1. SE axial image through the right ventricular outflow tract showing large aneurysm.

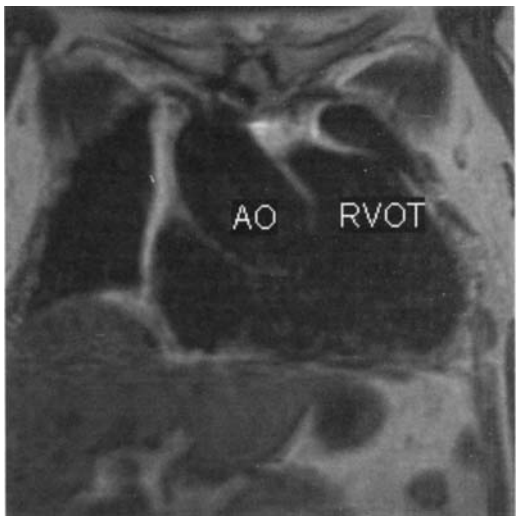

Figure 2. SE coronal image shows dilated ascending aorta and right ventricular outflow tract.

phology, volumes, and function. Volumes were calculated by manual segmentation of the endocardial borders.

Results:

Intracardiac Abnormalities: Twenty-two patients (70%) had pulmonary regurgitation, 12 mild, 5 moderate, 5 severe. Thirteen patients (42%) had a RV outflow tract aneurysm with a mean volume of 55.8cc, range 20–116cc. Seventeen patients (61%) had increased RVEDV with a mean of 199cc; all patients had reduced RVEF with a mean of 41%. The right atrium was enlarged in 27 patients (87%), mean of 5.45cm. Three patients (10%) had a small VSD. Seventeen patients (54%) had tricuspid incompetence, 14 mild and 3 moderate.

Pulmonary Abnormalities: Nineteen patients (61%) had PA narrowing. This involved both PA in 5 patients, only the right PA in 6 patients and the left PA in 8 patients. Of the 24 stenotic pulmonary arteries, 13 showed focal narrowing, 11 diffuse narrowing.

Extra Cardiac Non-Pulmonary Abnormalities: Ten patients (29%) had a right sided aortic arch, 8 of which had mirror branch origin of the arch vessels. The ascending aorta was dilated in 17 patients (53%) with a mean dimension of 4.3cm, 14 being maximally dilated at the aortic sinus. Four patients (13%) had residual aortopulmonary collaterals.

Conclusion: Our study suggests that the most common long term complications in adult postoperative Fallot patients are RV dysfunction and dilatation, right atrial enlargement, pulmonary and tricuspid incompetence, PA narrowing, aortic dilatation and RVOT aneurysms.

MRI allows both identification and quantification of these complications.

113. Evaluation of Ventricular Function with MRI Using the New Blood Pool

Willem Dockum MD,[1] Mark Hofman,[2] Anja Lehning,[3] Albert van Rossum.[4] [1]*Academic Hospital VU Amsterdam, Boelelaan 1117, Amsterdam, The Netherlands;* [2]*Univ Hospital Vrije Universiteit, Clinical Physics & Engineering, Amsterdam, Netherlands;* [3]*Nycomed Amersham, Frauhoferstrasse 7, Munchen, Germany;* [4]*Academic Hospital VU, Boelelaan 1117, Amsterdam, The Netherlands*

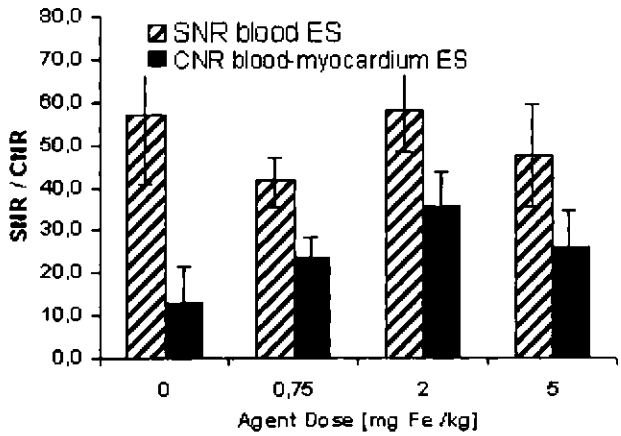

Figure 1. SNR of blood and CNR values of blood to myocardium at end systole as a function of blood pool agent dose.

Background: CLARISCAN™ (NC100150, Nycomed Amersham Imaging, Oslo, Norway) is a new blood pool agent for potential use in MRI. This agent reduces the T1 of blood, thereby increasing the MR contrast of left ventricular cavity to myocardium, which is expected to improve the image quality. The aim of the study was to determine the improvement and the optimal dose of this contrast agent for the evaluation of ventricular function.

Methods: Imaging data were acquired in this phase II clinical trial from 7 patients with a history of cardiac disease. The left ventricular ejection fraction (LVEF) as determined by echocardiography ranged from 13–60%. Imaging was performed at 1.5 T (Magnetom Vision, Siemens, Germany), using a phased-array RF receiver coil. The patients received three intravenous injections of CLARISCAN™ with a cumulative dose of 0.75, 2.0 and 5.0 mg Fe/kg body weight. This agent has a plasma half time longer than two hours, and subsequent injections were given within 20 minutes.

Imaging was performed using a 2D gradient-echo cine technique, acquiring one slice per breath-hold period of 15 heartbeats. Two variants were used, one optimized pre-contrast (TR 10 ms, TE 4.8 ms, α 20°, temp. resolution 50 ms, receiver bandwidth 195 Hz/pixel) and the other optimized post-contrast (TR 7 ms, TE 3 ms, α 35°, temp. resolution 35 ms, receiver bandwidth 390 Hz/pixel). Pre-contrast and after each injection a four-chamber view, a two-chamber view, and two short axis views were acquired.

The LVEF was calculated by the modified Simpson's rule [1]. LVEF's measured by MRI were compared with the data from radionuclide ventriculography. Signal-to-noise ratios (SNR) of LV blood and contrast-to-noise ratios (CNR) of blood to myocardium were calculated.

Results: With use of the blood pool contrast agent, CNR of blood to myocardium improved three-fold at a dose of 2 mg Fe/kg compared to non-enhanced imaging (see figure 1). The SNR of blood itself did not improve after contrast administration.

Bland-Altman analysis of LVEF of MR versus radionuclide ventriculography revealed a mean difference and standard deviation of 3 ± 7% and 2 − 7% for the pre- and post-contrast MR scan, respectively. This is no significant improvement.

The time used for analyzing the LVEF was scored, and found to be not different pre and post-contrast.

Conclusion: Administration of the blood pool agent CLARISCAN™ resulted in a strong improvement of contrast in 2D cine images of the left ventricle, especially at end systole and early diastole. This facilitates post-processing especially in patients with bad ventricular

function. The SNR of blood did not improve which is caused by the high MR signal pre-contrast due to inflow refreshment, and in part by the contrast agent induced reduction of the T2* value of blood.

No significant improvement in LVEF determination was found post-contrast, maybe due to the small number of subjects and inaccuracy in the nuclear technique. Comparison with LVEF determined by the more accurate MR full coverage 2D cine is under analysis.

114. Comparison of MRI, TEE and Invasive Measurement for Evaluation of Atrial Septal Defect II Before and After Transcatheter Closure

Thorsten Dill,[1] Anna John,[2] Thomas Neumann,[1] Wolfgang Ricken,[1] Georg Bachmann,[1] Ali Rad,[1] Matthias Rau,[1] Roland Brandt,[1] Christian Hamm.[1] [1]*Kerckhoff-Heart Center, Benekestrasse 2-8, Bad Nauheim, Germany Germany;* [2]*Royal Brompton Hospital, Sydney Street, London, United Kingdom United Kingdom*

Purpose: The defect diameter, shunt volume and size of the right atrium and ventricle are essential data for planning a transcatheter closure of an atrial septal defect (ASD II) and for post procedure follow up. Invasive balloon sizing of the defect is still mandatory. We tested the value of MRI in the evaluation of those patients and compared the findings to transesophageal echocardiography (TEE) and invasive balloon sizing before closure and on follow up at 1 month.

Patients and Methods: In 20 pts, female 11, mean age 43 yrs (18–64) the MR study was performed either on a 1.5 Tesla Siemens Vision or Sonata system. The endsystolic and enddiastolic volumes and diameters of the LV, RV, LA and RA were measured. Flow measurement in aorta and pulmonary artery were performed. The shunt ratio was calculated. For defect imaging, a Flash 2D cine gradient echo sequence (TR 60 ms, TE 5 ms, slice 6 mm) and a TruFISP cine sequence (TR 32 ms, TE 1.6 ms, slice 5 mm) was used. The data were compared to the 2 D-TEE measurements and the invasively measured Qp/Qs ratio. Transcatheter closure was performed with the Amplatzer® septal occluder system. On follow up, MRI and TEE were performed in the same way on the same day. Investigators were blinded to the results of the other technique.

Results: The medium size of the ASD as measured by MRI was 15 ± 5 mm (8–23mm), TEE 14 ± 5 mm (8–22 mm), the median balloon stretched defect diameter was 23 ± 4 mm (15–30). The mean Qp/Qs ratio as measured by MRI was 1.6 ± 0.26 (1.3–2.3), invasively measured 1.7 ± 0.3 (1.3–2.9). MR data and invasively measured data showed a correlation coefficient of r = 0.85 (95% confidence interval 0.55–0.96). On follow up, a decrease of the diameter of the RA and RV could clearly be demonstrated as an indicator for improved hemodynamics. As evaluated by MRI and TEE, a complete closure of the defect at one month follow up was achieved in 100% of the patients. No procedural related complications occured.

Conclusion: Transcatheter closure with the Amplatzer® occluder system of atrial septal defects is save and successful. MRI demonstrated to be feasible and reliable for complete pre- and post procedure evaluation compared to invasive or TEE measurements.

115. Gadolinium Enhanced Three-Dimensional Magnetic Resonance Angiography of Patients with Glenn Cavopulmonary Shunts or Fontan Operations

Reza Razavi,[1] Marc Miquel,[2] Paul Summers,[3] Joanne Goodey,[4] Edward Baker.[5] [1]*King's College London, Department of Congenital Heart Disease, London, UK;* [2]*King's College, London, Radiological Sciences, London, UK;* [3]*Kings College, London, Radiological Sciences, London, UK;* [4]*King's College, London, Radiological Sciences, London, UK;* [5]*Kings College, London, Department of Congenital Heart Disease, London, UK*

Introduction: In complex congenital heart disease it is often not possible to surgically repair the defect to achieve a bi-ventricular circulation. In these cases staged palliative surgery is performed with commonly the final two stages being the bi-directional Glenn cavopulmonary shunt followed by the Fontan operation. X-ray angiography at cardiac catheterisation has been used to look at the cavo-pulmonary anatomy in these patients. We investigated the use of Gadolinium enhanced magnetic resonance angiography (MRA) as an alternative to x-ray angiography.

Patients and Methods: Between January 1998 and September 2000, seventeen patients, 9 following Glenn cavopulmonary shunts and 8 following the Fontan operation were studied. Age at the time of Gd MRA was 2.18–19.25 years median 7.32 years. An MRI examination of the heart and great vessels had been requested as part of their clinical investigation. All but 2 examinations were performed under general anaesthesia. Images were acquired on a 1.0 Tesla Siemens Expert magnet with a phased array body coil. The 3D contrast enhanced MRA data set was acquired during a breath-hold using a 3D FISP (Fast Imaging with Steady State Precession) (TR/TE 6.7/2.8 msec) sequence in the coronal plane with an acquisition time of 30 seconds. The sequence was first run without contrast to obtain a background mask used for subtraction. The sequence was then repeated with a contrast injection of 0.15 mmol/kg Gd-DTPA. The injection was timed using a previous test bolus injection. Immediately following the contrast enhanced study the GD-MRA scan was repeated to provide information about late filling structures. As it was important to visualise the systemic veins and their connections the contrast dose was diluted fivefold with normal saline. This ensured that T2* shortening by the contrast agent did not produce susceptibility related signal loss in the vessels of interest. In all cases, the bolus was followed by a 20 ml saline flush. Manual injection was used to control bolus timing and duration, with the injection rate varying between 2 and 3 ml/sec. In all patients the site of injection was the right cephalic vein or right internal jugular vein. In the Fontan patients, a simultaneous separate injection was also made via the veins in either foot to obtain enhancement of both the inferior vena cava and superior vena cava (SVC). Following the subtraction of the pre contrast mask, the volume nature of the data was used to generate two types of views. Firstly, the data set was re-sliced in any given plane (multiplanar reformatting). Secondly, projection views through the data sets were obtained using the maximum intensity projection algorithm.

Results: High quality clear MRA images of the systemic veins, cavopulmonary connections and pulmonary vascular tree were obtained in all but two patients. In these two patients with fenestrated Fontan operations who had had their fenestration's closed with an umbrella device there was degradation of the gradient echo images around the metallic umbrella device. However clear images of the SVC and pulmonary arteries were still obtained. At the time of their MRA a low central venous pressure was confirmed in the Glenn patients by measurement via the venous access in the internal jugular vein. In three of the patients with Glenn shunts it was decided not to proceed with Fontan surgery for the present. The MRA of one these patients who had had a right Glenn shunt showed a disconnected hypoplastic left pulmonary artery. Six of the patients with Glenn shunts have had or are awaiting surgical completion of their Fontan, four of them solely on the bases of the MRA images without cardiac catheterisation. One patient with bilateral bi-directional Glenn shunts was found to have a complete obstruction of the left Glenn shunt with a large hemi-azygous vein draining the left sided upper venous return down to the IVC. The MRA findings were confirmed at cardiac catheterisation and the patient then proceeded to Fontan surgery. Another patient who had also had aortic arch surgery was also found to have mild residual coarctation. Cardiac catheterisa-

tion with a view to possible balloon dilation of the coarctation was performed with the MRA findings being confirmed. The gradient across the mild coarctation was not sufficient to require balloon dilation and the patient proceeded to Fontan surgery. Two of the Fontan patients were found on MRA to have proximal branch pulmonary artery stenosis. Both proceeded to cardiac catheterisation were the MRA findings were confirmed and balloon dilation of the proximal branch pulmonary artery stenosis performed. A third patient was studied following Fontan surgery, as he had remained cyanosed with reduced exercise tolerance. Two attempted cardiac catheterisations were unsuccessful, as it was not possible to gain venous access. MRA confirmed occlusion of both internal jugular and subclavian veins with collaterals draining into the SVC. There was some narrowing of the proximal IVC with hepatic collaterals draining into the right atrium outside the total cavopulmonary connection tunnel. He underwent repair of the narrowing in the IVC and rerouting of the hepatic veins into the cavopulmonary connection with an excellent result.

Conclusion: MRA provides detailed three-dimensional information regarding the anatomy of patients with Glenn cavopulmonary shunts or Fontan operations and allows planing of surgical or interventional cardiac catheter procedures without the need for diagnostic cardiac catheterisation.

116. Blood-Oxygen-Level-Dependent Magnetic Resonance Imaging Visualizes Vasodilatory Endothelial Function

Matthias Friedrich,[1] Thoralf Niendorf,[2] Jeanette Schulz-Menger,[3] Rainer Dietz.[1] [1]*Franz-Volhard-Klinik, Charite, Humboldt-Universitaet zu Berlin, Wiltbergstr. 50, Berlin, Berlin Germany;* [2]*GE Medical Systems, PO Box 414, Milwaukee, WI USA;* [3]*Franz-Volhard-Klinik, Charite, Humboldt-Universitaet zu Berlin, Wiltbergstrasse 50, Berlin, Berlin Germany*

Vasodilatory endothelial function plays a key role in the pathophysiology of atherosclerotic and other cardiovascular diseases. Reactive hyperemia after intermittent ischemia as an important feature of endothelial function was found to be altered in arterial hypertension. Established methods to visualize reactive hyperemia suffer from certain limitations such as low temporal and spatial resolution (plethysmography) or variability of results (measurement of brachial artery diameter or area). Due to changes of muscular relaxation times by inflow of oxygenated blood, BOLD-MRI is able to visualize blood supply to tissues, dependent on blood volume and the ratio of oxygenated to deoxygenated hemoglobin.

We visualized reactive hyperemia after 2 minutes of cuff-induced ischemia in the forearm of 7 patients with arterial hypertension and 8 healthy controls by a T2*-sensitized EPI sequence (TE 17.4ms) using an extremity coil on a 1.5T system (Signa CV/i, GE Medical Systems, Milwaukee) with continuous image acquisition (TR 333ms). Two sets of 500 images each allowed a complete coverage of the protocol.

Baseline signal scatter was found to be very low (0.5% of the signal). Fig. 1 demonstrates a typical signal intensity time course of a healthy volunteer during the protocol. The percentual signal overshoot after cuff release, which showed a very good reproducibility in volunteers (interstudy variability of repeated measurements in controls 7 ± 4%), was significantly reduced in patients with arterial hypertension as compared to controls (0.9 ± 0.9 vs. 3.5 ± 0.5%, $P < 0.01$) and was also different between males and females in the control group (2.6 ± 0.4 vs. 4.4 ± 0.6%, $P < 0.05$).

We conclude that BOLD-MRI is suitable to reliably demonstrate reactive hyperemia in volunteers and patients. BOLD-MRI derived reactive hyperemia measurements are advantageous as compared to other techniques due to a high temporal and spatial resolution and the small variability of the observed signal.

This is the first report of this simple, noninvasive approach for the assessment of parameters of endothelial function on the capillary level.

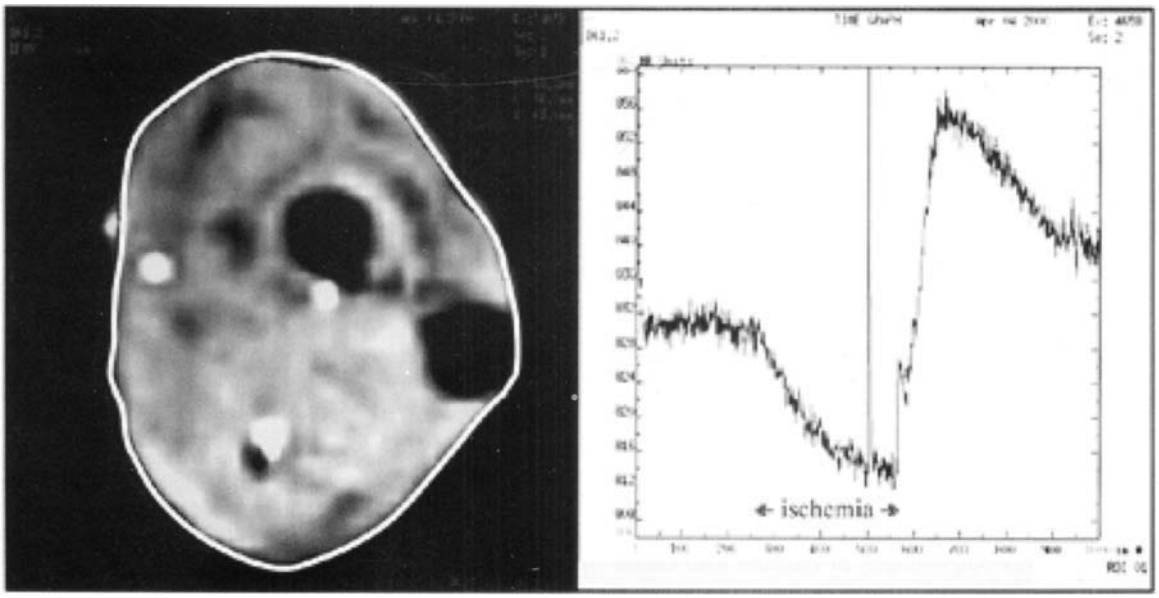

Figure 1. BOLD-MRI signal in a healthy volunteer. Left panel: Cross-sectional BOLD-MRI view of the right forearm 10cm below the elbow joint. The white line depicts the region of signal intensity measurement. Right panel: Time to signal intensity curve before, during and after 3 minutes of cessation of blood flow. The signal decrease during and the signal overshoot after cuff-induced ischemia is demonstrated The narrow peak after 500 images represents the start of the second image series.

117. Right Ventricular Involvement in Patients with Inferior Myocardial Infarction—Correlation of Contrast-Enhanced Magnetic Resonance Imaging to Other Findings

Matthias Friedrich,[1] Jeanette Schulz-Menger,[2] Anja Wagner,[1] Thoralf Niendorf,[3] Rainer Dietz.[4] [1]*Franz-Volhard-Klinik, Charite, Humboldt-Universitaet zu Berlin, Wiltbergstr. 50, Berlin, Berlin Germany;* [2]*Franz-Volhard-Klinik, Charite, Humboldt-Universitaet zu Berlin, Wiltbergstrasse 50, Berlin, Berlin Germany;* [3]*GE Medical Systems, PO Box 414, Milwaukee, WI USA;* [4]*Franz-Volhard-Klinik, Humboldt-Universitaet zu Berlin, Wiltbergstr. 50, Berlin, Berlin Germany*

The proportion of right ventricular involvement in inferior infarction is not well studied. RV involvement, however, may have a strong impact on the therapeutic strategy. The sensitivity of diagnostic criteria such as ST segment elevation in right ventricular leads or echocardiographic evidence for RV wall motion abnormalities is not well known.

Magnetic resonance imaging (MRI) visualizes myocardial edema (signal increase in T2-weighted MRI) and necrosis (delayed contrast enhancement in T1-weighted MRI).

We studied 15 consecutive patients 3 ± 1 days after acute inferior MI in a 1.5 T MR system (Signa CV/i, GE Medical Systems, Milwaukee) using a cardiac phased array coil. Breathheld fast spin echo techniques are applied for both, T2-weighted MRI (STIR; TE 64ms) and contrast-enhanced T1-weighted MRI (gradient echo, TE 1.7ms, 8 to 10 minutes after 0.1 mmol Gd-DTPA /kg BW).

Due to electrocardiographic (inferior MI + ST elevation in RV leads), echocardiographic (RV hypokinesia), or hemodynamic criteria (systolic blood pressure <100 mmHg), only one of these patients showed evidence for RV involvement. Edema as defined by regional myocardial signal increase in T2-weighted images was present in 8/15 patients (53%). Using contrast-enhanced MRI, RV necrosis was found in 4/15 patients (27%).

In 4 patients, the edema associated to the infarcted area included the RV myocardium, but was not associated with late contrast enhancement of the RV.

In conclusion, right ventricular involvement may be more frequent in inferior infarction than it is detected by echocardiography and electrocardiography in clinical routine. Contrast-enhanced MRI may serve as an important diagnostic tool for the detection of right ventricular involvement in patients with inferior myocardial infarction.

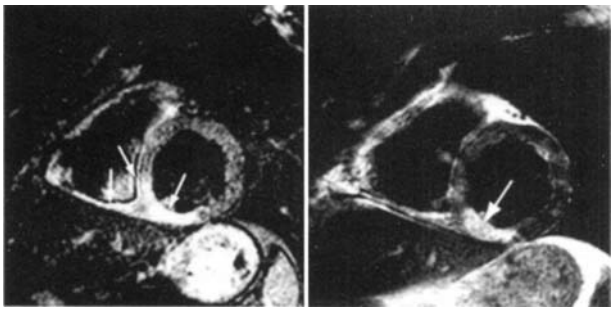

Figure 1. Right ventricular involvement in inferior infarction (day 3 after the clinical event). Left panel: Signal increase in a T2-weighted MR image in a short axis view reflecting myocardial edema (arrows). Right panel: Late contrast enhancement after administration of Gd-DTPA with mostly intramural extent (arrow).

118. MR Imaging of Arterial Wall Enhancement with MS-325 Facilitates Plaque Detection and Characterization

Jeffery Maki M.D.,[1] Gregory Wilson,[2] Randall Lauffer,[1] Robert Weisskoff,[4] Jeremiah O'Regan,[5] Chun Yuan.[6] [1]*University of Washington, Puget Sound VAHCS, Seattle, Washington United States;* [2]*Puget Sound VAHCS, Department of Radiology (114), Seattle, WA USA;* [3]*EPIX Medical, Inc., 71 Rogers Street, Cambridge, MA USA;* [4]*Massachusetts General Hospital, East Cny2 Bldg 149, Charlestown, Massachusetts United States;* [5]*University of Washington, Hospital Box 357115, Seattle, WA USA;* [6]*University of Washington, Box 357115, Seattle, Washington United States*

Introduction: Leaky vasa vasorum capillaries appear to accompany atherosclerosis and may be linked to inflammation and plaque growth. Presently there are no noninvasive methods of detecting and character-

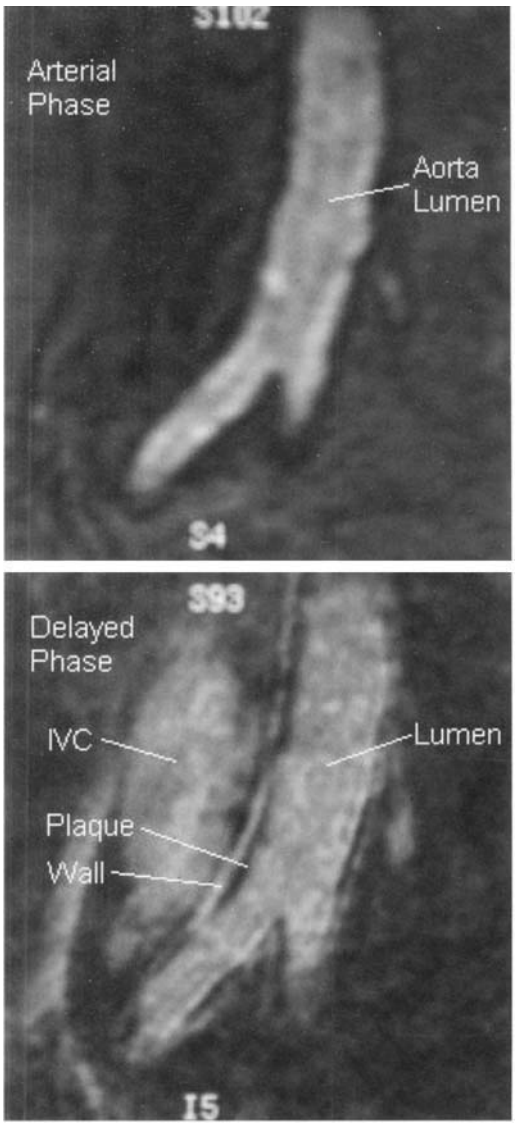

Figure 1.

izing this phenomenon in vivo. We used MS-325, a gadolinium blood pool MRI contrast agent which binds reversibly to albumin, to evaluate vessel wall enhancement.

Methods: Aorto-iliac vessels in 14 male patients (age 47–71) with known or suspected aorto-iliac atherosclerotic disease were imaged with high resolution 3D spoiled gradient MRI pre-, during arterial phase, and 15 min post IV bolus of MS-325 in a randomized dose, phase 2 trial. The delayed (equilibrium) images were acquired using fat suppression with a spatial resolution of 0.8 × 1.1 × 1.8 mm.

Results: In the 13/14 patients that did not receive placebo, delayed imaging clearly demonstrated regions where enhanced arterial lumen is surrounded by a band of low signal intensity (SI), with a more peripheral band of high SI (figure 1). In addition, diameter and SI of lumen, plaque, and vessel wall were measured in 7 areas (n = 3 patients). Lumen diameter comparison (arterial–delayed) confirms the low and high SI bands on delayed images represent elements of arterial wall–presumably non-enhancing plaque and enhancing media/adventitia. Plaque varied in thickness and was greatest in areas of stenosis. Low and high SI portions of vessel wall measured 19.3 ± 5.1 and 64.3 ± 17.8% of lumen SI, respectively. In general, SI of the outer wall is greater than that of highly vascular tissue such as liver (52.4 ± 18.3% of lumen SI), and therefore is greater than expected if contrast were merely confined to the vasa vasorum.

Conclusion: The strong vessel wall enhancement seen in this study may reflect MS-325 diffusing through leaky vasa vasorum capillaries and binding to extravasated albumin in the vessel wall. Future studies will address whether this enhancement is useful in characterizing the degree of inflammation or vascularity in arterial wall. Delayed imaging with MS-325 should provide a method of quantifying plaque load as well.

119. Correlation of Adenosine-BOLD MRI Findings to Coronary Angiography in Patients with Suspected Coronary Artery Disease

Matthias Friedrich,[1] Thoralf Niendorf,[2] Jeanette Schulz-Menger,[3] Rainer Dietz.[4] [1]*Franz-Volhard-Klinik, Charite, Humboldt-Universitaet zu Berlin, Wiltbergstr. 50, Berlin, Berlin Germany;* [2]*GE Medical Systems, PO Box 414, Milwaukee, WI USA;* [3]*Franz-Volhard-Klinik, Charite, Humboldt-Universitaet zu Berlin, Wiltbergstrasse 50, Berlin, Berlin Germany;* [4]*Franz-Volhard-Klinik, Charite, Humboldt-Universitaet zu Berlin, Wiltbergstr.50, Berlin, Berlin Germany*

The myocardial signal obtained by Blood-oxygen-level-dependent (BOLD) MRI is dependent on the perfusion. However, the relation of adenosine-induced signal changes to the presence or degree of coronary artery stenosis is unknown. In a prospective, blinded fashion we studied the relation of adenosine-BOLD MRI signal changes to the degree of stenosis as measured by quantitative angiography. Results were compared to quantitative Thallium SPECT.

We applied a T2*-sensitized gradient echo EPI (TE 17.4 ms) in a 1.5 T cardiovascular scanner (CV/i, GE Medical Systems, Milwaukee, Wisconsin, USA) to 26 patients/156 segments with stress-inducible angina before, during and after continuous infusion of adenosine (140g/kg/min.) over 6 minutes.

25 segments had to be excluded because of nondiagnostic image quality. Fig. 1 shows the relation of the BOLD signal changes to the degree of coronary stenosis. In higher degrees of coronary lumen reduction, the signal increase during adenosine was lower, and in non-perfused segments it was absent. 38 segments were related to coronary stenosis of equal to or more than 75%. When accepting a lack of signal increase during adenosine as a marker for hypoperfusion, adenosine-BOLD MRI correctly classified 15/38 segments with stenotic arteries

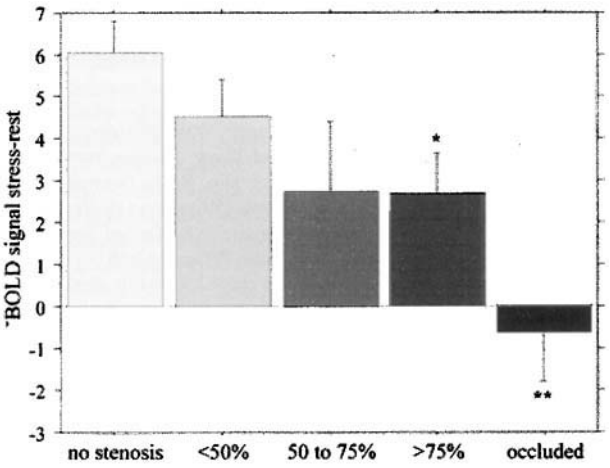

Figure 1. Relation of BOLD signal intensity changes during adenosine to the degree of coronary stenosis (n = 131 segments). With increasing degrees of coronary obstruction there is a loss of signal increase during adenosine. *:statistical difference to segments without stenosis/$p < 0.05$; **:statistical difference to segments without stenosis/$p < 0.01$.

(sensitivity 39%) and excluded stenoses correctly in 80/93 segments (specificity 86%). Quantitative Thallium SPECT showed a sensitivity of 66% and a specificity of 51%.

We conclude that adenosine-BOLD-MRI signal changes reflect the degree of coronary artery stenosis. However, a clincal application of the technique used in our study is hampered by a low sensitivity to detect relevant myocardial stenosis. Specificity, however, is markedly higher than a comparable approach using Thallium SPECT imaging. Further developments will have to focus on sensitivity.

120. Image Registration Improves Accuracy in Serial Quantitative Analysis of Human Carotid Artery Atherosclerosis with Magnetic Resonance Imaging

Shaoxiong Zhang,[1] William Kerwin,[2] Chun Yuan.[3] [1]*University of Washington, 1959 NE Pacific, Seattle, Washington United States;* [2]*University of Washington, Department of Radiology, Seattle, WA USA;* [3]*University of Washington, Box 357115, Seattle, Washington United States*

Background: We have previously shown that high-resolution magnetic resonance imaging (MRI) is capable of quantifying atherosclerotic lesion size and identifying tissue types in carotid atherosclerosis (1,2). This non-invasive imaging technique is ideal for serial examination of the lesions of atherosclerosis. Serial examination of these lesions will lead to a better understanding of its pathogenesis, and permit direct evaluation of the effects of pharmacological interventions over time. However, the spatial location mismatching of different scans will impair the accuracy of quantified analysis of carotid disease using MRI. The goal of this study was to assess the value of image registration for improved quantification of carotid artery lesion size in vivo.

Methods: Fifteen patients (mean age = 66) with <80% carotid stenosis by duplex ultrasound were recruited. Two independent MR scans were performed within 2 weeks using a high-resolution protocol on a 1.5 T GE scanner. All patients had no further symptoms during this

Table 1

Lumen and Wall Area Measurement Comparison Results for Manual Registration

	Mdif (mm^2)	SD (mm^2)	P	R	Mean (mm^2)
Lumen	0.07	11.94	0.92	0.85	37.52
Outer wall	1.22	24.32	0.37	0.82	97.09
Wall	1.15	16.07	0.20	0.77	56.36

Table 2

Lumen and Wall Area Measurement Comparison Results for Automated Registration

	Mdif (mm^2)	SD (mm^2)	P	R	Mean (mm^2)
Lumen	1.52	6.61	0.40	0.95	38.98
Outer wall	4.18	15.07	0.17	0.90	94.35
Wall	2.66	13.20	0.12	0.76	55.37

period. A double inversion recovery technique was used to obtain T1 weighted images with TR/TE/TI = 800ms/9ms/650ms. The total longitudinal coverage was 30–50mm centered at the carotid bifurcation.

For each patient, two registration procedures were compared for alignment of the anatomy in the two scans. The first was a one-dimensional manual registration along the z direction, in which the image planes were shifted until the bifurcation in each was aligned. The bifurcation was defined as the last image plane containing a single lumen before it splits into two. The second registration procedure was an automated method that aligns edges apparent in the images using an energy minimization formulation related to active contour methods (3). This registration method also counteracts more complicated misalignments consisting of volume-preserving shears, stretches, rotations and translations. This particular registration method was designed in house specifically for carotid artery image analysis and is largely immune to carotid imaging artifacts such as brightness variations that confound many established registration methods.

To assess the performance of the two registration procedures, the carotid lumen and outer wall areas of all registered images were measured by one expert observer with a custom designed quantitative vascular analysis tool (QVAT). The repeatability of the measurements from scan 1 to scan 2 was then determined using the correlation coefficient of corresponding measurements as the criteria.

Results: Overall, images from 312 locations were obtained. After manual location matching, 290 images remained for analysis, with the remainder shifted out of view relative to the original scan. After automated registration, 243 images remained. Mean lumen and wall areas (Mean), mean difference of the lumen and wall area from different scans (Mdif) , standard deviation (SD), p values of a T-test (P) and correlation coefficients (R) are shown in Tables 1 and 2. The p values are included merely to show that in no case did the mean difference significantly differ from 0. The correlation coefficient R indicates that the repeatability of the lumen and outer wall area measurements improved after automated registration. Surprisingly, the wall area repeatability, which is simply the difference of the outer wall and lumen measurements, showed no improvement.

Conclusion: For serial analysis of atherosclerosis, prior image registration is critical, whether the manual or automated method is used. Based on this study, the automated registration method is more effective for improving the repeatability of lumen and outer wall boundary measurements. For the repeatability of wall area measurements, on the other hand, registration does not appear to be the limiting factor, but will likely prove to be equally important once better MRI protocols and processing methods are identified.

121. Myocardial Perfusion Imaging with Cardiac Magnetic Resonance in the Assessment of Patients with Significant Attenuation Artifacts on Stress Scintigraphy

Jane Mccrohon,[1] Shelley Rahman,[2] Christine Lorenz,[3] Dudley Pennell.[4] [1]*Royal Brompton Hospital CMR Unit, Sydney St, London, England United Kingdom;* [2]*Royal Brompton Hospital, Department of Nuclear Medicine, London, England United Kingdom;* [3]*Royal Brompton Hospital and Siemens Medical Engineering, CMR Unit, London, England United Kingdom;* [4]*Royal Brompton Hospital, CMR Unit, London, England United Kingdom*

Introduction: The presence of artifacts on stress scintigraphy, in particular inferior wall attenuation in males remains a significant limitation of nuclear techniques. Although experience and review of the raw data may in some cases aid interpretation of attenuation on scintigraphic images, a significant proportion of cases remain unclear and ultimately lead to invasive coronary angiography. We postulate that CMR may resolve this clinical problem.

Methods: 8 male patients reported to have significant inferior wall attenuation on scintigraphy were studied. Imaging was performed on a 1.5T Siemens Sonata (Siemens AG, Erlangen, Germany). First pass perfusion imaging using a saturation recovery TurboFLASH sequence (TE/TR 0.86/159 ms, flip angle 8 degrees, saturation recovery time 84 ms, in plane pixel size approximately 3 × 3 mm, slice thickness 8 mm) was performed in three short axis planes with one set of images acquired per heartbeat. Gd-DTPA (Magnevist, Schering AG, Germany) was administered using a power injector (Medrad Spectris) at 0.1 mmol/kg at a rate of 3 ml/sec. Resting wall motion was also assessed using a breathhold TrueFISP cine sequence (TE/TR 1.6/3.2, flip angle 60 degrees, in plane pixel size approximately 1.5 × 2 mm, temporal resolution 40–60 ms). Adenosine was administered at 140 mcg/kg/min for 4 minutes at which time a second first pass perfusion acquisition was performed. Ten minutes following the second injection of Gd-DTPA, late enhancement imaging was performed using both a 3-D inversion recovery gradient echo sequence (TE/TR/FL/TI 1.64/244/10/260), in plane pixel size 2.4 × 1.4 mm, slab thickness 80 mm, 20 partitions) to screen the

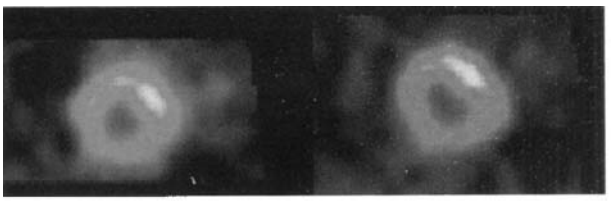

Figure 1A.

Figure 1B.

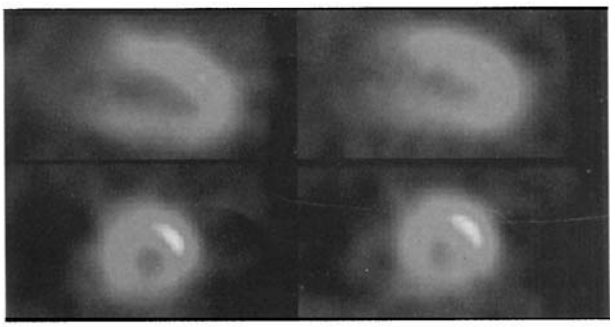

Figure 2A.

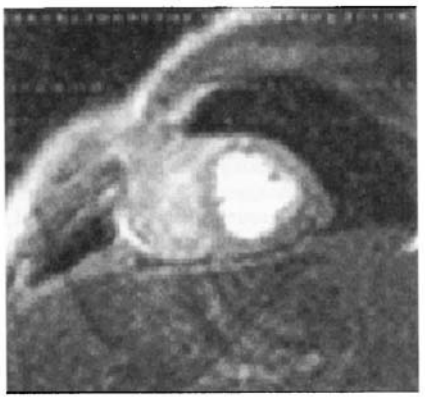

Figure 2B.

entire left ventricle, followed by 2-D inversion recovery gradient echo sequence (TE/TR/FL/TI 4/450/20/260-300), in plane pixel size 1.6 by 1.4 mm, slice thickness 8 mm).

Results: In 3/8 patients, the CMR findings suggested that the nuclear inferior attenuation could be explained by subendocardial infarction, with evidence of late gadolinium enhancement. In all three, visual analysis of the first pass perfusion was also abnormal at this level with one of the three having a marked circumferential perfusion defect suggestive of more widespread ischaemia (Fig. 1). Wall motion was mildly impaired at rest in only one patient. The remaining 5/8 patients with significant inferior attenuation on their nuclear scans did not show abnormal perfusion, abnormal wall motion or late gadolinium enhancement (example in Fig. 2). Two of these underwent coronary angiography due to persisting symptoms which confirmed normal coronary anatomy in these areas.

Conclusion: The above pilot data suggests that CMR is able to confirm whether inferior attenuation on scintigraphy is associated with coronary artery disease.

122. MR Detection of Coronary Artery Stenosis-Associated Flow Disturbance

Pamela Woodard,[1] Jie Zheng,[2] Dana Abendschein,[3] Nikolaos Tsekos,[4] Richard Kowalski,[5] Nasser Fatouraee,[6] Amir Amini,[7] Robert Gropler.[8] [1]*Mallinckrodt Institute of Radiology, Washington University, St. Louis, MO USA;* [2]*Mallinckrodt Institute of Radiology, Cardiovascular Imaging Lab, St. Louis, Missouri United States;* [3]*Washington University, Mailstop 8086, St. Louis, Missouri United States;* [4]*Mallinckrodt Institute of Radiology, Cardiovascular Imaging Laboratory, St. Louis, MO USA;* [5]*Northwestern University, School of Engineering, Chicago, IL USA;* [6]*Washington University, Cardiovascular Imaging Analysis Laboratory, St. Louis, MO USA;* [7]*Cardiovascular Image Analysis Laboratory, Campus Box 8086, 660 S. Euclid, St. Louis, Missouri United States;* [8]*Mallinckrodt Institute of Radiology, Cardiovascular Imaging Laboratory, Saint Louis, Missouri United States*

Purpose: To determine whether a 3D breath-hold, in-plane, phase-contrast method can detect post-stenotic flow disturbance in 4 mm diameter tubes and coronary arteries.

Background: Stenoses within a vessel lumen disrupt laminar flow, causing jetting effects and turbulence. This flow disturbance is determined by the geometry of the lesion, in particular the narrowness of the stenotic lumen and its abrupt expansion into the normal diameter artery. While researchers have used in-plane flow disturbance to detect the presence and assess significance of stenoses in larger vessels, none have used this technique in coronary artery disease assessment. We hypothesize that flow disturbance could be visualized using a 3D breath-hold MR phase- contrast technique.

Methods: Phantom: A flow phantom with multiple 4 mm tubes containing stenoses (0%–70% diameter) was imaged at flow rates simulating rest and stress. The phantom was connected to a pump that provided pulsatile flow in a physiologic waveform coupled to an EKG tracing. A 3D GRE flow-sensitive sequence (TR 5.56ms, TE 3.4ms, flip angle 20, Venc 100 cm/sec) with flow-encoding in the read out direction was used to visualize the flow pattern in-plane across the "stenoses" on phase images. Spatial resolution was 1.0(y) × .95(x) × 1.5(z) mm3. Animals: Five domestic swine with coronary artery lesions were imaged using the 3D breath-hold phase-contrast sequence. Stenoses were

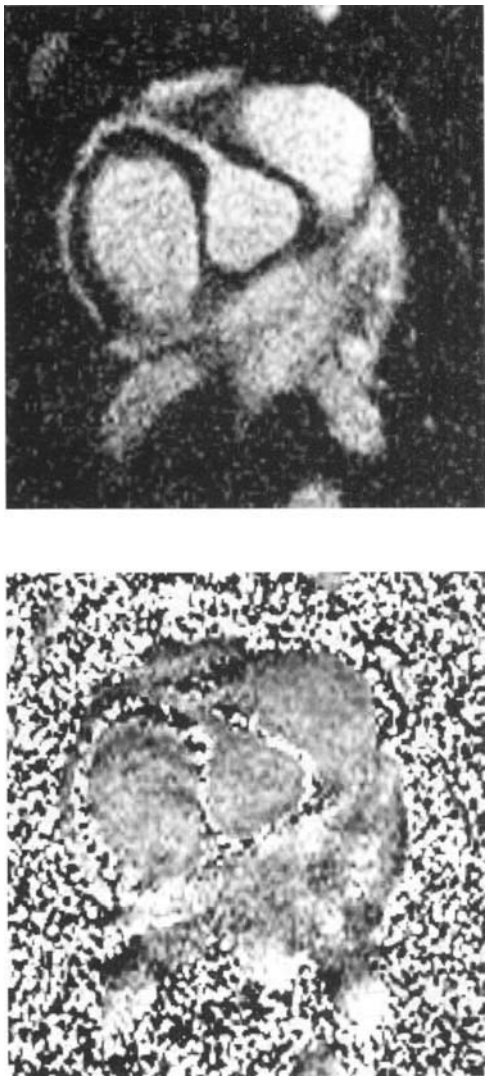

Figure 1. Magnitude (a) and phase (b) images acquired in a pig with a Teflon stenosis. Both a post-stenotic jet and prestenotic dephasing are visible.

created via atherogenic diet and overstretch injury in three animals, and by catheter placement of Teflon rings in two animals. Imaging was performed in-plane, and parameters were similar as that used in flow-phantom study, however, the sequence was performed after administration of 0.1 mM/Kg of Gadomer-17 (Schering AG, Berlin, Germany), an intravascular contrast agent. Sequence modifications for contrast included an IR pulse and a flip angle of angle 30 degrees. Spatial resolution was 1.2(y) × 0.78(x) × 1.5(z) mm3. Imaging time was 20 ~ 30 sec. Studies were performed on a 1.5T Siemens Sonata MR System.

Results: Phase-contrast images on both phantom and animal models showed visible dephasing in regions of all stenoses > = 50% of vessel or tube diameter.

Conclusions: 3D in-plane phase-contrast imaging can demonstrate turbulence caused by stenotic disruption in laminar flow in narrow diameter tubes and coronary arteries. This information could be coupled to 3D breath-hold MR angiography, potentially leading to increased accuracy and confidence in coronary stenosis detection.

123. A Quick Multi-Contrast High Resolution MR Protocol for Screening Atherosclerotic Carotid Artery and Brain Ischemic Events

Jianming Cai,[1] Shuihui Chen,[1] Chun Yuan.[2] [1]*The 301 Hospital, Department of Radiology, Beijing, Beijing China;* [2]*University of Washington, Box 357115, Seattle, Washington United States*

Purpose: To design and evaluate a high resolution MR protocol for screening carotid artery stenosis, atherosclerotic plaque tissue type and volume, and brain ischemic events. This protocol will assist in determining which plaques will lead to thrombosis/embolization and consequently cause stroke. While carotid endarterectomy is superior to medical therapy for lesions with >70% diameter reduction, it is not the degree of narrowing alone that is predictive of outcome. Recent literature suggests that MR imaging may be able to identify unstable vulnerable atherosclerotic plaques in the carotid artery in vivo [1–2]. This protocol is designed to acquire non-invasive information on plaque morphology, identify plaque tissue contents, monitor the plaque growth, disintegration over time, and determine the association of plaque progression with brain ischemic events.

Materials and Methods: 35 patients (25 male, 10 female, age range 55–82 years) suspected of carotid artery stenosis were recruited for the study. High-resolution MR images of the neck and brain were acquired with a 1.5T MR scanner (GE SIGNA Horizon EchoSpeed 5.8) in one session. Informed consent was obtained from the subjects for the study. Neurovascular and custom-made phased-array carotid coils were used.

The carotid MR protocol includes the following sequences: 1) 2D phase contrast for scout (20 seconds): TR/TE = 30/7.6ms, flip angle = 30, FOV = 24 × 18cm, matrix = 256 × 160, venc = 40cm/s; 2) Gated 2D time-of-flight (TOF) MR angiography (MRA) to find the bifurcation and obtain carotid MRA (3 minutes): TR/TE = 19.2/4.4ms, flip angle = 60, FOV = 13 × 9cm, matrix = 256 × 160, views per segment = 24; 3) Gated fast spin echo (FSE) for proton density and T2-weighted imaging (4 minutes): TR/TE = 3200 ~ 4000/10, 70ms, ETL = 12, slice thickness = 2mm, FOV = 13 × 9cm, matrix = 256 × 256 (with ZIP reconstruction); 4) Double inversion recovery T1-FSE imaging (7 minutes): TR/TE/TI = 800/10/650ms, ETL = 8, slice thickness = 2mm, FOV = 13 × 9cm, matrix = 256 × 256 (with ZIP reconstruction); and 5) 3D TOF (90 seconds): TR/TE = 23/3.8ms, flip angle = 25, slice thickness = 2mm (overlap 1 mm), FOV = 13 × 9cm, matrix = 256 × 256 (with ZIP reconstruction). The coil was switched while the patient remained in the same position. Then an axial T2-, fast FLAIR- and diffusion-weighted brain scan was acquired to evaluate the brain condition.

Results: The carotid artery scan could be finished within 30 minutes and the brain scan within 10 minutes (Figure 1 A-G). All patients tolerated the scan. The voxel size for carotid imaging was 0.25 × 0.25 × 2 mm3 and for brain imaging was 1 × 1 × 1mm3. This protocol provided information on lumen narrowing (through MRA and the black blood T1-, T2, and proton density- weighted), plaque tissue characterization (through multiple contrast weighting) and plaque volume as well as brain ischemic sites. 96% of the image data were interpretable.

Conclusion: This imaging protocol can be used conveniently for screening patients suspected of having carotid artery atherosclerosis and stroke. It can be a powerful tool to evaluate the association between lesion types found at the carotid artery and the development of clinical symptoms. It may also be used in determining the optimal treatment plan for patients.

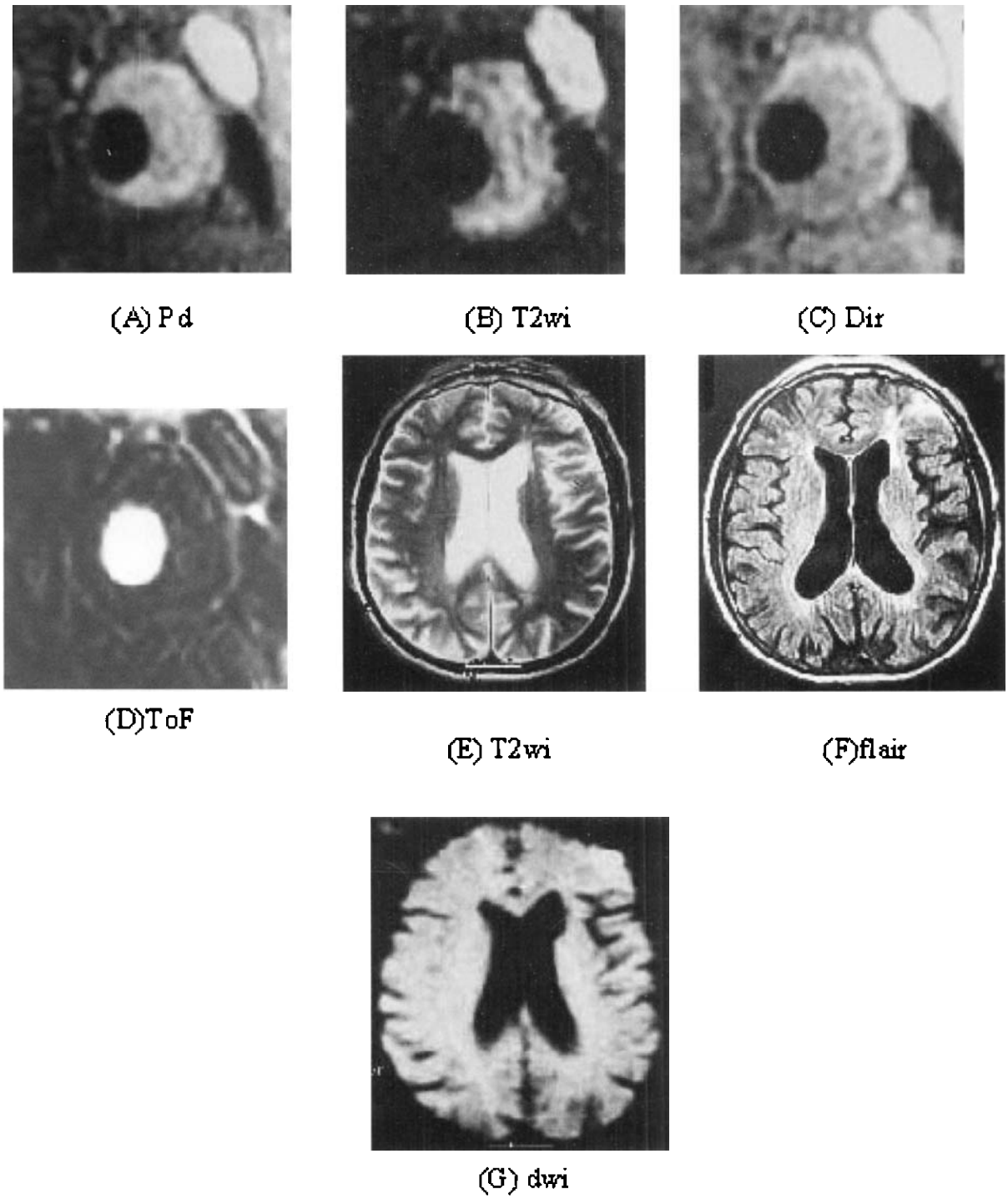

Figure 1. Severe stenosis involving the carotid bifurcation. Eccentric plaque is shown on PDWI (A), T2WI (B), DIR T1WI (C) and TOF (D) of the carotid artery. T2WI (E), fast FLAIR (F) and Diffusion weighted imaging (G) of the brain scan showed the ischemic lesions primarily located in the left frontal lobe.

124. Gadolinium MRI Angiography with a Real Time Bolus-Tracking Technique in Pediatric Patients with Coarctation

Giles Vick,[1] William Ravekes,[2] Raja Muthupillai,[3] Ricardo Pignatelli,[3] John Kovalchin.[4] [1]*Texas Children's Hospital, Division of Pediatric Cardiology, Houston, TX United States;* [2]*Baylor College of Medicine, Division of Pediatric Cardiology, Houston, Texas United States;* [3]*Baylor College of Medicine, Texas Children's Hospital, Houston, TX USA;* [4]*Baylor College of Medicine, Baylor College of Medicine, Houston, Texas United States*

Background: Aortic coarctations have complex structures that are often best appreciated in three and four dimensional reconstructions. The fidelity of these reconstructions and their ease of generation is directly dependent on the contrast between arterial lumen and surrounding tissue present in the original datasets. With the gadolinium enhancement technique this contrast is highly temporally dependent. First pass arterial phase datasets are much superior to subsequently acquired equilibrium datasets in this regard. Pediatric patients represent an especial challenge for acquisition of arterial phase datasets because these patients vary widely in size, circulation time, and ability to cooperate.

Purpose: To evaluate a bolus tracking method for acquisition of arterial phase images in pediatric patients with coarctation.

Methods: Fifteen pediatric patients with aortic coarctation underwent gadolinium enhanced magnetic resonance angiography with a bolus tracking method (BolusTrak, Phillips Medical Systems). This method employs thick-slice coronal two dimensional gradient echo acquisition and rapid complex subtraction to produce real-time visualization of the contrast bolus. Acquisition of repetitive three-dimensional angiographic datasets was triggered when contrast was visualized in the left atrium. Several types of reconstructions, including maximal intensity projections, three-dimensional shaded surface displays, and volume renderings were made from the acquired arterial phase and equilibrium phase three dimensional datasets.

Results: The bolus tracking method greatly facilitated the acquisition of arterial phase volumes. Arterial phase volumes were acquired in the initial angiographic dataset in every instance in which bolus tracking was employed. Subsequently acquired datasets were of equilibrium phase. Reconstructions performed from the arterial phase volumes were of substantially better quality than reconstructions performed from equilibrium phase images. Reconstructions performed from the arterial phase volumes could also be performed more rapidly and with more automation than reconstructions performed from the equilibrium phase volumes.

Conclusion: Gadolinium bolus tracking is a reliable technique for ensuring the acquisition of arterial phase volumes in pediatric patients with coarctation. Excellent, highly reproducible MRI angiographic results are readily obtained with this method.

125. Detection of Arrhythmogenic Substrate by Magnetic Resonance Imaging

Reza Razavi,[1] Daniel Rueckert,[2] Paul Summers,[3] Julia Anne Schnabel,[4] Marc Miquel,[5] Eric Rosenthal,[6] Edward Baker.[6] [1]*King's College London, Department of Congenital Heart Disease, London, UK;* [2]*Visual Information Processing (VIP), Dept of Computing, Imperial College, London, 180 Queens' Gate, London, UK;* [3]*King's College, London, Radiological Scinces, London, UK;* [4]*King's College, London, Radiological Sciences, London, UK;* [5]*King's College, London, Radiological Sciences, London, London UK;* [6]*King's College, London, Department of Congenital Heart Disease, London, UK*

Introduction: In most tachyarrhythmias radiofrequency ablation has become the treatment of choice. Accurate mapping of the arrhythmogenic substrate is essential for successful ablation. In some patients this can be difficult to achieve during electrophysiological study, leading to a prolonged procedure, which at times is unsuccessful. A number of new electro-anatomical mapping systems have recently been developed to overcome these problems. Magnetic resonance imaging gives excellent cardiac anatomical information. We hypothesis that as electrical activity leads to myocardial contraction, electrical mapping of the heart may be possible by studying changes in myocardial motion.

Methods: We studied 2 normal volunteers and 5 patients with a history of re-entry supraventricular tachycardia and one patient with ventricular tachycardia. MRI was performed on a 1.0 Tesla Siemens Expert magnet with a phased array body coil. Following planning scans a short axis cut just bellow the atrioventricular valves was obtained. A FLASH 2D cine tagged scan (TR 15 TE 7.2) was performed in this plane to look at left ventricular and right ventricular motion. The scan was repeated with an acquisition delay equal to 90% of the R-R interval to capture end diastolic/early systolic motion. In the patient who was in ventricular tachycardia, 5 parallel short axis cine tagged images were obtained from the base towards the apex. To calculate motion and deformation maps from tagged cine MR images we used a non-rigid registration algorithm, which we have previously employed to assess the contrast agent uptake in breast MR images [1] and to quantify brain deformation in intra-operative MR images [2]. To quantify ventricular motion we used the first cine (time 0) tagged MR image as a reference image and registered all successive time frames to this image. To avoid any artifacts due to flowing blood we have restricted the registration to voxels within the myocardium. This provides a motion and deformation map for each point in the myocardium relative to the first time frame. The time frames were 15 ms apart. The non-rigid registration algorithm uses a two-stage transformation model. The first stage captures the global motion of the left ventricle and is modeled by a rigid transformation. The second stage captures the local motion of the left ventricle and is modeled by a free-form deformation (FFD) based on B-Splines. The registration is achieved by maximizing normalized mutual information as a similarity measure between the first time frame of the tagged MR image sequence and any successive time frames. For each time frame the motion was displayed as a color map with maximal motion being displayed as the red end of the color spectrum. All the patients underwent electrophysiological study and conventional mapping of their arrhythmogenic substrate.

Results: Looking at the first systolic time frame the position of earliest motion appeared to correlate reasonably with what would be expected from the electrophysiological studies. In the patient with ventricular tachycardia the slice and anatomical position of earliest motion again correlated with the focus of the ventricular tachycardia.

Conclusion: Although these are very preliminary results it may be possible to produce electro-anatomical maps of the arrhythmogenic substrate of tachyarrhythmias by magnetic resonance imaging.

126. Impact of the Voxelsize on the Metabolite Ratios in Phosphorus-31 Magnetic Resonance Spectroscopic Imaging (31P MRSI) of the Human Heart

Michael Schocke,[1] Bernhard Metzler,[2] Christian Wolf,[3] Peter Steinboeck,[2] Otmar Pachinger,[2] Werner Jaschke.[3] [1]*University Innsbruck, Department of Radiology, Innsbruck, tyrol Austria;* [2]*University of Innsbruck, Department of Internal Medicine, Innsbruck, Tyrol Austria;* [3]*University of Innsbruck, Department of Radiology, Innsbruck, Tyrol Austria*

The aim of this study was to evaluate the impact of voxelsize on the ratio of phosphocreatine (PCr) to adenosine-triphosphate (ATP) in car-

diac phosphorus-31 magnetic resonance spectroscopic imaging (31P MRSI).

Using a 1.5 Tesla whole-body MR scanner cine MR imaging (MRI) and 31P MRSI were performed in 10 male healthy volunteers and eight patients with coronary artery disease (CAD). Fourier transformation with zero-filling of the spectral data resulted in matrices of 8 × 8 (64 ml), 16 × 16 (16 ml), and 32 × 32 (4 ml). Spectra were obtained from the chest muscle (CM), the interventricular septum (SP), the right (RV) and the left ventricle (LV). The matrix of 8 × 8 only permitted the recruitment of voxels of interest (VOI) in the chest muscle and the left ventricle. Cardia high energy phosphate metabolism was quantitated by the ratio of PCr to ATP. Regarding the healthy volunteers blood contamination was assessed by the ratio of 2,3-diphosphoglycerate (2.3-DPG) to PCr.

VOIs of 4 and 16 ml revealed significant differences ($p < 0.05$) in PCr to β ATP between patients and volunteers for CM, SP, RV and LV, whereas VOIs of 64 ml failed to show any significant effects. Generally, the VOIs taken from the left ventricle showed the lowest blood contamination. Regarding the different voxelsizes the blood contamination was the highest in the VOIs of 64 ml.

In conclusion, differences in high energy phosphate metabolism assessed by 31P MRS become clearer by means of smaller VOIs. This effect might be explained by the lower blood contamination of VOIs with a smaller volume.

127. Cardiac-MR in Genotype Positive/Phenotype Negative or Positive Patients with Hypertrophic Cardiomyopathy

Carsten Rickers,[1] Andrey Zenovich,[2] Michael Jerosch-Herold,[1] Prasad Panse,[1] Neeta Panse,[1] Yimei Huang,[1] Ravi Seethamraju,[1] Olaf Muehling,[1] Barry Maron,[3] Norbert Wilke.[1] [1]*University of Minnesota, Dept. of Radiology, MMC#292, Mayo, 420, Delaware St SE, Minneapolis, MN USA;* [2]*University of Minnesota, Dept. of Radiology, MMC#292, Mayo, 420, Delaware St SE, Minneapolis, MN USA;* [3]*Minneapolis Heart Institute and Foundation, Minneapolis, Minneapolis, MN USA*

Background: Sudden death resulting from hypertrophic cardiomyopathy (HCM) has been reported to be directly related to ventricular thickening with particular reference to septal thickness. We compared cardiac-MR (CMR) and echocardiography in patients (pts) with HCM (n = 9; obstructive: n = 4, non-obstructive: n = 4, genotype-positive/phenotype-negative: n = 1) regarding the extent and location of left ventricular (LV) hypertrophy as well as symptoms.

Methods: All pts were imaged with a 1.5T MR Scanner (SIEMENS Vision, Germany) for quantification of global myocardial function as well as segmental wall thickness. 10–12 Double-oblique short axis slices were acquired throughout the entire heart (slice thickness 8mm, interslice gap of 2mm, matrix size 128 × 260, phase encoding × readouts, field of view 300–350mm, and the flip angle 20 degrees, 12–15 phases/slice). Additionally two-to-three slices with a vivid myocardial hypertrophy were selected for assessment of myocardial tissue tagging. MR tagging images were obtained using SPAMM (TR = 3.2ms, TE = 8ms, flip angle = 10 degrees, FOV = 260mm, pixel dimension = 1.015mm).

The data were analyzed for global and segmental function measurements using MASS software (Version 4.0, Leiden/ Netherlands). LV and RV end-systolic and end-diastolic mass, stroke volumes, and ejection fraction were determined. Centerline method was used to assess wall thickening. SPAMM-tagged images were evaluated using SPAMMVU. We determined the transmural thickening (based on the maximum principle strain), circumferencial shortening (based on the minimal principle strain lambda 2) and the rigid body displacement D. Echo: Standard M-mode and cross-sectional views of the left ventricle were obtained.

Results: In our group of genotype positive patients septal hypertrophy (>12 mm) was detected in 40% of pts by echo and in 80% by CMR. The pt who was described as phenotype negative by echo standards had a regional septal hypertrophy (15 mm) as detected by CMR. With respect to the detection of the thickest LV-wall section, there was a good agreement (<2 mm difference) in 40% of the pts and no concordance between CMR and echocardiography in 60% of the pts. All pts (80%) with abnormal LV-mass (mean: 316 ± 302.92g; range 106.7 to 850.9) had symptoms but septal wall thickness was not correlated to symptoms. Hypertrophied segments exhibited heterogenious function compared to non-hypertrophied segments expressed by circumferential shortening and principal strain values on MR tagging.

Conclusions: Our findings suggest that CMR is superior to echocardiography in the assessment of regional wall thickness and LV-mass in genotype positive HCM pts. In accordance with previous studies maximal regional wall thickness does not correlate with symptoms, but total LV-mass may be a potential prognostic parameter.